INTERNATIONAL DOCTORAL
SCHOOL OF THE USC

Juan José
Tarrío Cordeiro

PhD Thesis

Poly(diphenylacetylene)s: Design, Synthesis and Applications

Santiago de Compostela, 2022

Doctoral Programme in Chemical Science and Technology

TESE DE DOUTORAMENTO

Poly(diphenylacetylene)s: Design, Synthesis and Applications

Juan José Tarrío Cordeiro

ESCOLA DE DOUTORAMENTO INTERNACIONAL DA UNIVERSIDADE DE SANTIAGO DE COMPOSTELA
PROGRAMA DE DOUTORAMENTO EN CIENCIA E TECNOLOXÍA QUÍMICA

SANTIAGO DE COMPOSTELA
2022

DECLARACIÓN DEL AUTOR/A DE LA TESIS

D./Dña. **Juan José Tarrío Cordeiro**

Título da tese: **Poly(diphenylacetylene)s: Design, Synthesis and Applications**

Presento mi tesis, siguiendo el procedimiento adecuado al Reglamento y declaro que:

1) La tesis abarca los resultados de la elaboración de mi trabajo.
2) De ser el caso, en la tesis se hace referencia a las colaboraciones que tuvo este trabajo.
3) Confirmo que la tesis no incurre en ningún tipo de plagio de otros autores ni de trabajos presentados por mí para la obtención de otros títulos.
4) La tesis es la versión definitiva presentada para su defensa y coincide la versión impresa con la presentada en formato electrónico.

Y me comprometo a presentar el Compromiso Documental de Supervisión en el caso que el original no esté depositado en la Escuela.

En **Santiago de Compostela**, **12 de julio de 2022**.

Firma electrónica

AUTORIZACIÓN DEL DIRECTOR / TUTOR DE LA TESIS

Poly(diphenylacetylene)s: Design, Synthesis and Application

D./Dª. **Emilio Quiñoá Cabana**
D./Dª. **Félix Freire Iribarne**

INFORMA/N:

Que la presente tesis, se corresponde con el trabajo realizado por D/Dª. **Juan José Tarrío Cordeiro**, bajo mi dirección/tutorización, y autorizo su presentación, considerando que reúne los requisitos exigidos en el Reglamento de Estudios de Doctorado de la USC, y que como director de esta no incurre en las causas de abstención establecidas en la Ley 40/2015.

De acuerdo con lo indicado en el Reglamento de Estudios de Doctorado, declara también que la presente tesis doctoral es idónea para ser defendida en base a la modalidad de Monográfica con reproducción de publicaciones, en los que la participación del doctorando/a fue decisiva para su elaboración y las publicaciones se ajustan al Plan de Investigación.

En Santiago de Compostela, 12 de julio de 2022

Contents

Abbreviations and Acronyms

AEE	Aggregation Enhanced Emission
AFM	Atomic Force Microscopy
AIB	α-aminoisobutyric acid
[α]	Specific Optical Rotation
ap	Antiperiplanar
CD	Circular Dichroism
c-c	*Cis-cisoidal*
CCPMs	Cross-linked Polymeric Microspheres
cod	*Cis-cis*-1,5-cyclooctadiene
CPs	Conjugated Polymers
CPL	Circular Polarized Luminiscence
CSP	Chiral Stationary Phase
c-t	*Cis-transoidal*
d	Doblet
δ	Chemical shift
D	Diameter
DCM	Dichloromethane
DIPEA	Diisopropyethylamine
DLS	Dynamic Light Scattering
DMF	N,N-Dimethylformamide
DMSO	Dimethyl sulfoxide
DSC	Differential Scanning Calorimetry
EDX	Energy Dispersive X-Ray spectroscopy
equiv	Equivalents
e.g	Latin expression "*exempli gratia*", for example

et al.	Latin expression "*et Alii*", and others
FSL	Functionalized Stabilizing Ligand
FWt	Formula molecular weight
g	Grams
GPC	Gel Perfomance Chromatography
h	Hour
HATU	(2-(7-Aza-1H-benzotriazole-1-yl)-1,1,3,3-tetramethyluronium hexafluorophosphate)
HMPC	Helical Polymer-Metal complex
HOPG	Highly Oriented Pyrolitic Graphite
HOAt	1-hydroxy-7-azabenzotriazole
HPLC	High-Performance Liquid Chromatography
Hz	Hertz
IR	Infrared
KPS	Potassium persulfate
LB	Langmuir-Blodgett
LBL	Layer-by-Layer
LS	Langmuir-Schaefer
M helix	Counterclockwise helix
m	Multiplet
m.r.u.	Monomeric repetition unit
mg	Milligrams
min	Minute
mL	Milliliters
mM	Millimolar
mmol	Milimol
MPA	α-methoxy-α-phenylacetic acid

MTPA	α-methoxy-α-trifluoromethyl-α-phenylacetic acid
MS	Mass spectroscopy
nm	Nanometer
M_w	Molecular weight
nbd	2,5-norbornadiene
NMR	Nuclear Magnetic Resonance
^oC	Celsius degree
P helix	Clockwise helix
PA	Poly(acetylene)
PDI	Polydispersion index
PDPA	Poly(diphenylacetylene)
PDSA	Poly(disubstitutedacetylene)
PGME	Phenylglycine methyl ester
Prof.	Professor
PPA	Poly(phenylacetylene)
s	Singlet
syn	synperiplanar
sa	Broad signal
S&S	Sergeants and Soldiers
SIFC	Surfactant-Induced Fluorescence Change
SEM	Scanning Electron Microscopy
STM	Scanning Tunneling Microscopy
sp	Synperiplanar
SCAT	Selective Photocyclic Aromatization
SDS	Sodium Dodecyl Sulphate
SIEE	Swelling-Induced Emission Enhancement

TEM	Transmission Electron Microscopy
TGA	Thermogravimetric Analysis
THF	Tetrahydrofuran
TMS	Trimethylsilane
TrMA	Triphenylmetracrilate
UV-Vis	Ultraviolet-Visible Spectroscopy

List of publications

During the development of this Thesis, the following article has been published in a scientific journal. Furthermore, the results of this article have been included within this manuscript.

1) Juan José Tarrío, Rafael Rodríguez, Berta Fernández, Emilio Quiñoá and Félix Freire. *Angew. Chem. Int. Ed.* **2022**, *61*, e202115070

Impact factor: 16.823

Category: Chemistry, multidisciplinary (Q1).

J. J. T. has contributed to the experimental part (synthesis and characterization) discussion of results and the manuscript preparation.

The authorization of the journal can be found in the following link:

https://s100.copyright.com/CustomerAdmin/PLF.jsp?ref=25ef2004-e80f-4b28-a4c7-63a3d87f10d

Chapter I

Introduction

Chapter I. Introduction

In nature, helix is one of the most representative chiral structures. Thus, left- and right-handed helices cannot be superimposed. This structure can be found in many molecules, supramolecules, oligomers and polymers and it is known the relationship between this structure and its properties.

a- **helix in proteins** **Helical structure in sugars** **DNA secondary structure**

Figure 1. Representation of natural biomacromolecules with helical structure.

In the early 50´s, it took place the discovery of the α-helix for proteins[1] proposed by Pauling and the double helical structure of DNA proposed by Watson and Crick.[2] These were two of the most important research progresses at that time in molecular biology. In each case, the homochirality of *L*-amino acids and *D*-sugars is the responsible of the axial chirality in the helices. Focused on these findings, the scientific community has spent efforts and time in trying to emulate the properties of helices in nature creating the synthetical helical polymers field.

At 1955, Natta reported the first helical structure in a non-natural polymer. This corresponds to the isotactic poly(propylene) which adopts a helical structure in solid state. Moreover, he described this polymer has an equal ratio of left- and right-handed helices in its structure.[3]

Since the discovery of Natta there have had new advances in this field, generating polymers with a helical structure even in solution. Pinno and co-workers developed in the 60´s

[1] Pauling, L.; Corey, R. B.; Branson, H. R. *Proc. Natl. Acad. Sci. U.S.A.* **1951**, *37*, 205.

[2] Watson, J. D.; Crick, F. H. C. *Nature*. **1953**, *171*, 737.

[3] Natta, G.; Pino, P.; Corradini, P.; Danusso, F.; Mantica, E.; Mazzanti, G.; Moraglio, G. *J. Am. Chem. Soc.* **1955**, *77*, 1708.

a series of isotactic poly(vinyl) polymers by polymerization of chiral olefins, where the inclusion of a chiral center in the pendant moiety promotes an excess of a predominant helical sense acting as chiral inductor.[4]

After these important findings, it was in 70s when several research groups started to work in helical polymers making some of the greatest advances in this area. Nolte *et al.* resolved the structure of poly(tert-butyl isocyanide) into enantiomeric left- and right-handed helices applying chiral HPLC.[5] Later, Okamoto and co-workers obtained the first helical polymer through the polymerization of an achiral monomer with a chiral catalyst.[6]

In the 80's, Green and co-workers reported the synthesis of a new family of helical polymers, the poly(isocianyte)s. These polymers can adopt either a right- or left-handed helical structure depending on the application of different external stimuli. This is due to the presence of a mixture of interconvertible left-handed (*M*) and right-handed (*P*) helices connected by helical reversals.[7] This was the first example of dynamic helical polymers.

1.1 Classification of helical polymers

Helical polymers can be classified into three main groups based on the dynamism of their helical properties.[8] These dynamic properties are directly related to the interconversion energetic barriers between the *P* (clockwise direction) and *M* (counterclockwise direction) helical conformations.

I) Static helical polymers

These materials are a family of polymers that adopt a rigid structure with a define helical sense during the polymerization. These polymers present a high energetic barrier that hinders the interconversion of the helical sense by applying external stimuli. Usually, they are prepared from monomers that contain bulky substituents that favor the formation of one preferred helical sense by steric hindrance. Different families of static helical polymers have been prepared such as poly(methacrylate)s (poly-**1**), poly(methylacrylamide)s (poly-**2**), poly(quinoxaline-2,3-diyl)s (poly-**3**) or poly(guanidine)s (poly-**4**).[9]

[4] Pino, P.; Lorenzi, G. P. *J. Am. Chem. Soc.* **1960**, *82*, 4745.

[5] Nolte, R. J. M.; Van Beijnen, A. J. M.; Drenth, W. *J. Am. Chem. Soc.* **1974**, *96*, 5932.

[6] Okamoto, Y.; Suzuki, K.; Ohta, K.; Hatada, K.; Yuki, H. *J. Am. Chem. Soc.* **1979**, *101*, 4763.

[7] Green, M. M.; Andreola, C.; Munoz, B.; Reidy, M. P.; Zero, K. *J. Am. Chem. Soc.* **1988**, *110*, 4063.

[8] a) Yashima, E.; Maeda, K.; Iida, H.; Furusho, Y.; Nagai, K.; *Chem. Rev.* **2009**, *109*, 6102. b) Cornelissen, J. J. L.; Rowan, A. E.; R. J. M. Nolte, R. J. M.; Sommerdijk, N. A. J. M.; *Chem. Rev.* **2001**, *101*, 4039.

[9] Okamoto, Y.; T. Nakano, T.; *Chem. Rev.* **1994**, *94*, 349

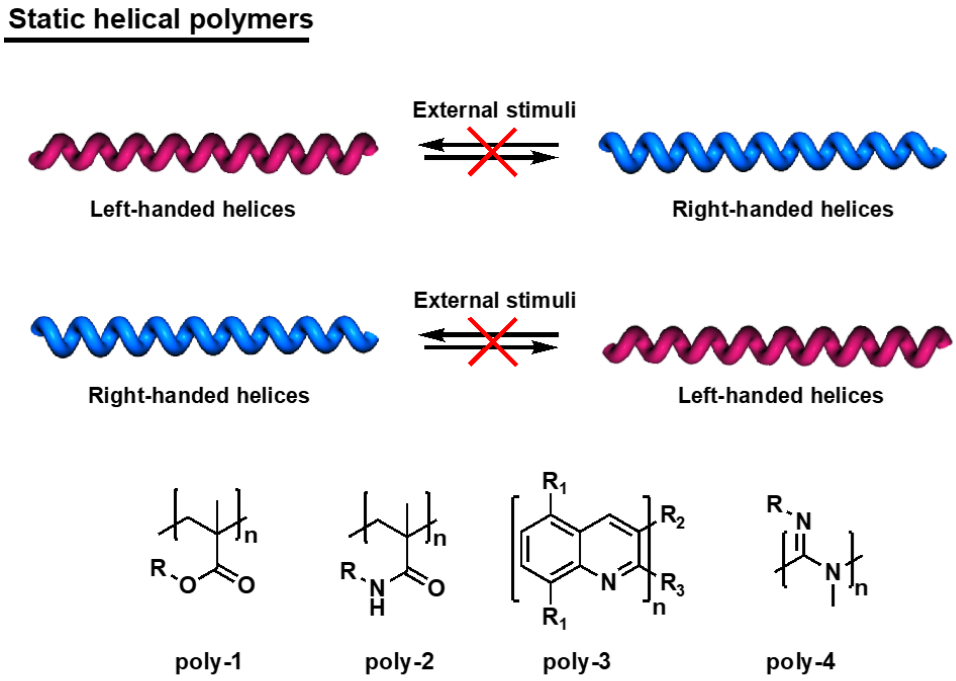

Figure 2. Conceptual representation of different types of static helical polymers.

II) Dynamic helical polymers

Dynamic helical polymers are those that present a low interconversion barrier energy between the two helical senses (right- and left-handed). This is achieved by polymerization of achiral monomers, or chiral ones that present at least two stable conformers in equilibrium in the pendant group. Thus, the helical sense can be easily modulated by the presence of external stimuli such as: pH, solvents, temperature or the addition of metal ions (Figure 3). Examples of this type of dynamic polymers are poly(isocyanate)s (poly-**5**), poly(silane)s (poly-**6**) and poly(acetylene)s (poly-**7**).[10]

[10] Louzao, I.; Seco, J. M.; Quiñoá, E.; Riguera, R.; *Angew. Chem., Int. Ed.* **2010**, *49*, 1430.

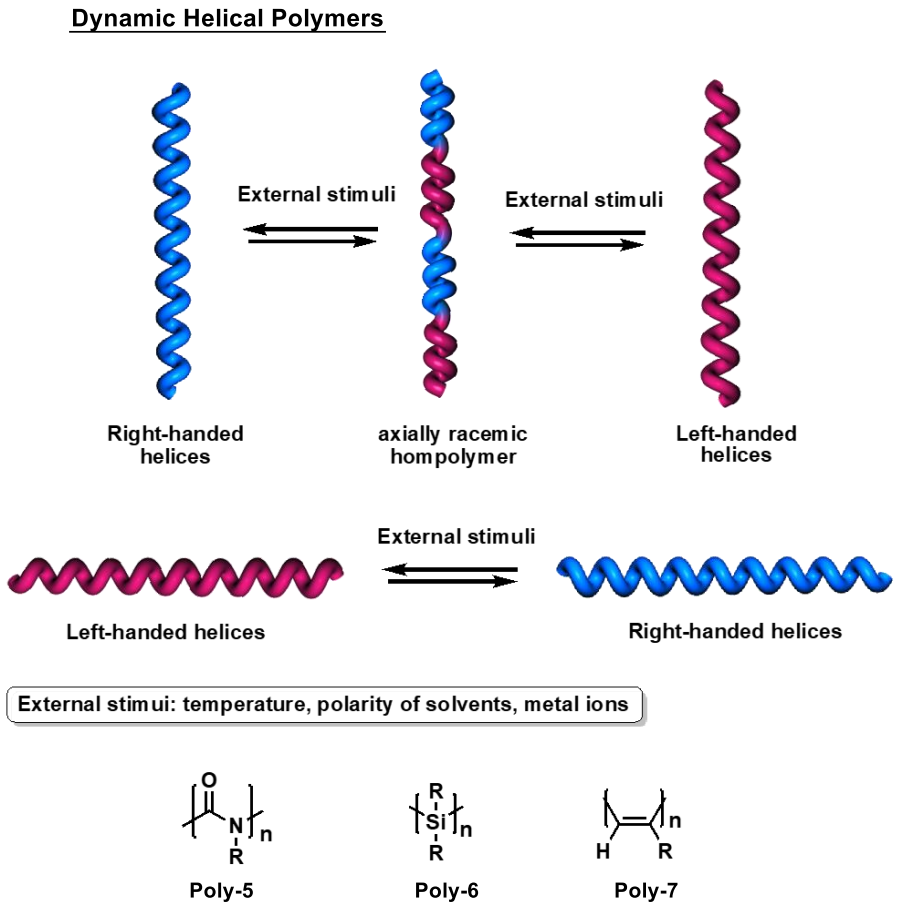

Figure 3. Conceptual representation of different types of dynamic helical polymers.

III) Foldamers

Foldamers are defined as any polymer with a strong tendency to adopt a specific pack conformation. The helical structure is in equilibrium with an unfolded structure and turns them in interesting targets in supramolecular chemistry.[11]

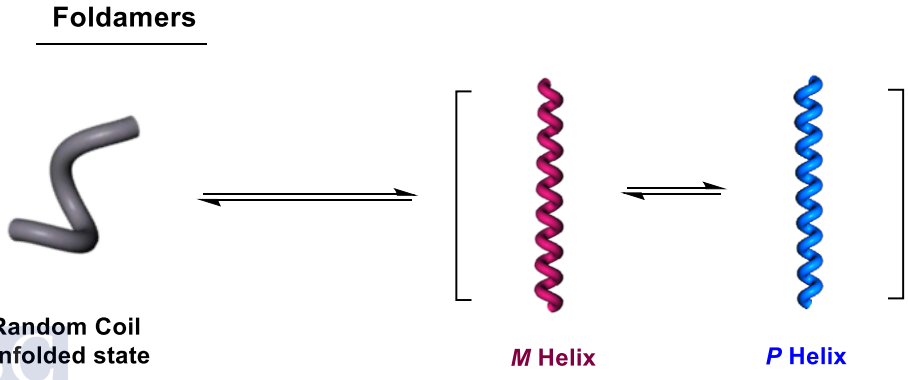

Figure 4. Conceptual representation of the different structures that foldamers can adopt.

[11] a) Hill, D. J.; Mio, M. J.; Prince, R.B.; Hughes, T.S.; Moore, J.S.; *Chem.Rev.* **2001**, *101*, 3893. b) Appella, D. H.; Christianson, L. A.; Karle, I. L.; Powell, D. R.; Gellman, S. H.; *J. Am. Chem. Soc.* **1996**, *118*, 13071.

2. Poly(acetylene)s and Poly(phenylacetylene)s

Poly(acetylene)s (PAs) are one of the most studied families of dynamic helical polymers. PAs are derived from acetylenic monomers that presents π-conjugated double bonds along the polymeric chain. In the last decades, different examples of PAs have been prepared and studied (Figure 5a) due to their optical and chiroptical properties which make them suitable for applications such as Chiral Stationary Phases (CSPs) for HPLC, sensors or asymmetric catalysts. Moreover, PAs are highly stable in solid state, dissolved and can be obtained easily. Thus, Ciardelli *et al.* started to prepare many π-conjugated PAs[12,13] with optical activities during the 60s-70s.

At 1995, professor Yashima made a huge step in the dynamic helical polymers field by developing a new method to obtain them. This method consists in generating polymers with a helical structure stabilized by non-covalent interactions. These novel structures were derived from PA substituted with one phenyl ring and called poly(phenylacetylene)s (PPAs).[14]

As mention before, PPAs are a class of PAs that have as the monomeric repetition unit (m.r.u) an ethynylbenzene derived monomer. As dynamic helical polymers, the helical sense of these macromolecules can be modulated by the addition of different external stimuli such as: temperature, polarity of solvents and metal ions, among others.[15]

One important feature to obtain PPAs with helical structure is the need of a *cis* configuration of the double bonds in the conjugated polyenic skeleton. There are 4 possibilities that can be adopted during the polymerization: *cis-cisoidal* (*c-c*), *cis-transoidal* (*c-t*), *trans-cisoidal* (*t-c*) and *trans-transoidal* (*t-t*) (Figure 5c). Notice that in a *trans* configuration is not possible to obtain a folded helical structure probably due to the distance between functional groups that stabilize the helical structure through non-covalent forces. For these reasons, Rh(I) catalysts, initially developed by Noyori and co-workers, are used because they produce polymers with a high content of *cis* double bonds, great stereoregularity and high molecular weight in good yields due to a living polymerization process.[16]

[12] Ciardelli, F.; Benedetii, E.; Pieroni, O.; *Makromol. Chem.* **1967**, *103*, 1.

[13] Ciardelli, F.; Lanzillo, S.; Pieroni, O.; *Macromolecules* **1974**, *7*, 174.

[14] Maeda, K.; Yashima, E.; *Top. Curr. Chem.* **2006***, 265*, 47.

[15] Simonescu, C. I.; Persec, V.; Dumitrescu. S.; *J. Polym. Sci. Polym. Chem.* **1977***, 15,* 2497. (b) Simonescu, C. I.; Percec, V.; *J. Polym. Sci., Part C: Polym. Lett.* **1979**, *17*, 421.

[16] a) Ke, Z.; Abe, S.; Ueno, T.; Morokuma, K.; *J. Am. Chem. Soc.* **2011**, *133*, 7926. b) Hirao, K.; Ishii, Y.; Terao, T.; Kishimoto, Y.; Miyatake, T.; Ikariya, T.; Noyori, R.; *Macromolecules* **1998**, *31*, 3405. (c) Kishimoto, Y.; Eckerle, P.; Miyatake, T.; Ikariya, T.; Noyori, T.; *J. Am. Chem. Soc.* **1994**, *116*, 12131.

Different types of Rh(I) catalysts such as $[Rh(nbd)Cl]_2$ (nbd: 2,5-norbornadiene), $[Rh(cod)Cl]_2$ (cod: *cis-cis*-1,5-cyclooctadiene), $[Rh(nbd)BF_4]$ can be used to obtain these polymers in different organic solvents or in water. Furthermore, Rh (I) catalysts are tolerant to polar groups and can be applied even with unprotected amines.[17]

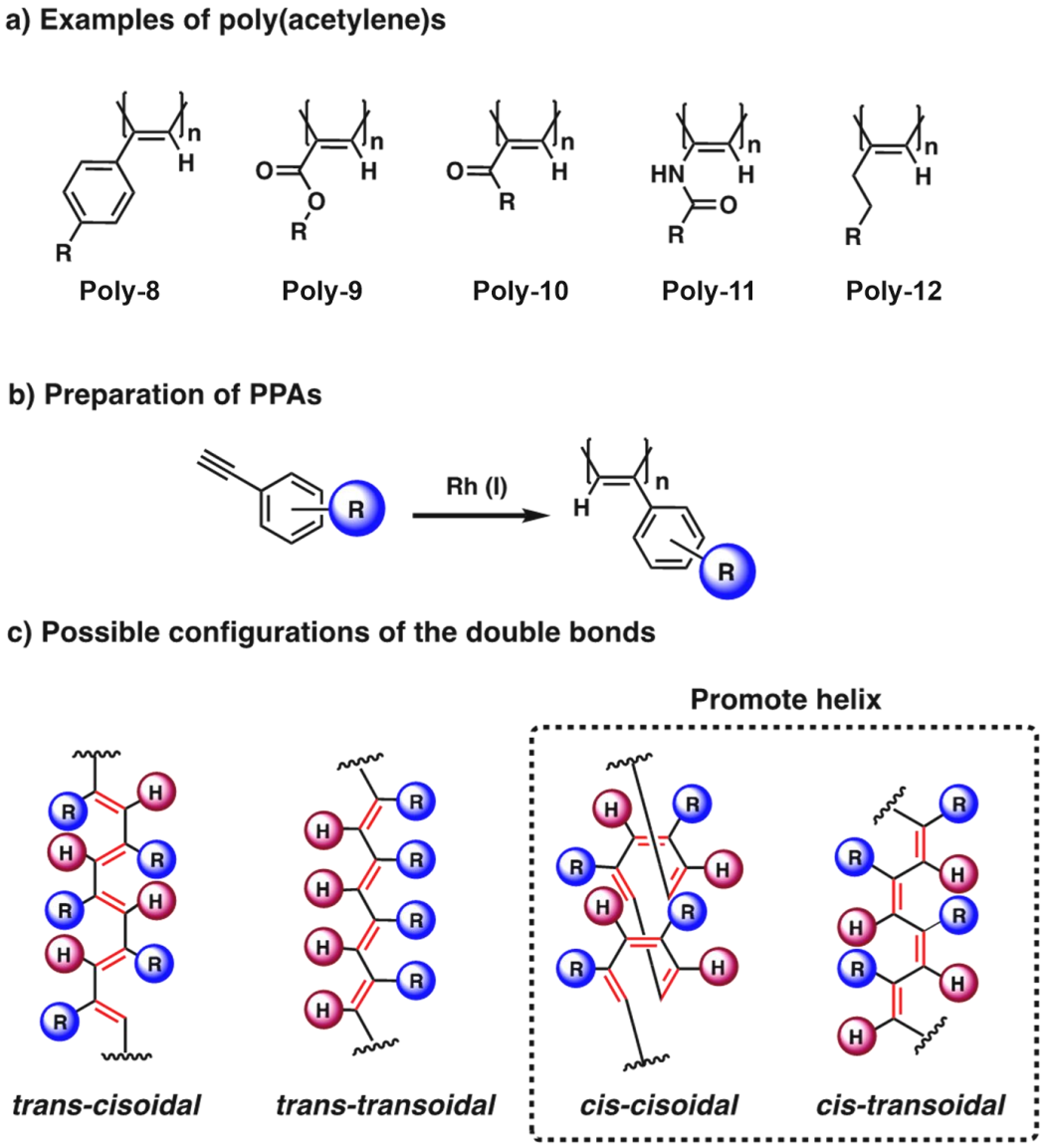

Figure 5. a) Examples of PAs**.** b) General method for the preparation of PPAs. b) Four possible configurations of the conjugated double bonds in PPAs.

The PPAs polymerization mechanism with a Rh(I) catalyst is a 2,1-insertion, with a head to tail stereospecific and regioselective process. This mechanism is produced due to steric repulsion between pendant units (Figure 6).[18]

[17] Suárez-Picado, E.; Quiñoá, E.; Riguera, R. and Freire, F. *Chemistry of Materials*. **2018**, 30, 6908.

[18] Ke, Z.; Abe, S.; Ueno, T.; Morokuma, K.; *J. Am. Chem. Soc*. **2011**, *33*, 7926.

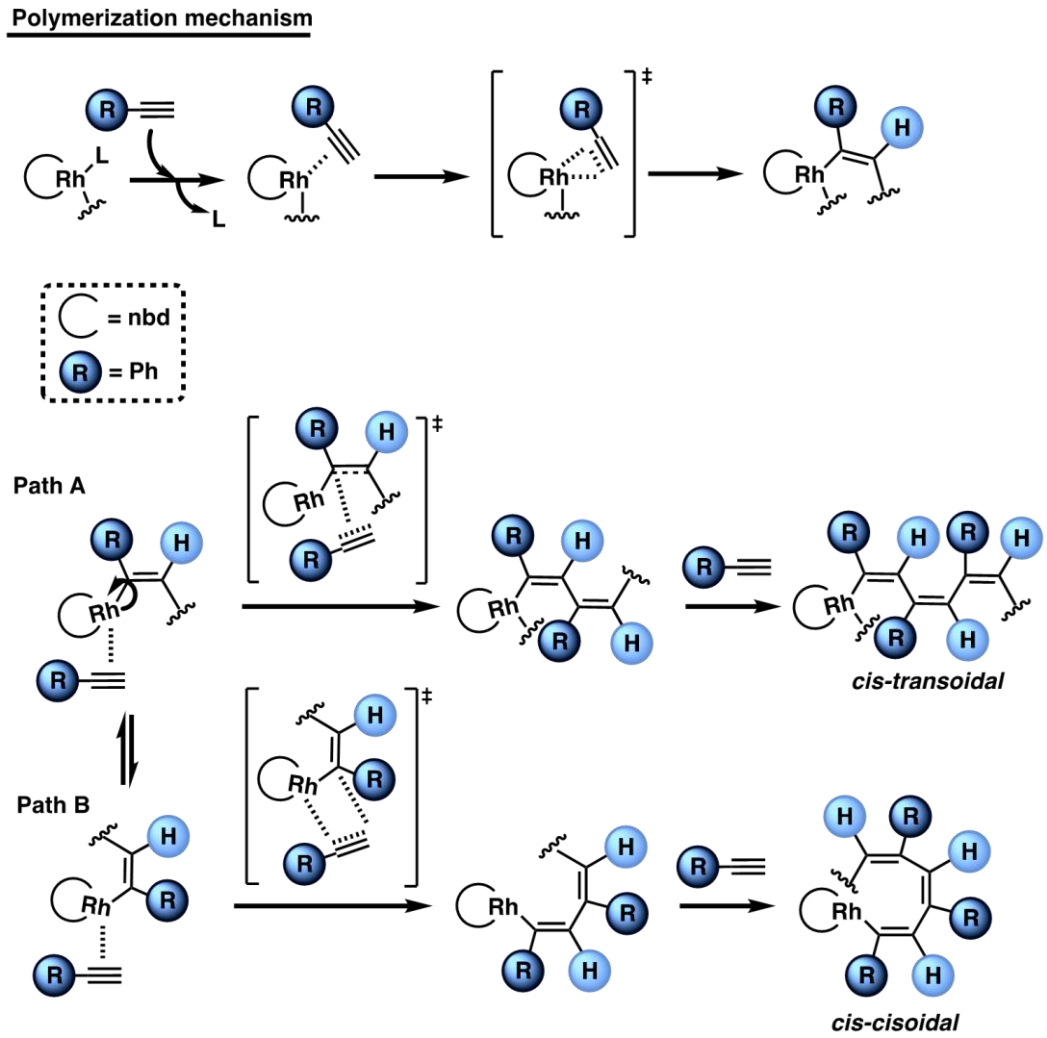

Figure 6. Polymerization mechanism for PPAs using Rh (I) catalyst.

2.1 Poly(phenylacetylene)s' stability

As it was mentioned before, helical polymers have a strong potential application in different fields. For this, to know if they can be applied at industrial level or only at laboratory scale, the stability of PPAs is a very important feature that must be measured.[19]

Interestingly, Percec *et al.* noticed how the *cis* content of the *c-t* PPAs shows a decrease when the polymers are dissolved in chloroform as well as in solid state. The reason was attributed to an electrocyclization mechanism followed by a breakage of the polymer chain to produce an 1,3,5-triphenylbencene (Figure 7a). On the one hand, this degradation occurs faster in solution than in solid state and the kinetics of this phenomenon decrease under inert atmosphere or vacuum. On the other hand, the degradation velocity increases at high

[19] a) Liu, l.; Namikoshi, T.; Zang, Y.; Aoki, T.; Hadano, S.; Abe, Y.; Wasuzu, I.; Tsutsuba, T.; Teraguchi, M.; Kaneko, T.; *J. Am. Chem. Soc.* **2013**, *135*, 602. b) Huang, K.; Mawatari, Y.; Miyasaka, A.; Sadahiro, Y.; Tabata, M.; Kashiwaya, Y.; *Polymer* **2007**, *48*, 6366. c) Miyasaka, A.; Mawatari, Y.; Sone, T.; Tabata, M.; *Polym. Degrad. Stab.* **2007**, *92*, 253. d) Percec, V.; Rudick, J. G.; *Macromolecules* **2005**, *38*, 7241.

temperatures as demonstrated by ^{1}H NMR experiments. For this reason, these polymers are thermosensitive and unstable.[20]

Tabata and co-workers determined by electron spin resonance the *cis* to *trans* isomerization in PPAs. The process undergoes a radical mechanism and can be mediated by heat, pressure or electric field (Figure 7b).[19]

Most recently, Liu *et al.* described the possibility of a photocyclic degradation in *cis-cisoidal* PPAs in solid state, resulting in 1,3,5-trisubstitued benzene derivatives (cyclotrimers). The new products can organize in supramolecular polymers by hydrogen bonding and π-stacking. These products were successfully characterized by Gel Performance Chromatography (GPC), ^{1}H NMR and TOF-MS (Figure 7c).[21]

[20] Vohlidal, J.; Redrova, D.; Pacovska, M.; Sedlacek; *J. Collect Czech Chem. Commun.* **1993**, *58*, 2651.

[19] a) Liu, l.; Namikoshi, T.; Zang, Y.; Aoki, T.; Hadano, S.; Abe, Y.; Wasuzu, I.; Tsutsuba, T.; Teraguchi, M.; Kaneko, T.; *J. Am. Chem. Soc.* **2013**, *135*, 602. b) Huang, K.; Mawatari, Y.; Miyasaka, A.; Sadahiro, Y.; Tabata, M.; Kashiwaya, Y.; *Polymer* **2007**, *48*, 6366. c) Miyasaka, A.; Mawatari, Y.; Sone, T.; Tabata, M.; *Polym. Degrad. Stab.* **2007**, *92*, 253. d) Percec, V.; Rudick, J. G.; *Macromolecules* **2005**, *38*, 7241.

[21] Miyata, M.; Masahiro, T.; Hiromichi, E.; Takashi, K.; Toshiki, A.; *Chem. Lett.* **2014**, *43*, 1476.

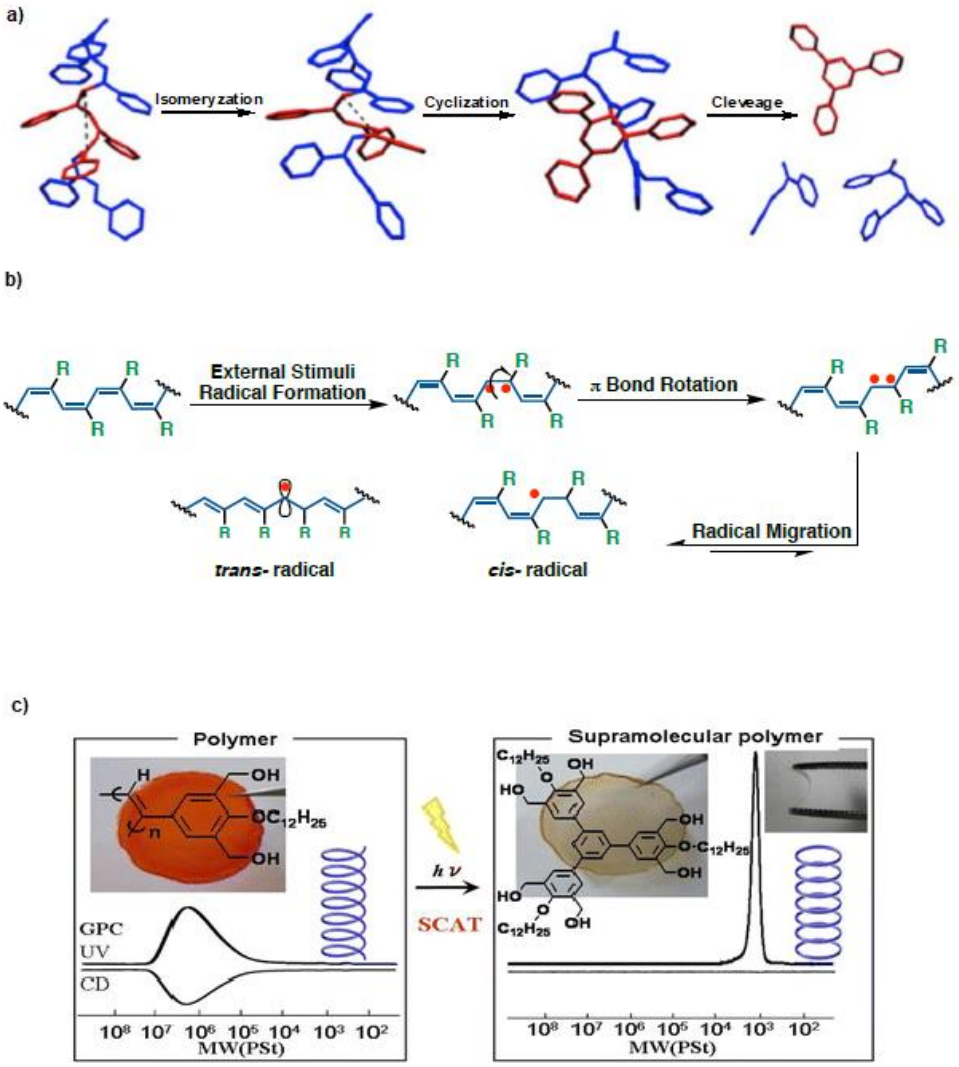

Figure 7. a) Schematic representation for the degradation of PPAs by electrocyclization. b) Isomerization *cis-trans* in PPAs described by Tabata. c) Schematic representation of photocyclic aromatization in *cis-cisoidal* PPAs in solid state.

In 2020, Rey-Tarrío et al., in a great contribution to the topic, demonstrated that this photocyclization of PPAs is possible also in *cis-transoidal* polymers. Thus, they created a new tool to elucidate the internal structure of PPAs based on the decomposition velocity measured by the time under irradiation with light.[22]

3. Structural Elucidation of Helical Scaffolds: Approaches in PPAs

The secondary structure of non-natural helical polymers is directly related with their properties and functions as it occurs in nature. Thus, knowing the structure-properties relationship is essential to determine the helix formation mechanism and for the rational

[22] Rey-Tarrío, F.; Rodríguez, R.; Quiñoá, E.; Riguera, R. and Freire, F; *Angew. Chem. Int. Ed.*, **2021**, *133*, 8176.

design of monomers/polymers. Nevertheless, the complete elucidation of the secondary structure of a helical polymer is a huge challenge and it is only attainable with the combination of different techniques.

3.1 Architecture of Poly(phenylacetylene)s

PPAs are composed by two coaxial helices (internal and external ones). Many published works deal with changes on the internal helix, but don't give information about the external one. ECD is a powerful technique to follow the changes produced in the internal helix. Nowadays, the reason for these changes is explained by computational studies.[23,24]

The internal helix is formed by conjugated double bonds and is characterized by its flexibility. Thus, the adoption of a preferred helical sense will be determined by the conformational composition of the pendant groups and the supramolecular interactions produced among them. The elongation of this helix will depend on the dihedral angle between the conjugated double bonds (ω_1) —negative values of ω_1 form an *M* helix (negative CD), while positive values form a *P* helix (positive CD)—. As consequence, ω_1 also determine the presence of a *cis-cisoidal* or *cis-transoidal* structure —$\omega_1 < 90^o$ indicates a *c-c* configuration and $\omega_1 > 90^o$ form a *c-t* configuration—.

Otherwise, the external helix is described by the pendant groups and can follow the same direction of the internal helix or the opposite.[25] In order to know the helical sense of this helix is necessary to observe it directly by AFM measurements. With this technique is also possible to obtain structural parameters as helical pitch and packing angle.

Taking all this into account, it is demonstrated that is not possible to refine the final secondary structure of a helical polymer only with one technique.

[23] Fernández, B.; Rodríguez, R.; Quiñoá, E.; Riguera, R.; Freire, F. *ACS Omega* **2019**, *4*, 5233.

[24] Fernández, B.; Rodríguez, R.; Rizzo, A.; Quiñoá, E.; Riguera, R.; Freire, F. *Angew. Chem. Int. Ed.* **2018**, *57*, 3666.

[25] Leiras, S.; Freire, F.; Seco, J. M.; Quiñoá, E.; Riguera, R. *Chem. Sci.* **2013**, *4*, 2735.

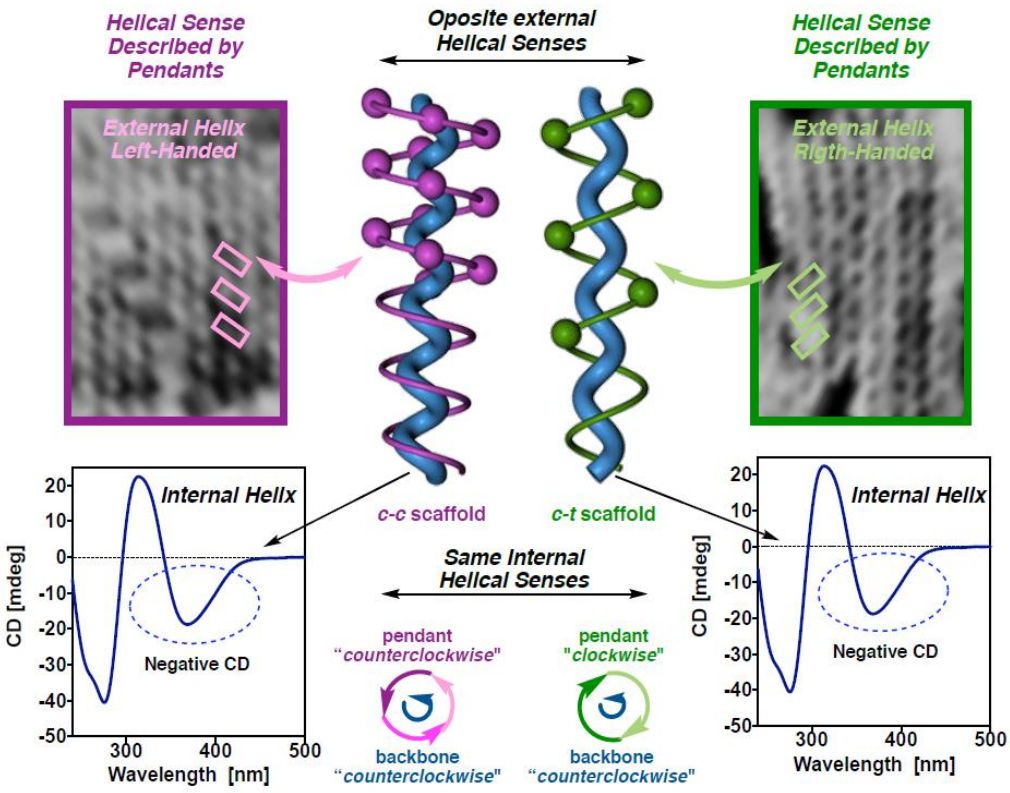

Figure 8. Schematic representation of the different helices that a PPA can adopt.

3.2 Determination of the Polyene Backbone Configuration

As stated before, there are four possible configurations that the acetylenic monomers can adopt during the polymerization —*cis-cisoidal*, *cis-transoidal*, *trans-cisoidal* and *trans-transoidal*—. The polymerization of the phenylacetylene monomers using Rh(I) catalysts produces polymers with a *cis* configuration, in high yields and low polydispersity.[26,27]

Percec *et al.* carried out studies to distinguish the different configurations that can adopt the conjugated double bonds in PPAs. For that, NMR studies and other theoretical studies were carried out throwing interesting results. Thus, *trans* PPAs show the vinylic protons signals between 6.20-7.20 ppm in ^{1}H-NMR, while *cis* polymers present the vinylic proton around 5.60-6.00 ppm.

They also could calculate the *cis*-content in the polymers in the following way:

[26] a) Kishimoto, Y.; Eckerle, P.; Miyatake, T.; Ikariya, T.; Noyori, R.; *J. Am. Chem. Soc.* **1994**, *116*, 12131. b) Tabata, M.; Yang, W.; Yokota, K.; *Polym. J.* **1990**, *22*, 1105. c) Furlani, A.; Napoletano, C.; Russo, M. V.; Feast, W.; *J. Polym. Bull.* **1986**, *16*, 311.

[27] a) Simonescu, C.I.; Percec, V.; *Prog. Polym. Sci.* **1982**, *8*, 133. b) Simonescu, C.I.; Percec, V. J.; *Polym. Sci.: Polymer Symposia* **1980**, *67*, 43. c) Simionescu, C. I.; Percec, V.; J. *Polym. Sci., Polym. Chem. Ed.* **1980**, *18*, 147. d) Simionescu, C. I.; Percec, V.; J. Polym. Sci., *Polym. Lett. Ed.* **1979**, *17*, 421. e) Simionescu, C. I.; Percec, V.; Dumitrescu, S. J. *Polym. Sci., Polym. Chem. Ed*. **1977**, *15*, 2497.

For example, a *cis-cisoidal* polymer shows in ^{1}H-NMR, the vinylic proton resonances at 5.80 ppm, 1H *ortho*- at 6.70 ppm, 1H *para*- and *meta*- at 6.85 ppm. To calculate the *cis*-content in PPAs, Percec *el Al.* propose the following equation.

$$\%\ cis\text{-content} = [A_{cis}/(A_{total} \times H_{total})] \times 100$$

Equation 1. Mathematical statement to determine the % of *cis*-content in PPAs.

Where A_{cis} is the area of vinylic proton in ^{1}H-NMR (5.60 - 6.00 ppm), A_{total} is the total area observed in^{1}H-NMR and H_{total} is the number of protons in the pendant group.

Another important technique is Raman spectroscospy. This is very useful because double bonds present characteristic signals depending on the configuration. For example, in the case of *cis-cisoidal* or *cis-transoidal*, they present characteristic resonances bands of the polyene skeleton around 1580 cm^{-1} (C=C$_{cis}$), 1335 cm^{-1} (C-C$_{cis}$) and 965 cm^{-1} (C-H$_{cis}$) (Figure 9b). On the other hand, in the case of *trans*- configuration PPAs, Raman characteristic bands appear shifted to low energy wavenumber. Thus, 1500 cm^{-1} (C=C$_{trans}$), 1200 cm^{-1} (C-C$_{trans}$) and 740 cm^{-1} (C-H$_{trans}$) are typical bands of the *trans* configuration.[28] Moreover, in a seminal work, made by Simionescu *et al.*, they could decipher the *cis/trans* configuration in different PA and PPA through IR spectroscopy. Also, it can give information about C-H deformation bands around 1015 cm^{-1} (C-H$_{trans}$) and 740 cm^{-1} (C-H$_{cis}$).[27, 29] However, the assignation and interpretation of the bands in the fingerprint is difficult. For this, it is highly advisable to use this technique in combination with others.

As explained above, both Raman and ^{1}H-NMR techniques are powerful techniques by themselves, and IR can provide important information in some cases. Nevertheless, with the combination of them it is not possible to distinguish between *cis-cisoidal* and *cis-transoidal* conformations. For this reason, Differential Scanning Calorimetry (DSC) is employed to determine the configuration of the PPAs too.

DSC shows different thermograms depending on if the PPAs adopt a *cis-cisoidal* or *cis-transoidal* configuration. Thus, *c-c* PPAs just show an exothermic transition peak around 200-

[28] a) Misayaka, A.; Sone, T.; Mawatari, Y.; Setauesh, S.; Müllen, K.; Tabata, M.; *Macromole. Chem. Phys.* **2006**, *207*, 1938. b) Huang, K.; Mawatari, Y.; Miyasaka, A.; Sadahiro, Y.; Tabata, M.; Kashiwaya, Y.; *Polymer* **2007**, *48*, 6366. c) Miyasaka, A.; Mawatari, Y.; Sone, T.; Tabata, M.; *Polym. Degrad. Stab.* **2007**, *92*, 253.

[27] a) Simonescu, C.I.; Percec, V.; *Prog. Polym. Sci.* **1982**, *8*, 133. b) Simonescu, C.I.; Percec, V. J.; *Polym. Sci.: Polymer Symposia* **1980**, *67*, 43. c) Simionescu, C. I.; Percec, V.; J. *Polym. Sci., Polym. Chem. Ed.* **1980**, *18*, 147. d) Simionescu, C. I.; Percec, V.; J. Polym. Sci., *Polym. Lett. Ed.* **1979**, *17*, 421. e) Simionescu, C. I.; Percec, V.; Dumitrescu, S. J. *Polym. Sci., Polym. Chem. Ed*. **1977**, *15*, 2497.

[29] a) Ito, T.; Shirakawa, H.; Ikeda, S. *J. Polym. Sci., Part A: Polym. Chem.* **1974**, *12*, 11-20. b) Shirakawa, H.; Ikeda, S.; *Polym. J.* **1971**, *2,* 231.

240°C due to the isomerization process from *c-c* to *t-t*. On the other hand, *cis*-transoidal thermograms shows two exothermic peaks around 140°C and 240°C corresponding to isomerizations from *c-t* to *c-c* and *c-c* to *t-t* respectively (Figure 9c).[30]

As mentioned before, the photocyclic aromatization reaction of PPAs in solution permits to distinguish between *c-c* and *c-t* helices.[22]

Another interesting technique is Ultraviolet-Visible spectroscopy (UV-Vis). This can provide information about the elongation or compression produced in the polymer when an external stimulus is applied. Thus, a bathochromic shift appears due to the increase in the conjugation of double bonds when the helix is stretched. In the opposite way, when the helix is compressed a hypsochromic shift is observed meaning a decrease in the conjugation of the polyenic chain. It is important to remark that this technique cannot provide information about the configuration (*c-c* or *c-t*) of the double bonds.[31]

[30] a) Motoshige, A.; Mawatari, Y.; Yoshida, Y.; Motoshige, R.; Tabata, M.; *Polym. Chem.* **2014**, 5, 971. b) Yoshida, Y.; Mawatari, Y.; Motoshige, A.; Motoshige, R.; Hiraoki, T.; Wagner, M.; Müllen , K.; Tabata, M.; *J. Am. Chem. Soc.* **2013**, 135, 4110. c) Motoshige, A.; Mawatari, Y.; Motoshige, R.; Yoshida, Y.; Tabata, M.; J. Polym. Sci., Part A: *Polym. Chem*. **2013**, *51*, 5177.

[22] Rey-Tarrío, F.; Rodríguez, R.; Quiñoá, E.; Riguera, R. and Freire, F; *Angew. Chem. Int. Ed.*, **2021**, *133*, 8176.

[31] a) Percec, V.; Peterca, M.; Rudick, J. G.; Aqad, E.; Imam, M. R.; Heiney, P. A.; *Chem. Eur. J*. **2007**, *13*, 9572. b) Percec, V.; Rudick, J. G.; Peterca, M.; Aqad, E.; Imam, M. R.; Heiney, P. A.; *J. Polym. Sci., Part A: Polym. Chem.* **2007**, *45*, 4974. c) Percec, V.; Aqd, E.; Peterca, M.; Rudick, J. G.; Lemon, L.; Ronda, J. C.; De, B. B.; Heiney, P. A.; Meijer, E. W.; *J. Am. Chem. Soc.* ***2006***, *128*, 16365. d) V. Percec, J. G. Rudick, M. Peterca, M. Wagner, M. Obata, C. M. Mitchell, W. D. Cho, V. S. K. Balagurusamy and P. A. Heiney.; *J. Am. Chem. Soc*. **2005**, *127*, 15257.

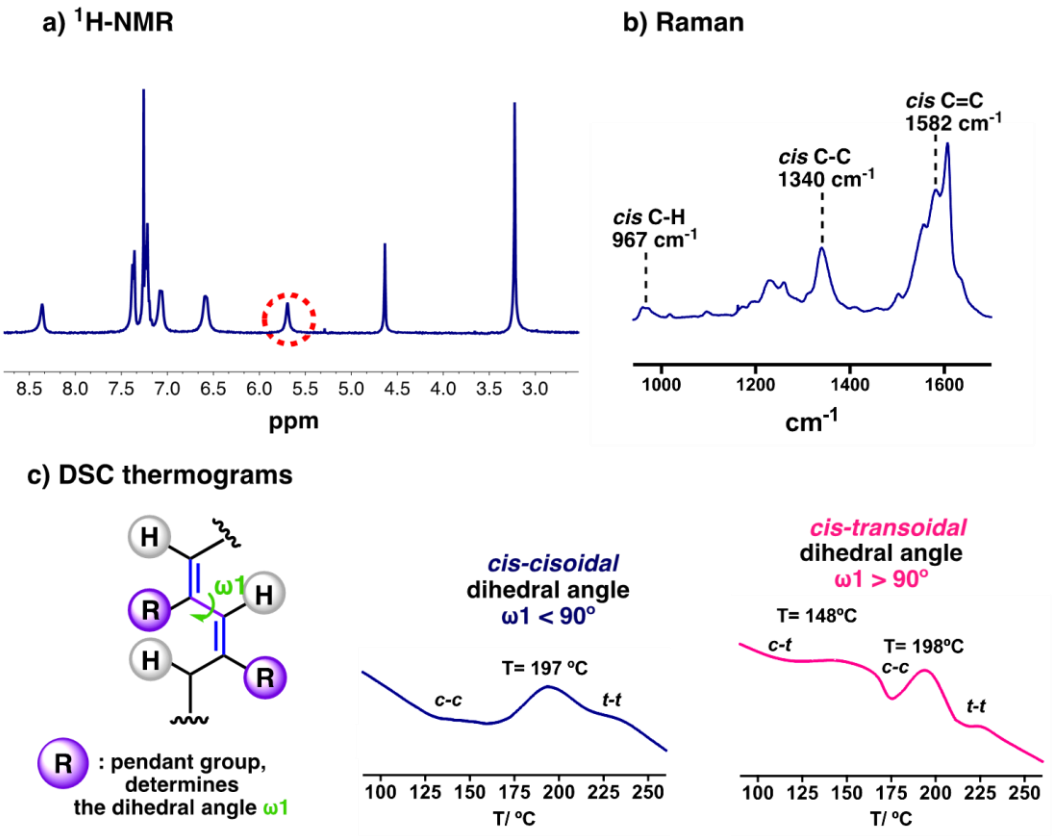

Figure 9. a) ¹H-NMR, b) Raman spectra and c) DSC thermograms of PPAs with conjugated double bonds in *cis* configuration.

3.3 Determination of the Screw Sense in PPAs

To determine the helical sense in PPAs it is necessary to use a combination of several techniques. Usually, techniques with polarized light such as CD and optical rotation are used.

3.3.1 Specific rotation

The observed optical rotation (α) gives values related to the degree of deviation of the polarized light when it interacts with chiral molecules in solution. The optical rotation depends on the concentration, solvent, temperature and cell length. To avoid ambiguities, it was established a standard value of α, the specific rotation $[\alpha]_\lambda^t$. This value is calculated from equation 2, where *t* is the temperature, λ is the wavelength, α is the observed optical rotation (degrees), *l* is the length of the cubet (dm) and *c* is the concentration (g·mL^{-1}) for the solution.[32]

$$[\alpha]_\lambda^t = \frac{\alpha}{l \cdot c}$$

Equation 2. Equation to calculate the specific rotation

[32] Vollhardt, P.; Schore, N.; *Organic Chemistry: Structure and Function.;* 5nd ed., Omega, **2008**, p 174.

This technique presents some disadvantages compared to CD. For example, it has a low sensitivity because a high amount of sample is necessary to obtain α measurement. In helical macromolecules such as PPAs, $[\alpha]$ value is at least one order of magnitude higher when compared with the obtained data for the monomeric unit.

3.3.2 Circular Dichroism

Circular Dichroism (CD) is a very useful technique to determine a screw sense excess in helical macromolecules, as well as a preferred conformation in discrete chiral molecules. When a Circularly Polarized Light beam interacts with a sample containing molecules bearing chromophores (light-absorbing groups), the light path gets altered. The CD records the differences in the absorption between right-handed (*R*-CD) and left-handed (*L*-CD) circularly polarized light.

CD spectroscopy has been used to determine the folding in biomacromolecules such as peptides, to distinguish the secondary structure between an α-helix and a β-sheet folding or a random coil unfolding state. Moreover, with CD it is possible to determine different structural, kinetic and thermodynamic parameters.[33,34]

Interestingly, by applying CD spectroscopy in helical polymers, changes on the CD traces (helical enhancement or helical inversion) can be detected due to the interaction of the macromolecules with external stimuli such as temperature, metal ions and pH among others. By comparing the CD spectrum of a monomer with the former polymer it is possible to see a Cotton effect in the vinylic region (400 nm) indicating the presence of a helical structure. In our researcher group, there are published several articles where the external stimuli affect to the secondary structure of the PPAs.

Finally, the amount of sample needed to employ CD spectroscopy is smaller than in the case optical rotation. Less than 1 mg of sample is enough to carry out the experiments indicating a better sensitivity what becomes the CD in a very powerful technique.

The combination of these techniques (IR, NMR, CD, DSC, optical rotation and Raman) is enough to determine the primary structure and the helical sense of the PPAs but it is not possible to build a 3D model of the helical polymer's secondary structure. To do that, it is

[33] a) Hammes, G. G.; Circular Dichroism, Optical Rotatory Dispersion, and Fluorescence Polarization, In *Spectroscopy for the Biological Sciences*, John Wiley & Sons, Inc. **2005**, p 63. b) Bereova, N.; Nakanishi, K., Woody, R. W., *Circular Dichroism: Principles and Applications*, 2nd ed., Wiley-VCH: New York, **2000**, p 912.

[34] a) Nakanishi, K.; Berona, N; Circular Dichroism: Principles and Applications; ed por N. Berova, K. Nakanishi, W. R Woody, **2000**, *Wiley-VCH,* 2nd ed, Cap 13, p 361.b) Harada, N.; Nakanishi, K. *Circular Dichroic Spectroscopy-Exciton Coupling in Organic Stereochemistry*, 2nd ed., University Science Books: Mill Valley, CA, **1983**.

necessary to obtain other parameters such as packing angle and helical pitch. To solve this problem, X-ray diffraction and Atomic Force Microscopy (AFM) are employed.

3.3.3 Theoretical Calculations of Circular Dichroism

Theoretical calculations have emerged in the last years as a useful tool for the elucidation of the helical structure. MMFF94 energy minimization together with ECD simulation, using the time-dependent self-consistent field (SCF) ZernerQs Intermediate Neglect of Differential Overlap (ZINDO/S) method, have been explored to solve the secondary structure of some helical polymers. For example, Masuda and co-workers confirmed the formation of two different helical scaffolds (different dihedral angle at the single bond along the main chain, ω1), while studying the substitution effect on a series of polymers derived from propargylamides.[35]

In the case of PPAs only one example had been reported focusing on the CD bands corresponding to the pendant and not talking about those related to the polyene backbone, probably due to the complexity of the helical structure (presence of two coaxial helices).[36] Recently, Rodríguez *et al.* succeeded in stablishing a relation between the CD signal in the vinylic region and the helical sense of the internal helix. To calculate the ECD spectra, the Time-Dependent Density Function Theory (TD-DFT) was employed and as base, the 3-21G basis set with the CAM-B3LYP functional were selected. The good match between the calculated ECD spectra for small oligomers and the experimental ECD spectra for some PPAs, with a known helical structure, allowed to correlate the experimental CD with the internal helical sense of the PPA. From all the data obtained it was determined that a PPA with a positive Cotton effect in the vinylic region describes a *P* internal helix, whereas if a negative band is observed the polymer will be describing an *M* internal helix. Moreover, the robustness and reliability of this finding was confirmed by evaluating some PPAs taken from literature.[23,24]

After this important contribution to the field, it has been possible to apply theoretical calculations in different works such as predicting the dynamic and structural behavior by

[35] Suzuki, Y.; Tabei, J.; Shiotsuki, M.; Inai, Y.; Sanda, F.; Masuda, T. *Macromolecules,* **2008**, *41*, 1086

[36] Kaneko, T.; Umeda, Y.; Yamamoto, T.; Teraguchi, M.; Aoki, T. *Macromolecules,* **2005**, *38*, 9420

[23] Fernández, B.; Rodríguez, R.; Quiñoá, E.; Riguera, R.; Freire, F. *ACS Omega,* **2019**, *4*, 5233.

[24] Fernández, B.; Rodríguez, R.; Rizzo, A.; Quiñoá, E.; Riguera, R.; Freire, F. *Angew. Chem. Int. Ed.,* **2018**, *57*, 3666.

rational design of polymers,[37] in more complex helices with rigid spacers between pendants and the polyenic chain[38] and even in the formation of supramolecular helical scaffolds.[39,40]

3.3.4 Vibrational Circular Dichroism and Raman Optical Activity

Vibrational Circular Dichroism (VCD) and Raman Optical Activity (ROA) are the chiral version of traditional IR and Raman techniques.

On the one hand, VCD is the extension of the CD to infrared and near infrared wavelengths. VCD has shown an interesting sensitivity in the formation of protein fibril structures in solution,[41] it permits the direct observation and control of supramolecular chirality[42] or even to distinguish between different conformations of pendant groups in PPAs and to see how an achiral solvent can organize in a helical manner interacting with the helical polymer.[43]

On the other hand, in ROA it exists a nonequivalence between the incident and scattered circular polarization light beam.[44] Although ROA effect is weak and needs large amounts of sample,[45] it has been applied recently not only as a new tool to elucidate the helical structure of PPAs but also to determine the screw sense of this helix (Figure 10).[46]

[37] Cobos, K.; Rodríguez, R.; Domarco, O.; Fernandez, B.; Quiñoá, E.; Riguera, R.; Freire, F. *Macromolecules,* **2020**, *53*, 3182.

[38] Fernández, Z.; Fernández, B.; Quiñoá, E.; Riguera, R.; Freire, F. *Chem. Sci.* **2020**, *11*, 7182.

[39] Fernández, Z.; Fernández, B.; Quiñoá, E.; Freire, F. *Angew. Chem. Int. Ed*. **2021**, *60*, 9919.

[40] Fernández, B.; Fernández, Z.; Quiñoá, E.; Freire, F; *Molecules*, **2021**, *26*, 3530.

[41] Ma, S.; Cao, X.; Mak, M.; Sadik, A.; Walkner, C.; Freedman, T. B.; Lednev, I. K.; Dukor, R. K.; Nafie, L. A.; *J. Am. Chem. Soc*. **2007**, *129*, 12364.

[42] Kurouski, D.; Lombardi, R. A.; Dukor, R. K.; Lednev, I. K.; Nafie, L. A.; *Chem. Commun.*, **2010**, *46*, 7154.

[43] Nieto-Ortega, B.; Rodríguez, R.; Medina, S.; Quiñoá, E.; Riguera, R.; Casado, J.; Freire, F.; Ramírez, F. J. *J. Phys. Chem. Lett.,* **2018**, *9*, 2266.

[44] Nafie, L. A.; *Theor. Chem. Acc.*, **2008**, *119*, 39.

[45] Li, G.; Kessler, J.; Cheramy, J.; Wu, T.; Poopari, M. R.; Bour, P.; Xu, Y.; *Angew.Chem. Int. Ed.* **2019**, *58*, 16495; *Angew. Chem.* **2019**, *131*, 16647.

[46] Palomo, L.; Rodríguez, R.; Medina, S.; Quiñoá, E.; Casado, J.; Freire, F.; Ramírez, F. J; *Angew. Chem. Int. Ed.*, **2020**, *132*, 9165.

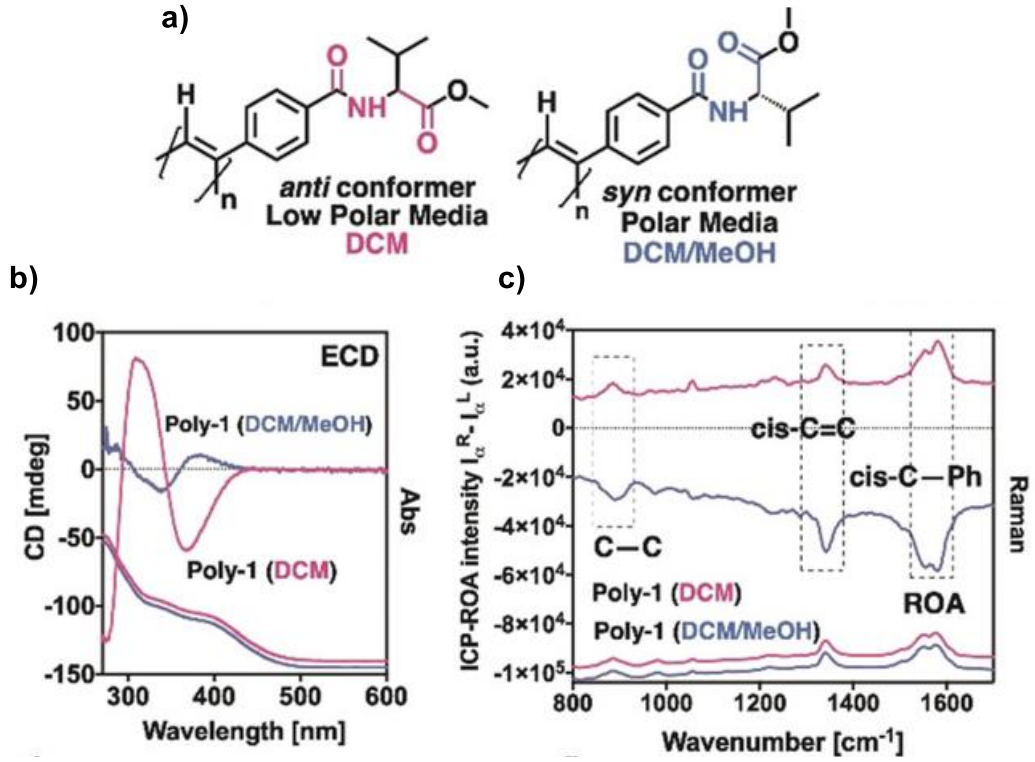

Figure 10. a) Main conformers of PPA-ValOMe in low-polar and polar solvents. b) ECD/UV and c) Raman/ROA spectra of PPA-ValOMe in low-polar (DCM) and polar (DCM/MeOH) solvents.

3.3.5 X-Ray Diffraction

X-ray diffraction has a strong limitation because it requires the preparation of an oriented film of sample. This is only possible if the polymer has a rod-like structure with a tendency to form liquid crystals. Different methods to prepare these films are by physical shearing or under electric or magnetic fields.[47]

Although this technique can provide information about the secondary structure of the polymer — helical pitch, helix length or helix width —, no information about the helical sense of PPAs can be obtained.

3.3.6 Atomic Force Microscopy (AFM)

AFM allows the visualization of individual helices providing some important information about the secondary structure of helical polymers. Using this technique, different parameters such as helical sense, helical pitch or packing angle can be obtained in PPAs. To determine this information, sample preparation becomes a very important step because only well-ordered self-assembled monolayers are suitable to distinguish the information in the AFM image.[48,49]

[47] Yashima, E.; *Polym. J.* **2010**, *42*, 3.

[48] Kumaki, J.; Sakurai, S.-I.; Yashima, E.; *Chem. Soc. Rev.* **2009**, *38*, 737.

Moreover, the substrate used as supporting plays an important role. Thus, highly oriented pyrolytic graphite (HOPG) is typically used for low polar polymers and mica for polar ones. The selection of an adequate substrate will allow to improve the intermolecular interactions between the helical PPAs and the substrate permitting a better well-ordering. Different protocols have been developed during the last years to prepare polymeric monolayers and high-resolution AFM images.

- **Drop casting**

Yashima *et al.*, in a pioneering work, studied the structure of PPAs analyzing with AFM monolayers prepared by drop casting of polymer solutions in different substrates: mica and HOPG. Thus, a copolymer based on two pendant groups, an achiral C_{60}-bound and an optically active amine, was studied. When this copolymer was drop casted on mica, the AFM images showed isolated spherical particles due to the aggregation of C_{60} by the repulsive interaction with the hydrophilic mica substrate. On the contrary, when the copolymer was drop casted over HOPG, the AFM images revealed some isolated and individual copolymer chains with a few particles (Figure 11). From these images, it can be concluded that the attractive forces between pendants and the substrate play a critical role in the scaffold adopted by this type of copolymers. Also, the images suggest how important it is the correct choice of the substrate to achieve the obtention of some information of the helical parameters.[50]

[49] Freire, F.; Quiñoá, E.; Riguera, R. *Chem. Rev.* **2016**, *116*, 1242.

[50] Nishimura, T.; Takatani, K.; Sakurai, S.; Maeda, K.; Yashima, E.; *Macromolecules* **2002**, *41*, 3602.

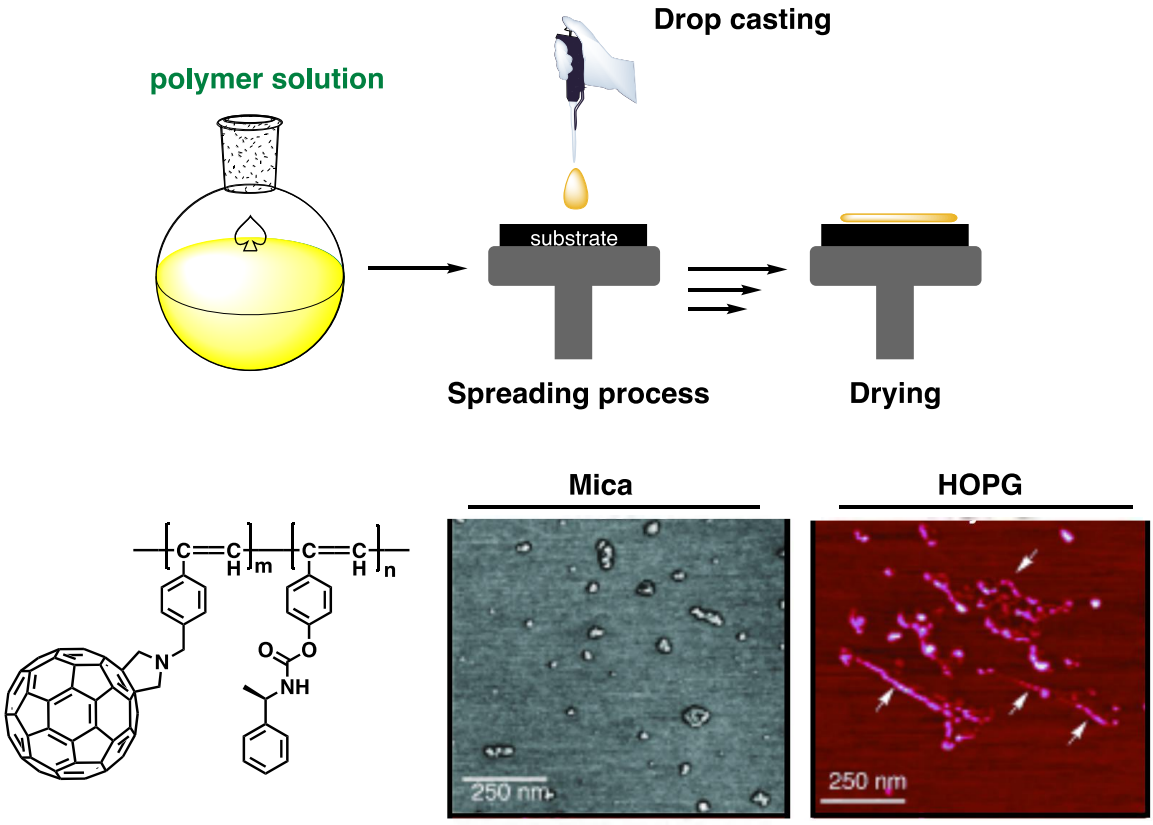

Figure 11. Schematic representation for the drop casting procedure.

- **Spin coating and solvent vapor exposure**

Considering the previous information, Yashima *et al.* developed a new approach. Introducing long alkyl chains as pendants, the self-assembly of PPA chains should be favored due to the interdigitation among long chain groups.[51,52,53]

The deposition manner was employing a spin coater in this case. Thus, a diluted solution of PPA was added onto the HOPG substrate and then kept under a solvent atmosphere overnight to favor the self-assembly of polymer chains and growth of 2D crystals.[54] Using this approach, they obtained the helical structure of the PPAs derived from *L* and *D*-alanine decyl ester by the direct observation of AFM images (Figure 12).[54] These images of poly-(*L*)-**13** revealed the presence of a helical pitch of 2.34 nm and a packing angle of 40º where the PPA describes a (external) *M* helix with two residues per turn. Moreover, the internal helix adopts a *c-t* configuration and describes the opposite helical sense (*P* helix).

[51] Okoshi, K.; Sakurai, S.-I.; Ohsawa, j. K.; Kumaki, J.; Yashima, E.; *Angew. Chem. Int. Ed.* **2006**, *45*, 8173.

[52] Sakurai, S.-I.; Okoshi, K.; Kumaki, J.; Yashima, E.; *Angew. Chem. Int. Ed.* **2006**, *45*, 1245.

[53] Sakurai, S.-I.; Okoshi, K.; Kumaki, J.; Yashima, E.; *J. Am. Chem. Soc.* **2006**, *128*, 5650.

[54] a) Bing, L; Lam, J. W.; Zhen-Qiang, Y.; Tang, B. Z.; *Langmuir* **2012**, *28*, 5770. b) Li, B.; Kang, Z. K.; Cheuk, K.; Wan, L.; Ling, L.; Bai, C.; Tang, B. Z.; *Langmuir* **2004**, *20*, 7598.

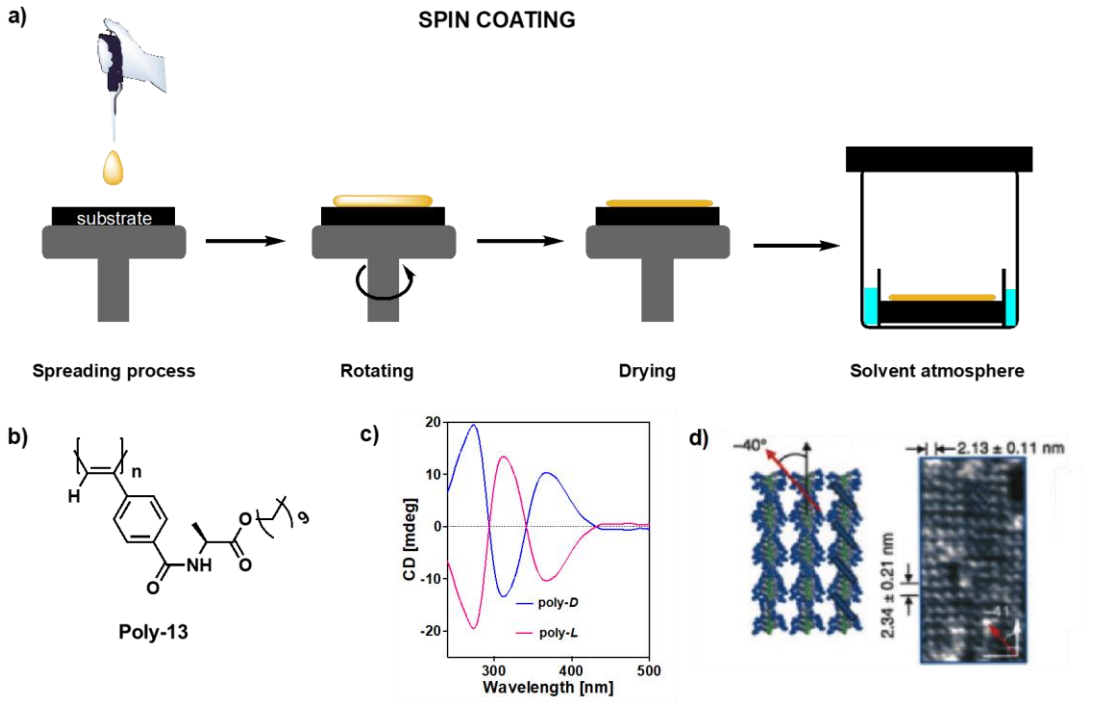

Figure 12. a) Schematic representation of spin coating deposition. b) Structure of poly-(*L*)-**13**. c) CD spectra of poly-(*L*)-**13** and poly-(*D*)-**13**. d) AFM images of 2D crystals self-assembled poly-(*L*)-**13** on HOPG.

In our research group, this protocol was applied with an axially racemic helical polymer [poly-(*R*)-**14**] onto HOPG. In this case, it was not observed the presence of 2D crystals due to the dynamic behavior of this PPA.

The dynamism in the polymer is related to the two possible conformations in the pendant group. This PPA, derived from the anilide of (*R*)-α-methoxy-α-phenylacetic acid [poly-(*R*)-**14**], presents two conformations in equilibrium (*ap*: carbonyl and methoxy groups in an antiperiplanar orientation and *sp*: carbonyl and methoxy groups synperiplanar oriented).[55] This conformational equilibrium in the pendant groups is transmitted to the helix in a 1:1 equilibrium between *P/M* helices in the same polymeric chain.

Interestingly, well 2D crystals can be obtained when the 1:1 equilibrium is shifted to *P* or *M* helix by the addition of divalent or monovalent metal ions.[55] Thus, when a diluted solution of helical polymer-metal complex (HMPC) is spin coated onto HOPG and left under a THF atmosphere overnight, well ordered 2D-crystals can be obtained. These AFM images revealed that the helical pitch is 3.2 nm, the packing angle is 60° and the helical sense depends on the type of metal ions added (*M* helix for monovalent metal ions and *P* helix for divalent metal

[55] Freire, F.; Seco, J. M.; Quiñoá, E.; Riguera, R.; *Angew. Chem. Int. Ed.* **2011**, *50,* 11692.

ions). This information in combination with NMR, Raman, DSC and CD allows the elucidation of the secondary structure of the PPA (Figure 13).

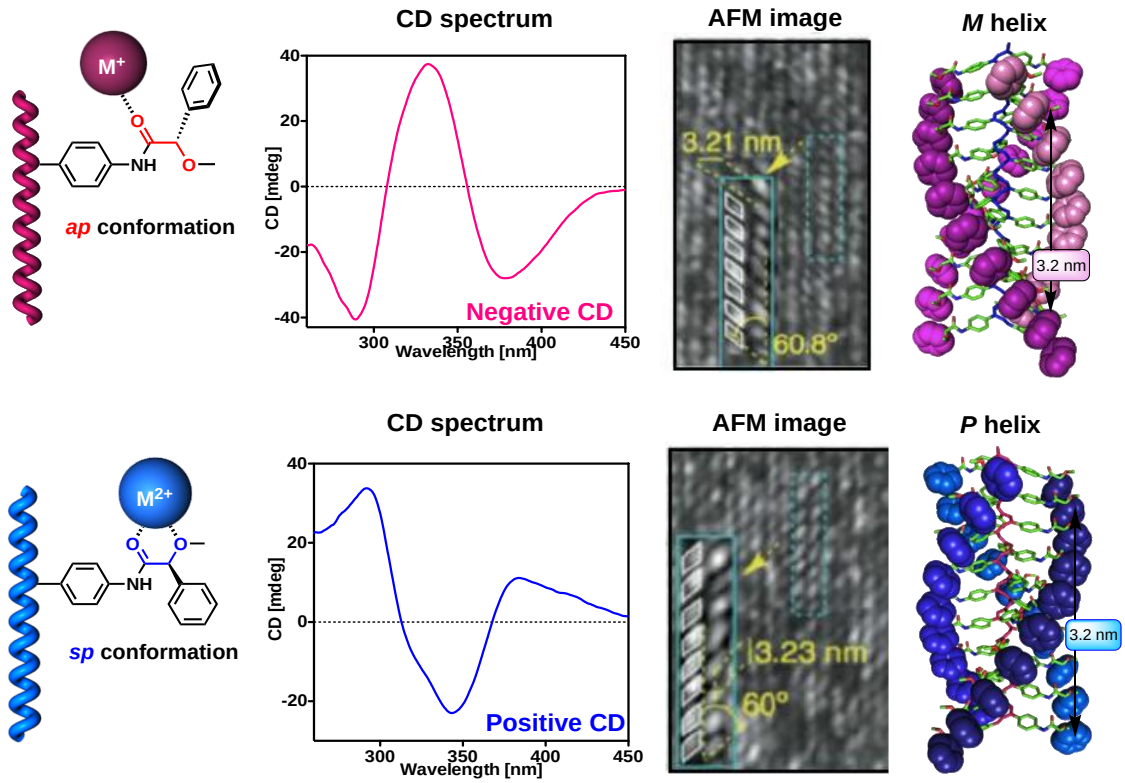

Figure 13. Chiral amplification for poly-(*R*)-**14** in presence of monovalent and divalent metal ions and the corresponding AFM images.

- **Spin coating and thermal annealing**

Another interesting protocol, developed by Percec and co-workers, is based on spin coating procedure, but in this case the sample is also subjected to thermal annealing instead of solvent atmosphere annealing. Using this protocol, they produced 2D crystals on HOPG and mica and visualized the self-organization of individual dendronized PPAs using AFM. A library of dendronized PPAs with long alkyl chains were prepared for doing those experiments.[56,57]

Thus, individual polymer chains of a *c-t* poly(carbazolyacetylene), after being spin coated on HOPG with thermal annealing at 100°C, were observed using AFM. This example shows the high potential of these polymers to obtain well-ordered monolayers (Figure 14).

[56] Percec, V.; Obata, M.; Rudick, J. G.; De, B. B.; Glodde, M.; Bera, T. K.; Magonov, S. N.; Balagurusamy, V. S. K.; Heiney, P. A.; *J. Polym. Sci. Part A: Polym. Chem.* **2002**, *40*, 3509.

[57] Percec, V.; Rudick, J. G.; Peterca, M.; Staley, S. R.; Wagner, M.; Obata, M.; Mitchell, C. M.; Cho, W.-D.; Balagurusamy, V. S. K.; Lowe, J. N.; Glodde, M.; Weichold, O.; Chung, K. J.; Ghionni, N.; Magonov, S. N.; Heiney, P. A.; *Chem. Eur. J.* **2006**, *12*, 5731.

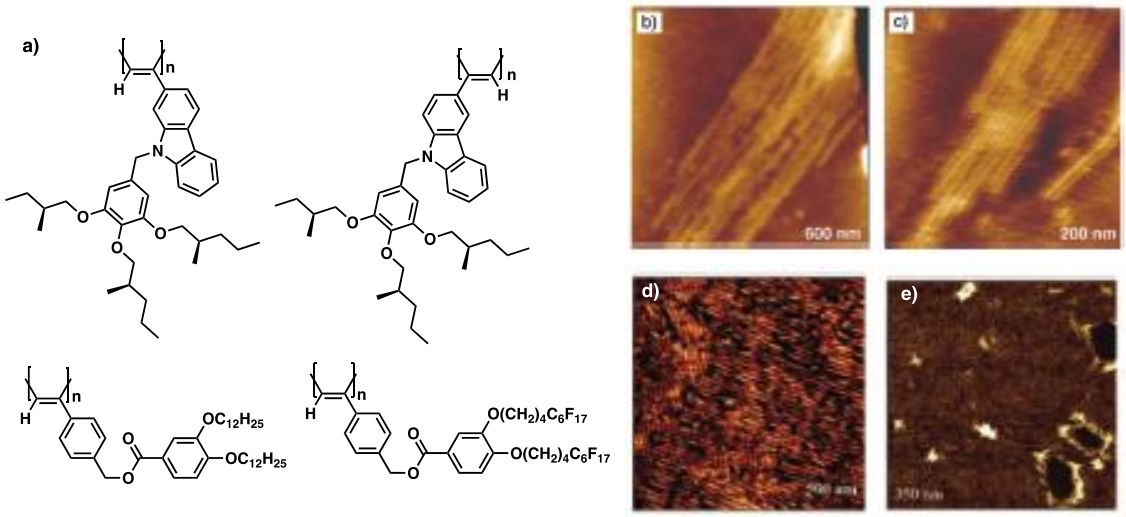

Figure 14. a) Structure of dendronized PPAs. b), c), d) and e) AFM images on graphite for these polymers.

- **Langmuir-Blodgett (LB)**

The previous methods for the monolayer's preparation consist on the evaporation of a solution of the polymer onto a solid substrate. Then, the monolayer is formed at the air/solid interface. As mentioned before, in these protocols it plays a very important role the interactions of the polymer with the substrate and the evaporation rate of the solvent.

The Langmuir-Blodgett method (LB) is used as alternative to the previous method, to prepare monolayers in an air/water interphase when the substrate is introduced in a water pool.[58,59] Herein, the hydrophobic/hydrophilic interactions between polymer and support have a special relevance.

To perform these experiments, a dilute solution of polymer in an organic solvent as $CHCl_3$ is employed. Thus, this solution is spread drop by drop using a Hamilton syringe. Then, after the solvent evaporation, an increase of the surface pression is needed to form the monolayer. For this, two barriers move compressing the sample. Once the monolayer is formed, the support is removed from the pool with the monolayer attached to it (Figure 15).

Tang *et al.* reported the formation of monolayers using this method in PPAs with hydrophobic backbone and with hydrophilic pendants groups derived from aminoacids. They prepared PPAs derived from *L*-alanine and *L*-valine methyl ester where the PPA can self-assembly due to their amphiphilic character. To obtain the AFM images, mica was used as

[58] Roberts, G. G.; *Langmuir-Blodgett Films*, Plenum, New York, 1990.

[59] Kawauchi, T.; Kumaki, J.; Kitaura, A.; Okoshi, K.; Kusanagi, H.; Kobayashi, K.; Sugai, T.; Shinohara, H.; Yashima, E.; *Angew. Chem. Int. Ed.* **2008**, *47*, 515.

substrate where the hydrophilic amino acids residues interact with it.[54] Nevertheless, the AFM images were not so good to obtain the helical parameters (helical pitch, packing angles, or helical sense).

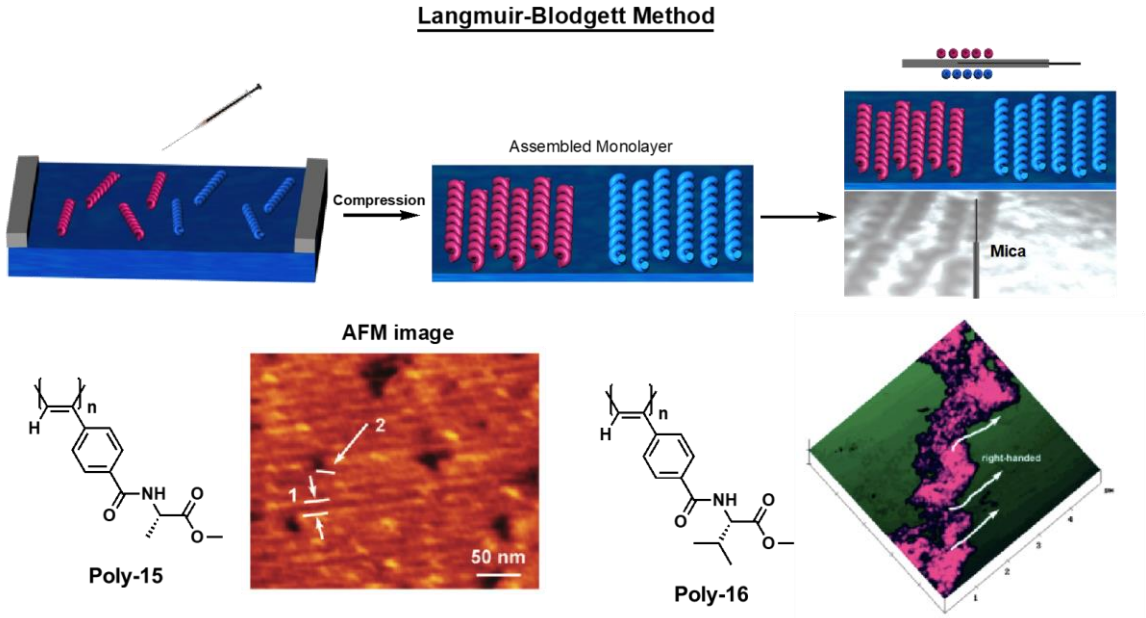

Figure 15. Schematic illustration of Langmuir-Blodgett method.

- **Langmuir-Schaefer (LS)**

When an amphiphilic character is presented in our sample, LB can be the best choice to form monolayers. However, in literature it can be found that HOPG is the best substrate to obtain AFM images with good quality for PPAs. This substrate is more hydrophobic than mica and can interact better with the PPAs to form the monolayer. Unfortunately, the HOPG hydrophobic properties are incompatible with its use with LB because of the water.[60]

To prepare a good monolayer of PPAs in HOPG, Langmuir-Schaefer[61] approach (LS) is employed. This method consists in a modification of LB procedure where the monolayer is exfoliated from the water/air interphase allowing its transference to HOPG.[62]

Following LS protocol, good monolayers were obtained for the highly dynamic poly-(*R*)-**14**. AFM images showed well-ordered monolayers, with uniform fields composed by right-handed or left-handed helical chains. The good quality of the AFM images allows to determine

[54] a) Bing, L; Lam, J. W.; Zhen-Qiang, Y.; Tang, B. Z.; *Langmuir* **2012**, *28*, 5770. b) Li, B.; Kang, Z. K.; Cheuk, K.; Wan, L.; Ling, L.; Bai, C.; Tang, B. Z.; *Langmuir,* **2004**, *20*, 7598.

[60] Freire, F.; Quiñoá, E.; Riguera, R.; *Chem. Commun.* **2017**, *53*, 481.

[61] Ulman, A.; *An introduction to Ultrathin, Organic films –From Langmuir-Blodgett To Self-Assembly,* Academic Press, New York, **1991**.

[62] Rodríguez, R.; Ignés-Mullol, J.; Sagués, F.; Quiñoá, E.; Riguera, R.; Freire, F.; *Nanoscale,* **2016**, *8*, 3362.

the helical sense as well as the helical pitch (3.2 nm) and the packing angle (±60°). These values are in concordance with those of the polymer complexed with monovalent and divalent metal ions mentioned before.[55] This indicates that poly-**14** adopts a *c-c* polyene backbone where the helices defined by the polyene and the pendant groups are following the same direction (Figure 16). Interestingly, AFM images reveal also the presence of left- and right-handed oriented superhelices.[63,64,65,66]

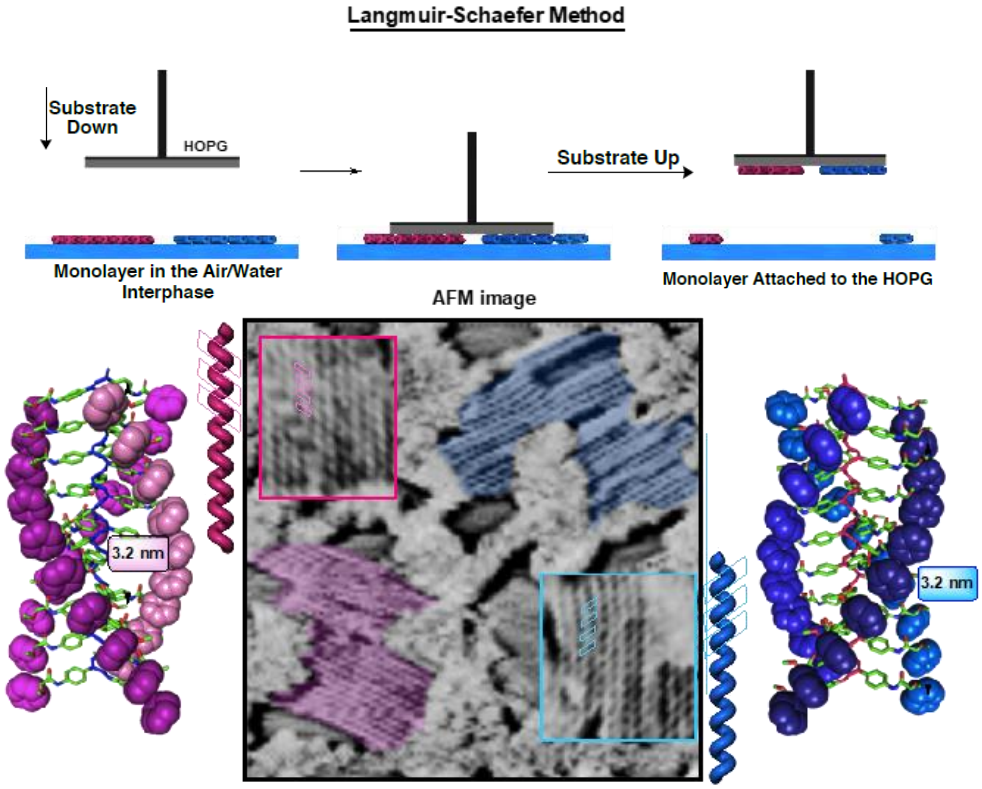

Figure 16. Conceptual representation of Langmuir-Schaefer method and AFM images obtained of poly-(*R*)-**14**.

LS has also demonstrated its versality by being able to elucidate the secondary structure of PPAs with different substitution patterns. Thus, in another interesting work from our group, LS method was used to study the secondary structure of *m*-poly-**14**, bearing the *meta* anilide of (*R*)-α-methoxy-α-phenylacetic acid and *m*-poly-**17**, bearing the meta benzamide of phenylglycine methyl ester (PGME) as the pendant.[67]

[55] Freire, F.; Seco, J. M.; Quiñoá, E.; Riguera, R.; *Angew. Chem. Int. Ed.* **2011***, 50,* 11692.

[63] Sakurai, S.; Kuroyanagi, K.; Nunokawa, R.; Yashima, E.; *J. Polym. Sci. Part A: Polym. Chem.* **2004**, *42*, 5838.

[64] Matsushita, S.; Azagi,K.; *J. Am. Chem. Soc.* **2015**, *137*, 9077.

[65] Mori, T.; Kyotani, M.; Azagi, K.; *Chem. Sci.* **2011**, *2*, 1389.

[66] Akagi, K.; *Chem. Rev.* **2011**, *109*, 5354.

[67] Rodríguez, R.; Quiñoá, E.; Riguera, R.; Freire, F. *J. Am. Chem. Soc.* **2016**, *138*, 9620.

In the case of *m*-poly-**14**, it exists in solution an equilibrium between a compressed *c-c* helix (3.2 nm of helical pitch and 60º of packing angle) and a more stretched *c-t* one (5.2 nm of helical pitch and 40º of packing angle). The internal helical senses of both helices are the same (*P* helices), whereas the external helix described by the pendants rotates in the opposite direction (*P* helical sense for the compressed and *M* helical sense for the stretched one) (Figure 17).

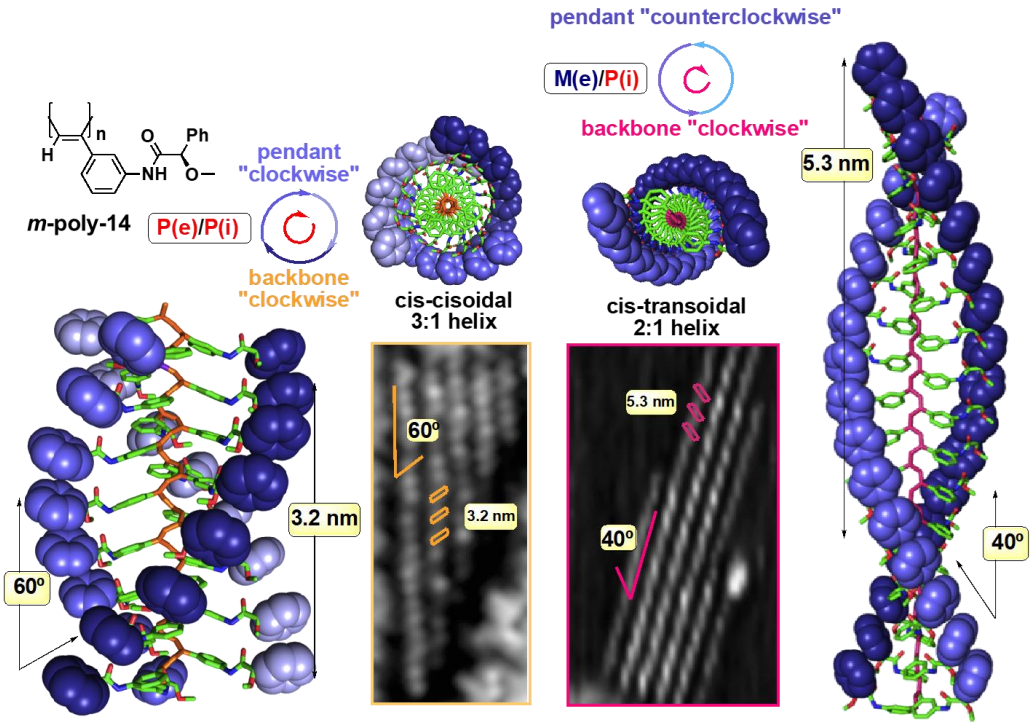

Figure 17. Molecular models and AFM images for the compressed and stretched helices of *m*-poly-**14**.

4. Supramolecular assemblies of PPAs

The evolution of chemistry in the last 60 years can be illustrated by the introduction of three new concepts. One is *macromolecule*,[68] whose importance was recognized in the 1953 Nobel Prize to Prof. Staudinger, and the other two are *molecular recognition* and *supramolecular assembly*,[69,70] which gave the 1987 Nobel Prize to Profs. Cram, Lehn and Petersen.

Supramolecular assemblies may present different architectures (films, layers, membranes, spheres, etc.) and in biological systems they may confer some properties with

[68] Hierarchical Macromolecular Structures: 60 years after the Staudinger Nobel Prize I; Percec, V.; Ed.; *Advances in Polymer Science*, Vol. *261*; Springer: New York, **2013.**

[69] Lehn, J.-M.; *Supramolecular Chemistry: Concepts and Perspectives*; Wiley-VCH: Weinheim, Germany, **1995**.

[70] Steed, J. W.; Atwood, J. L.; *Supramolecular Chemistry*; John Wiley & Sons: West Sussex, U.K., **2005.**

relevant importance due to their sophisticated functions. Theses structure depend on the type of bonding —hydrogen bonding, π-π interactions, ionic bonding, charged electrostatic interactions or their combinations— that binds the molecular components together and how they are spatially arranged. Moreover, if the components are chiral, their absolute configuration will be transferred to the assembly and the presence of supramolecular chirality constitutes an especially attractive topic.[71,72,73,74,75]

After the explanation of how to completely elucidate the secondary structure of PPAs, in this section it will be summarized the main types of supramolecular assemblies that PPAs can adopt reaching the next level in the complex-structure characterization scale.

4.1 Fibers and Superhelices

Helical PPAs can establish supramolecular interactions between pendants groups of different chains and can self-assemble into fiber-like structures. The aggregation requires the presence of adequate functional groups in the pendant as well as a certain complementarity between polymer chains. Stereocomplexes are a good example of stereochemically complementary interactions that can be formed by stereoregular PPAs. Generally, the stereocomplexes show better mechanical and thermal resistance than the former polymers. Also, the degradation process of these is slower. Usually, the forces that stabilize these supramolecular structures are Van der Waals and electrostatic interactions.

One example in the field of PPAs was described by our group reporting the formation of a fiber-like stereocomplex. The starting PPAs were formed with (*R*)- and (*S*)-α-methoxy-α-trifluoromethyl-α-phenylacetamide (MTPA) as pendant groups [poly-(*R*)-**18** and poly-(*S*)-**18**]. These polymers dissolved in donor solvents, like THF, present the amide groups in *cis* conformation favoring cooperative supramolecular interactions between enantiomeric helices.[25] These interactions are favored by the stretching of the helical scaffold exposing in the external crest of the helix the functional groups able to interact with the complementary helix. These type of stereochemically interactions starts with a dimer formation and after this gives rise to supramolecular fiber-like aggregates that at higher concentrations result in gels (Figure

[71] Duan, P.; Cao, H.; Zhang, L.; Liu, M.; *Soft. Matter* **2014**, *10*, 5428.

[72] Zhang, L.; Qin, L.; Wang, X.; Cao, H.; Liu, M.; *Adv. Mater.* **2014**, *26*, 6959.

[73] Yang, Y.; Zhang, Y.; Wei, Z.; *Adv. Mater.* **2013**, *25*, 6039.

[74] Wang, Y.; Xu, J.; Wang, Y.; Chen, H.; *Chem. Soc. Rev.* **2013**, *42*, 2930.

[75] Miyake, H.; Tsukube, H.; *Chem. Soc. Rev.* **2012**, *41*, 6977.

[25] Leiras, S.; Freire, F.; Seco, J. M.; Quiñoá, E.; Riguera, R. *Chem. Sci.* **2013**, *4*, 2735.

18). These interactions are reversible because the modification of the amide *cis-trans* conformation by temperature or solvent polarity allows to control the formation of the stereocomplex. For example, the addition of high polar solvents (*e.g.* MeOH) cleavage the intermolecular and intramolecular hydrogen-bonding interaction disrupting the formation of the stereocomplex.

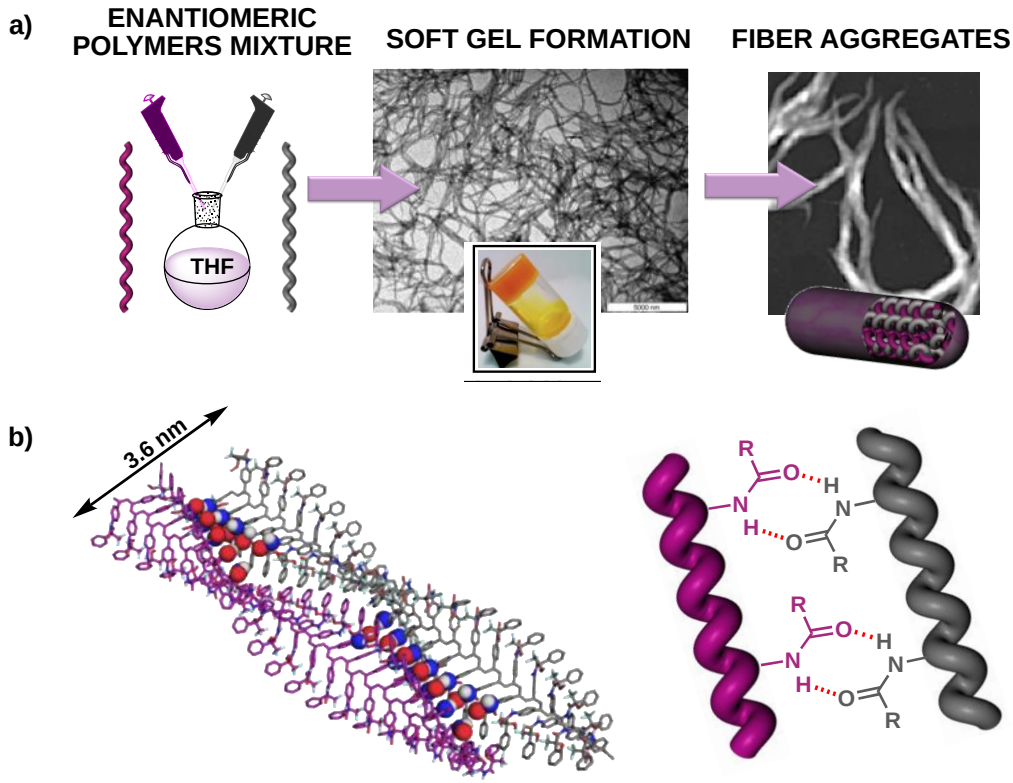

Figure 18. Conceptual representation of the complexation process for poly-**18**.

Many other examples of fiber-like aggregates based on PPAs were reported. In some of them, the PPA helicity is conserved while in others the aggregation leads to the disappearance of the helical structure. Yashima *et al.* reported an example of fiber-like aggregates based on 4-carboxyphenylacetylene (poly-**19**) where the PPA helicity is conserved. This polymer can increase the organization in a helical manner when a small amount of chiral amine is added. The deposition of this complex onto a mica substrate shows in AFM two-helix bundles probably formed by hydrogen bonding between the carboxyl groups of two different helical chains.[76]

Another example was reported by Shinohara and co-workers. In this case, they demonstrated by Scanning Tunneling Microscopy (STM) the formation of double helices based on an optically active PPA. The deposition of the PPA, bearing a methoxycarbonylamino group

[76] Sakurai, S.I.; Kuroyanagi, K.; Morino, K.; Kunitake, M.; Yashima, E.; *Macromolecules* **2003**, *36*, 9670.

as pendant (poly-**20**), onto HOPG shows the formation of double-helical structures. Interestingly, the researcher observed that the molecules of the polymer deposited on HOPG were easy to move by the effect of the probe scanning losing the helical structure during the process of interaction.[77]

In a similar way, Tang's group studied the supramolecular interactions in PPAs containing different aminoacids methyl ester as pendant groups (i.e. Alanine, Leucine, Valine or Phenylglycine). In this work, NMR analysis confirms an intermolecular hydrogen bonding interaction between pendant groups in low polar solvents as $CHCl_3$. In addition, AFM images demonstrated the formation of different length and diameter fibers when the polymers are deposited onto mica and slowly evaporated.[78] All this information suggests that a supramolecular interaction exists by intermolecular hydrogen-bonding between amide and carbonyl groups of different polymeric chains (C=O···H-N) (Figure 19).

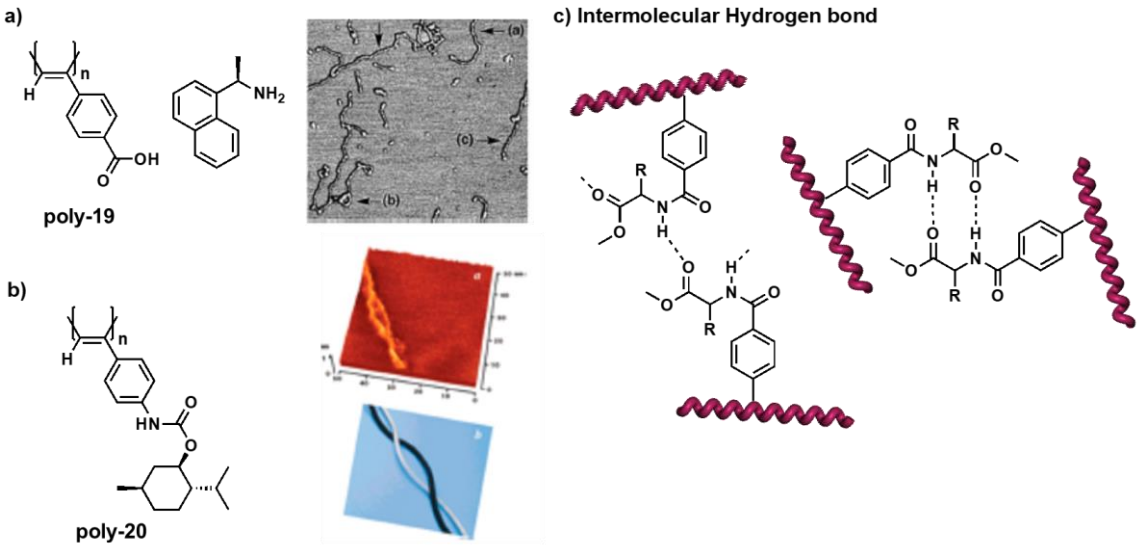

Figure 19. a) AFM images from drop casted solutions of polymer. b) STM images on HOPG substrate. c) Representation of possible intermolecular hydrogen bonds between helical polymers.

Interestingly, when PPAs containing aminoacids derivatives are dissolved in polar solvents (*e.g.* MeOH), this leads to the formation of micelle-like aggregates with the backbone inside forming the core and aminoacids pendants exposed to the solvent in the shell. This is due to the amphiphilic character of these PPAs.[79] Due to the high content of aminoacid residues present in the outside of these micelles, it leads them to stick together by hydrogen-bonding interactions forming even larger fiber-like structures.

[77] Shinohara, K.; Yasuda, S.; Kato, G.; Fujita, M.; Shigekawa, H.; *J. Am. Chem. Soc.* **2001**, *123*, 3619.

[78] Cheuk, K. K. L.; Li, B. S.; Lam, J. W. Y.; Xie, Y.; Tang, B. Z.; *Macromolecules* **2008**, *41*, 5997.

[79] Li, B.; Cheuk, K. K. L.; Yang, D.; Lam, J. W. Y.; Wan, L. J.; Bai, C.; Tang, B. Z.; *Macromolecules* **2003**, *36*, 5447.

4.2 Layer-by-Layer assembly of PPAs

Yashima and co-workers published an interesting work where they apply the layer-by-layer (LBL) assembly. In this work, charged polymers can generate multilayer structures by interaction among polyanions and polycations. They prepared three different LBLs constituted by a) an anionic phosphonate derivative PPA with a poly(allylamine), b) a cationic ammonium PPA with poly(acrylic acid) and c) the mixture of the anionic phosphonate bearing PPA with the cationic ammonium bearing PPA.[80]

These polymers are optically inactive, but they can induce a unique helical sense with the addition of a chiral agent (chiral amine or a chiral carboxylic acid) that binds to the PPA. The addition of the corresponding counterion polyelectrolyte [poly(allylamine or poly(acrylic acid)] replaces the chiral molecule added, generating a LBL assembly with a macromolecular helicity memory.

In another work of the Yashima's group, they used the repulsive forces (steric and electrostatic hindrance), instead of attractive, among pendats to produce supramolecular aggregates (Figure 20).[81,82]

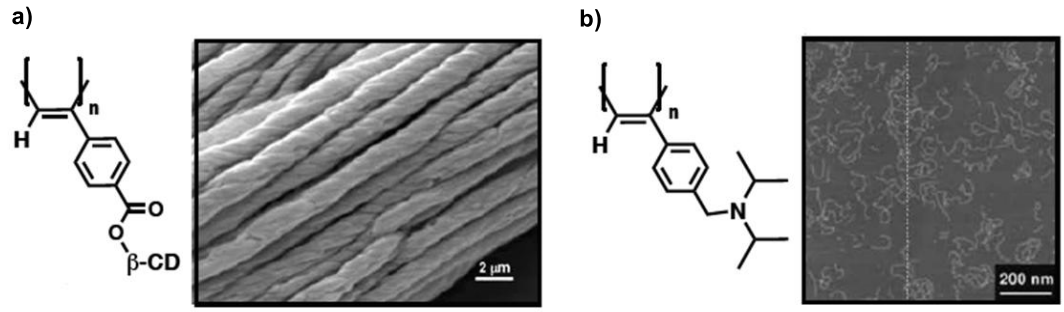

Figure 20. a) SEM (Scanning Electron Microscopy) image of the superhelices formed by a PPA. b) AFM image of the individual fibres obtained for a PPA due to repulsive forces after the addition of a chiral acid.

4.3 Nanoparticles based on PPAs

Polymer Nanoparticles are usually defined as nanospheres or nanocapsules made of any type of polymer whose size is in the range of 10-1000 nm. Nanospheres are spherical and solid and, frequently, are used to attach molecules on their surface or even encapsulate molecules inside them. Nanocapsules are colloidal particles consisting on a hollow core surrounded by

[80] Maeda, K.; Matsushita, Y.; Ezaka, M.; Yashima, E.; *Chem. Commun.* **2005**, 4152.

[81] Maeda, K.; Mochizuki, H.; Osato, K.; Yashima, E. *Macromolecules* **2011**, *44*, 3217

[82] Nagai, K.; Maeda, K.; Takeyama, Y.; Sato, T.; Yashima, E. *Chem. Asian J.* **2007**, *2*, 1314

the polymeric cover. These particles are usually employed to encapsulate substances due to their empty nature.[83,49]

Due to the possibility of selective variation of morphology and size of the particles, even the introduction of chirality in these systems, scientific community has explored with great interest during the last decade several ways to produce them. Two main strategies will be described next: the emulsification method and the emulsion polymerization.[84,85]

4.3.1 Emulsification Method

This method consists in the mixture of a polymer solution with a surfactant that produces the polymer particles as an emulsion (Figure 21). Using this method, Deng and co-workers prepared particles of PPAs by dropwise addition of a concentrated polymer solution in THF to a solution of the surfactant sodium dodecyl sulphate (SDS) in water. Interestingly, they concluded that the size is highly dependent of the SDS concentration: higher concentration produces smaller particles and more micelles in the medium.[86]

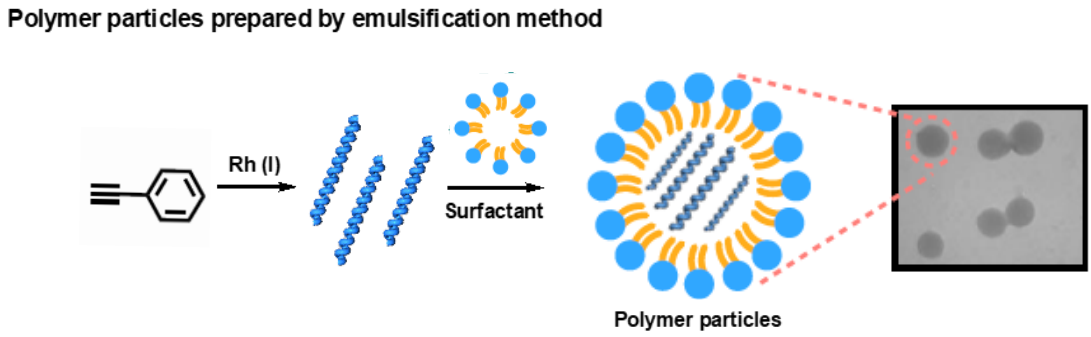

Figure 21. Schematic illustration of the emulsification method to form polymer particles.

4.3.2 Emulsion Polymerization

Deng and co-workers also explored the emulsion polymerization method. This methodology starts with a low soluble monomer in water which with help of an initiator and a surfactant is polymerized *in situ* (Figure 22). Using this method, Deng *et al.* employed different

[83] a) Li, W.; Huang, H.; Li, Y.; Deng J. P. *Polym. Chem*. **2014**, *5*, 1107. b) Song, C.; Liu, X.; Liu, D.; Ren, C.; Yang, W. Deng, J.; P. *Macromol. Rapid Commun.* **2013**, *34*, 1426. c) Zhao, B.; Deng, J.; Deng, J. P. *Macromol. Rapid Commun.* **2016**, *37*, 568. d) Zhang, Y. Y.; Luo, X. F.; Deng, J. P.; Yang, W. T.; *Macromol. Chem. Phys*. **2011**, *212*, 353. e) Rao, J. P.; Geckeler, K. E.; *Prog. Polym. Sci.* **2011**, *36*, 887.

[49] Freire, F.; Quiñoá, E.; Riguera, R. *Chem. Rev.* **2016**, *116*, 1242.

[84] Li, W.; Huang, H.; Li, Y.; Deng, J.; *Polym. Chem* **2014**, *5*, 1107.

[85] Song, C.; Liu, X.; Liu, D.; Ren, C.; Yang, W.; Deng, J.; *Macromol. Rapid Commun.* **2013**, *34*, 1426.

[86] Zhang, Y.; Luo, X.; Deng. J.; *Macromol. Chem. Phys.* **2011**, *212*, 353.

types of monomers, including chiral ones and therefore, they could obtain chiral particles with sizes around 10^2 nm.[87]

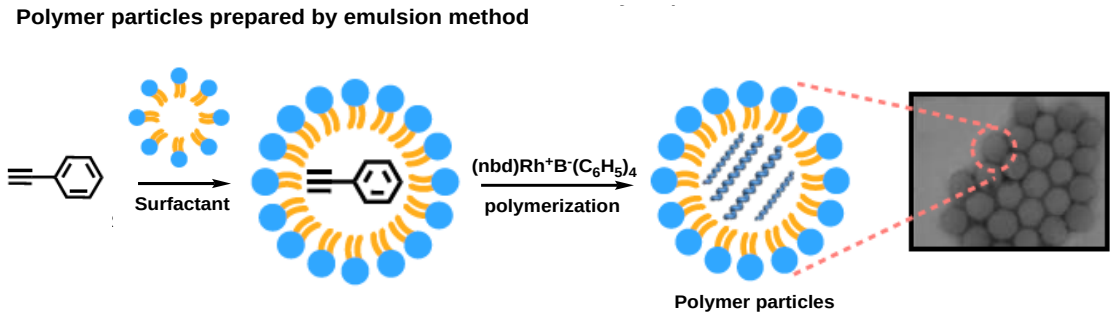

Figure 22. Schematic illustration of the emulsion polymerization method to form polymer particles.

This group also described the formation of macroscopically racemic PPAs particles. The formation of them is due to the presence of a surfactant such as SDS or Triton X-100 in water. Thanks to the liquid nature of the phenylacetylene monomer it is unnecessary the use of organic solvent to dissolve it, and in fact, it gets into the micelles as soon as it is added to the water solution. In this work, $[(nbd)Rh^+B^-(C_6H_5)_4]$ is used as catalyst and their hydrophobic nature results in its rapid dispersion into the micelles in the aqueous mixture. Because of the micelles are preformed, this type of polymerization produces small-diameter particles that can be controlled with the amount of surfactant employed.[87]

In order to control the nanoparticles size, D'Amato *et al.* developed different protocols. Thus, they found that when the organometallic catalyst is substituted by a radical initiator such as potassium persulfate (KPS),[88] the polydispersity of the particles decreased due to the emulsion stabilization by the presence of charged species in the reaction mixture. Moreover, the size of the particles can be easily changed by modification of the initiator concentration.

4.3.3 PPAs Nanoparticles via Metal-Driven Nanostructuration

Nanoparticles based on PPAs can be also obtained by using non-covalent cross-linking agents like metal cations. Riguera *et al.* reported for the first time the formation of Helical Polymers Metal-Complexes (HPMCs) using this approach. Thus, a PPA bearing either (*R*)- or (*S*)-α-methoxy-α-phenylacetic acid (poly-**14**) connected to the phenylacetylene through amide bond was converted into nanospheres by addition of monovalent or divalent metal ions (perchlorate salts in THF).

[87] a) Chen, B.; Liu, X.; Xu, C.; Song, C.; Luo, X.; Yang, W.; Deng, J. *Macromol. Chem. Phys*. **2012**, *213*, 603-609. b) Luo, X. F.; Kai, N. W.; Li, L.; Deng, J. P.; Yang, W. T. J. *Polym. Sci., Part A: Polym. Chem.* **2010**, *48*, 1661-1668. c) Chen, B.; Deng, J.; Tong, L.; Yang, W. Macromolecules **2010**, 43, 9613−9619. d) Deng, J. P.; Chen, B.; Luo, X. F.; Yang, W. T. *Macromolecules* **2009**, *42*, 933-938.

[88] Venditti, I.; D'Amato, R.; Russo, M. V.; Falconeri, M.; *Sens. Actuators B* **2007**, *126*, 35.

Poly-**14** dissolved in different organic solvents ($CHCl_3$, THF, DMSO, DMF) presents an equilibrium between left-handed (*M*) and right-handed (*P*) helices showing null CD signal at the vinylic region. Interestingly, the addition of monovalent or divalent metal ions can increase its left-handed or right-handed helical sense. For example, the left-handed helical sense of poly-(*R*)-**14** is obtained when a perchlorate salt of a monovalent metal ion is added, while the right-handed helical sense is achieved when a salt of divalent metal ion is employed.

The metal ion can act not only as chiral inducer but also as a cross-linking agent between polymer chains forming chiral nanospheres. The size and chiral content of these nanospheres can be modulated controlling the polymer/metal ratio.[89] Finally, it was demonstrated the encapsulation ability of these nanostructures by the encapsulation of iron oxide magnetic nanoparticles, quantum dots or organic molecules such as fluorescent dyes (Figure 23).[90]

Moreover, poly-**14** can be converted into other nanostructures (toroids, nanotubes) with the help of a cosolvent or solvent variation. In the case of nanotubes, they are formed when a cosolvent with a high boiling point is added while toroidal nanostructures are obtained upon addition of a solvent in which the polymer is poorly dissolved.[91]

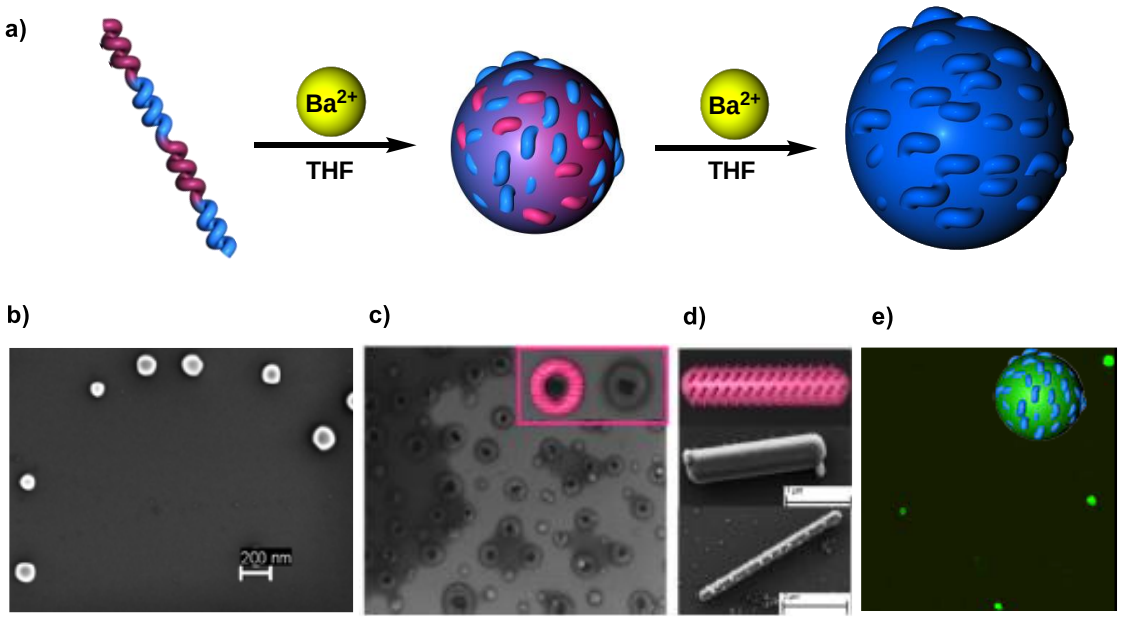

Figure 23. a) Schematic representation for the nanostructuration of poly-**14** with metal ions. b) SEM images of poly-**14** converted into nanospheres, c) toroids d) nanotubes and e) confocal image of HPMCs encapsulating fluorescein.

[89] Arias, S.; Núñez-Martínez, M.; Quiñoá, E.; Riguera, R.; Freire, F. *Small* **2017**, *13*, 1602398.

[90] Freire, F.; Seco, J. M.; Quiñoá, E.; Riguera. R. *J. Am. Chem. Soc.* **2012**, *134*, 19374.

[91] Arias, S.; Freire, F.; Quiñoá, E.; Riguera, R.; *Angew. Chem. Int. Ed.* **2014**, *53*, 13720.

In another work of our group, PPAs derived from *L*-aminoacids methyl ester (*e.g*. *L*-alanine, *L*-isoleucine, *L*-leucine, etc) can be converted into chiral nanospheres (*P* or *M*) varying the polymer/metal/cosolvent ratio. Thus, the addition of divalent or monovalent metal ions produce the complex I (chelation of the two carbonyl groups; *syn* conformation) associated to a helical inversion an also the formation of *M* nanospheres. With the addition of a small amount of MeOH, it is possible to transform complex I to complex II and to produce a second inversion leading to the formation of *P* nanospheres (Figure 24).[92]

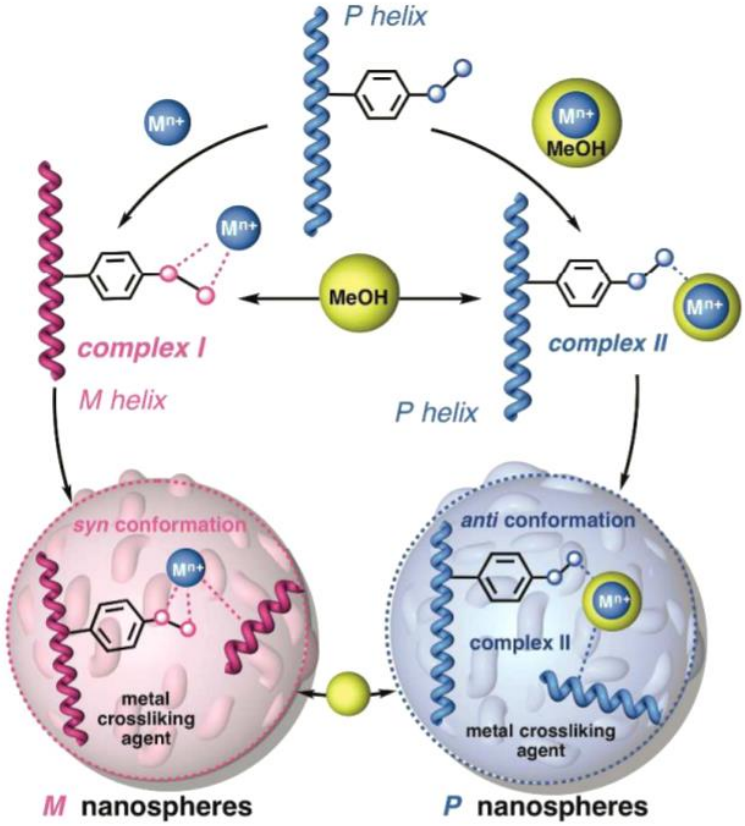

Figure 24. Schematic representation for the selective nanostructuration in *P* or *M* nanospheres by structural changes in the PPA/M^{n+}/cosolvent ratio.

5. Properties of Dynamic Helical Polymers

In the last years, the groups that studied dynamic helical polymers have been working on having a total control of the helix motif —helical sense and elongation—. To achieve this goal is fundamental for the possible applications that have these materials. Sensing, memory storage, drug delivery, chiral recognition and asymmetric catalysis are some of them. The rational design of monomers is very important to observe the properties expected in the

[92] Arias, S.; Freire, F.; Quiñoá, E.; Riguera, R.; *Polym. Chem*. **2015**, *6*, 4725.

polymer. For this, an advanced characterization of the polymers is essential to better understand the relationship between structure-function.

In the next sections, the most important properties discovered until now in dynamic helical polymers will be described in detail.

5.1 Helix Induction in Dynamic Helical Polymers

The helix induction takes place in axially racemic polymers where the both helices are present in equilibrium (*P* and *M* helices are in the same population). An axially racemic polymer can be obtained by polymerizing an achiral monomer or even with some chiral monomers where there are two stable conformational states in equilibrium. The interaction of these optically inactive polymers with chiral external stimuli (*e.g.* chiral solvent or chiral molecules) will promote the formation of a helix with one preferred helical sense and creating an optically active helical polymer. This helix will have a diastereomeric character due to the chirality of the helix and the chirality of the external agent.

Yashima and co-workers were the first group in reporting the first example of a helix induction in PPAs using chiral external stimuli. In this work, they synthetized an inactive optically PPA that bears an achiral carboxylic acid as pendant group. The addition of a chiral amine produces an acid-base complexation that induces one preferred helical sense in the PPAs transferring the chirality of the amine to the helical polymer. This process is reversible and if a strong acid is added, the preferred helical sense is lost. Interestingly, the helix induction was observed in solution, gel and solid state (Figure 25).[93,94]

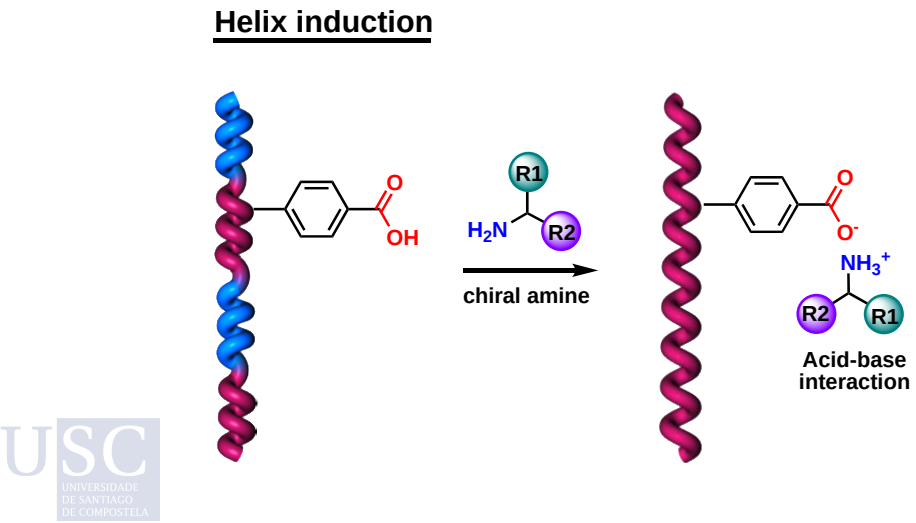

Figure 25. Schematic representation of the helix induction in PPAs.

[93] Yashima, E.; Matsushima, T.; Okamoto, Y.; *J. Am. Chem. Soc.* **1995**, *117*, 11596

[94] Hase, Y.; Nagai, K.; Iida, H.; Maeda, K.; Ochi, N.; Sawabe, K.; Sakajiri, K.; Okoshi, K.; Yashima, E.; *J. Am. Chem. Soc.* **2009**, *131*, 10719.

5.2 Memory Effect of Macromolecular Helicity

Interestingly, after observing the helix induction explained above, Yashima's group described a new phenomenon called Memory Effect. This process can be explained as the maintenance of the helical sense after removing the chiral external stimulus. Thus, interchanging the chiral amine by an achiral one, the macromolecular helicity remained unaltered.

When the chiral amine is totally replaced, the CD signal presents the same intensity indicating the same helical sense in the polymer. The mechanism of this memory effect consists on stablishing salt bridges among the carboxylic groups and the achiral amines when these replace the chiral ones. Moreover, the electrostatic repulsions formed sustain the helix (Figure 26).[95]

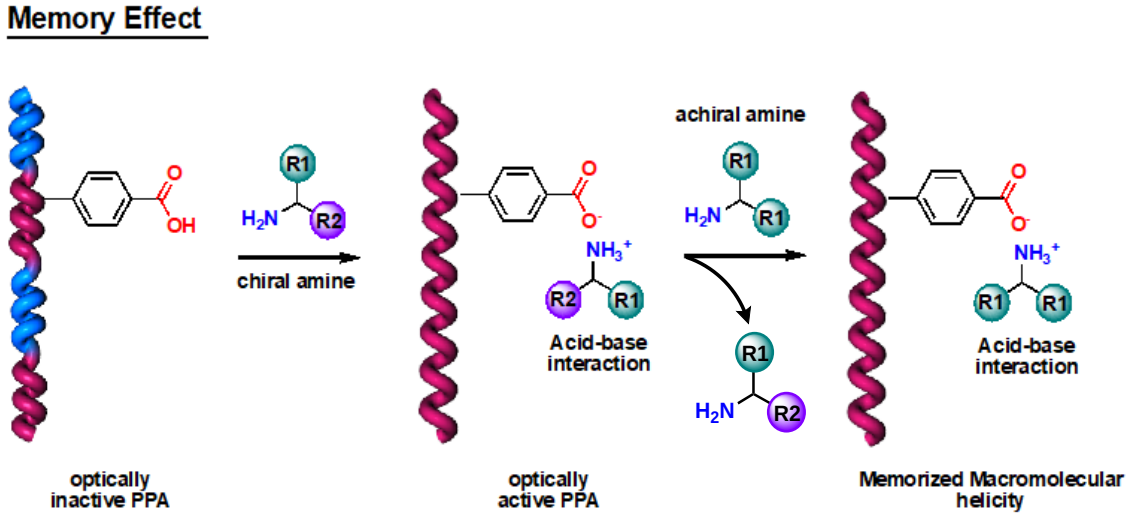

Figure 26. Schematic illustration of the Memory Effect.

5.3 Chiral Enhancement or Chiral Amplification

When to a starting racemic helical polymer formed by a chiral pendant, an external stimulus that promotes the formation of a preferred helical sense is added, this is called chiral enhancement. This process must be differentiated of the helix induction that is produced with PPAs formed from achiral monomers. Chiral enhancement phenomenon also allows to increase the screw sense excess of a starting optically active helical polymer by the addition of a small amount of an external stimulus (*e.g.* temperature, metal ions, polarity of solvents,

[95] Yashima, E.; Maeda, K.; Okamoto, Y.; *Nature*. **1999**, *399*, 449.

[55] Freire, F.; Seco, J. M.; Quiñoá, E.; Riguera, R.; *Angew. Chem. Int. Ed.* **2011***, 50,* 11692.

etc.). The mechanism is based on the formation of a covalent or non-covalent interaction between the polymer and the external stimuli that induce the helical sense excess.

Working on this topic, our group developed a new PPA derived from the anilide of α-methoxy-α-phenylacetic acid (poly-**14**) that presents an equilibrium with 50% of right- and left-handed helices. This fact makes the helical polymer axially racemic, therefore it presents a null CD signal in the vinylic region (CD_{380} = 0). The equilibrium is due to the presence of a conformational equilibrium between two conformations: the carbonyl and the methoxy group in antiperiplanar position [*ap* conformer, dihedral angle for (O-)C—C(=O) 180° ca] and a synperiplanar conformation between these functional groups [*sp* conformer, dihedral angle for (O-)C—C(=O) 0° ca].[55]

Interestingly, the addition of a small amount of metal ions (*e.g.* Li^+, Ag^+, Ba^{2+}, etc) to the polymer can disarrange the equilibrium due to the formation of a PPA/M^{n+} complex. Thus, with the addition of monovalent metal ions (*e.g.* Li^+, Na^+ and Ag^+), the *ap* conformation is stabilized in the pendant group due to the coordination of the metal ion to the carbonyl and the presence of a cation-π interaction between the cation and the phenyl ring. In contrast, the addition of divalent metal ions (Ba^{2+}, Co^{2+}, Ni^{2+}, etc.) stabilizes the *sp* conformation by the coordination of the metal to the carbonyl and the methoxy groups (Figure 27). Thus, poly-**14** behaves as a metal ion sensor due to its ability to change the coordination mode depending on the metal ion oxidation state.

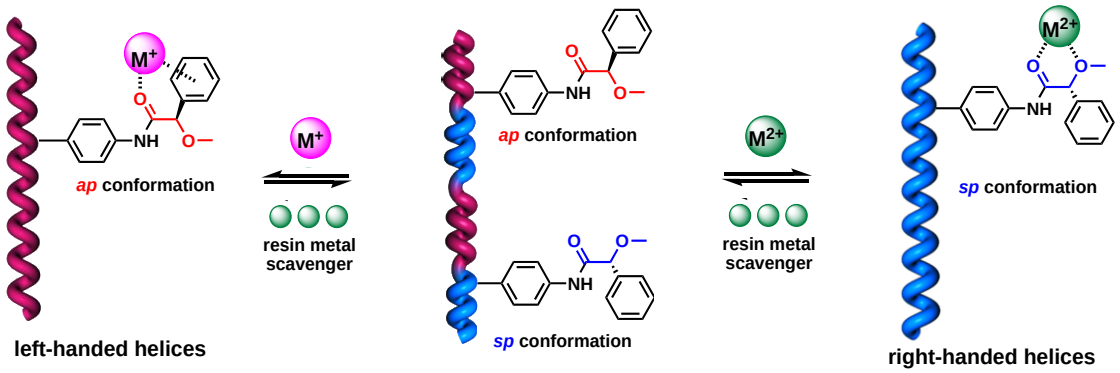

Figure 27. Schematic representation of chiral enhancement by complexation of monovalent and divalent metal ions to poly-**14**.

In addition, Arias *et al.* demonstrated that it is possible to have a total control of the helical scaffold in poly-**14** achieving both helical senses using only monovalent metal ions (Na^+ and Ag^+). This is reached by controlling the presence or absence of cation-π interactions. Thus, the addition of a small amount of a donor cosolvent (*e.g.* MeOH, MeCN) is able to break the interaction between the metal ion and the aryl ring stabilizing the *sp* conformation in the pendant group (Figure 28).[92]

The chiral amplification phenomenon has been widely studied by Green *et al.* in poly(isocyanate)s. During the last decades, the processes described by them have been also observed in others helical systems. These processes will be explained next.

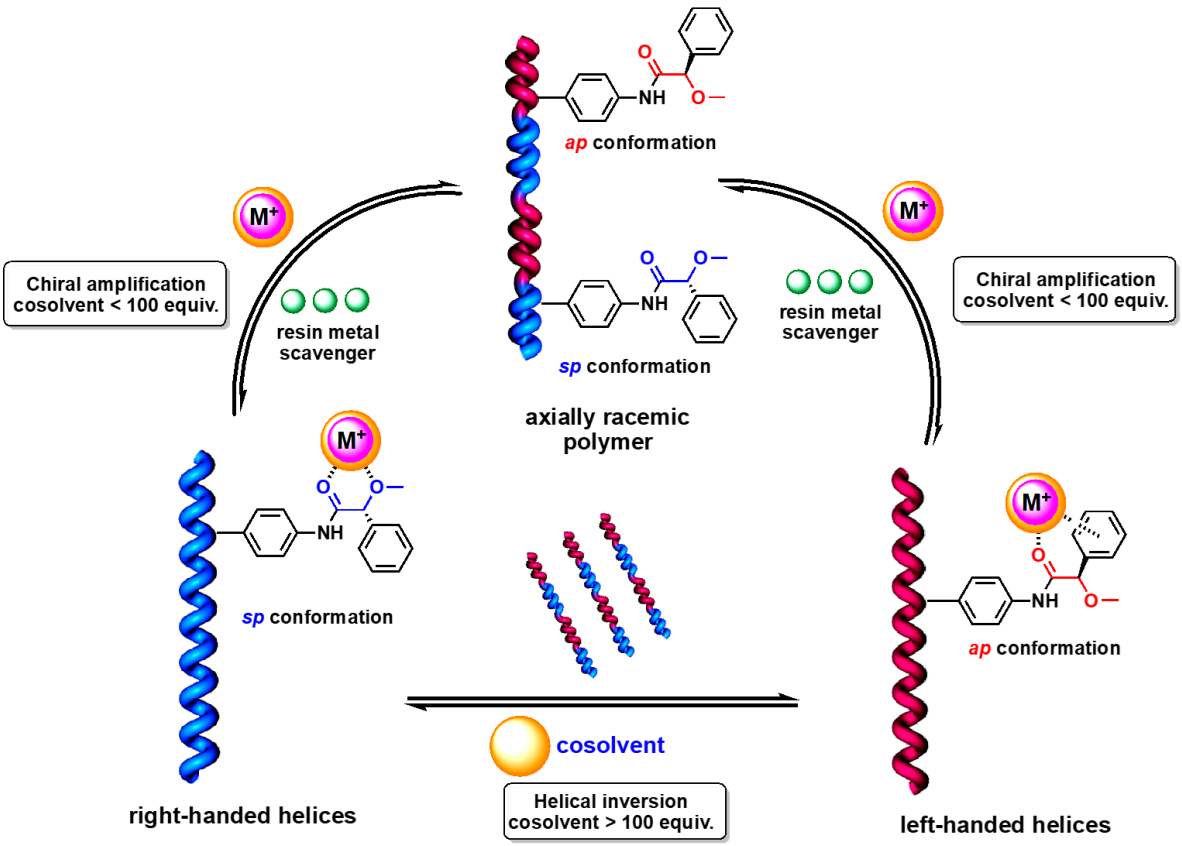

Figure 28. Modulation of the helical sense in poly-**14** by the activation/deactivation of the cation-π interactions.

5.3.1 Sergeants and Soldiers Effect

The Sergeants and Soldiers Effect is a chiral amplification process produced in copolymers composed by chiral and achiral monomers. With the introduction of a small amount of chiral monomer (less than 1%) and through a cooperative communication mechanism, this chiral unit is able to control the helical sense of the entire copolymer. For this reason, copolymers with a small amount of chiral monomers present the same CD intensity than the chiral homopolymers (Figure 29a). This process was described by Green and co-workers in poly(isocyanate)s at 1988.[96] Since this work based on poly(isocyanate)s, this effect

[96] a) Green, M. M.; Park, J.-W.; Sato, T.; Teramoto, A.; Lifson, S.; Selinger, R. L. B.; Selinger, J. V. *Angew. Chem. Int. Ed.* **1999**, *38*, 3138. b) Green, M. M.; Peterson, N. C.; Sato, T.; Teramoto, A.; Cook, R.; Lifson, S. *Science* **1995**, *268*, 1860. c) Green, M. M.; Garetz, B. A.; Munoz, B.; Chang, H. P.; Hoke, S.; Cooks, R. G. *J. Am. Chem. Soc.* **1995**, *117*, 4181.

was also observed in other helical polymers (e.g. Poly(silane)s, poly(acetylene)s, etc) obtaining similar results.

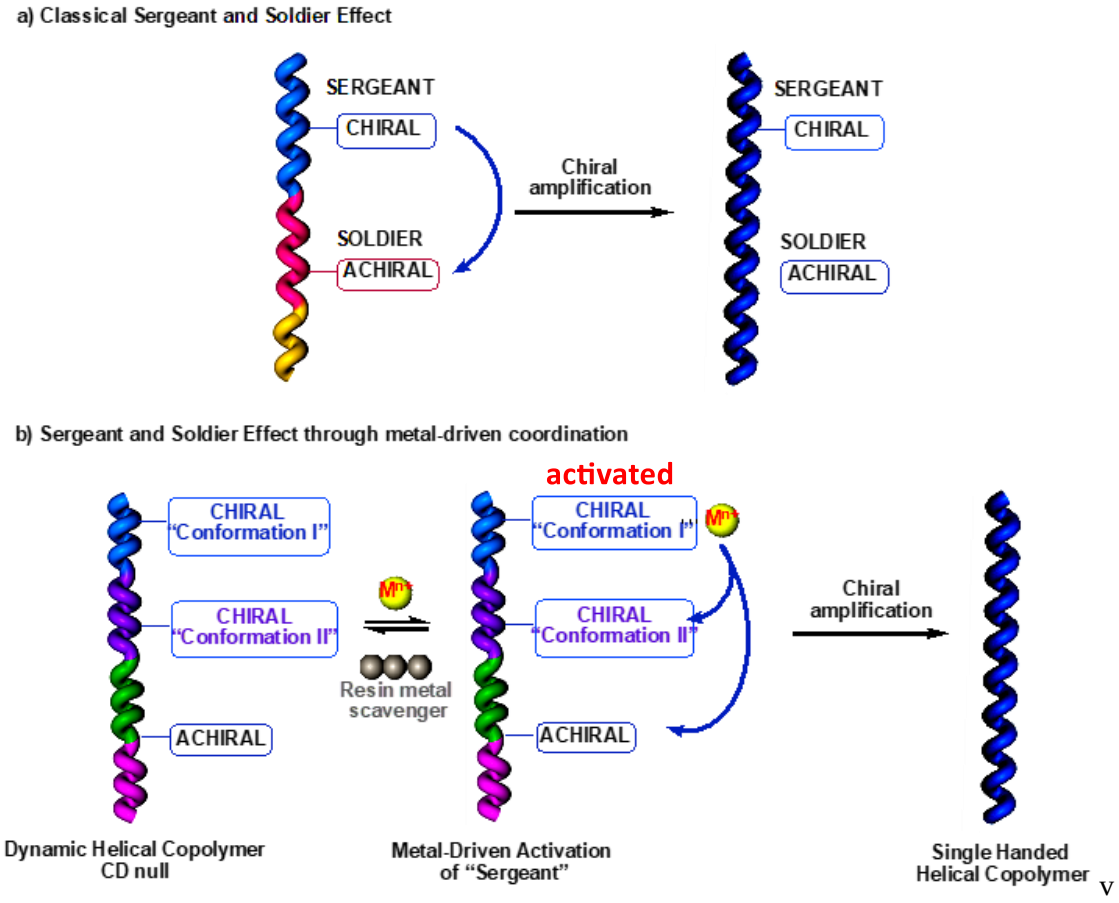

Figure 29. a) Conceptual representation for the classical Sergeants and Soldiers Effect resulting into a chiral enhancement. b) Sergeant and Soldiers Effect mediated by metal ion coordination.

At 1997, Meijer *et al.* described the Sergeants and Soldiers Effect in supramolecular polymers. To carry out this work, chiral BiPy-BTA and achiral BiPy-BTA were employed derived from aliphatic chains. They observed that when the chiral BiPy-BTA units are dissolved in low-polar solvents, the formation of chiral helical aggregates is observed. These structures show a strong response in the CD spectrum. Alternatively, the achiral units also formed these aggregates but did not show CD response. Remarkably, copolymers formed by at least a 2.5% of chiral monomers dissolved in hexane exhibit a strong CD intensity comparable with the counterpart chiral homopolymers.[97]

In this type of supramolecular polymers, the Sergeants and Soldiers Effect is very limited and influenced by the organization of the entire system where the design of the different

[97] Palmans, A. R. A.; Vekemans, J.; Havinga, E. E.; Meijer, E. W. *Angew. Chem. Int. Ed*. **1997**, *36*, 2648.

monomer plays an important role. This problem is not as significant in covalent polymers as in supramolecular polymers.

Considering this information, Freire *et al.* described a new Sergeants and Soldiers Effect based on poly-**14** (sergeant) and achiral units (soldiers). As explained before, from previous studies it was demonstrated that poly-**14** presents an equilibrium of left- and right-handed helices motivated by the presence of two possible conformations in the pendant. This conformational equilibrium can be modified with the coordination of metal ions. Thus, the *ap* conformation [dihedral angle for (O-)C—C(=O) 180º ca] can be predominant with monovalent metal ions (*e.g.* Na^+, Li^+ and Ag^+) due to the presence of the cation-π interaction, whereas divalent metal ions (*e.g.* Ba^{2+}, Ca^{2+}, etc.) stabilize the *sp* conformation [dihedral angle for (O-)C—C(=O) 0º ca]. On the other hand, as achiral units (soldiers), anilides derived from the phenylacetic and diphenylacetic acid were selected because the parent homopolymers do not show a preferred helical sense (null CD in the vinylic region).[98]

As it was demonstrated, poly-**14** can act as a metal ions sensor distinguish between monovalent and divalent metal ions stabilizing one preferred helical sense. Taking this information in account, a small amount of metal ions was added to the axially racemic copolymers to activate the Sergeant (MPA moiety) and produce the Sergeants sand Soldiers Effect. As result, one preferred helical sense is stabilized in function of the metal's valence employed, due to the ability of MPA to command and order the achiral units (Figure 29b).

Moreover, the reversibility of the process is proven by adding some metal scavenger resin because the starting axially racemic copolymer is recovered. This work constitutes the first time that a reversibility Sergeants and Soldiers Effect is reported.

Furthermore, as it was explained before, it is possible to control the helical sense of poly-**14** by activation/deactivation of the cation-π interactions. Thus, the addition of monovalent metal ions (*e.g.* Na^+) in presence of small amount of donor cosolvent (*e.g.* MeOH) induces an *ap* conformation leading to one preferred helical sense. On the other hand, the presence of high amount of donor cosolvent breaks the Na^+-π stabilizing a *sp* conformation in the pendant group. Applying this information, it was possible to control the Sergeants and Soldiers Effect in the same copolymers formed by MPA, phenylacetic and diphenylacetic monomers. Thus, with a unique external stimulus, it is possible to produce the two helical senses (*P* and *M* helices) varying the stabilized conformation of MPA moiety.[99]

[98] Bergueiro, J.; Freire, F.; Wendler, E. P.; Seco, J. M.; Quiñoá, E.; Riguera, R. *Chem. Sci.* **2014**, *5*, 2170.

[99] Arias, S.; Bergueiro, J.; Freire, F.; Quiñoá, E.; Riguera, R. *Small* **2016**, *12*, 238.

5.3.2 Chiral Coalition

Classical Sergeants and Soldiers Effect consists on a chiral-achiral communication. Recently, our group has described a novel approach to this classic phenomenon using a chiral sergeant and a chiral soldier. In this work, it is possible to have a total control over the internal helical sense and the chirality of the periphery. In these systems, the chiral soldier is the major component and it is possible to obtain the same internal helical sense from either enantiomers, even a racemic mixture of them. As a result, it was demonstrated that the chirality of the appropriated Sergeant is enough to control the internal helical sense of a copolymer organized by Sergeants and Soldiers Effect with chiral to chiral communication. (Figure 30).[100,101]

To obtain an effective Chiral Coalition, the two monomers must obey some rules: (1) both monomers have to be chiral and promote similar helical scaffolds in the corresponding homopolymers (*c*-*t* or *c*-*c*); (2) the chiral soldier must have two possible conformations (null CD in the homopolymer); (3) the chiral sergeant must have a defined conformation that promotes a preferred helical sense in the corresponding homopolymer.

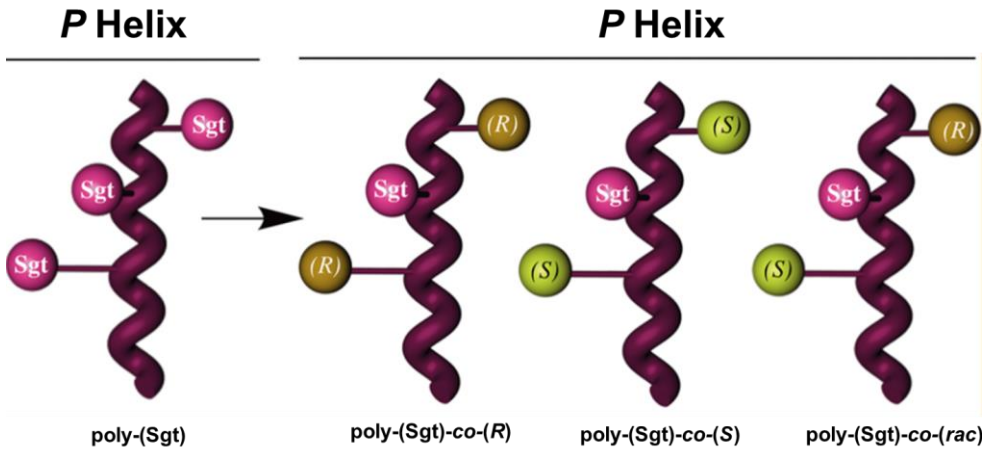

Figure 30. Conceptual representation of chiral to chiral communication by Chiral Coalition.

5.3.3 Chiral Conflict

On the opposite side of Chiral Coalition is the Chiral Conflict. This phenomenon was first described by Green and co-workers in (isocyanate)s copolymers formed by two chiral monomers with different structure and configuration. Thus, both monomers must induce

[100] Cobos, K.; Quiñoá, E.; Riguera, R.; Freire, F.; *J. Am. Chem. Soc.* **2018**, *38*, 12239.

[101] Arias, S.; Rodríguez, R.; Quiñoá, E.; Riguera, R.; Freire, F; *J. Am. Chem. Soc.* **2018**, *140*, 667.

opposite helical senses in the polymer chain resulting in a non-order structure.[102] In this way, the ratio of both monomers will define the initial helical sense, but also the inversion temperature. Thus, with a specific ratio of monomers, there is a conflict temperature (T_c) where the CD is null. Above or below that T_c the copolymer becomes an optically active material achieving opposite helical senses (Figure 31).

Our group has reported the unique practical application for Chiral Conflict in dynamic helical polymers, using this non-communication mechanism as sensor of metal valences.[103]

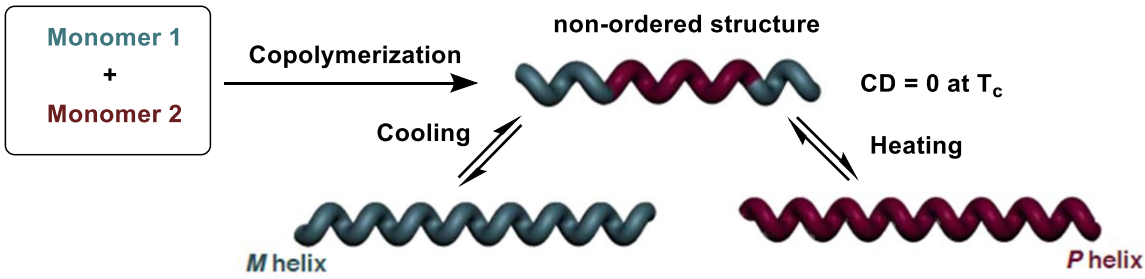

Figure 31. Conceptual representation of Chiral Conflict (lack of chiral to chiral communication).

5.3.4 Majority rules

In another seminal work of Green and co-workers, it was reported another Chiral Enhancement phenomenon in poly(isocyanate)s. In this case, they observed that in mixtures of (*R*)- and (*S*)-isocyanate monomers, when there is a small imbalance (*e.g.* copolymer based on 51% of (*R*)-monomer and 49% of (*S*)-monomer), this produces one preferred helical sense in the copolymers. The CD intensity is identical to the parent homopolymer of the major monomer due to cooperative effects. In this mechanism of communication, the minor component adopts the helical sense of the major component to avoid the presence of helix reversals energetically unfavored (Figure 32).[104]

[102] a) V. Jain, K.-S. Cheon, K. Tang, S. Jha, M. M. Green *Isr. J. Chem.* **2011**, *51*, 1067–1074. (b) Tang, K.; Green, M. M.; Cheon, K. S.; Selinger, J. V.; Garetz, B. A. *J. Am. Chem. Soc.* **2003**, *125* ,7313-7323.

[103] Alzubi, M.; Arias, S.; Rodríguez, R.; Quiñoá, E.; Riguera, R.; Freire, F. *Angew. Chem. Int. Ed.* **2019**, *58*, 13365.

[104] Green, M.; Garetz, B.; Munoz, B.; Chang, H.; Hoke, S.; Graham-Cooks, R.; *J. Am. Chem. Soc.* **1995**, *117*, 4181.

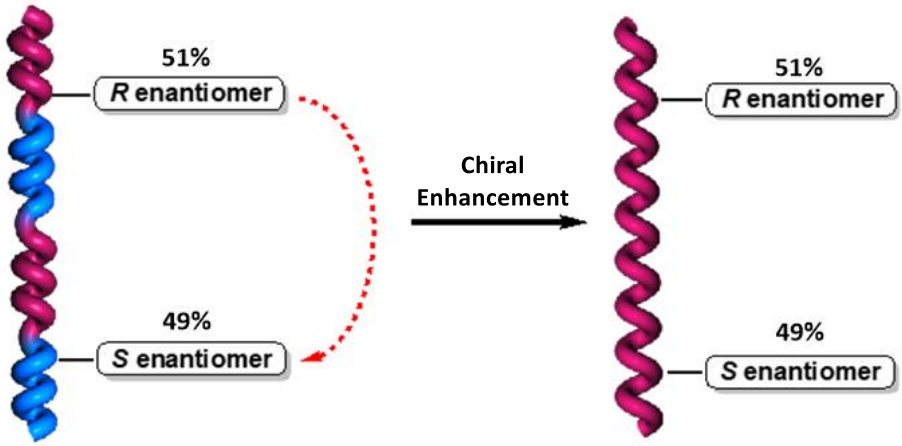

Figure 32. Conceptual representation of Majority Rules in helical polymers.

5.3.5 Domino effect

This type of Chiral Enhancement is based on the introduction of a chiral residue at the end of an achiral oligomer. Thus, the helix induction is possible in oligomers by covalent interactions.[105] For example, synthetic peptides with the N-terminal position unprotected, based on an achiral α-aminoisobutyric acid (Aib) and Z-α,β-dehydrophenylalanine (Δ^ZPhe) residues, adopt a racemic helical structure.[106] The covalent insertion of chiral α-amino acid residues transmits the chiral information into the racemic peptides resulting into a folded helix with a screw sense defined.[107]

Following these works, Inai and co-workers reported a helical induction in optically inactive oligopeptides consisting on an achiral Aib and Δ^ZPhe bearing a *N*-terminal amino group upon interactions with carboxylic acids but through non-covalent interactions (Figure 33b).[108,109] These peptides showed an active CD in the vinylic region due to the presence of an excess of one helical sense. This is due to the acid-base interactions produced with the chiral carboxylic acids.

[105] Okamoto, Y.; Matsuda, M.; Nakano, T.; Yashima, E.; *Polym. J.* **1993**, *25*, 391.

[106] Venkatraman, J.; Shankaramma, S. C.; Balaran, P.; *Chem. Rev.* **2001**, *101,* 3131.

[107] Pengo, B.; Formaggio, F.; Crisma, M.; Toniolo, C.; Bonora, G. M.; Broxterman, Q. B.; Kamphuis, J.; Saviano, M.; Iacovino, R.; Rossi, F, Benedetti, E.; *J. Chem. Soc., Perkin Trans.* **1998**, 2, 1651.

[108] Inai, Y.; Komori, H.; Ousaka, N.; *Chem. Rec.* **2007**, *7*, 191.

[109] Ousaka, N.; Inai, Y.; *J. Org. Chem.* **2009**, *74*,1429.

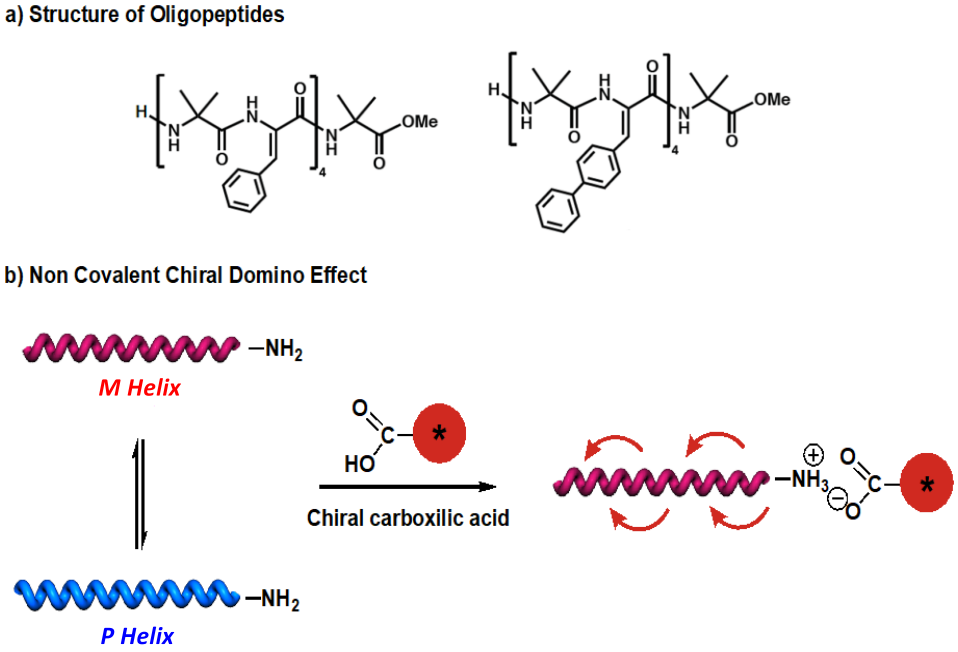

Figure 33. a) Structure of Oligopeptides and b) schematic representation of Domino Effect.

Recently, our group reported a new helix induction phenomenon based on this transmission of chiral information from the end (*(R)*/(*S*) - MTPA units) of an oligopeptide [$(Aib)_n$ (n = 1-3)] that compose the pendant groups of a PPA (poly-AIB_n-**18**). In this macromolecular gear phenomenon, the chiral information of the MTPA enantiomer is transmitted along the achiral AIB through chiral tele-induction and chiral harvesting to the polyene backbone. Interestingly, the polymer shows a dynamic behavior to polarity of solvents changing the helical sense or modifying the length of the AIB oligopeptide (Figure 34).[110]

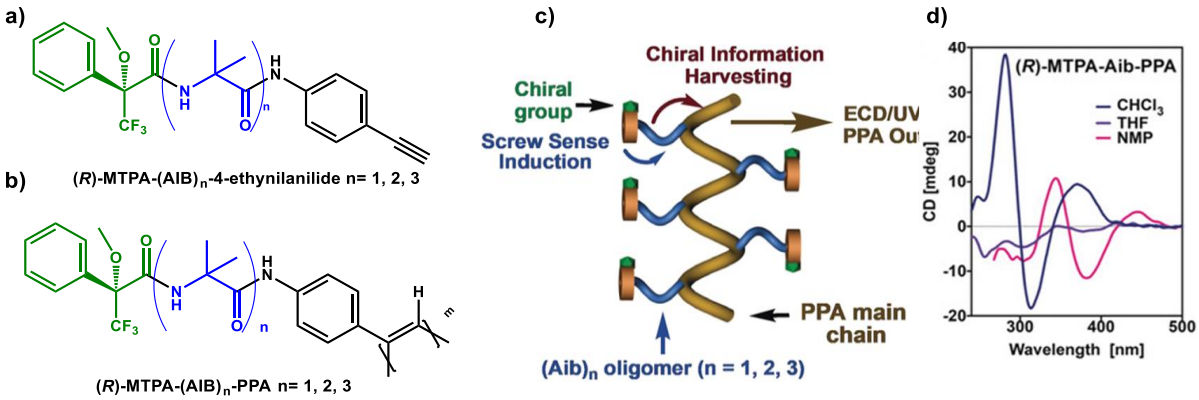

Figure 34. a) Structure of monomers. b) Structure of poly(AIB_n-**18**). c) Conceptual illustration of the chiral information transmission mechanism and d) the resulting CD spectra of the poly(AIB_n-**18**) in different solvents.

[110] Rodriguez, R.; Suárez-Picado, E.; Quiñoá, E.; Riguera, R.; Freire, F.; *Angew. Chem., Int. Ed.* **2020**, *132*, 8694.

5.4 Helix inversion

The helical inversion is one of the most interesting features that present dynamic helical polymers. This property allows the polymer to change the helical sense from *P* to *M* and *vice versa*. This phenomenon is triggered by the addition of external stimuli such as metal ions, light, temperature or solvent's polarity.

In our group, it was developed a dynamic PPA that bears the (*S*)-pheylglycine methyl ester as pendant (poly-**17**). This PPA presents the ability to switch the helical sense with the solvent's polarity and with the coordination of metal ions. In low polar solvents (*e.g.* $CHCl_3$), the polymer shows a negative Cotton effect due to the *anti*-conformation adopted by the carbonyl groups on the pendant —dihedral angle 180º between carbonyl groups—. This conformation leads to *M* helices. On the other hand, when poly-**17** is dissolved in high polar solvent (*e.g.* DMSO, DMF), the pendant groups adopt a *syn* orientation between the two carbonyl groups —dihedral angle 0º between carbonyl groups— leading to *P* helices. The same behavior is achieved when in low polar solvents a metal cation is added (*e.g.* Ba^{2+}) due to the coordination of the metal to both carbonyl groups. Thus, in this way *P* helices are also obtained (Figure 35).[10]

Moreover, in our group it was studied the helical inversion reversibility in polymers derived from *L*-aminoacids methyl ester (*e.g.* Alanine, Valine, Leucine…). All these polymers adopt *M* helices in low polar solvents (*e.g.* $CHCl_3$) due the stabilization of the *anti* conformation of the carbonyls on the pendant group by hydrogen bonds between neighboring pendants. This conformation can be switched by the addition of metal ions (*e.g.* Li^+, Ba^{2+}, Ca^{2+}, etc.) due to the coordination of the cations to both carbonyl groups promoting a helix inversion obtaining *P* helices. Then, the addition of a cosolvent as MeOH promotes another helical inversion and the polymer recover the original helical sense (*M* helices) due to the solvation of the cations by the cosolvent (Figure 35b).[111]

[10] Louzao, I.; Seco, J. M.; Quiñoá, E.; Riguera, R.; *Angew. Chem., Int. Ed.* **2010**, *49*, 1430.
[111] Arias, S.; Núñez-Martínez, M.; Quiñoá, E.; Riguera, R.; *Polym. Chem.* **2017**, *8*, 3740.

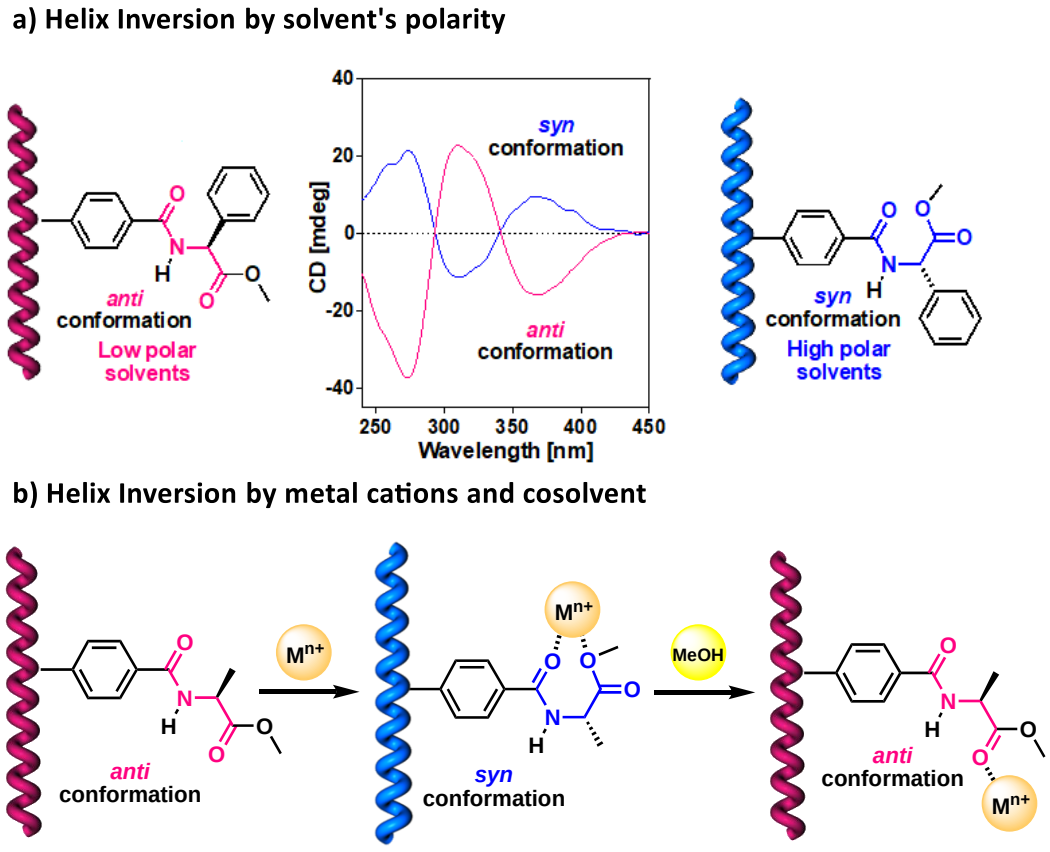

Figure 35. a) Helical inversion produced by solvent's polarity and b) by the addition of metal ions with the recovery of initial helicity by addition of a cosolvent.

5.5 Elongation Control of the Polymer Chains

Until now, different mechanisms and properties to modulate the helical sense of PPAs have been described. In this family of helical polymers, there is another parameter that can be easily modulated: the elongation (compression/stretching). Being able to control both —elongation and helical sense— opens the possibility for the potential applications of these materials.

The elongation of the helical scaffold is dependent of the nature of pendant groups. Thus, if they can interact with external stimuli producing an increase of the repulsions among them, the helix will stretch, while if an attraction between pendants occurs, the helical scaffold will compress. This changes on the helix can be easily observed by UV-Vis technique by the alterations in the double bonds conjugation.[112]

Taking this in account, Yashima *et al.* developed new optically active PPAs with β-cyclodextrins (β-CyD) (poly-**21**) as pendant group (Figure 36). They discovered that poly-**21**

[112] Motoshige, A.; Mawatari, Y.; Yoshida, Y.; Matsuyama, C. S.; Tabata, M.J. *Polym. Sci., Part A: Polym. Chem.* **2012**, *50*, 3008.

presents the ability of colorimetric detection of some enantiomers. For instance, in the presence of (*R*) and (*S*)-1-phenylethylamine the polymer presents a different CD pattern and a small different color resulting in a chiral recognition to these enantiomers (Figure 36c).

In addition, when poly-**21** is dissolved in DMSO, it shows a preferred helical sense and an elongated backbone as it can be seen in the UV spectra (Figure 36b). The addition of increasing amounts of water promotes a change in the color from red to yellow (hypsochromic shift) indicating compression in the backbone of the PPA. Interestingly, at high ratios of water/DMSO the elongation of the PPA is also accompanied with a helical inversion. (Figure 36b).[113]

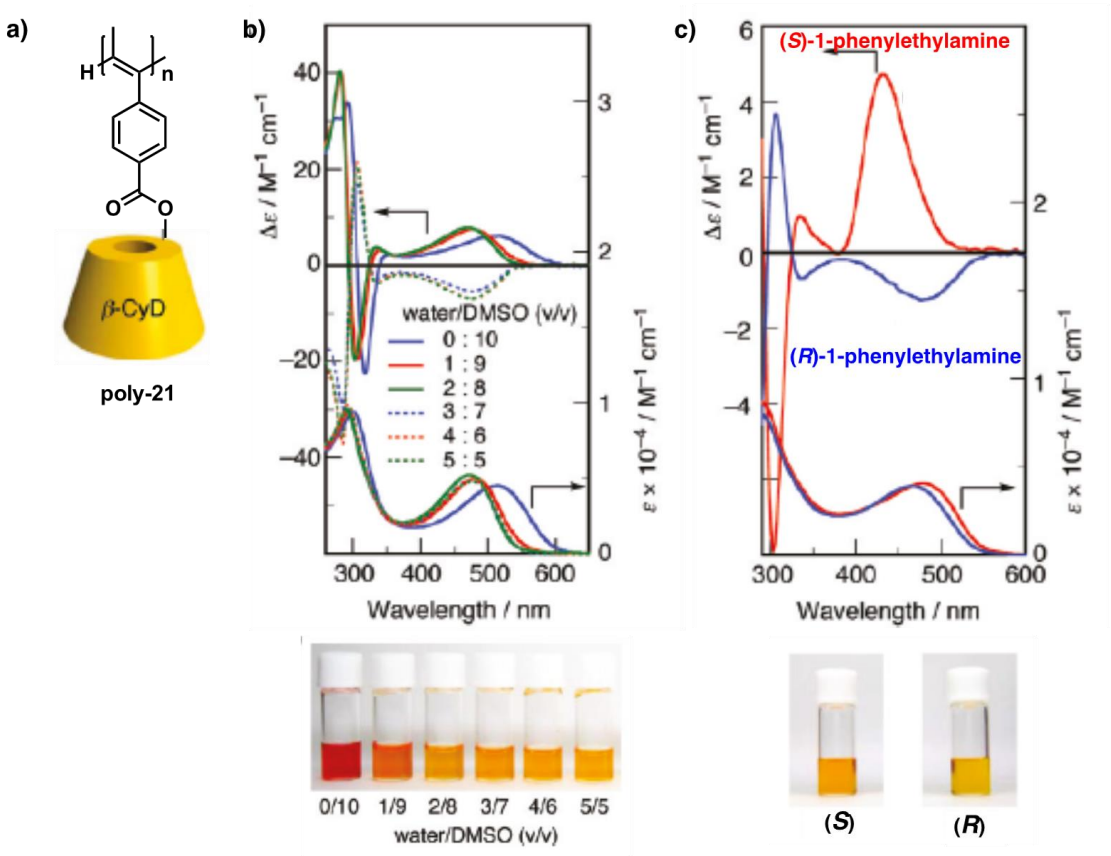

Figure 36. a) Structure of poly-**21**. b) CD and UV spectra of poly-**21** dissolved in different ratios of water/DMSO. c) CD spectra of poly-**21** in presence of (*S*) and (*R*)-1-phenylethylamine showing a chiroptical and optical recognition.

In our research group, Seila *et al.* prepared a new PPA derived from the anilide from (*R*)-α-methoxy-α-trifluoromethyl-α-phenylacetic acid [(*R*)-MTPA] (poly-**18**), in which both features can be selectively modulated. Thus, the helical sense can be switched depending on the

[113] Maeda, K.; Mochizuki, H.; Osato, K.; Yashima, E.; *Macromolecules* **2011**, *44*, 3217.

[25] Leiras, S.; Freire. F.; Seco, J. M.; Quiñoá, E.; Riguera, R.; *Chem. Sci.* **2013**, *4*, 2735.

donor/acceptor character of the solvent; and the elongation can be tuned depending on the polarity of the solvent.[25]

This PPA presents two different bonds that can be manipulated to change the conformation of the pendant group.

On the one hand, the amide bond can be switched from *cis* (donor solvents) to *trans* (non-donor solvents). This functional group is responsible of the elongation control of the polymer that can be easily tracked by UV-Vis technique.

On the other hand, the second bond that can be manipulated is the (O-)C—C(=O) bond. MTPA presents two conformers dependent on the dihedral angle of the carbonyl and methoxy groups. Thus, in low polar solvents (*e.g.* $CHCl_3$, DCM) the (O-)C—C(=O) bond adopts an *ap* conformation where the carbonyl and methoxy groups are oriented in opposite directions. Secondly, when the polymer is dissolved in high polar solvents (*e.g*. DMF and DMSO) the (O-)C—C(=O) bond adopts a *sp* conformation where the carbonyl and methoxy groups are oriented in the same direction. In this work, it has been demonstrated that with the selective manipulation of two bonds it is possible to obtain four different helical structures (Figure 37).[25]

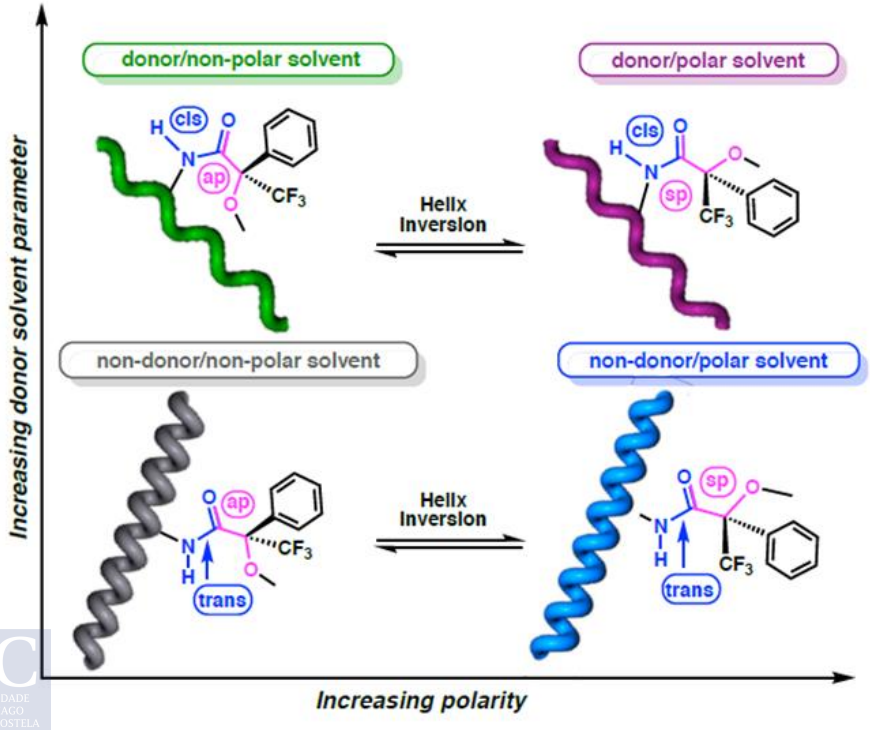

Figure 37. Schematic illustration for the conformation changes in poly-**18** depending on the donor/acceptor and polar/non-polar character of the solvent.

[25] Leiras, S.; Freire. F.; Seco, J. M.; Quiñoá, E.; Riguera, R.; *Chem. Sci.* **2013**, *4*, 2735.

Recently, our group described how the substitution pattern of the phenyl rings (*para*, *meta* and *ortho*) affects the structure of the helix. In this work, it is studied the dynamic behavior and elongation of poly-**14** with the different substitution pattern. It was observed that *p*-poly-**14** and *m*-poly-**14** presents the ability to respond at the presence of metal ions. In the case of *meta* substituted poly-**14**, the ability to respond at external stimuli is lower than in the case of *para* substituted polymer due to less dynamic behavior. Moreover, *m*-poly-MPA presents the combination of two helices, one more compressed *cis-cisoidal* structure like the *p*-poly-**14**; and the second one, a more stretched *cis-transoidal* helix. In the case of *ortho-substituted* polymers (*o*-poly-**14**), it was found that it does not respond to the presence of external stimuli due to the quasi-static behavior and that it presents a highly stretched helix with an almost planar structure (Figure 38).[67]

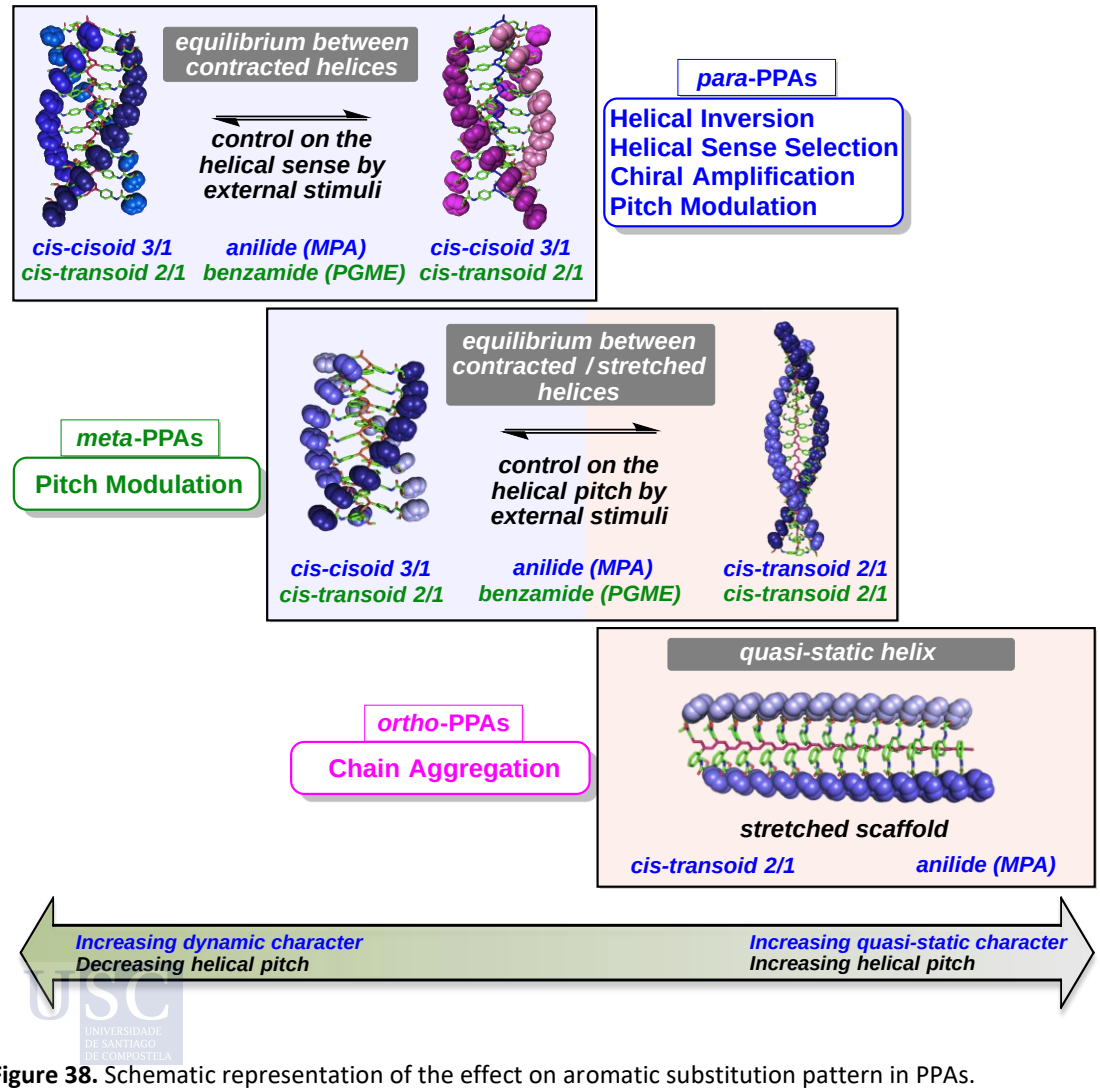

Figure 38. Schematic representation of the effect on aromatic substitution pattern in PPAs.

[67] Rodríguez, R.; Quiñoá, E.; Riguera, R.; Freire, F. *J. Am. Chem. Soc.* **2016**, *138*, 9620.

6. Applications of Poly(phenylacetylene)s

Due to the properties explained before, dynamic helical polymers and specifically PPAs have several potential applications in fields such as sensing, chiral separation, chiral recognition or nanoreactors among others. The easily manipulation of parameters such as helical sense and elongation permits these applications. In this section, they will be summarized.

6.1 PPAs as Sensors

Helical polymers and the possibility of tuning their structure by the addition of different external stimuli makes these materials appropriate for their use as sensors. In this way, several PPAs have been designed for sensing different metals,[116] anions[117] or even as thermal sensors.[118]

In our group, they have been prepared several polymers that can act as sensor. For instance, poly-**14**,[55] that was previously described, can differentiate between monovalent and divalent metal ions due to the left- and/or right-handed helicities obtained in each case.

In another work of the group that was also described before, several PPAs bearing a *L*-aminoacids methyl ester as pendant groups were prepared showing different chiroptical properties depending on the solvent employed.[10] Thus, these polymers can discern between low polar and high polar solvents displaying different CD spectra. This different behavior is achieved due to the presence of two conformations in the pendant that can be switched by solvent or metal ions.

Going deeper in the previous detection of solvent's polarity, our group developed poly-**18**[25] that can act as solvent sensor distinguishing between two parameters: the polar/low polar and donor/non donor characters. Thus, this polymer can present four different helices that can be detected by CD and UV-Vis spectra. These helices are achieved in function of the already mentioned features of the solvent.

On the other hand, colorimetric sensors are a rapid and direct way of determination. In this sense, they have been developed several polymers with this function. For instance,

[116] Alzubi, M.; Arias, S.; Louzao, I.; Quiñoá, E.; Riguera, R.; Freire, F. *Chem. Commun.* **2017**, *53*, 8573.

[117] Leiras, S.; Suárez-Picado, E.; Quiñoá, E.; Riguera, R.; Freire, F. *Giant*, **2021**, *100068*.

[118] Zhou, Y.; Zhang, C.; Qiu, Y.; Liu, L.; Yang, T.; Dong, H.; Satoh, T.; Okamoto, Y. *Molecules* **2016**, *21*, 1583.

[55] Freire, F.; Seco, J. M.; Quiñoá, E.; Riguera, R.; *Angew. Chem. Int. Ed.* **2011***, 50,* 11692.

[10] Louzao, I.; Seco, J. M.; Quiñoá, E.; Riguera, R.; *Angew. Chem., Int. Ed.* **2010**, *49*, 1430.

[25] Leiras, S.; Freire. F.; Seco, J. M.; Quiñoá, E.; Riguera, R.; *Chem. Sci.* **2013**, *4*, 2735.

Yashima *et al.* developed new optically active PPAs with β-cyclodextrins (β-CyD) (poly-**21**) as pendant group that present the ability of colorimetric detection of some enantiomers (*e.g.* (*R*)/(*S*)-1-phenylethylamine).[113]

6.2 Chiral Recognition

High-Performance Liquid Chromatography (HPLC) with chiral stationary phases (CSP) is one of the most important techniques for the separation of enantiomers.[119] To obtain a good separation of racemic mixtures, the CSP must present a good chiral recognition of the racemate mixture.

Several examples of CSPs were developed based on small molecules (*e.g.* polysaccharides, peptides) or polymers. However, there are still several racemic mixtures that cannot be separated using commercially available CSPs. Working on this, helical polymers with one preferred helical sense such as poly(triphenylmethylmethacrylates)s (PTrMA)[120] or polysaccharides[121] were prepared to resolve this problem. Although helical polymers have demonstrated a good resolution of several racemates, they still present some limitations.

In the last decade, PPAs have begun to be employed as CSP in HPLC. Thus, Yashima *et al.* reported the first example of PPAs with this use. In this work, PPA bearing a 2-2'-biphenol derivative as pendants (poly-**22**) that presents an axially racemic chirality (*P*/*M* helices in the same population) was prepared. This PPA experiences a chiral enhancement in presence of (*S*)- or (*R*)-phenylethanol and the helical sense can be memorized in absence of the external stimulus. Thus, this polymer was the first example of a PPA used to separate racemate mixtures (*e.g. trans*-stilbene). Interestingly, the elution order of the enantiomers can be easily tuned by switching the helical sense of the PPA.[122]

Recently, Maeda and Freire used as CSP in HPLC a helical PPA derived from a chiral (*R*)-α-methoxy-α-phenylacetic acid unit as pendant (poly-**14**). This PPA can achieve both helical senses by the addition of catalytic amounts of sodium and cesium tetrakis[3,5-bis(trifluromethyl)phenyl]borate salts (MBArF), respectively. In this work, it has been

[113] Maeda, K.; Mochizuki, H.; Osato, K.; Yashima, E.; *Macromolecules,* **2011**, *44*, 3217.

[119] a) Andersson, S.; Allenmark, S. G., *J. Biochem. Biophys. Methods*, **2002**, *54*, 11. b) Liu, Y.; Lantz, A. W.; Armstrong, D. W., *J. Liq. Chromatogr. Relat. Technol.* ***2004****, 27,* 1121.

[120] a) Yuki, H.; Okamoto, Y.; Okamoto, I., *J. Am. Chem. Soc*. **1980**, *102*, 6356. b) Okamoto, Y.; Honda, S.; Okamoto, I.; Yuki, H.; Murata, S.; Noyori, R.; Takaya, H., *J. Am. Chem. Soc*. **1981**, *103*, 6971. c) Nakano, T., *J. Chromatogr. A.* **2001**, *906*, 205-225.

[121] a) Okamoto, Y.; Yashima, E., *Angew. Chem. Int. Ed*. **1998**, *37*, 1020. b) Yashima, E.,*J. Chromatogr. A*, **2001**, *906*, 105. c) Ikai, T.; Okamoto, Y.; *Chem. Rev.* **2009**, *109*, 6077.

[122] Shimomura, K.; Ikai, T.; Kanoh, S.; Yashima, E., *Nat. Chem.* **2014**, *6*, 429.

demonstrated that a novel three-state switchable PPA forming a CSP (left-handed, right-handed and racemic mixture) can alter or even invert the elution order of different racemic mixtures (Figure 39).[123]

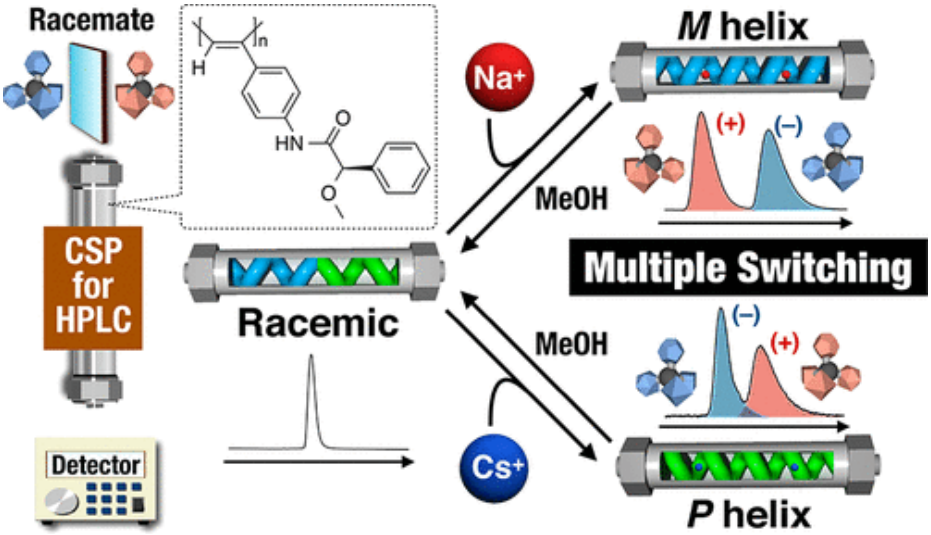

Figure 39. Conceptual representation of three-state switchable PPA forming a CPS for racemates separation.

6.3 Asymmetric Catalysis

Catalysis is one of the most interesting topics in which scientific community has been focused in the last decades. On the one hand, achiral polymers offer the possibility of including chiral ligands as pendant governing the enantioselectivity of the reaction while the polymer just act as support.[124] On the other hand, helical polymers have the inherent chirality of the helix. Thus, optically active helical polymers can act as asymmetric catalysts without employing chiral ligands in the periphery.

Reggelin *et al.,* using a helical poly(methacrylate)s (poly-**23**), described the first example of asymmetric C-C bond formation reaction. The polymers were synthetized by polymerization with TrMA obtaining a one-handed helical polymer. After the polymerization, the complexation with palladium catalyst favors an asymmetric allylic alkylation reaction with a 40-60% *e.e*. (Figure 40a)[125,126]

Another example of helical polymer employed as catalyst consists on a copolymer derived from 4-carboxyphenyl isocyanide and piperazine units (poly-**24**). This copolymer was

[123] Hirose, D.; Isobe, A.; Quiñoá, E.; Freire, F.; Maeda, K.; *J. Am. Chem. Soc.* **2019**, *141*, 8592.

[124] Benaglia, M.; Puglisi, A.; Cozzi, F.; *Chem. Rev.* **2003**, *103*, 3401.

[125] Reggelin, M.; Schultz, M.; Holbach, M.; *Angew. Chem., Int. Ed.* **2002**, *41*, 1614.

[126] Reggelin, M.; Doerr, S.; Klussmann, M.; Schultz, M.; Holbach, M.; *Angew. Chem., Int. Ed.* **2004**, *101*, 5461.

developed by Yashima and co-workers, and presents one preferred helical sense and enantioselectivity in a catalyzed direct aldol reaction between aldehydes and ketones with an *e.e* around 12% (Figure 40b).[127]

Focus on PPA, Maeda and co-workers prepared a series of optically active PPAs derived with oligopeptides as pendants (poly-**25**) in order to know the organocatalytic activities for the epoxidation of chalcone (Figure 40c). The experiments show a great enantioselectivity (34% *e.e*) for the PPAs whereas the monomers yielded poor results (<2% *e.e.*).[128] With these results it is demonstrated the importance of the helical structure of the PPAs in the enantioselectivity of the reaction.

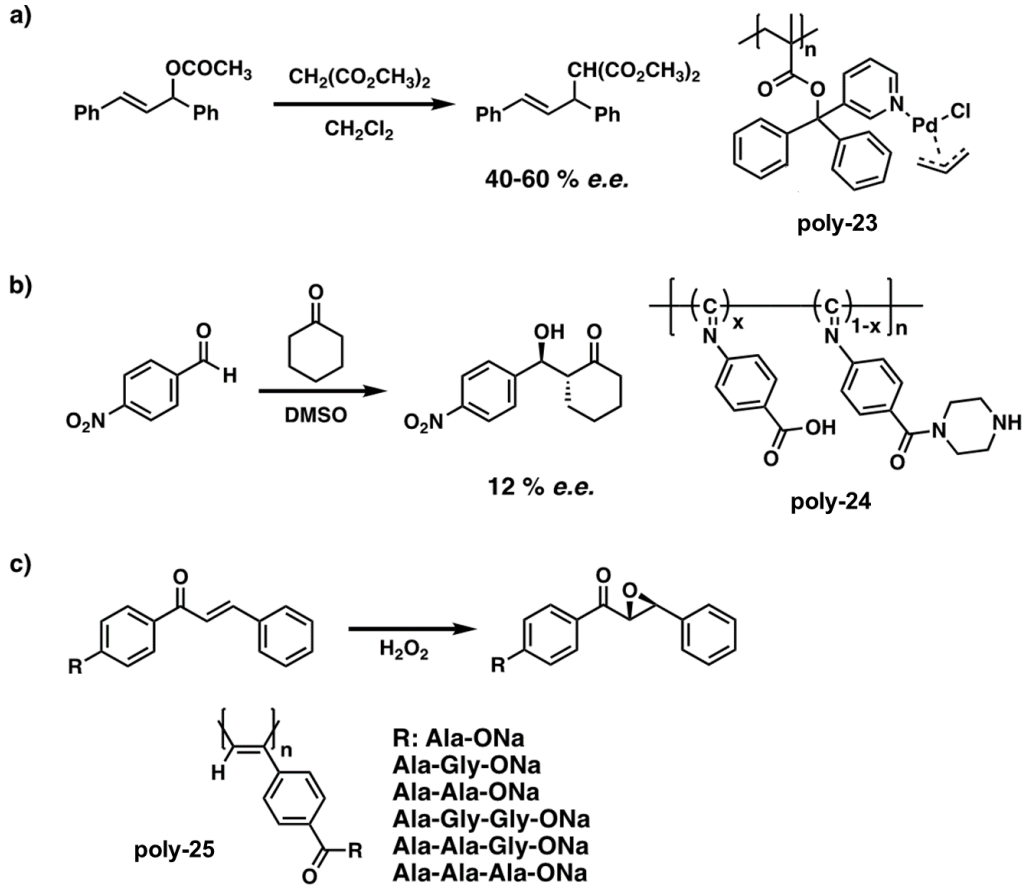

Figure 40. Schematic illustration showing the structure and the reaction of a) poly-**23**, b) poly-**24** and c) poly-**25**.

Recently, in another interesting work of Yashima *et al.*, they reported an unprecedented enantioselectivity of a PPA prepared by the polymerization of a racemic monomer. Thus, both right- and left-handed helical poly(biarylylacetylene) (PBA) composed of dynamically racemic

[127] Miyabe, T.; Hase, Y.; Lida, H.; Maeda, K.; Yashima, E.; *Chirality* **2009**, *21*, 44.

[128] Maeda, K.; Tanaka, K.; Morino, K.; Yashima, E.; *Macromolecules* **2007**, *40*, 6783.

2-arylpyridyl-N-oxide monomer units with N-oxide moieties located in the vicinity of the helical polymer backbone can be produced by noncovalent interaction with a chiral alcohol through deracemization of the biaryl pendants. In addition, the macromolecular helicity of the polymer and the axial chirality induced in the pendants are memorized after complete removal of the external stimulus allowing a remarkable enantioselectivity (86% *e.e.*) for the asymmetric allylation of benzaldehyde.[129]

7. Poly(disubstitutedacetylene)s (PDSAs)

During the last decades, conjugated polymers (CPs) have demonstrated to be excellent options to use as materials due to their optical and electronic properties. As explained, PAs and PPAs have interesting properties and possible application but they have some limitations. For instance, stability and processability are one of the most inconvenient for their use as practical materials. To avoid these problems, disubstitution of the acetylenic unit has emerged as an option to improve not only the depicted features, but also others like an efficient fluorescence emission or an excellent circular polarized luminescence (CPL) among others.[130]

7.1 Polymerization of Poly(disubstitutedacetylene)s

PDSAs have demonstrated some advantages in contrast to monosubstituted acetylenes. Thus, higher thermal and chemical stability are obtained when bulky substituents are used due to the protection of the polyenic skeleton. However, the polymerization of disubstituted acetylenes is complicated and some considerations must be considered. For instance, monomers bearing polar groups cannot be polymerized directly due to the poisoning of the catalysts employed during these reactions. This occurs because the Rh-based catalyst employed in the polymerization of monosubstituted PAs cannot polymerize disubstituted ones and it is necessary to employ traditional metathesis catalysts as Mo, W or Nb.[131,132]

The polymerization of acetylenic monomers has demonstrated a selectivity between the monomer structure and catalyst employed. Thus, a slight variation in the monomer structure can completely change the catalyst required (Figure 41, 42a).[131]

[129] Ikai, T.; Ando, M.; Ito, M.; Ishidate, R.; Suzuki, N.; Maeda, K.; Yashima, E. *J. Am. Chem. Soc.* **2021***, 143*, 12725.

[130] Wang, X.; Sun, J. Z.; Tang, B. Z. *Progress in Polymer Science*, **2018,** *79*, 98.

[131] Lam, J. W.; Tang, B. Z. *Acc. Chem. Res.*, **2005**, *38*, 745.

[132] Liu, J.; Lam, J. W.; Tang, B. Z. *Chem. Rev.*, **2009**,*109*, 5799.

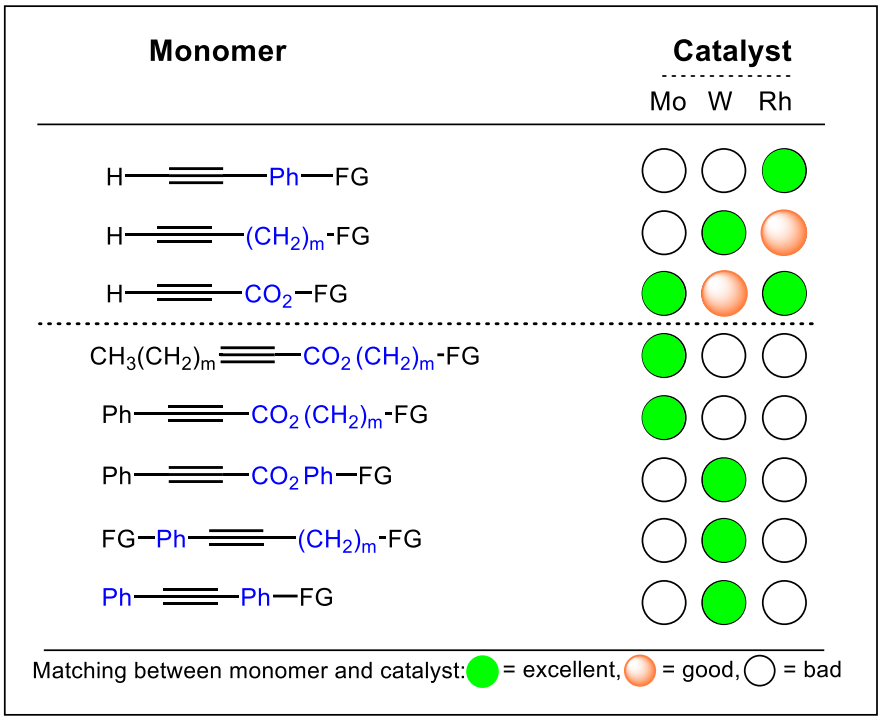

Figure 41. Illustration of the relation between monomer structure and catalyst for a better polymerization.

Moreover, additional points (co-catalyst, solvent, temperature…) must be considered. On the one hand, it is usual to employ these catalysts with a co-catalyst based on Sn (*e.g.* Ph_4Sn or Bu_4Sn). The appropriate choice of this co-catalyst depends on the monomer structure and it will permit its polymerization (Figure 42b). [131]

On the other hand, polymerization of monosubstituted acetylenes occurs easily at room temperature and in polar solvents (*e.g.* Dioxane, DMF) and has poor yields in low polar solvents. In the case of disubstituted acetylenes, they are usually polymerized at high temperature in non-polar solvents (*e.g.* toluene) to avoid the poisoning of the catalyst (Figure 42c). [131]

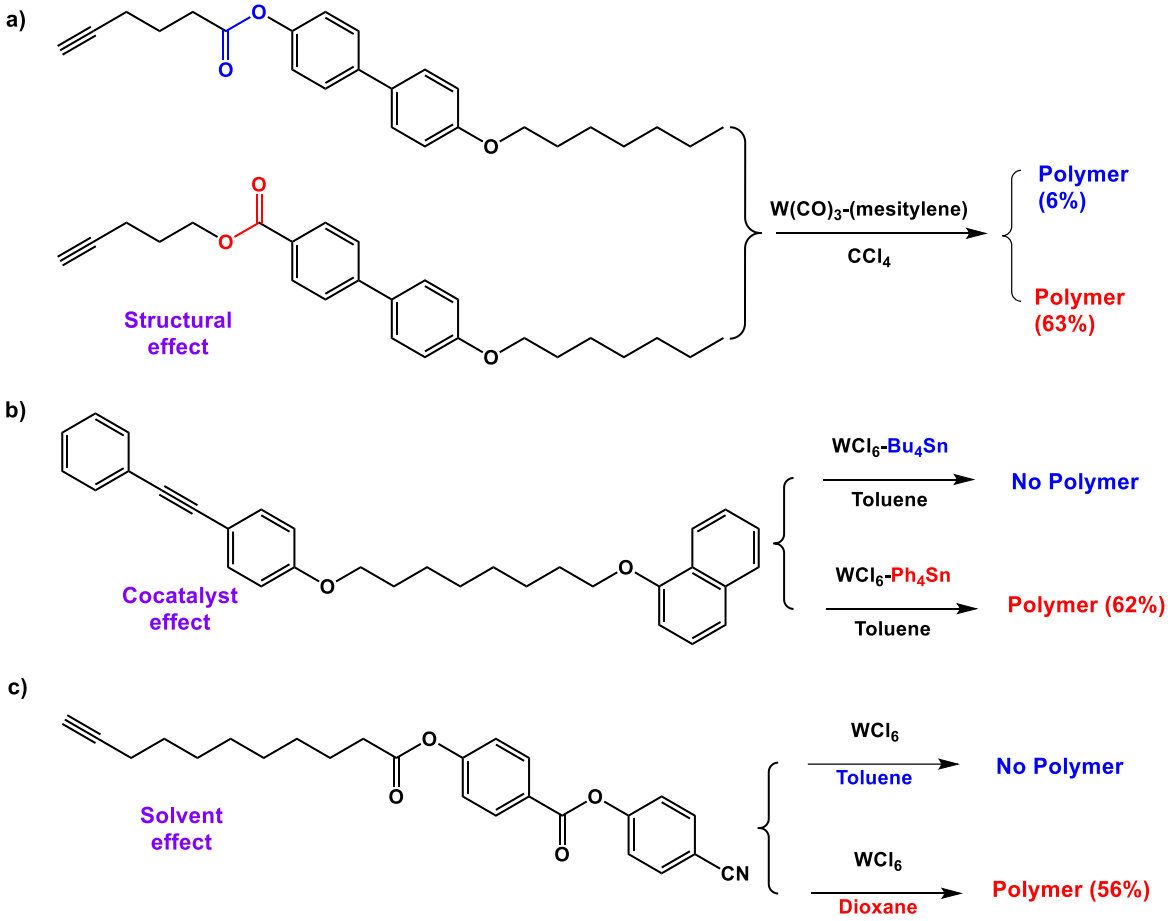

Figure 42. Illustration of different conditions of polymerization yielding final polymers or not.

In recent years, some advances have been achieved in the development of new catalysts to polymerize disubstituted acetylenes bearing polar functional groups. Moving to late transition metals as Pd, with lower oxophilicity and higher resistance to polar groups, would permit a wide variety of polymer synthesis.

In 2014, Sanda *et al.* prepared a Pd-monophosphine catalyst with good results (Figure 43a). The yield was over 77% with high molecular weights of the polymers synthetized. These results are comparable with the classical transition metals (*e.g.* W, Nb, Ta…). In this case and contrary to the classical catalysts, a *cis*-rich double bonds content was obtained in the polymers after analyzing them by ^{13}C NMR and Raman spectroscopy.[133]

In 2015, the same group discovered that increasing the electro-withdrawing of the phosphine ligand used in the catalyst of Pd (Figure 43b), also increased the polymerization activity. In this way, the monomer coordination is higher and offers better results during the polymerization.[134]

[133] Castanon, J. R.; Sano, N.; Shiotsuki, M.; Sanda, F. *ACS Macro Letters*, **2014**, *3*, 51.

[134] Castanon, J. R.; Murayama, Y., Sano, N.; Sanda, F. *Chem. Lett.*, **2015**, *44*, 1200.

These incursions in the development of new catalysts were very successful. However, Pd-based catalysts, until now, can only polymerize chloro-disubstituted acetylenes.

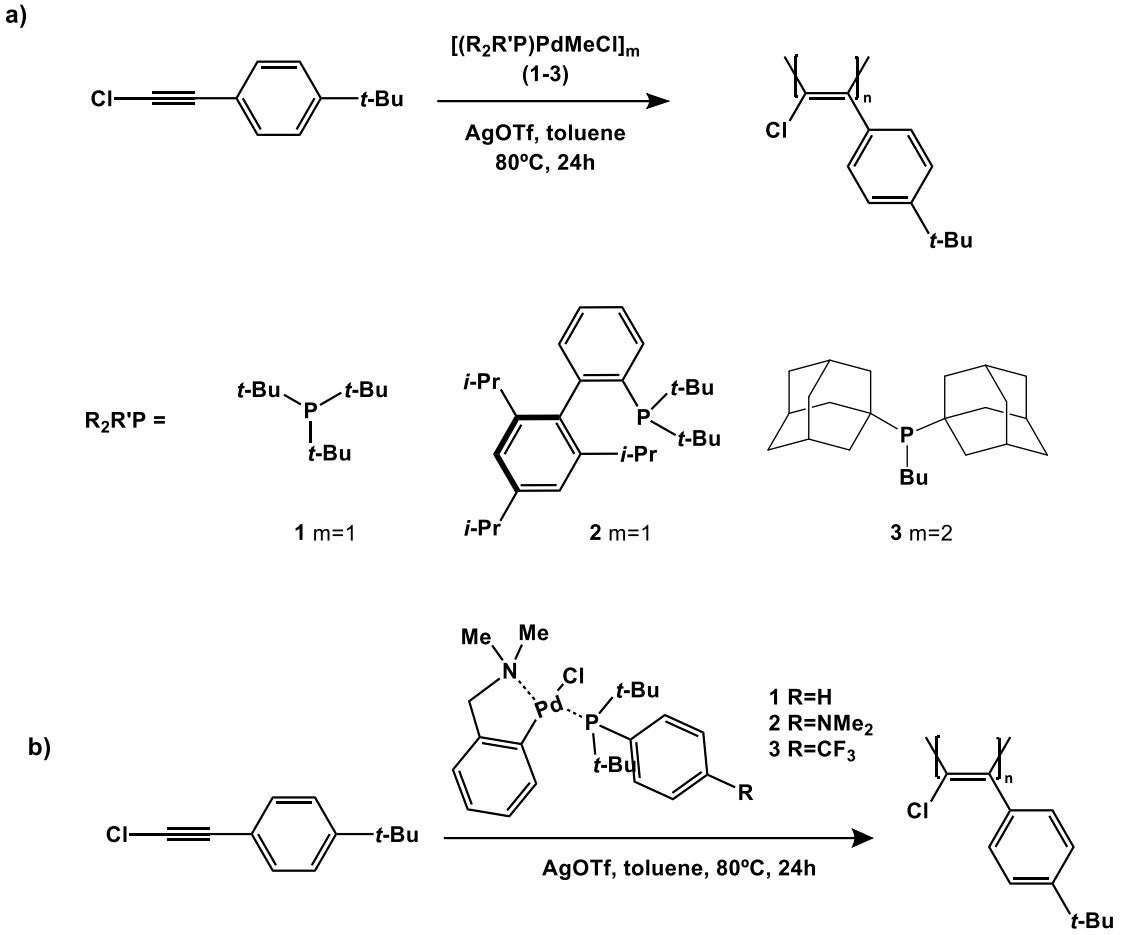

Figure 43. Polymerization of 1-chloro-2-(4-*tert*-butyl)phenylacetylene with different Pd-based/AgOTf catalysts.

7.2 Post-Polymerization Strategies

Taking in account the previously considerations reported, the low tolerance of the catalysts to the polar functional groups creates an important limitation in the development of functional and practical materials. To avoid this problem, post-polymerization reactions have been employed to introduce several polar functionalities into the main polymer.

Tang's group made some of the best contributions to this field during the last two decades. They worked mainly with asymmetrically substituted poly(diphenylacetylene)s (PDPAs). This family of PDSA has demonstrated a great thermal resistance due to the presence of two bulky aryl rings that protect the double bonds skeleton of the thermolytic attack.[135]

[135] Masuda, T.; Tachimori, H. *J. Macromol. Sci., Part A*, **1994**, *31*, 1675.

Some of the reactions used include: photopolymerizable vinyl groups as pendants,[136] Michael addition,[137] direct substitution via activated ester strategy[138] or even the use of click chemistry (Figure 44).[139,140]

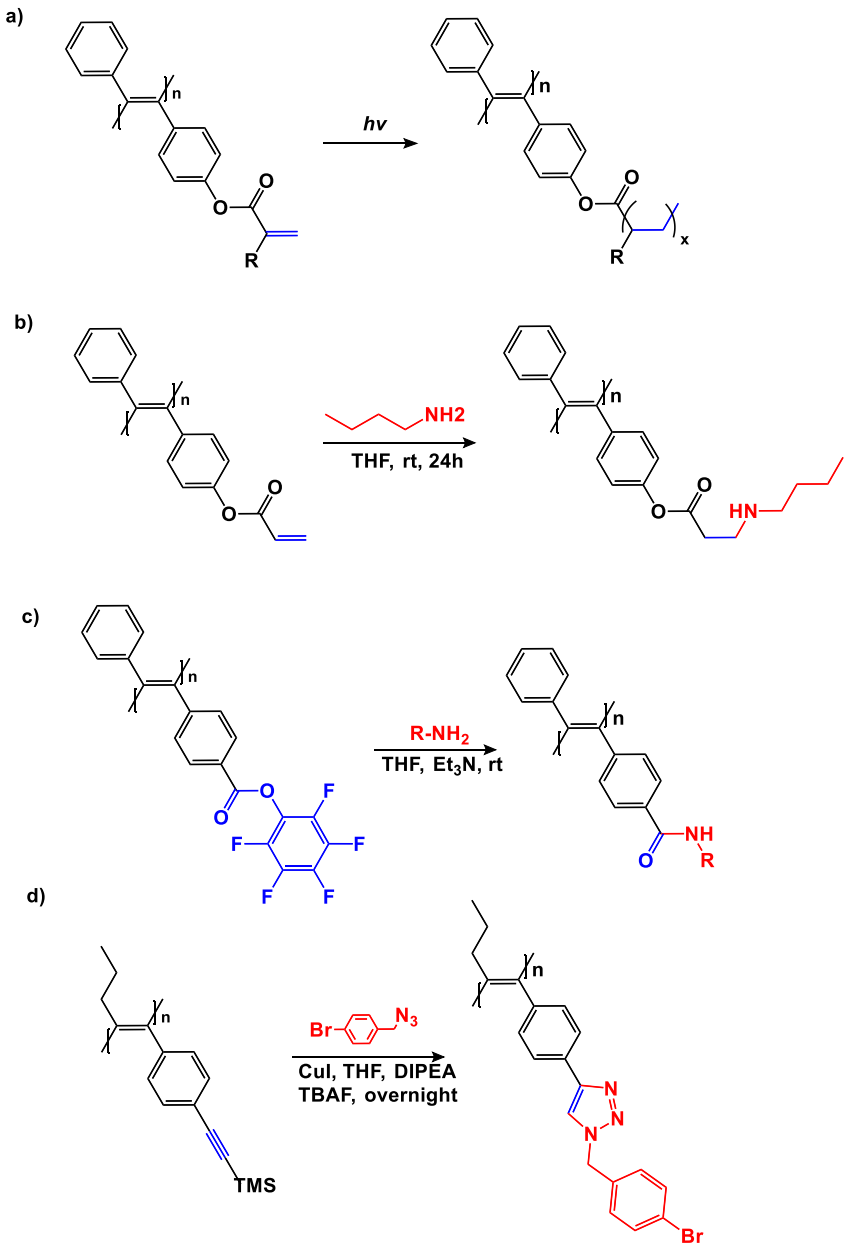

Figure 44. Different post-polymerization reactions carried out on several PDSAs. a) Photopolymerization of vinyl group. b) Michael addition. c) Direct substitution. d) Click reaction.

[136] Yuan, W. Z.; Qin, A.; Lam, J. W.; Sun, J. Z.; Dong, Y.; Häussler, M.; Liu, J.; Xu, H. P.; Zheng, Q.; Tang, B. Z. *Macromolecules*, **2007**, *40*, 3159.

[137] Gao, Y.; Wang, X.; Tong, L.; Qin, A.; Sun, J. Z.; Tang, B. Z. *Polym. Chem.*, **2014**, *5*, 2309.

[138] Zhang, X. A.; Qin, A.; Tong, L.; Zhao, H.; Zhao, Q.; Sun, J. Z.; Tang, B. Z. *ACS Macro Letters*, **2012**, *1*, 75.

[139] Tong, L.; Qin, A.; Zhang, X.; Mao, Y.; Sun, J.; Tang, B. Z. *Science China Chemistry*, **2011**, *54*, 1948.

[140] Wang, X.; Hu, H.; Wang, W.; Qin, A.; Sun, J. Z.; Tang, B. Z. *Polym. Chem.*, **2015**, *6*, 7958.

7.3 Structural Elucidation of PDPAs

As it was mentioned for PPAs, the complete elucidation of the secondary structure of a helical polymer is a huge challenge and only attainable with the combination of different techniques. Moreover, it is an essential work that must be done to understand the correlation between structure-function of a material to attain practical applications. This work starts knowing the stereoregularity of the double bonds that conforms the helical structure of these polymers.

On the one hand, there are only a few examples of works where the structure of a PDPA is mentioned. In these, some basic calculations[141] are used or directly ascribe the structure to the catalyst employed just by the knowledge of this. Thus, classical transition metals (*e.g.* W, Mo, Ta, Nb) adopt to play an important role in achieving *trans*-rich configuration of double bonds.[142]

In addition, there are a few examples where some differences between *cis*-rich polymers and *trans*-rich polymers are found.[143] Techniques used to observe these differences are ^{1}H-NMR or Raman spectroscopy.[144]

On the other hand, it is well known that Rh-based catalysts provide *cis*-rich polymers, but its impossibility to polymerize disubstituted acetylenes doesn't allow to take them in account. Nevertheless, there are some examples already mentioned where *cis*-PDSAs have been synthetized. This was achieved using Pd-based catalysts and the polymers were characterized by Raman and ^{13}C-NMR, but the monomers are restricted to be chloro substituted in one side of the acetylenic unit. Moreover, the synthetized polymers are shorter

[141] a) Lee, W. E.; Oh, C. J.; Park, G. T.; Kim, J. W.; Choi, H. J.; Sakaguchi, T.; Fujiki, M.; Nakao, A.; Shinohara K.; Kwak, G. *Chem. commun.*, **2010**, *46*, 6491.; b) Kim, H.; Lee, D.; Lee, S.; Suzuki, N.; Fujiki, M.; Lee, C. L.; Kwak, G. *Macromol. Rapid Commun.*, **2013**, *34*, 1471.

[142] a) Lam, J. W. Y.; Dong, Y.; Cheuk, K. K. L.; Tang, B. Z. Macromolecules, **2003**, 36, 7927.; b) Lam, J. W. Y.; Dong, Y. P.; Cheuk, K. K. L.; Law, C. C. W.; Lai, L. M.; Tang, B. Z. Macromolecules, **2004**, 37, 6695.; c) Grubbs, R. H. Handbook of Metathesis; Wiley-VCH: New York, **2003**.; d) Metathesis Polymerization of Olefins and Polymerization of Alkynes; Imamoglu, Y., Ed.; Kluwer: Dordrecht, **1998**.; e) Choi, S. K.; Lee, J. H.; Kang, S. J.; Jin, S. H. Prog. Polym. Sci. **1997**, 22, 693.; f) Charvet, R.; Novak, B. M. Macromolecules, **2001**, 34, 7680.; g) Benedicto, A. D.; Novak, B. M.; Grubbs, R. H. Macromolecules, **1992**, 25, 5893.; h) McGowan, K. P.; O'Reilly, M. E.; Ghiviriga, I.; Abboud, K. A.; Veige, A. S. *Chem. Sci.*, **2013**, *4*, 1145.

[143] a) Pauly, A. C.; Theato, P. *Polym. Chem.* **2012**, *3*, 1769.; b) Pauly, A. C.; Theato, P.; *Macromol. Rapid Commun.* **2013**, *34*, 516.; c) Gunay, K. A.; Theato, P.; Klok, H.-A. *J. Polym. Sci., Part A: Polym. Chem.* **2013**, *51*, 1.; d) Jin, Y. J.; Kim, H.; Hwang, D. Y.; Teraguchi, M.; Kaneko, T.; Aoki, T.; Kwak, G. *Molecular Crystals and Liquid Crystals*, **2017**, *645*, 50.

[144] Fujii, A.; Hidayat, R.; Sonoda, T.; Fujisawa, T.; Ozaki, M.; Vardeny, Z. V.; Teraguchi, M.; Masuda, T.; Yoshino, K. *Synthetic metals*. **2001**, *116*, 95.

than those attained with a classical catalytic system (*e.g.* WCl_6/Ph_4Sn).[133,134] This is probably due to the very congested structures that would produce many phenyl rings attached to consecutively *cis* double bonds.

Recently, Maeda *et al.* have made some important contributions in the field of symmetrically substituted PDPAs. These polymers have, *a priori*, a structural advantage for its characterization because they avoid the problem of regioregularity during the polymerization (Figure 45b).

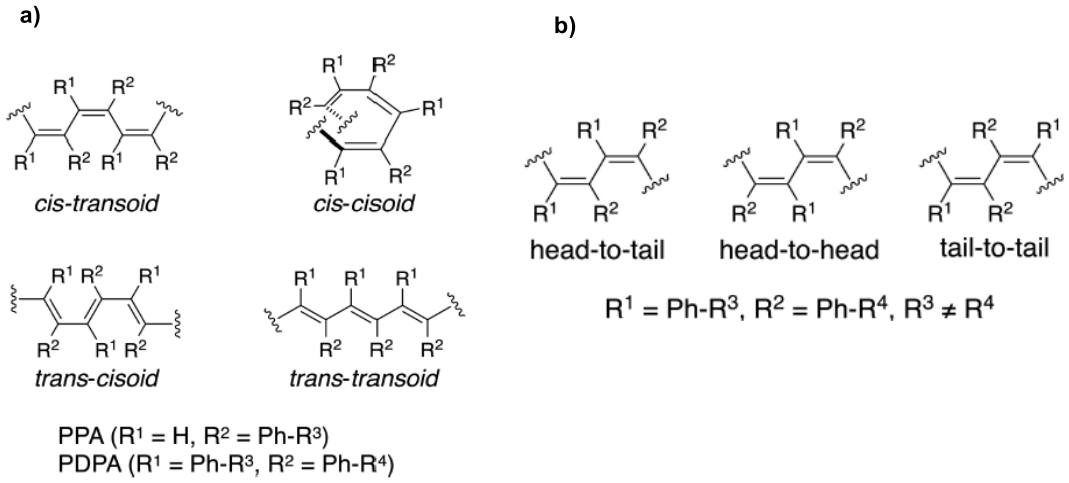

Figure 45. a) Comparative of the four possible stereoregularities for double bonds in PPAs and PDPAs. b) Possible regioregularities that can reach asymmetric PDPAs during the polymerization.

In 2020, they started proposing a *cis*-stereoregular structure of a PDPA derived with a carboxylic acid in each side of the acetylenic unit that can achieve both helical senses with the interaction of different amines (*R*/*S*). It must be mentioned that the monomer employed is polymerized with the classical catalytic system WCl_6/Ph_4Sn that should provide *trans*-rich polymers. They could also observe a memory effect when the amine is removed, and it is not necessary to replace it by an achiral one to preserve the helix. They confirm the *cis* configuration with different techniques such as Raman, NMR and theoretical calculations. Nevertheless, the calculations are ambiguous because they match a *c-t* structure but also a *t-t* one, and the NMR studies are made with the assumption that only the *c-t* structure generates the anisotropy necessary to observe a nonequivalent splitting of the proton signals of the aromatic rings.[145]

[133] Castanon, J. R.; Sano, N.; Shiotsuki, M.; Sanda, F. *ACS Macro Letters*, **2014**, *3*, 51.

[134] Castanon, J. R.; Murayama, Y., Sano, N.; Sanda, F. *Chem. Lett.*, **2015**, *44*, 1200.

[145] Maeda, K.; Nozaki, M.; Hashimoto, K.; Shimomura, K.; Hirose, D.; Nishimura, T.; Watanabe, G.; Yashima, E.; *J. Am. Chem. Soc.*, **2020**, *142*, 7668.

Following the previous work, they revisited the polymerization with the classical catalytic system based on WCl_6/Ph_4Sn to propose a new alternative mechanism to the established of metathesis polymerization. Herein, they could observe by mass spectrometry how a migratory insertion of a phenyl ring of the Ph_4Sn is produced at first step of the polymerization and no evidence could be observed of a metathesis intermediate (Figure 46).[146]

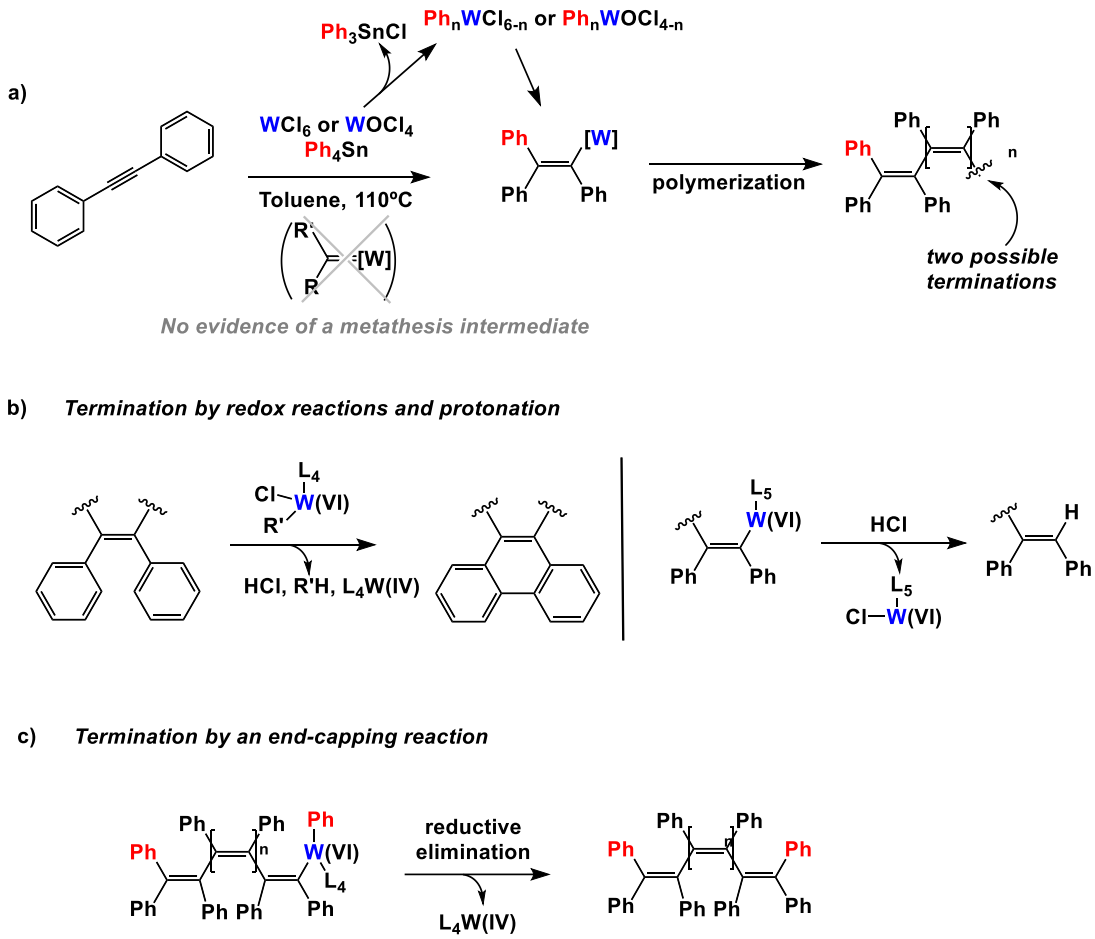

Figure 46. a) Schematic illustration of a polymerization with WCl_6/Ph_4Sn system through a migratory insertion mechanism with a possible termination by b) redox reaction and protonation and c) an end-capping reaction.

Although this work clears out some steps of the polymerization mechanism such as the beginning and the end, the intermediate steps remain unclear. At the high temperature at which the reaction is made, it is well known the *cis*/*trans* isomerization of double bonds in PPAs, so this cannot be completely discarded.[27]

[146] Miyairi, M.; Taniguchi, T.; Nishimura, T.; Maeda, K. *Angew. Chem. Int. Ed.*, **2020**, *59*, 14772.

[27] a) Simonescu, C.I.; Percec, V.; *Prog. Polym. Sci.* **1982**, *8*, 133. b) Simonescu, C.I.; Percec, V. J.; *Polym. Sci.: Polymer Symposia* **1980**, *67*, 43. c) Simionescu, C. I.; Percec, V.; J. *Polym. Sci., Polym. Chem. Ed.* **1980**, *18*, 147. d) Simionescu, C. I.; Percec, V.; J. Polym. Sci., *Polym. Lett. Ed.* **1979**, *17*, 421. e) Simionescu, C. I.; Percec, V.; Dumitrescu, S. J. *Polym. Sci., Polym. Chem. Ed*. **1977**, *15*, 2497.

7.4 Properties and Applications of PDPAs

PDPAs are a special class of helical polymers so they present many of the properties already explained in previous sections. For this, a recompilation of those more important will be summarized next.

7.4.1 Stiffness and Resistance

PDPAs have a better chemical, thermal and photochemical resistance than their homologous PPAs. This is ascribed to the disubstitution of the polyene backbone with bulky aryl rings.[135] This fact increases a lot the restriction of movement along the polyenic chain resulting in structures with a high stiffness. For this, PDPAs just adopt one preferred helical sense and this cannot be modified. Then, PDPAs can be classified as static helical polymers.

7.4.2 Chiral Induction and Memory Effect

During the polymerization of DPAs monomers, it is usual to obtain polymers non-active in CD. Moreover, most of the reported polymers are formed from achiral monomers and to give them a specific handedness it is necessary to apply an external stimulus. As it is mentioned above, PDPAs adopt one preferred helical sense after a thermal annealing at high temperature through a chiral induction phenomenon. This occurs with achiral solvents[147,148,138] when a chiral pendant is presented on the polymer or even with chiral solvents[141b,149] when the pendant is achiral.

In the best of my knowledge, just one PDPA has been reported with the ability of achieve both helical senses (*M*/*P*) using another external stimulus different to solvent change. This is the symmetrically substituted PDPA derived with carboxylic acids in each side prepared for Maeda and co-workers that can achieve both helical senses changing the chirality of the amine employed for the supramolecular interaction. Moreover, after removed this amine, the

[135] Masuda, T.; Tachimori, H. *J. Macromol. Sci., Part A*, **1994**, *31*, 1675.

[147] Maeda, K.; Maruta, M.; Shimomura, K.; Ikai, T.; Kanoh, S. *Chemistry Letters*, **2016**, *45*, 1063.

[148] Kim, H.; Seo, K. U.; Jin, Y. J.; Lee, C. L.; Teraguchi, M.; Kaneko, T.; Aoki, T.; Kwak, G. *ACS Macro Letters*, **2016**, *5*, 622.

[138] Zhang, X. A.; Qin, A.; Tong, L.; Zhao, H.; Zhao, Q.; Sun, J. Z.; Tang, B. Z. *ACS Macro Letters*, **2012**, *1*, 75.

[141] b) Kim, H.; Lee, D.; Lee, S.; Suzuki, N.; Fujiki, M.; Lee, C. L.; Kwak, G. *Macromol. Rapid Commun.*, **2013**, *34*, 1471.

[149] Seo, K. U.; Jin, Y. J.; Kim, H.; Sakaguchi, T.; Kwak, G. *Macromolecules*, **2018**, *51*, 34.

[145] Maeda, K.; Nozaki, M.; Hashimoto, K.; Shimomura, K.; Hirose, D.; Nishimura, T.; Watanabe, G.; Yashima, E. **2020**, *J. Am. Chem. Soc.*, *142*, 7668.

helical conformation remains unaltered observing a memory effect of the macromolecular helicity.[145]

7.4.3 Abnormal Sergeants and Soldiers Effect

Informational transmission mechanisms have been widely studied in different helical polymers such as poly(phenylacetylene)s[55,92,98,100,101] or poly(isocyanate)s.[96] However, these are not so studied on poly(diphenylacetylene)s.

Maeda *et al.* in another work of symmetrically substituted PDPAs could evaluate an abnormal Sergeants and Soldiers (S&S) effect. The S&S effect occurs when a chiral sergeant is able to organize an achiral soldier in a copolymer observing the same CD than the sergeant homopolymer. Thus, the abnormal S&S effect consists in stabilizing the opposite helical sense of the sergeant homopolymer.

Herein, they evaluated the chiroptical properties of the PDPA by changing the chiral/achiral amine ratio employed in the post-polymerization coupling. Thus, in function of the ratio used, they could achieve both helical senses of the helix. Using these two different helices as CSP for HPLC, they could also observe how different enantiomers can be completely separated and the elution time inverts depending on the helix (*M* or *P*) used.[150]

[55] Freire, F.; Seco, J. M.; Quiñoá, E.; Riguera, R.; *Angew. Chem. Int. Ed.* **2011***, 50,* 11692.

[92] Arias, S.; Freire, F.; Quiñoá, E.; Riguera, R.; *Polym. Chem*. **2015**, *6*, 4725.

[98] Bergueiro, J.; Freire, F.; Wendler, E. P.; Seco, J. M.; Quiñoá, E.; Riguera, R. *Chem. Sci.* **2014**, *5*, 2170.

[100] Cobos, K.; Quiñoá, E.; Riguera, R.; Freire, F.; *J. Am. Chem. Soc.* **2018**, *38*, 12239.

[101] Arias, S.; Rodríguez, R.; Quiñoá, E.; Riguera, R.; Freire, F; *J. Am. Chem. Soc.* **2018**, *140*, 667.

[96] a) Green, M. M.; Park, J.-W.; Sato, T.; Teramoto, A.; Lifson, S.; Selinger, R. L. B.; Selinger, J. V. *Angew. Chem. Int. Ed.* **1999**, *38*, 3138. b) Green, M. M.; Peterson, N. C.; Sato, T.; Teramoto, A.; Cook, R.; Lifson, S. *Science* **1995**, *268*, 1860. c) Green, M. M.; Garetz, B. A.; Munoz, B.; Chang, H. P.; Hoke, S.; Cooks, R. G. *J. Am. Chem. Soc.* **1995**, *117*, 4181.

[150] Maeda, K.; Maruta, M.; Sakai, Y.; Ikai, T.; Kanoh, S. *Molecules*, **2016**, *21*, 1487.

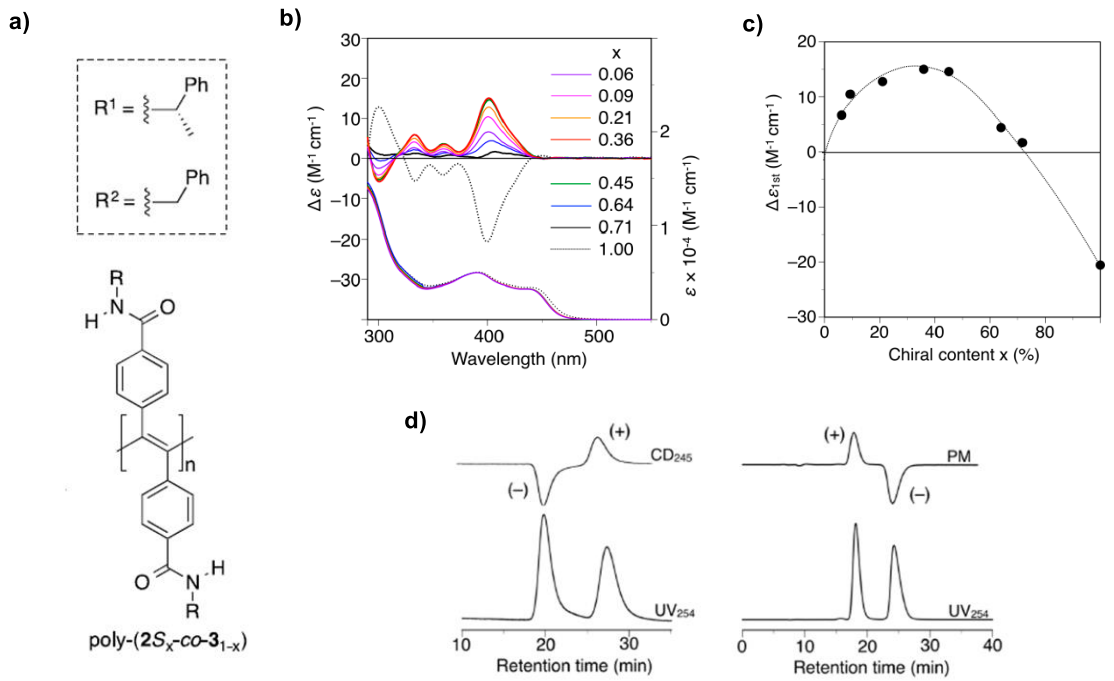

Figure 47. a) Schematic illustration of copolymer structure. b) CD spectra of different copolymers in DMF after thermal annealing. c) the Δε1st values vs chiral content. d) Inversion of the elution time of two enantiomers using poly-**2***S* and poly-(**2**$S_{0.36}$-co-**3**$_{0.64}$) respectively as CSP.

7.4.4 Nanostructuration

Although helical polymers, specifically PPAs, have a huge amount of works based on nanostructuration,[49] in PDPAs this ability has not been so explored.

Recently, Jianping Deng and co-workers have prepared some polymeric spherical particles based on PDSAs. They used the precipitation polymerization methodology to prepare them. This approach consists on the polymerization of a monomer in a solvent mixture where the formed polymer is insoluble (Figure 48a).

On the one hand, they prepared chiral cross-linked polymeric microspheres (CCPMs) using a chiral disubstitutedacetylenic monomer together with a crosslinker. These CCPMs show CD activity demonstrating that are formed by chiral helical polymers. On the other hand, they could prepare some achiral polymeric spherical NPs based on PDSAs following the same approach.[151]

Kwak's group has also developed some chiral spherical NPs through the nanoprecipitation method. This consists on developing the polymer particles by precipitation adding to the polymer solution a cosolvent where it has poor solubility (Figure 48b). In this

[49] Freire, F.; Quiñoá, E.; Riguera, R. *Chem. Rev.* **2016**, *116*, 1242.

[151] Zhang, Y.; Wu, Y.; Xu, R.; Deng, J. *Polym. Chem.*, **2019**, *10*, 2290.

work, the polymer used is achiral and the solvent's chirality is transferred to the polymeric NPs.[152]

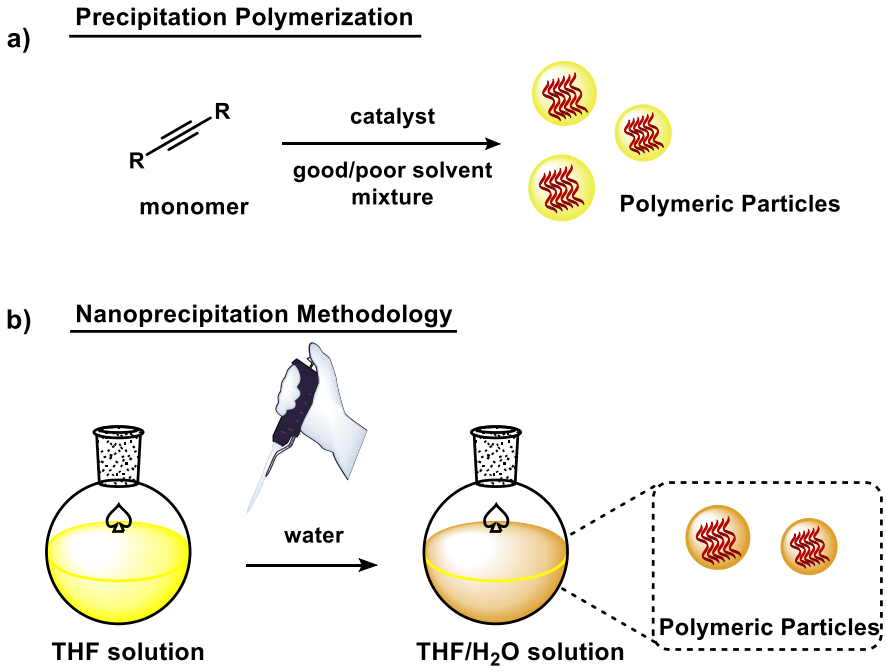

Figure 48. Schematic illustration of a) precipitation polymerization and b) nanoprecipitation methodologies to prepare polymeric particles.

7.4.5 Fluorescence Emission

Emission ability is one of the most important features of PDPAs that opens new possibilities to use them as materials in contrast to non-fluorescent PPAs. Kwak's group has made the best contributions in this topic and they will be depicted following.

In 2010, Kwak *et al.* analyzed the effect of the substitution position in an achiral PDPA on the photoluminescence emission. Thus, they could observe a decreasing in the fluorescence recorded when the pendant is in *meta* position in contrast to the *para* position. They explained this phenomenon because of the difference in the intramolecular π-stacking in the polymer structure proposing a zig-zag scaffold to the *para* and a helical structure to the *meta* polymers.[141a,153]

Through a nanoprecipitation method, Tang's group demonstrated an Aggregation Enhanced Emission (AEE) solving a PDPA bearing a chiral menthyl pendant group. Thus, with

[152] Kim, H.; Jin, Y. J.; Kim, B. S. I.; Aoki, T.; Kwak, G. *Macromolecules*, **2015**, *48*, 4754.

[141] a) Lee, W. E.; Oh, C. J.; Park, G. T.; Kim, J. W.; Choi, H. J.; Sakaguchi, T.; Fujiki, M.; Nakao, A.; Shinohara K.; Kwak, G. *Chem. commun.*, **2010**, *46*, 6491.

[153] Jin, Y. J.; Seo, K. U.; Choi, Y. G.; Teraguchi, M.; Aoki, T.; Kwak, G. *Macromolecules*, **2017**, *50*, 6433.

different mixtures of THF/H_2O or THF/Hexane, they could observe the raising of the fluorescence emission with the increase of cosolvent amount.[154]

Working in the interphase of two immiscible phases, Kwak *et al.* applied in PDPA a new phenomenon named Surfactant-Induced Fluorescence Change (SIFC). Thus, with the use of a surfactant and promoting changes on the surface tension of the water, they reveal a significant enhanced emission of the polymer.[155]

Recently, Kwak and co-workers have studied the influence of the substituent's size on the fluorescence emission. They used an achiral PDPA derived with different alkyl chains. Thus, they observed how the quantum efficiency of the fluorescence emission increased together with the size of the pendant. This is due to the suppression of collisional quenching and decreasing of non-radiative processes of relaxation.[156,148]

7.4.5.1 Circularly Polarized Luminescence

Circularly polarized luminescence (CPL) of organic and polymeric materials has attracted the interest of several groups in the most recent years. This is due to the possibility of creating new photoelectronic devices, light-emitting diodes and optical information storage.[157]

In PDPAs this property has not been widely studied. Thus, only a few examples of PDPAs have been described with this feature.

In 2012, in a fantastic work of Akagi *et al.*, it was described how different PDPAs can form liquid crystals. In this state, they could observe and record the CPL spectrum that is not found in solution or cast films despite they are active in CD.[158]

Recently, Maeda and co-workers working on symmetrically substituted PDPAs have developed two polymers capable of emitting this CPL.

On the one hand, they used a non-covalent interaction with different chiral amines to promote a helical sense in a PDPA bearing two carboxylic acids on each side of the monomeric

[154] Jim, C. K.; Lam, J. W.; Leung, C. W.; Qin, A.; Mahtab, F.; Tang, B. Z. *Macromolecules*, **2011**, *44*, 2427.

[155] Kim, S. I.; Jin, Y. J.; Lee, W. E.; Yu, R.; Park, S. J.; Kim, H. J., Song, K. H.; Kwak, G *Adv. Mater. Interfaces*, **2014**, *1*, 1300029.

[156] Jin, Y. J.; Choi, Y. G.; Kwak, G. *Polym.*, **2019**, *171*, 127-1.

[148] Kim, H.; Seo, K. U.; Jin, Y. J.; Lee, C. L.; Teraguchi, M.; Kaneko, T.; Aoki, T.; Kwak, G. *ACS Macro Lett.*, **2016**, *5*, 622.

[157] Sang, Y.; Han, J.; Zhao, T.; Duan, P.; Liu, M. *Adv. Mater.*, **2020**; *32*, 1900110.

[158] San Jose, B. A.; Matsushita, S.; Akagi, K. *J. Am. Chem. Soc.*, **2012**, *134*, 19795.

[145] Maeda, K.; Nozaki, M.; Hashimoto, K.; Shimomura, K.; Hirose, D.; Nishimura, T.; Watanabe, G.; Yashima, E.; *J. Am. Chem. Soc.*, **2020,** *142*, 7668.

[150] Maeda, K.; Maruta, M.; Sakai, Y.; Ikai, T.; Kanoh, S. *Molecules*, **2016**, *21*, 1487.

repetition unit (m.r.u.). Thus, depending on the helicity promoted (*P* or *M*) in the PDPA, they can achieve a positive or negative CPL spectra.[145]

On the other hand, based on the same acidic PDPA, in this case they employed a covalent coupling with different ratio of chiral/achiral amines achieving both helical senses of the helix. These polymers were used as CSP for HPLC, but also presented the CPL ability.[150]

7.4.6 Applications

Due to the properties explained before, PDPAs have several potential applications in fields such as sensing, chiral separation or chiral recognition among others. In this section, they will be summarized the most interesting and important described up to now.

One of the main applications of PDPAs is their use as sensors. For example, some nanofibers of a PDPA have demonstrated to be especially sensitive to explosive nitroaromatic compound vapors. Thus, when the polymer is exposed to the saturated vapor of 2,4-dinitrotoluene, the nanofibers showed a very fast fluorescence quenching.[159]

Taking advantage of the fluorescent ability of PDPAs, some practical applications can be found also in forensic science. A high visualization method of latent fingerprints has been developed based on the use of a PDPA film. Due to the oily components present in fingerprints, a migration of these to the PDPA film occurs revealing the latent fingerprint in fluorescent images (Figure 49a). This is produced by a swelling-induced emission enhancement (SIEE) phenomenon.[160] SIEE is related to the molecular-scale porosity and conformation-variable structure. For this, it also permits the determination of various solvent viscosities.[161]

The fluorescent quenching also permits the detection of water in solvents. Thus, when a film is immersed in solvents the fluorescence decreases due to deswelling. Based on this, a fluidic channel with the inner wall coated with a PDPA was fabricated to real-time monitoring of water in flowing solvents (Figure 49b).[162]

Working in water, a sulfonated PDPA can be turned on/off in presence or absence of a positive charged protein as lysozyme. Depending on the size of the protein, fluorescence and average lifetime vary significantly which permits to the PDPA the discrimination of different proteins based on the highly sensitive fluorescence turn-on response.[163]

[159] Lee, W. E.; Oh, C. J.; Kang, I. K.; Kwak, G. *Macromol. Chem. Phys.*, **2010**, *211*, 1900.

[160] Kwak, G.; Lee, W. E.; Kim, W. H.; Lee, H. *Chem. Commun.* **2009**, 2112.

[161] Lee, W. E.; Lee, C. L.; Sakaguchi, T.; Fujiki, M.; Kwak, G. *Macromolecules*, **2011**, *44*, 432.

[162] Han, D. C.; Jin, Y. J.; Lee, J. H.; Kim, S. I.; Kim, H. J.; Song, K. H.; Kwak, G. *Macromol. Chem. Phys.*, **2014**, *215*, 1068.

[163] Lee, W. E.; Jin, Y. J.; Kim, S. I.; Kwak, G.; Kim, J. H.; Sakaguchi, T.; Lee, C. L. *Chem. Commun.*, **2013**, *49*, 9857.

Finally, the high stability of PDPAs to photooxidation[164] enables to create a down-conversion layer in organic cell devices. This allows to enhance the operation lifetime of the organic cell because the PDPA absorbs the UV radiation that is the responsible of the active layer degradation and permits the visible light to pass. The PDPA layer can convert this UV light and emit it as fluorescence in the visible region that overlaps with the absorption spectrum of the active layer (Figure 49c).[165]

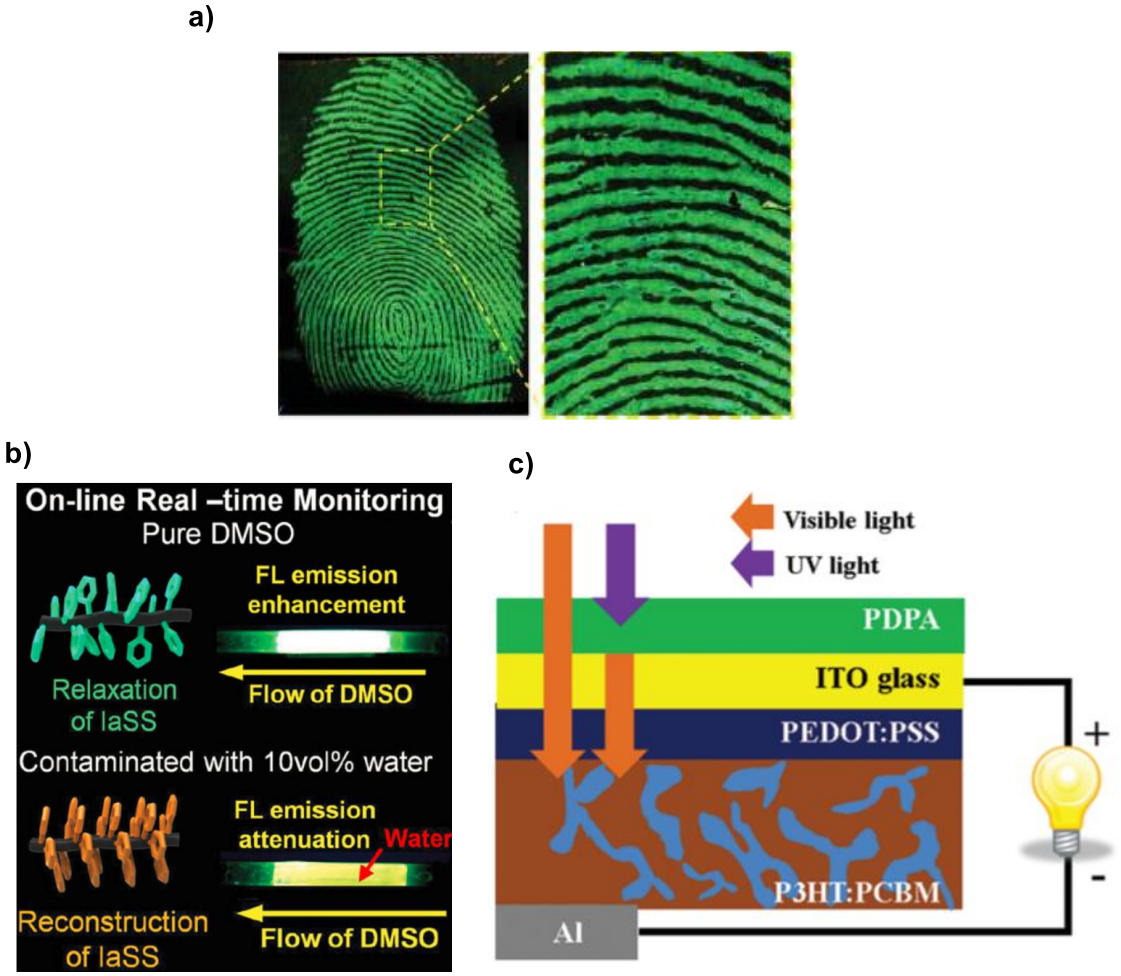

Figure 49. a) FL image of a PDPA film to which a fingerprint was transferred. b) Fluidic channel with the inner wall coated with a PDPA for real-time monitoring of water in flowing solvents. c) Schematic representation of an organic solar cell with a down-conversion layer based on a PDPA.

This thesis is focused on the development of new chiral PDPAs and its complete structural elucidation as well as the evaluation of their properties.

[164] Kwak, G.; Fujiki, M.; Sakaguchi, T.; Masuda, T. *Macromolecules*, **2006**, *39*, 319.

[165] Han, D. C.; Kwak, G.; Kim, Y. B.; Bae, J. J.; Lee, W. H.; Seo, Y. S.; Byun, J. H.; Kang, S. W. *J. Nanosci. Nanotechnol.*, **2014**, *14*, 5937.

Chapter II

Objectives

Objectives

Helical polymers have been widely studied in the last years due to their special properties inherent to the helical scaffold. Fields of possible application of these materials are as varied as asymmetric catalysis, energy storage or conversion, chromatographic separation, or chiral recognition, among others.

This thesis is focused on the synthesis and structural characterization of a novel family of helical polymers denominated poly(diphenylacetylene)s (PDPAs). PDPAs are a type of helical polymers that have been reported in recent years and described as static polymers. In most cases, the different groups that have worked on this topic, they developed achiral PDPAs and did not consider the secondary structure of the polymers. The study of this structure is key for further control of the material's properties, something that only can be achieved by rational design of monomers/polymers.

Taking into account this information, the main objectives of this Doctoral Thesis will be depicted bellow in five chapters.

- ***CHAPTER III. Dissymmetric Chiral Poly(diphenylacetylene)s: Secondary Structure Elucidation and Dynamic Luminescence***

In literature, it can be found several PDPAs asymmetrically substituted by achiral pendants and some examples of chiral substituted. These last have been described as static helical polymers. This means that they can achieve one helical sense, and this cannot be tuned by external stimuli. Moreover, the elucidation of the secondary structure is something avoided due to the difficulty of this kind of analysis in macromolecules.

In this chapter, the main objective was the preparation of a dynamic PDPA and the full analysis of the secondary structure of this polymer to understand from where the properties of the material arise.

Publication associated with this objective: Tarrío, J. J.; Rodríguez, R.; Fernández, B.; Quiñoá, E.; Freire, F. *Angew. Chem. Int. Ed.* **2022**, *61*, e202115070.

- ***CHAPTER IV. The Degree of Polymerization Drastically Determines the Chiroptical Properties of Dynamic Asymmetric Poly(diphenylacetylene)s***

Preliminary computational calculations showed a different behavior in ECD calculated spectra, when different length oligomers were used as model compounds. This is due to the different orientation and contribution to the spectra of the functional groups presented in the polymeric chain (polyene backbone, inner part; phenyl rings, external part of the helix).

Moreover, these results were different from the theoretical calculations reported for similar compounds as PPAs.

The objective of this chapter was to synthetize polymers and oligomers with different length to see if these differences in the CD spectra are also originated experimentally, and to corroborate that is not a different polymerization pathway the reason of these variations.

CHAPTER V. Dynamic P/M Memory Effect of the Macromolecular Helicity in Chiral Poly(diphenylacetylene)s: Kinetic and Thermodynamic Studies

Due to the intrinsic hindered structure of PDPAs provoked by the presence of two aryl rings attached to the acetylenic unit, in this chapter we proposed to take advantage of this to memorize the chiroptical and emissive properties of the PDPAs.

Moreover, kinetic and thermodynamic studies of the helical inversion were calculated to explain why it is necessary to apply a thermal annealing at high temperature to promote the formation – and/or the inversion – of the helical structure.

- ***CHAPTER VI. Complex Aggregation Pathways in Covalent Helical Polymers: Consecutive Mechanism and Kinetically Trapped Aggregates in a PDPA/Mn+ complexes***

In this chapter, our objective was to surpass the stability problems associated to the PPA/M^{n+} complexes and to prepare stable dynamic chiral polymeric particles which can be stored dispersed in solution for months using a PDPA. Moreover, we explored the formation of smart nanomaterials whose induced chirality can be memorized once the external stimulus is removed.

Thus, to perform these studies we used a chiral PDPA that shows a kinetically controlled dynamic helical behavior. Therefore, the two *P*/*M* screw senses can be induced in the PDPA by playing with the conformational composition at the pendant group at high temperature. On the other hand, different metal perchlorate salts [$LiClO_4$ and $Ba(ClO_4)_2$] were used as crosslinking agents to assemble the PDPAs into the desired nanostructures in solvents where the polymer is completely dissolved such as DCE.

- ***CHAPTER VII. Evaluation of Substitution Effects in the Structure, Optical and Chiroptical Properties of Chiral Poly(diphenylacetylene)s***

In literature, there is just one example dealing with *meta*-substituted non-symmetric PDPAs. In that work, Prof. Kwak and collaborators prepare two achiral *meta*- and *para* substituted PDPAs bearing a trimethylsilyl group as pendant. Interestingly, they found that while it is possible to induce a helical sense in the *para*-PDPA by dissolving it into a chiral

solvent such as (*R*)- or (*S*)-limonene, in the *meta*-substituted PDPA the helix induction does not take place.

The objective of this work is to create different chiral helical materials and to compare their properties and structure. For this, a library of several *para*- and *meta*-substituted PDPAs were prepared, and their chiroptical and optical properties, as well as their structure, were analyzed.

Chapter III

Dissymmetric Chiral Poly(diphenylacetylene)s: Secondary Structure Elucidation and Dynamic Luminescence

Chapter III: Dissymmetric Chiral Poly(diphenylacetylene)s: Secondary Structure Elucidation and Dynamic Luminescence

Adapted from: Juan José Tarrío,[a] Rafael Rodríguez,[b] Berta Fernández,[c] Emilio Quiñoá,[a] and Félix Freire[a]*

Author affiliations: [a]Centro Singular de investigación en Química Biolóxica e Materiais Moleculares (CiQUS), Departamento de Química Orgánica and Universidade de Santiago de Compostela, E-15782 Santiago de Compostela, Spain.

[b]WPI Nano Life Science Institute (WPI-NanoLSI), Kanazawa University, Kakuma-machi, Kanazawa 920-1192, Japan.

[c]Departamento de Química Física, Universidade de Santiago de Compostela, Santiago de Compostela 15782, Spain.

Angew. Chem. Int. Ed. **2022**, *61*, e202115070.

Abstract

The secondary structure of a dissymmetric and chiral poly(diphenylacetylene) (PDPA) is elucidated by combining the data from NMR experiments —regioregular head to tail structure—, Raman and IR studies —*E* configuration of the polyene double bonds— and high-resolution AFM images —helical pitch, packing angle and orientation of the external helix—. As a result, an *E-transoidal* polyene backbone describing three coaxial helices is obtained. Theoretical ECD studies of the structure show a good correspondence between experimental and theoretical data and allow deciphering that the first Cotton band is generated by the poly(diphenylacetylene) core and not only by the polyene backbone. The dynamic behavior of poly-(*S*)-**2** is also demonstrated by a helix inversion effect produced by conformational changes at the pendant groups when annealed in solvents with different donor abilities. This phenomenon is accompanied with an inversion of the circular polarized luminescence of the PDPA (CPL switch).

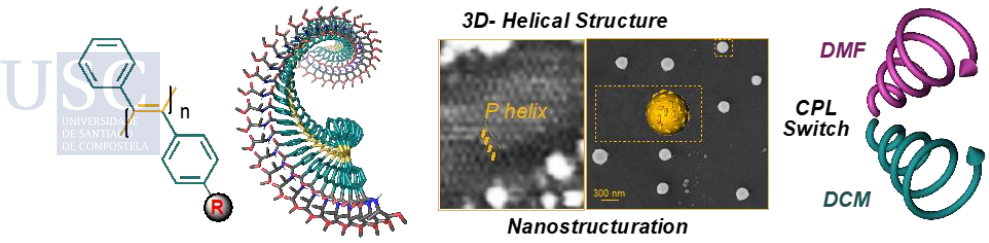

1. Introduction

Molecular engineering allows the design of novel materials with a certain structure and specific properties related to it. Within this topic, modelling new helical structures based on non-natural building blocks —helicenes,[1-3] foldamers,[3-6] supramolecular[7-9] or covalent helical polymers[10-17]— has attracted the attention of the scientific community. These studies are inspired by the structure/function relationships present in biomacromolecules such as peptides, proteins, DNA or polysaccharides. Among non-natural helical scaffolds, dynamic helical polymers constitute a very interesting family due to the possibility of tunning their helical sense or elongation through external stimuli.[19-23] The use of non-natural building blocks to synthetize these polymers allows the creation of smart materials with applications in different fields such as sensing,[24-31] asymmetric synthesis,[32-36] chiral recognition[37] and separation.[38-41] However, in molecular engineering it is mandatory to establish structure/function relationships for these materials, a fact that will allow to determine and, if possible, refine the structural features involved in the functionality of the material.

Unfortunately, the structural elucidation of helical polymers is not straightforward due to the presence of monomer repeating units (m.r.u.) along the polymer chain, rendering powerful structural techniques such as nuclear magnetic resonance (NMR) or X-ray diffraction (XRD) useless. During the last decade a great effort has been made in the structural characterization of poly(phenylacetylene)s (PPAs), fundamentally through a combination of techniques —NMR,[42-43] XRD,[44-52] atomic force microscopy (AFM),[53-61] differential scanning calorimetry (DSC),[62] Raman,[63] circular dichroism (CD),[64-65] vibrational circular dichroism (VCD),[66] Raman optical activity (ROA)[67]—,computational studies[68-69] and reactivity experiments —photochemical electrocyclization of PPAs [67]— that were used to obtain information about different structural parameters of these complex macromolecules and combined to solve the puzzle of the secondary structure of helical polymers.

Another interesting family of helical polymers are the poly(diphenylacetylene)s (PDPAs)[71-94] that resemble PPAs in the main chain, which in both cases is made up of conjugated double bonds. However, the presence of a phenyl group on each carbon of the double bond in PDPAs makes the properties of both materials very different. For instance, PDPAs show better chemical, thermal and photochemical stability compared

to PPAs.[72-85] Moreover, PDPAs exhibit another interesting property that PPAs do not have, i.e. photoluminescence.[82-85,90] As a negative characteristic, PDPAs show a poor dynamic behavior, being necessary to heat them to 80º to induce a helical sense once the external stimuli are modified.[79-85] This depletion of dynamic behavior is a consequence of the introduction of the second phenyl ring in the m.r.u., which congests the helical backbone and where steric repulsion does not favor chiral amplification and helix inversion effects.

PDPAs can be classified in two different groups, symmetric (Scheme 1a) or asymmetric (Scheme 1b), depending on the substitution of the two phenyl rings. Moreover, in both groups the stereoregularity of the polymer depends on the configuration of the double bonds —*Z* or *E*— (Scheme 1a-b), and the dihedral angle between conjugated double bonds, which can adopt either cisoidal or transoidal configuration— $\omega_1 < 90°$ (cisoidal); $\omega_1 > 90°$ (transoidal) (Scheme 1c). Thus, four different possible stereoregularities can be obtained in PDPAs —*Z-cisoidal, Z-transoidal, E-cisoidal and E-transoidal*—, where the *Z*/*E* content depends on the catalyst used for the polymerization reaction and the cisoidal/transoidal configuration is related to the steric hindrance between pendant groups.

The complexity of the system increases in the case of asymmetric PDPAs where different products can be obtained depending on the regioregularity of the polymerization reaction. Thus, head to tail, head to head or tail to tail polymerizations can occur (Scheme 1d), each of them with the four possible stereoregularities at the conjugated polyene backbone.

This fact, in combination with the fully substitution of the double bonds, and therefore of the polyene backbone, makes the extrapolation of structural information obtained for PPAs useless to elucidate the structure of PDPAs.

Only a few examples related to chiral PDPAs[72-85] are found in the literature compared to the large amount of work that has been done with PPAs.[12-33,37-51,95-98] This is due to the difficulty of obtaining the former polymers in the laboratory by polymerization of the corresponding diphenylacetylene monomers (DPA). Thus, while PPAs bearing a large variety of functional groups are easily prepared using a Rh(I) catalyst,[45,51] the synthesis of PDPAs is more complex due to the low tolerability towards polar groups shown by the catalysts used to prepare these materials. For instance, Tang and coworkers developed a synthetic procedure that uses a combination of WCl_6-Ph_4Sn in toluene to polymerize achiral diphenylacetylenes,[74-76] although

following this approach it is not possible to polymerize diphenylacetylenes bearing polar groups due to the poisoning of the catalyst. To prepare polar PDPAs, it is neccessary to first polymerize a diphenylacetylene in which one or both of the aryl rings carry an active pentafluorophenyl ester group (PFP), which is efficiently transformed into a chiral PDPA by a post-functionalization reaction.[81] Interestingly, all the polymers prepared in these conditions do not show an induced helical structure once they are obtained. Thermal annealing is necessary, i.e., 4h at 80 °C, to induce a preferred handedness in the PDPA main chain.[81,86,88,100]

Recently, Maeda and coworkers studied the secondary structure of symmetric PDPAs bearing para-substituted carboxy pendant groups.[79,80] By using a combination of ^{1}H and ^{13}C NMR, IR, Raman, VCD and ECD spectroscopies, they found that this polymer adopts a preferred *cis-transoidal* structure, where *P* or *M*-helical senses can be induced by thermal annealing in water in the presence of chiral amines. On the other hand, in the case of asymmetric PDPAs, Kwak, Aoki and coworkers made great contributions to the study of their luminescent properties and to the achiral-to-chiral transformations of PDPAs.[78,82,85-90] To perform these studies, a catalyst developed by Masuda [$TaCl_5$-n-Bu_4Sn] was used.[77] Also with asymmetric PDPAs, Tang and coworkers reported polymers prepared with the WCl_6-Ph_4Sn[83,84] catalyst that Maeda also employed for the preparation of optically active PDPAs with application as chiral stationary phases.[71] Nevertheless, although several examples of asymmetric PDPAs are found in literature, their secondary structure remains unclear. From these studies it is found that the helical structure adopted by a PDPA depends on the monomer structure[99] and, therefore, to assume that symmetric and asymmetric PDPAs have the same scaffold is a mistake.

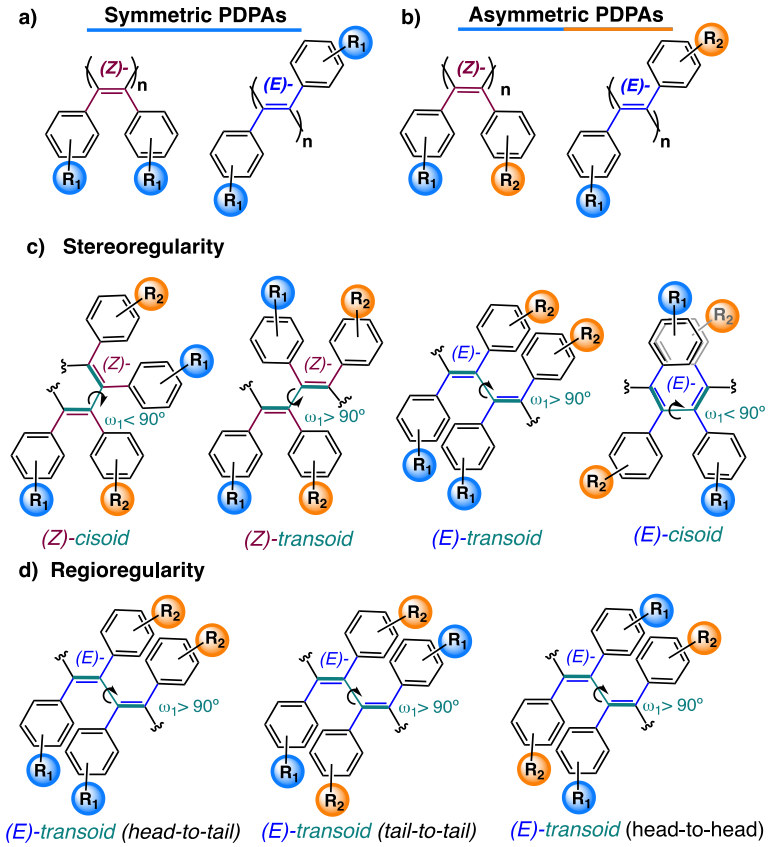

Scheme 1. General molecular structure of (a) symmetric and (b) asymmetric PDPAs. c) Stereoregularity of a PDPA obtained via head to tail polymerization. d) Regioregularity in a PDPA with an (*E*)-transoidal polyene backbone.

Herein, we will study the secondary structure of chiral and asymmetric PDPAs obtained from polymerization of an achiral diphenylacetylene, where one of the aryl rings carries an active pentafluorophenyl ester (PFP) group, while the other phenyl ring remains unaltered.[81] This approach is one the most widely used in the preparation of asymmetric PDPAs. The stereo and regioregularity of the polymer will depend on the synthesis of the first PDPA, which bears the PFP as pendant group and that is further transformed in a chiral PDPA. Thus, through a post-functionalization reaction, the PDPA bearing the 4-benzamide of alanine methyl ester as pendant group will be prepared and its secondary structure elucidated.

2. Results and Discussion

The synthesis of the achiral and asymmetric precursor, perfluorophenyl 4-(phenylethynyl)benzoate, and its subsequent polymerization to obtain poly-**1** using a mixture of WCl_6-Ph_4Sn as catalyst, was carried out according to the methods previously reported.[83,84]

The number average molar mass (M_n) and molar mass dispersity (M_w/M_n) of poly-**1** were 1.4 x 10^4 and 1.43 respectively, as determined by gel permeation chromatography (GPC) using THF as eluent and polystyrene narrow standards (PSS) as calibrants. Taking advantage of the active ester present as pendant group, poly-**1** was effectively transformed into poly-(*S*)-**2** by coupling with NH_2-Ala-OMe under common peptide coupling conditions (Figure 1), as confirmed by ^{19}F NMR and IR studies that corroborated the disappearance of the signals corresponding to the pentafluorophenol moeity (See SI).

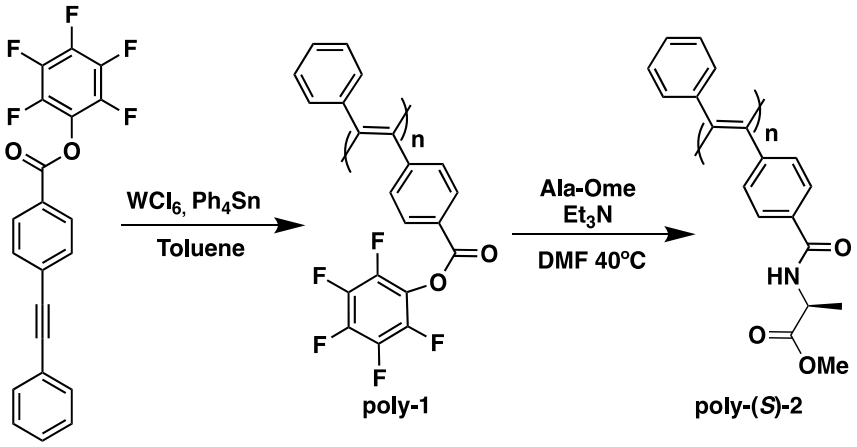

Figure 1. Synthetic approach to prepare poly-1 and poly-(S)-2.

Once poly-**1** and poly-(*S*)-**2** were obtained, their stereo- and regioregularity were analyzed using IR, Raman, and NMR techniques as structural tools.

Raman spectroscopy is a powerful structural technique that provides useful information related to the stereoregularity of the conjugated double bonds.[83] It is commonly applied to assess *cis*- or *trans*-content in PPAs and PDPAs.[51,100,101] Catalysts based on tungsten (W) are known to provide *trans*-rich PDPAs as shown in many examples in the literature,[100,101] albeit Maeda recently demonstrated that in the case of symmetric PDPAs, polyene backbones with a predominant *cis*-content of double bonds are also obtained.[79-80]

Herein, we will study the stereoregularity of poly-**1** and poly-(*S*)-**2** by comparison of their Raman spectra with those obtained for PPAs with well-known secondary structure. Therefore, as model compounds we chose poly-(**3**-**6**) (Figure 2a). Poly-**3**[101] and poly-**4**[54] were selected due to their resemblance with poly-**1** and poly-(*S*)-**2**, while poly-**5**[70] and poly-**6** were chosen due to the possibility of generating a *trans*-PPA (*E*-PPA, poly-**6**) by isomerization of a *cis*-PPA (*Z*-PPA, poly-**5**) (Figure 2a). The isomerization

of the polyene backbone proceeds through the generation of a delocalized radical cation in the polyene when the anilide group of the PPA interacts with Au^{3+} (see SI).

Carefully examination of the Raman spectra unambiguously reveals clear differences for the polymeric backbones containing *cis* or *trans* double bonds. While polymers with a high content of *cis* (*Z*) double bonds [poly-(**3**-**5**)] showed an intense Raman band at ca. 1585 nm together with a weak one at ca. 1550 nm, for polymers with a *trans* (*E*) configuration [poly-(**1**-**2**), poly-**6**] of the double bonds, the opposite scenario is obtained, a weak band at ca. 1585 nm followed by a strong band at ca. 1557 nm (Figure 2b).

Another structural technique that provides useful information related to the *Z*/*E* configuration of double bonds in polyene backbones is IR. In a seminal work, Simionescu *et al.* were able to determine the *cis*/*trans* (*Z*/*E*) configuration of the double bonds by analyzing the ratio between the bands at 1500 and 1450 cm^{-1} of different model compounds.[102] Thus, while PPAs with a 1500/1450 (cm^{-1}/cm^{-1}) ratio> 1 have a majority *trans* configuration of the double bonds, those with a 1500/1450 (cm^{-1}/cm^{-1}) ratio≈ 1 have a prevalent *cis* configuration of the double bonds. Hence, we decided to analyze these bands for all the polymers used in this study —PPAs and PDPAs— and determine if the reported pattern found by Simionescu *et al.* for PPAs can be extended to PDPAs. Interestingly, in all PDPAs and PPAs with a *trans*- *(E*) content of the double bonds, the ratio between the 1500/1450 (cm^{-1}/cm^{-1}) bands is greater than 1, while in those cases where the polyene is formed by *cis*- (*Z*) double bonds, the ratio between those two bands is ≈ 1, indicating that this PPA protocol can be extended to PDPAs (Figure 2c).

To determine the *Z*/*E* configuration of the double bonds, it is recommended to analyze both the Raman and IR spectra, being necessary to check the ratio of signals at ca.1585/1550 (cm^{-1}/cm^{-1}) for Raman studies and ca.1500/1450 (cm^{-1}/cm^{-1}) for IR experiments.

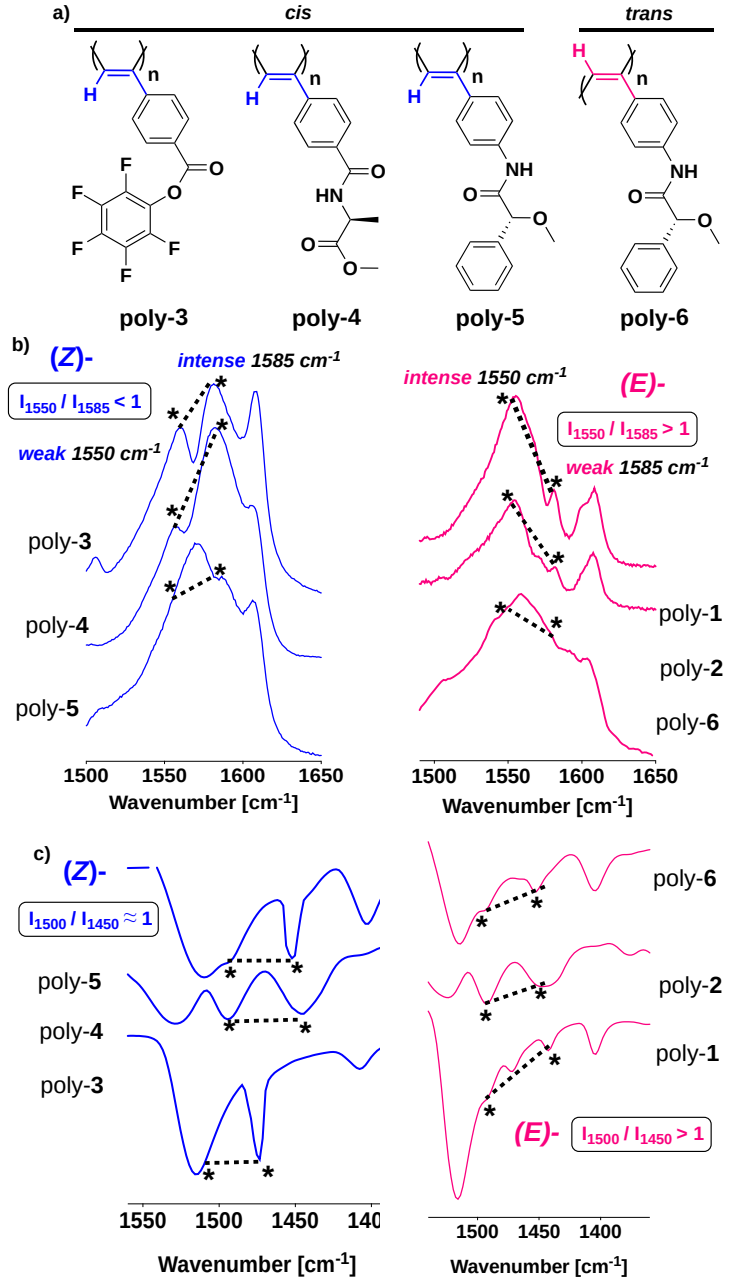

Figure 2. a) Structure of poly-(**3**-**6**). Partial (b) Raman and (c) IR spectra of poly-(**1**-**6**) showing the 1300-1600 cm^{-1} regions.

Once the *trans* (*E*) configuration of the double bonds was demonstrated in asymmetric PDPAs prepared with WCl_6/Ph_4Sn catalysis, the regioregularity of these polymers was explored.

As stated above, different regioregularities (head-to-tail, head-to-head, and tail-to-tail) can be generated in these systems during the polymerization of asymmetric DPA monomers (Scheme 1d). ^{1}H-NMR spectra of poly-(*S*)-**2** in different solvents show a single set of NMR signals indicating the presence of a regioregular polymer (Figure 3c and SI). Otherwise, a mixture of regioregularities should result in more complicated

NMR spectra due to the different anisotropic environments experienced by the protons of the m.r.u. within the different regiochemistries (Figure 3a). To discriminate between the different regioregularities, long-distance 2D-NMR experiments such as NOESY were carried out. Detailed observation, after modeling structures containing the three possible regioregularities (head-to-tail, head-to-head, and tail-to-tail) of poly-(*S*)-**2** and *trans* (*E*) configuration of the double bonds in the polyene backbone, reveals that in head-to-head or tail-to-tail regioregularities, all the aromatic protons of the unsubstituted benzene ring are in close contact with the different protons of the alanine residue of n-1 and n+1 m.r.u. (Figure 3a). This fact is due to the alternating distribution of alanine residues and aromatic rings on the helix ridges. On the contrary, in the case of a head-to-tail regioregularity, the unsubstituted and the substituted aromatic rings are located in the opposite helix ridges (Figure 3a). As a result, the proton at the *para* position of the unsubstituted benzene ring should afford a long-distance NOE cross peak with some alanine protons in a head-to-head or tail-to-tail sequence, whereas this NOE should not be observed in the case of a head-to-tail sequence. Therefore, the absence of this cross peak in the NOESY spectrum corroborates the head-to-tail regioregularity during the polymerization of poly-**1** (Figure 3c).

Interestingly, the head-to-tail structure observed for poly-(*S*)-**2** resembles the packing observed for a diphenylacetylene derivatized with an alanine methyl ester group [m-(*S*)-**2**] by X-ray[103] (Figure 3b).

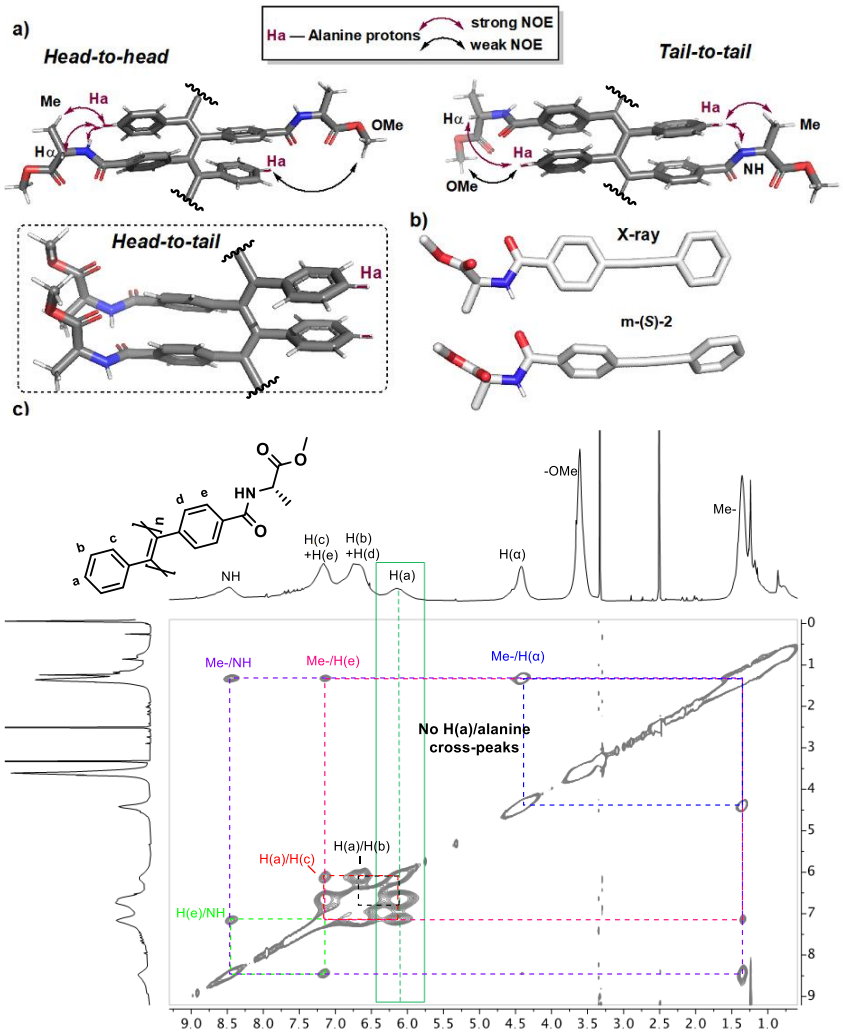

Figure 3. a) Dimeric model structures for a head-to-head, tail-to-tail and head-to-tail regioregularities of poly-(*S*)-2, emphasizing the expected NOE cross peaks for Ha. b) X-ray structure of m-(*S*)-2. c) NOESY spectrum of poly-(*S*)-2 in DMSO.

Next, ECD studies were carried out for poly-(*S*)-**2** in DMF. As expected, no ECD signal was obtained until the sample was annealed at 80 °C for 4 hours. After annealing, an ECD trace with a first positive Cotton effect at 400 nm was obtained (Figure 4b). The dissymmetry factor (g_{abs}) obtained for poly-(*S*)-**2** was 1.8×10^{-3}, within the same range as the values reported for symmetric PDPAs or PPAs,[10,12,79] fact that corroborates both good stereo and regioregularities within poly-(*S*)-**2** with a screw sense excess.

To obtain more structural information, and to refine the helix adopted by poly-(*S*)-**2**, a 2D-crystal of this polymer was prepared using the protocol described by Yashima *et al.*, which consists of spin coating a dilute DMF solution of poly-(*S*)-**2** on highly oriented pyrolytic graphite (HOPG) followed by annealing under the corresponding solvent atmosphere.[59] In our case, before spin coating the sample, the

polymer was annealed in DMF at 80 °C for 4 h to induce a screw sense excess in the polyene backbone. High-resolution AFM images of poly-(*S*)-**2** reveal the presence of 2D crystals where single PDPA chains are packed in a parallel manner, one after the other, to form a right-handed (clockwise) pendant disposition with the periodic oblique stripes in 50° angles and a helical pitch of 6.35 nm (Figure 4a).

By combining the information obtained from the ECD and AFM studies of poly-(*S*)-**2** in DMF, we can state that the first positive Cotton band (CD_{400}> 0) corresponds to a *P* helical structure described by the pendant groups (external helix). As with PPAs, PDPAs are made up of two coaxial helices, one described by the polyene backbone and the other described by the pendants.[70]

In order to stablish a relationship between internal and external helices, computational studies [TD-DFT(CAM-B3LYP)/3-21G][104-107] were performed on a *P* helix (n= 20 m.r.u.) for a PDPA with *trans-transoidal* skeleton —ω_1= -165°, ω_2= 180°, ω_3= 40°— (Figure 4a, d). In this model, the chiral substituents were removed to reduce the computational demands. The simulated ECD spectrum (Figure 4c and SI for detailed information) is in good agreement with the experimental one, which indicates that the proposed model is a good approximation to the structure of poly-(*S*)-**2**.

The helical structure described by an asymmetric PDPA in a *trans-transoidal* configuration is very different from the *cis-transoidal* helix described by a PPA. In a PDPA helix, three different helices coexist: a) helix 1, which is the classical internal helix described by the orientation between conjugated double bonds (ω_1= -165°) and which in this example (i.e., poly-(*S*)-**2**) is *M* oriented due to the negative value of ω_1 (Figures 4a, d); b) helix 2, which is the helix described between consecutive poly(diphenylacetylene) groups, and which rotates in the opposite direction to that defined by the dihedral angle between conjugated double bonds —helix 1= ω_1— (so, in poly-(*S*)-**2**, is *P*; Figure 4a); and c) helix 3, which is present in PDPAs but does not exist in PPAs. This helix appears when the polyene backbone grows because of the *trans-transoidal* configuration of the polyene, resulting in a twist of the whole scaffold. The helical sense described by helix 3 is coincident with that described by helix 2, in this case a *P* helix (Figure 4a).

When analyzing the data obtained from the theoretical calculations, we could observe that unlike the PPAs, the PDPAs show a first Cotton band given by a combination of the poly(diphenylacetylene) backbone and not only by the polyene (see SI). Therefore, these results indicate that the correlation between the ECD signal and

the helical sense of the polyene (ω_1) found in *cis*-PPAs cannot be applied to asymmetric PDPAs. In the latter it is found that, although the double bonds are *M* oriented (helix 1 $\omega_1 < 0$), the *P* orientation of consecutive diphenylacetylene m.r.u. (helix 2) in combination with the *P* orientation of the whole scaffold (helix 3), results in a final positive Cotton band. Thus, at this point we can state that in an asymmetric PDPA with a *trans-transoidal* helix, a first positive Cotton band at 400 nm indicates a helical structure with a *M*/*P*/*P* (helix 1/helix 2/helix 3) orientation. On the contrary, if the asymmetric PDPA shows a $CD_{400} < 0$, then the polymer adopts a *P*/*M*/*M* (helix 1/helix 2/helix 3) orientation.

Another interesting structural feature observed in PDPAs is found when the ECD and the UV spectra obtained for a DMF solution of poly-(*S*)-**2** are compared (Figure 4b). By looking at the two spectra, we can see that there is a mismatch between the first Cotton band in the ECD spectrum (400 nm) and the highest wavelength UV band (450 nm), corresponding the ECD Cotton band to the second band of the UV-spectrum (400 nm). To determine and characterize the electronic transitions responsible for these two UV-bands, theoretical ECD and UV studies were carried out for an n=12 oligomer. The theoretical UV-spectrum reproduced the experimental one, showing two maxima at ca. 400 and 450 nm, being the first transition the one that produces the first Cotton band.

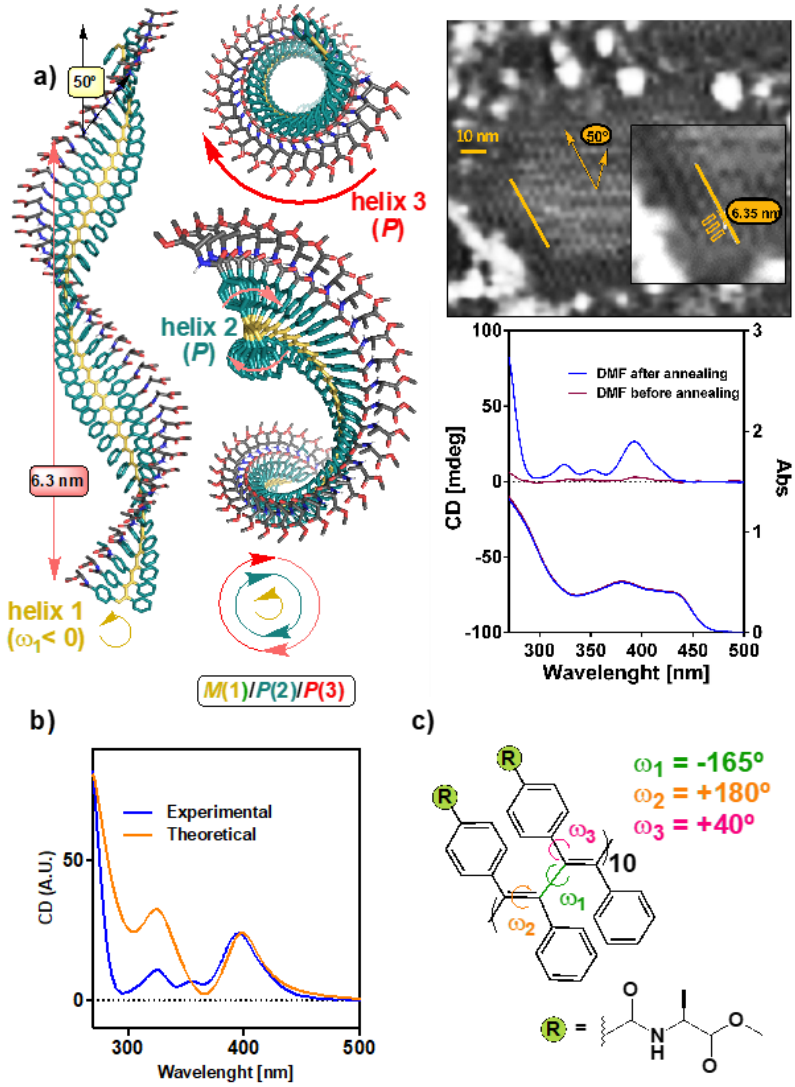

Figure 4. a) 3D structure of poly-(*S*)-**2**, AFM image of poly-(*S*)-**2** after annealing in DMF and CD/UV spectra of poly-(*S*)-**2** before and after annealing, c= 0.5 mg/mL. b) Comparison between the experimental and theoretical ECD spectrum obtained for poly-(*S*)-**2**. c) Dihedral angles for the 12-mer oligomer used to compute the theoretical spectra.

By analyzing the electron density differences involved in the transitions responsible of these bands, it was found that while the UV band at higher wavelengths —the one that is not ECD active— has an asymmetric contribution of the polyene and the aryl rings (Figure 5), the second UV band that corresponds to the first Cotton in the ECD spectrum shows a more symmetric contribution of each diphenylacetylene m.r.u. (Figure 5). These studies show how the UV and ECD Cotton bands appearing at ca. 400 and 450 nm are affected by the orientation of the diphenylacetylene m.r.u. and not just because of the polyene.

Interestingly, Kwak and coworkers found that a new ECD active signal could appear in the spectra of an asymmetric PDPA when measured in film or aggregated

state. This band appears at ca. 450 nm, has the same sign as the Cotton band at 400 nm and was associated to a longitudinal coupling between polyene chains.[89,90]

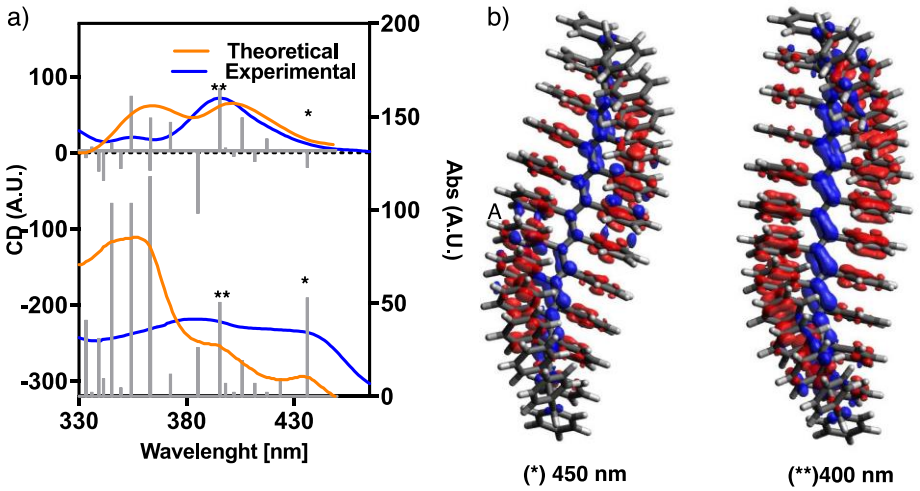

Figure 5. a) Comparison of calculated and experimental ECD and UV-Vis spectra of a 12-mer oligomeric PDPA model. b) Electron density differences of transitions responsible of UV and ECD bands at 400 and 450 nm.

Thus, we explored different solvents to try to study this ECD band further, choosing those where poly-(*S*)-**2** shows poor solubility and appears as a dispersed aggregate. Of the different poly-(*S*)-**2** (0.5 mg/mL) solutions tested, only the MeCN solution was found to produce an ECD signal at 450 nm after annealing at 80 °C for 4 h.

In this solvent, the PDPA shows a negative Cotton band at 400 nm indicative of a *P*/*M*/*M* (helix 1/helix 2/helix 3) helical scaffold. Interestingly, AFM studies of poly-(*S*)-**2** —prepared in MeCN— showed the presence of superhelices that have a helical pitch of 14 nm and a width of 8 nm, parameters that correspond to a bundle of PDPA helices (Figures 6a-c).

Additionally, controlled nanoprecipitation[108,109] studies of poly-(*S*)-**2** in a THF/H_20 1/1 v/v ratio were carried out to generate nanospheres that can produce this new ECD band at 450 nm due to the aggregation of poly-(*S*)-**2**. As expected, ECD studies of these nanospheres dispersed in THF/H_20 (Figure 6 d-f) show again the presence of this new ECD band, which therefore can be attributed to an interaction between different PDPA chains, and more precisely, to a longitudinal coupling between asymmetric contributions of the polyene and the aryl rings as extracted from computational studies (Figure 5).

Dynamic behavior of asymmetric PDPAs. Once the helical structure of an asymmetric PDPA (i.e., poly-(*S*)-**2**) was puzzled out by the different structural

techniques, the stimuli-responsive properties of poly-(*S*)-**2**, and therefore its dynamic behavior, were studied. In this case, the variation of the helical structures with solvents was analyzed after annealing at 80 ºC for 4h (Figure 7a). Interestingly, it is possible to observe the dynamic behavior of a chiral and asymmetric PDPA. This dynamic behavior was found before in achiral PDPAs bearing a *para*-benzoic group and where the sense can be enhanced towards *P* or *M* senses by interaction with the two enantiomers of a chiral amine.[79]

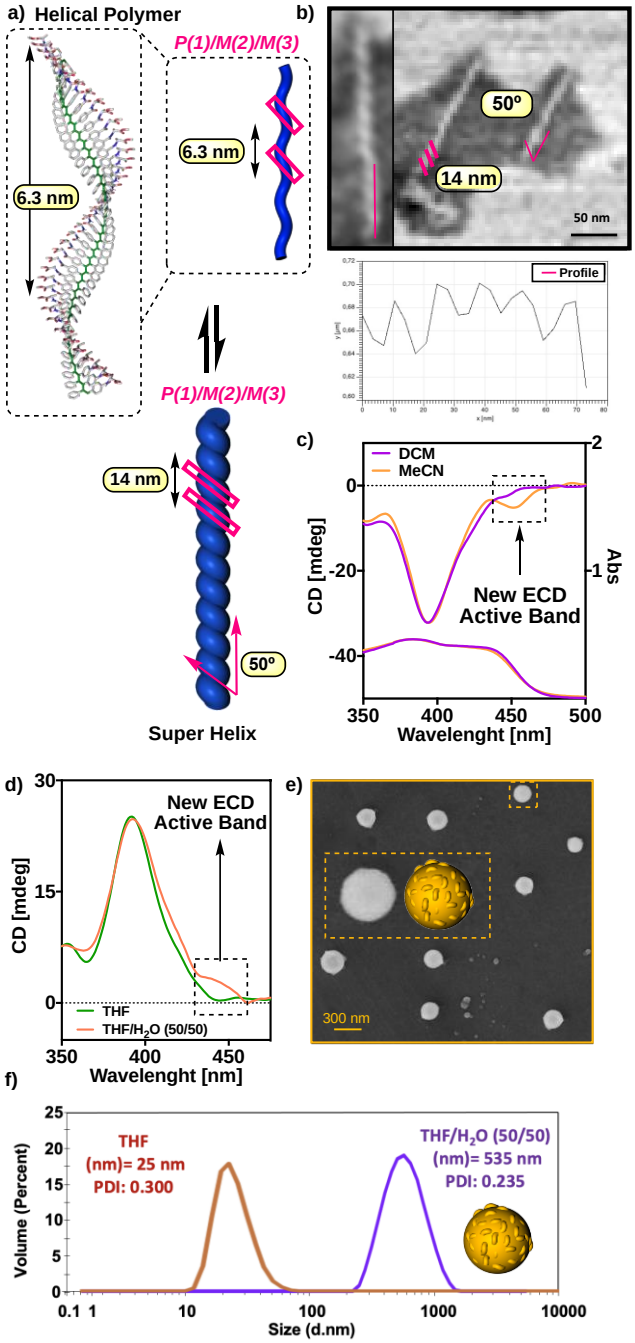

Figure 6. a) Conceptual representation of the superhelix formation. b) AFM image and height profile of the superhelical assemblies generated by poly-(*S*)-**2** during its annealing in MeCN. c) Comparison of the

ECD spectra of poly-(*S*)-**2** in DCM (good solvent, non-aggregated state) and after annealing in MeCN (bad solvent, aggregated state) displaying the new low-energy ECD active band due to the formation of supramolecular aggregates. d) Comparison of the ECD spectra of poly-(*S*)-**2** in THF (good solvent, non-aggregated state) and THF/H_2O (1/1) (nanoprecipitated state) displaying the new low-energy ECD active band due to the formation of nanospheres. e) SEM image of the nanospheres generated by nanoprecipitation. f) DLS traces monitoring the nanoprecipitation process.

VCD studies were carried out to demonstrate that the helix inversion is associated to a conformational change at the pendant group. So, VCD spectra of poly-(*S*)-**2** in both $CDCl_3$ and DMSO-d_6 show activity in the carbonyl fingerprint region (Figure 7d). More precisely, the C=O stretching bands of the amide and the ester groups —1650 and 1750 cm^{-1} respectively— show positive bands in $CDCl_3$ [ECD -, *P*/*M*/*M* (helix 1/helix 2/helix 3)] and negative ones in DMSO-d_6 [ECD +, *M*/*P*/*P* (helix 1/helix 2/helix 3)] which are ascribed to *anti* and *syn* conformations at the pendant group respectively, as inferred from VCD theoretical calculations of the monomeric unit in both conformations (Figures 7c, f).

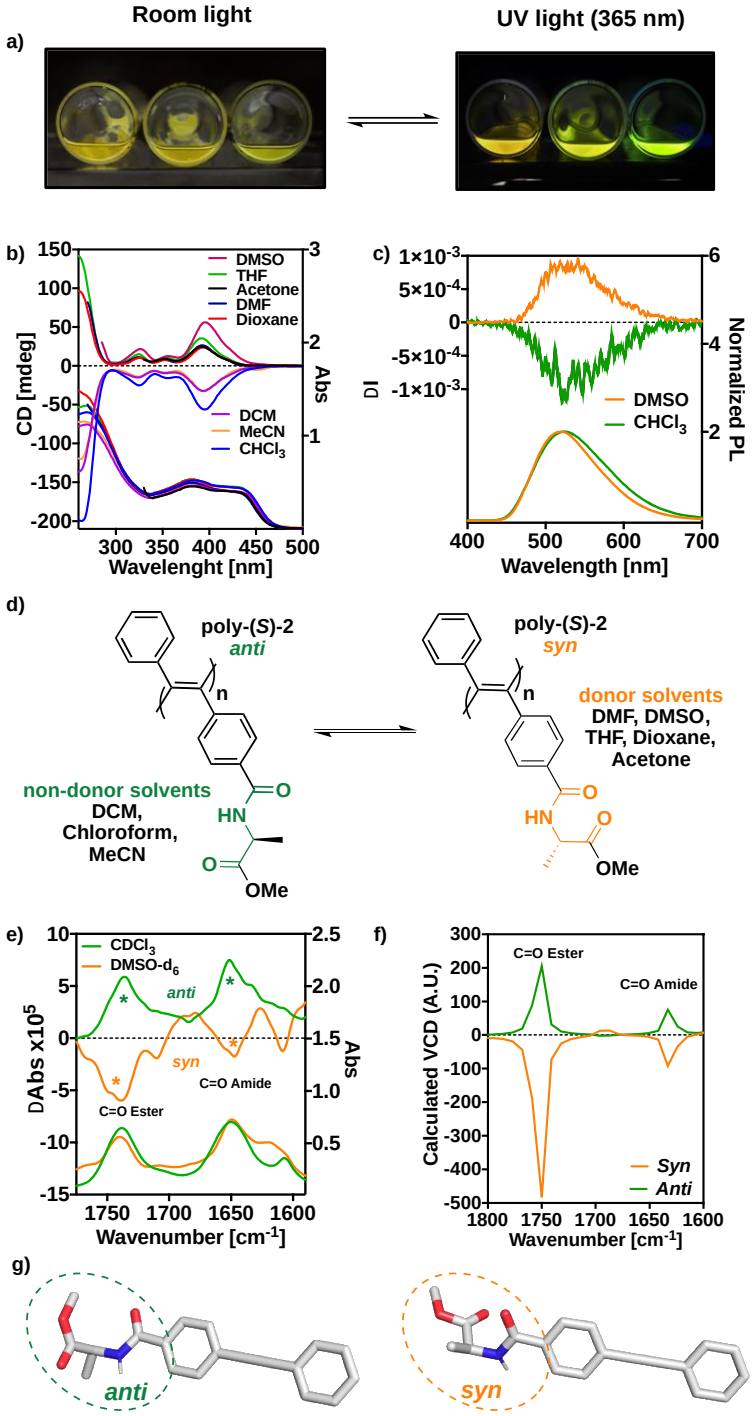

Figure 7. a) Photographs of poly-**1** and poly-(*S*)-**2** under room light and UV-light b) ECD and UV spectra of poly-(*S*)-**2** in different solvents (0.5 mg/mL, 1 mm path). c) CPL spectra of poly-(*S*)-**2** (λ_{Exc} = 365 nm, 0.3 mg/mL). d) Schematic illustration of the solvent-triggered conformational change in the pendant group that promotes helix inversion. e) Experimental VCD spectra of poly-(*S*)-**2** in $CDCl_3$ and DMSO-d_6. f) Calculated VCD spectra of the monomeric units with *anti* and *syn* conformations. g) Optimized structures of the monomeric DPA units with *anti* and *syn* conformations employed to obtain the theoretical spectra depicted in f).

One of the most interesting features of PDPAs is that after adopting a screw sense excess, they result in circular polarized luminescent (CPL) active materials.[110,111] This unique property has found many applications in different cutting-edge fields such as security encoding[112] or CP-OLEDs among many others.[113] Consequently, CPL studies were carried out for poly-(*S*)-**2** in *P*, *rac* and *M* helical states exhibiting *P*, null and *M* CPL activity respectively (Figure 7b). The CPL sign is, as expected, coincident with that of the high energy band in the ECD spectra, indicating that a CPL (+) is due to a *M*/*P*/*P* (helix 1/helix 2/helix 3) arrangement, while a CPL (-) is ascribed to a *P*/*M*/*M* (helix 1/helix 2/helix 3) helical orientation.

Moreover, recently experimental, and computational CPL studies support the *trans-transoidal* structure for PDPAs.[114] The poor conformational flexibility in the polyene of PDPAs creates a reversing in the excited energy levels that permit an electronically dipole-allowed transition resulting in emissive materials, such as is observed here in poly-(*S*)-**2**. However, in the case of PPAs the emissive form of the helical scaffold is when the polyene backbone adopts just a *cis-cisoidal* configuration.[114]

The CPL emission was gauged by the dissymmetric factor defined as $|g_{lum}| = 2(I_L - I_R)/(I_L + I_R)$, being I_L and I_R the left- and right-handed luminescent emissions respectively. In both cases a maximum g_{lum} value of ca. $+/-1x10^{-3}$ at 520 nm was obtained, with quantum yield values of Φ= 26 and of Φ= 44 for the $CHCl_3$ and DMSO solutions respectively. To the best of our knowledge, this system represents one of the few examples where the CPL sign can be switched,[115] paving the way to the design of new stimuli-responsive CPL active materials with enhanced properties and applications.

3. Conclusion

In summary, the combination of data collected from different structural techniques allowed us to build an approximated structure for an asymmetric PDPA prepared by polymerization with WCl_6/Ph_4Sn of a diphenyl acetylene monomer substituted with an active pentafluorophenyl ester (PFP) group. This polymer was further transformed into a chiral polymer by a post-functionalization reaction that incorporates *L*-alanine methyl ester into the pendants. To elucidate the secondary structure of the polymer, Raman and IR spectroscopies were used to discern between *Z* and *E* configurations of the double bonds. In this case, the polymer adopts mainly a *trans* configuration of the double bonds. 1D and 2D-NMR experiments helped us to

elucidate the regioregularity of the polymer, indicating a preferred head-to-tail polymerization reaction. AFM studies provided useful information related to different helical structural parameters such as helical pitch, packing angle and the orientation of the external helix described by the pendant groups. The use of molecular modelling, together with the constrains provided by the results of IR, Raman, NMR and AFM studies allowed us to build an approximate secondary structure for this polymer. Thus, poly-(*S*)-**2** adopts a preferred *trans-transoidal* helical scaffold that is formed by three different helices. Helix 1, described by the orientation between conjugated double bonds; helix 2, described by the pendant groups; and helix 3, described by a twisting degree of the whole polymer chain and observed when the polymer grows. Computational studies on the model compound result in a theoretical ECD spectrum that resembles the experimental one and that allows us to demonstrate that in an asymmetric PDPA, the sign of the first Cotton band is ruled by helices 2 and 3, and not just by the orientation of the polyene backbone. Moreover, the present study also made it possible to explain why in different aggregation states, such as superhelices or nanospheres, a new ECD band appears because of a longitudinal coupling between polymer chains. Additionally, this work reveals the dynamic behavior of poly-(*S*)-**2** and shows how *P* or *M* helical senses can be induced by conformational changes at the pendant groups using external stimuli such as solvent donor ability, fact corroborated by a combination of VCD experiments and theoretical calculations. Finally, associated to this dynamic helical behavior, a dynamic circular polarized luminescence switch with a $|g_{lum}| = +/-1x10^{-3}$ was obtained for poly-(*S*)-**2**, where a CPL (+) is produced by a *M*/*P*/*P* (helix 1/helix 2/helix 3) arrangement generated in donor solvents, while a CPL (-) is ascribed to a *P*/*M*/*M* (helix 1/helix 2/helix 3) helical orientation produced when poly-(*S*)-**2** is annealed in non-donor solvents.

The elucidation of the three-dimensional structure of a PDPA opens a new horizon in the development of functional materials due to the possibility of establishing structure/function relationships that can result in an improvement of the functionality of the polymer through a directed tuning of its secondary structure.

4. References

[1] Y. Shen, C. F. Chen, *Chem. Rev.* **2012**, *112*, 1463-1535.

[2] T. Mori, *Chem. Rev.* **2021**, *121*, 2373-2412.

[3] E. S. Gauthier, R. Rodríguez, J. Crassous, *Angew. Chem. Int. Ed.* **2020**, *59*, 22840-22856.

[4] K. L. George, W. S. Horne, *Acc. Chem. Res.* **2018**, *51*, 1220-1228.

[5] Y. Ferrand, I. Huc, *Acc. Chem. Res.* **2018**, *51*, 970-977.

[6] E. A. John, C. J. Massena, O. B. Berryman, *Chem Rev.* **2021**, *120*, 2759-2782.

[7] Y. Dorca, E. E. Greciano, J. S. Valera, R. Gomez, L. Sanchez, *Chem. Eur. J.* **2019**, *25*, 5848-5864.

[8] B. Adelizzi, N. J. Van Zee, L. N. de Windt, A. R. A. Palmans, E. W. Meijer, *J. Am. Chem. Soc.* **2019**, *141*, 6110-6121.

[9] P. Xing, Y. Zhao, *Acc. Chem. Res.* **2018**, *51*, 2324-2334.

[10] E. Yashima, K. Maeda, H. Lida, Y. Furusho, K. Nagai, *Chem. Rev.* **2009**, *109*, 6102-62111.

[11] M. Milton, R. Deng, A. Mann, C. Wang, D. Tang, M. Weck, *Acc. Chem. Res.* **2018**, *54*, 2397-2408.

[12] E. Yashima, N. Ousaka, D. Taura, K. Shimomura, T. Ijai, K. Maeda, *Chem. Rev.* **2016**, *116*, 13752-13990.

[13] J. G. Rudick, V. Percec, *Acc. Chem. Res.* **2008**, *41*, 1641-1652.

[14] E. Yashima, K. Maeda, Y. Furusho, *Acc. Chem. Res.* **2008**, *41*, 1166-1180.

[15] N. Liu, L. Zhou, Z. Q. Wu, *Acc. Chem. Res.*, **2021**, *54*, 3953-3967.

[16] L. Zhou, X. H. Xu, Z. Q. Jiang, L. Xu, B. F. Chu, N. Liu, Z. Q. Wu. *Angew. Chem. Int. Ed.*, **2021**, *60*, 806-812.

[17] J. H. Chu, X. H. Xu, S. M. Kang, N. Liu, Z. Q. Wu. *J. Am. Chem. Soc.*, **2018**, *140*, 17773-17781.

[18] T. Yamamoto, R. Murakami, S. Komatsu, M. Suginome, *J. Am. Chem. Soc.* **2018**, *140*, 3867-3870.

[19] M. Nuñez-Martínez, S. Arias, E. Quiñoá, R. Riguera F. Freire, *Chem. Mater.* **2021**, *33*, 4805-4812.

[20] C. Zhao, S. Sun, W. L. Tong, M. C. W. Chan, *Macromolecules*, **2017**, *50*, 6896-6902.

[21] R. Rodríguez, E. Suarez-Picado, E. Quiñoá, R. Riguera, F. Freire, *Angew. Chem. Int. Ed.* **2020**, *59*, 8616-8622.

[22] M. Alzubi, S. Arias, R. Rodríguez, E. Quiñoá, R. Riguera, F. Freire, *Angew. Chem. Int. Ed.* **2020**, *59*, 13365-13369.

[23] E. Suarez-Picado, E. Quiñoá, R. Riguera, F. Freire, *Angew. Chem. Int. Ed.* **2020**, *59*, 4537-4543.

[24] R. Ishidate, A. J. Markvoort, K. Maeda, E. Yashima, *J. Am. Chem. Soc.*, **2019**, *141*, 7605-7614.

[25] K. Maeda, H. Hirose, N. Okoshi, K. Shimomura, Y. Wada, T. Ikai, S. Kanoh, E. Yashima, *J. Am. Chem. Soc.,* **2018**, *140*, 3270−3276.

[26] R. Sakai, E. B. Barasa, N. Sakai, S. I. Sato, T. Satoh, T. Kakuchi, *Macromolecules*, **2012**, *45*, 8221-8227

[27] E. Yashima, K. Maeda, *Macromolecules*, **2008**, *41*, 3-12.

[28] K. Maeda, E. Yashima, *Top. Curr. Chem.* **2006**, *265*, 47-88.

[29] R. Nonokawa, E. Yashima, *J. Am. Chem. Soc.*, **2002**, *125*, 1278-1283.

[30] E. Yashima, K. Maeda, Y. Okamoto, *Nature*, **1999**, *399*, 449-451.

[31] E. Yashima, K. Maeda, T. Matsushima, Y. Okamoto, *Chirality*, **1997**, *9*, 593-600.

[32] M. Ando, R. Ishidate, T. Ikai, K. Maeda,E. Yashima, *J. Polym. Sci., Part A: Polym. Chem.* **2019**, 57, 2481-2490.

[33] C. Zhang, Y. Qiu, S. Bo, F. Wang, Y. Wang, L. Liu, Y. Zhou, H. Niu, H. Dong, T. Satoh, *J. Polym. Sci., Part A: Polym. Chem.* **2019**, *57*, 1024-1031.

[34] R. P. Megens, G. Roelfes, *Chem. Eur. J.* **2011**, *17*, 8514-8523.

[35] S. Ikeda, R. Takeda, T. Fujie, N. Ariki, Y. Nagata, M. Suginome. *Chem. Sci.* **2021**, *12*, 8811-8816.

[36] Y. Nagata, R. Takeda, M. Suginome, *ACS Cent. Sci.*, **2019**, *5*, 1235-1240.

[37] E. Anger, H. Iida, T. Yamaguchi, K. Hayashi, D. Kumano, J. Crassous, N. Vanthuyne, C. Roussel, E. Yashima, *Polym. Chem*. **2014**, *5*, 4909-4914.

[38] R. Ishidate, T. Sato, T. Ikai, S. Kanoh, E. Yashima, K. Maeda, *Polym. Chem.*, **2019**, *10*, 6260-6268

[39] D. Hirose, A. Isobe, E. Quiñoá, F. Freire, K. Maeda, *J. Am. Chem. Soc.* **2019**, *141*, 8592-8598.

[40] J. Shen, Y. Okamoto, *Chem. Rev*., **2016**, *116*, 1094-1138.

[41] K. Shimomura, T. Ikai, S. Kanoh, E. Yashima, K. Maeda, *Nat. Chem.* **2014**, *6*, 429-434.

[42] C. I. Simionescu, V. Percec, *Prog. Polym. Sci.*, **1982**, *8*, 133-214.

[43] K. Morino, K. Maeda, Y. Okamoto, E. Yashima, T. Sato, *Chem. Eur. J.*, **2002**, *8*, 5112-5120.

[44] J. G. Rudick, V. Percec. *Macromol. Chem. Phys.*, **2008**, *209*, 1759-1768.

[45] M. Asahi, Y. Mawatari, R. Motoshige, Y. Yoshida, M. Tabata. *J. Polym. Sci., Part A: Polym. Chem.*, **2013**, *51*, 5177-5183.

[46] X. Q. Liu, J. Wang, Sh. Yang, E. Q. Chen, *ACS Macro Lett.*, **2014**, 3, 834-838.

[47] V. Percec, E. Aqad, M. Peterca, J. G. Rudick, L. Lemon, J. C. Ronda, B. B. De, P. A. Heiney, E. W. Meijer, *J. Am. Chem. Soc*., **2006**, 128, 16365-16732.

[48] V. Percec, J. G. Rudick, M. Peterca, E. Aqad, M. R. Imam, P. A. Heiney, *J. Polym. Sci., Part A: Polym. Chem.*, **2007**, 45, 4974-4987.

[49] V. Percec, M. Peterca, J. G. Rudick, E. Aqad, M. R. Imam, P. A. Heiney, *Chem. Eur. J.*, **2007**, 13, 9572-9581.

[50] V. Percec, J. G. Rudick, M. Peterca, P. A. Heiney, *J. Am. Chem. Soc.*, **2008**, *130*, 7503-7508.

[51] A. Miyasaka, T. Sone, Y. Mawatari, S. Setayesh, K. Müllen, M. Tabata, *Macromol. Chem. Phys.* **2006**, *207*, 1938-1944.

[52] T. Ito, H. Shirakawa, S. Ikeda, *J. Polym. Sci., Part A: Polym. Chem.* **1974**, *12*, 11-20.

[53] Y. Yoshida, Y. Matawari, A. Motoshige, R. Motoshige, T. Hiraoki, M. Wagner, K. Müllen, M. Tabata, *J. Am. Chem. Soc.*, **2013**, *135*, 4110-4116.

[54] R. Rodríguez, J. Ignés-Mullol, F. Sagués, E. Quiñoá, R. Riguera, F. Freire, *Nanoscale*, **2016**, *8*, 3362-3367.

[55] J. Kumaki, *Polym. J.*, **2016**, *48*, 3-14

[56] J. Kumaki, S. I. Sakurai, E. Yashima, *Chem. Soc. Rev.*, **2009**, *38*, 737-746.

[57] S. Sakurai, K. Okoshi, J. Kumaki, E. Yashima, *J. Am. Chem. Soc.* **2006**, *128*, 5650-5651.

[58] K. Okoshi, S. Sakurai, S. Ohsawa, J. Kumaki E. Yashima, *Angew. Chem. Int. Ed.* **2006**, *45*, 8173-8176.

[59] S. I. Sakurai, K. Okoshi, J. Kumaki, E. Yashima, *Angew. Chem. Int. Ed.*, **2006**, *45*, 1245-1248.

[60] V. Percec, J. G. Rudick, M. Peterca, S.R Staley, M. Wagner, M. Obata, C. M. Mitchell, W. D. Cho, V. S. K. Balagurusamy, J. N. Lowe, M. Glodde, O. Weichold, K. J. Chung, N. Ghionni, S. N. Magonov, P. A. Heiney, *Chem. - Eur. J.* **2006**, *12*, 5731-5746.

[61] F. Freire, E. Quiñoá, R. Riguera, *Chem. Commun.*, **2017**, *53*, 481-492.

[62] I. Liu, T. Namikoshi, Y. Zang, T. Aoki, S. Hadano, Y. Abe, I. Wasuzu, T. Tsutsuba, M. Teraguchi, T. Kaneko, *J. Am. Chem. Soc.***, 2013**, *135*, 602-605.

[63] H. Shirakawa, S. Ikeda, *Polym. J.* **1971**, *2,* 231-244

[64] J. Tabei, M. Shiotsuki, F. Sanda, T. Masuda, *Macromolecules* **2005**, *38*, 9448.

[65] T. Kaneko, Y. Umeda, T. Yamamoto, M. Tereguchi, T. Aoki, *Macromolecules* **2005**, *38*, 9420-9426.

[66] B. Nieto-Ortega, R. Rodríguez, S. Medina, E. Quiñoá, R. Riguera, J. Casado, F. Freire, F. J. Ramírez, *J. Phys. Chem. Lett.*, **2018**, *9*, 2266-2270.

[67] I. Palomo, R. Rodríguez, S. Medina, E. Quiñoá, J. Casado, F. Freire, F. J. Ramírez, *Angew. Chem. Int. Ed.*, **2020**, *59*, 9080-9087.

[68] B. Fernández, R. Rodríguez, E. Quiñoá, R. Riguera, F. Freire, *ACS Omega*, **2019**, *4*, 5233-5240.

[69] B. Fernández, R. Rodríguez, A. Rizzo, E. Quiñoá, R. Riguera, F. Freire, *Angew. Chem. Int. Ed.* **2018**, *57*, 3666-3670.

[70] F. Rey-Tarrío, R. Rodríguez, E. Quiñoá, R. Riguera, F. Freire, *Angew. Chem. Int. Ed.* **2021**, *60*, 8095-8103.

[71] M. Nozaki, D. Hirose, K. Maeda, *J. Chromatogr. A*, **2021***, 1622*, 461173.

[72] Y. J. Jin, Y. G. Choi, G. Kwak, *Polymer*, **2019**, *171*, 127-132.

[73] T. Sakaguchi, H. Shimada, T. Hashimoto, *Polym. Chem.* **2020**, *11*, 6471-6478.

[74] M. Miyairi, T. Taniguchi, T. Nishimura, K. Maeda, *Angew. Chem. Int. Ed.*, **2020**, *59*, 14772-14780.

[75] X. Wang, H. Hu, W. Wang, A. Qin, J. Z. Sun, B. Z. Tang, *Polym. Chem.* **2015**, *6*, 7958-7963.

[76] X. Wan, Y. Gao, W. Wang, A. Qin, J. Z. Sun, B. Z. Tang, *Polym. Chem.* **2016**, *7*, 5312-5321.

[77] T. Aoki, Y. Kobayashi, T. Kaneko, E. Oikawa, Y. Yamamura, Y. Fujita, M. Teraguchi, R. Nomura, T. Masuda, *Macromolecules,* **1999**, *32*, 79-85.

[78] H. Kim, D. Lee, S. Lee, N. Suzuki, M. Fujiki, C. L. Lee, G. Kwak, *Macromol. Rapid Commun.* **2013***, 34*, 1471-1479.

[79] K. Maeda, M. Nozaki, K. Hashimoto, K. Shimomura, D. Hirose, T. Nishimura, G. Watanabe, E. Yashima, *J. Am. Chem. Soc*. **2020**, *142*, 7668-7682.

[80] K. Maeda, D. Hirose, M. Nozaki, Y. Shimizu, T. Mori, K. Yamanaka, Hashimoto, K. Ogino, T. Nishimura, T. Taniguchi, M. Moro, E. Yashima, *Sci. Adv.* **2021**, *7*, eabg5381.

[81] Y. Gao, X. Wang, J. Z. Sun, B. Z. Tang, *Chem. Rec.* **2015**, *15*, 524-532.

[82] K. U. Seo, Y. J. Jin, H. Kim, T. Sakaguchi, G. Kwak, *Macromolecules*, **2018**, *51*, 34–41

[83] W. Z. Yuan, A. Qin, J. W. Y. Lam, J. Z. Sun, Y. Dong, M. Häussler, J. Liu, H. P. Xu, Q. Zheng, B. Z. Tang, *Macromolecules* **2007**, *40*, 3159-3166.

[84] C. K. W. Jim, J. W. Y. Lam, C. W. T. Leung, A. Qin, F. Mahtab, B. Z. Tang, *Macromolecules*, **2011**, *44*, 2427–2437.

[85] H. Kim, K. U. Seo, Y. J. Jin, C. L. Lee, M. Teraguchi, T. Kaneko, T. Aoki, G. Kwak, *ACS Macro Lett.* **2016**, *5*, 622−625.

[86] Y. J. Jin, K. U. Seo, Y. G. Choi, M. Teraguchi, T. Aoki, G. Kwak, *Macromolecules*, **2017**, *50*, 6433-6438.

[87] H. Kim, Y. J. Jin, B. S. I. Kim, T. Aoki, G. Kwak, *Macromolecules*, **2015**, *48*, 4754–4757.

[88] K. U. Seo, Y. J. Jin, H. Kim, T. Sakaguchi, G. Kwak, *Macromolecules*, **2018**, *51*, 34–41.

[89] S. I. Kim, Y. J. Jin, W. E. Lee, R. Yu, S. J. Park, H. J. Kim, K. H. Song, G. Kwak, *Adv. Mater. Interfaces*, **2014**, *1*, 1300029.

[90] D. Lee, H. Kim, N. Suzuki, M. Fujiki, C. L. Lee, W. E. Lee, G. Kwak, *Chem. Commun.*, **2012**, *48*, 9275-9277.

[91] B. A. San Jose, S. Matsushita, K. Akagi, *J. Am. Chem. Soc*. **2012**, *134*, 19795−19807.

[92] K. Maeda, M. Maruta, K. Shimomura, T. Ikai, S. Kanoh, *Chem. Lett.* **2016**, *45*, 1063–1065.

[93] K. Maeda, M. Maruta, Y. Sakai, T. Ikai, S. Kanoh, *Molecules*, **2016**, *21*, 1487-1500.

[94] K. A. Günay, P. Theato, H. A. Klok, *Journal of Polymer Science Part A: Polymer Chemistry*, **2013**, *51*, 1-28.

[95] S. Leiras, E. Suarez-Picado, E. Quiñoá, R. Riguera, F. Freire, *Giant*, **2021**, *7*, 100068.

[96] K. Cobos, R. Rodríguez, E. Quiñoá, R. Riguera, F. Freire, *Angew. Chem. Int. Ed.* **2020**, *59*, 23724-23730.

[97] Z. Fernández, B. Fernández, E. Quiñoá, R. Riguera, F. Freire, *Chem. Sci.* **2020**, *11*, 7182-7187.

[98] S. Arias, M. Núñez-Martínez, E. Quiñoá, R. Riguera, F. Freire, *Polym. Chem.*, **2017**, *8*, 3740-3745.

[99] A. Takeda, T. Sakaguchi, T. Hashimoto, *Polymer*, **2009**, *50*, 5031-5036.

[100] Y. J. Jin, H. Kim, D. Y. Hwang, M. Teraguchi, T. Kaneko, T. Aoki, G. Kwak, *Molecular Crystals and Liquid Crystals*, **2017**, *645*, 50-57.

[101] A. C. Pauly, P. Theato, *Polym. Chem.,* **2012**, *3*, 1769-1782.

[102] C. I. Simionescu, V. Percec, S. Dumitrescu, *J. Polym. Sci., Polym. Chem. Ed.* **1977**, *15*, 15, 2497-2509.

[103] Deposition Number 2130256 contains the supplementary crystallographic data for this paper. These data are provided free of charge by the joint Cambridge Crystallographic Data Centre and Fachinformationszentrum Karlsruhe Access Structures service.

[104] E. Runge, E. K. U. Gross, *Phys. Rev. Lett.* **1984**, *52*, 997-1000.

[105] Y. Yanai, D. P. Tew, C. C. A. Handy, *Chem. Phys. Lett*. **2004**, *393*, 51-57.

[106] M. J. G. Peach, T. Helgaker, P. Salek, T. W. Keal, O. B. Lutnæs, D. J. Tozer, N. C. Handy, *Phys. Chem. Chem. Phys.* **2006**, *8*, 558-562.

[107] *Gaussian 03* (Revision B-04), M.J. Frisch, G.W. Trucks, H.B. Schlegel, G.E. Scuseria, M.A. Robb, J.R. Cheeseman, J.A. Montgomery Jr., T. Vreven, K.N. Kudin, J.C. Burant, J.M. Millam, S.S. Iyengar, J. Tomasi, V. Barone, B. Mennucci, M. Cossi, G. Scalmani, N. Rega, G.A. Petersson, H. Nakatsuji, M. Hada, M. Ehara, K. Toyota, R. Fukuda, J. Hasegawa, M. Ishida, T. Nakajima, Y. Honda, O. Kitao, H. Nakai, M. Klene, X. Li, J.E. Knox, H.P. Hratchian, J.B. Cross, C. Adamo, J. Jaramillo, R. Gomperts, R.E. Stratmann, O. Yazyev, A.J. Austin, R. Cammi, C. Pomelli, J.W. Ochterski, P.Y. Ayala, K. Morokuma, G.A. Voth, P. Salvador, J.J. Dannenberg, V.G. Zakrzewski, S. Dapprich, A.D. Daniels, M.C. Strain, O. Farkas, D.K. Malick, A.D. Rabuck, K. Raghavachari, J.B. Foresman, J.V. Ortiz, Q. Cui, A.G. Baboul, S. Clifford, J. Cioslowski, B.B. Stefanov, G. Liu, A. Liashenko, P. Piskorz, I. Komaromi, R.L. Martin, D.J. Fox, T. Keith, M.A. Al-Laham, C.Y. Peng, A. Nanayakkara, M. Challacombe, P.M.W. Gill, B. Johnson, W. Chen, M.W. Wong, C. Gonzalez, J.A. Pople, Gaussian, Inc., Pittsburgh, PA, **2003**.

[108] H. Fessi, F. Puisieux, J. Ph. Devissaguet, N. Ammoury, S. Benita. *Int. J. Pharm.*, **1989**, *55*, R1-R4.

[109] J. P. Rao, K. E. Geckeler. *Prog. Polym. Sci.*, **2011**, *36*, 887-913.

[110] Y. Deng, M. Wang, Y. Zhuang, S. Liu, W. Huang, Q. Zhao, *Light Sci. Appl.* **2021**, *10*, 1–18.

[111] H. Tanaka, Y. Inoue, T. Mori, *ChemPhotoChem* **2018**, *2*, 386–402.

[112] L. E. MacKenzie, R. Pal, *Nat. Rev. Chem.* **2021**, *5*, 109-124.

[113] K. Dhbaibi, L. Abella, S. Meunier-Della-Gatta, T. Roisnel, N. Vanthuyne, B. Jamoussi, G. Pieters, B. Racine, E. Quesnel, J. Autschbach, J. Crassous, L. Favereau, *Chem. Sci*. **2021**, *12*, 5522-5533.

[114] S. Wang, D. Hu, X. Guan, S. Cai, G. Shi, Z. Shuai, J. Zhang, Q. Peng, X. Wan, *Angew.Chem. Int. Ed*. **2021**, *60*, 21918–21926

[115] Y. Gao, C. Ren, X. Lin, T. He, *Front. Chem.* **2020**, *8*, 1–17.

Chapter IV

Polymerization Degree Drastically Determines the Chiroptical Properties of Dynamic Asymmetric Poly(diphenylacetylene)s

Chapter IV: Polymerization Degree Drastically Determines the Chiroptical Properties of Dynamic Asymmetric Poly(diphenylacetylene)s

Abstract

Non-symmetric poly(diphenylacetylene)s (PDPAs) shows a strong relationship between the size of the macromolecules and their electronic circular dichroism (ECD) spectra. This fact is related to the complex macromolecular 3D structure adopted by these polymers where three coaxial helices coexist —helix1: defined mainly by orientation of the polyene; helix2: defined mainly by orientation of the phenyl rings attached the double bonds, which rotate in opposite direction to the polyene; helix 3: generated as the polymer chain grows—. The large conjugation found between the two aryl rings and the polyene of the backbone produce complex electronic circular dichroism spectra where the main transitions are dominated by electron transfer from the polyene backbone (helix 1) to the substituted phenyl ring (helix 2) or from phenyl rings of the PDPA (helix 2) to the main chain (helix 1). Interestingly, depending on the DP of a non-symmetric PDPA, these two transitions have different contribution and results in ECD traces with different sign. Thus, while an oligomer of a non-symmetric PDPA shows a positive ECD when the dihedral angle between conjugated double bonds is $w_1>0$ (helix 1, *P* helix), a polymer with a DP >100 will show an ECD trace with opposite sign. This fact is not related to the opposite helical sense of the polyene, is due to the generation of a main transition in the ECD spectra that corresponds to helix 2, (*M* helix), which rotates opposite to helix w1 (*P* helix). Therefore, to assign the helical sense of a PDPA is necessary to know the DP of the polymer and its effect on the corresponding ECD spectrum.

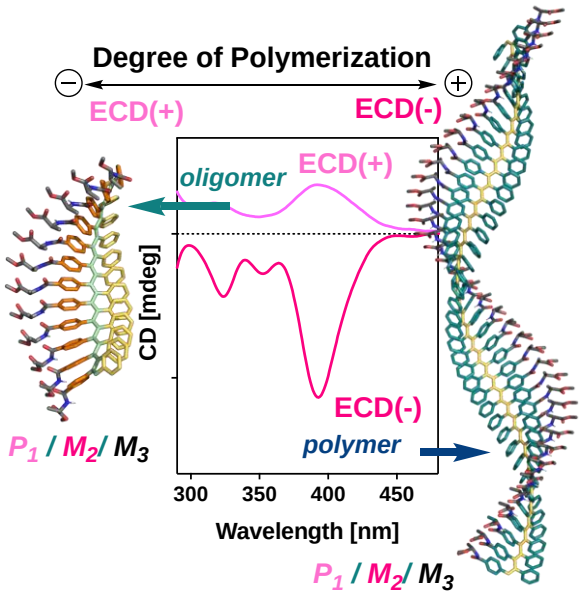

1. Introduction

During the last decades, the synthesis of chiral materials, like helical polymers,[1-7] has attracted worldwide attention due to their applications in different fields such as chiral recognition,[8] catalysis,[9-14] chromatographic separation[15-18] or CPL materials.[19-21] In these systems, the helical structure adopted by the polymer is responsible of its function. Therefore, to improve the features of actual materials, or even to prepare novel materials with better or new properties, it is necessary to have tools that allow us to elucidate the secondary structure of the polymer and/or to predict a possible scaffold from a certain monomeric structure. Thus, the scientific community has done a great effort recently to study the tridimensional structure of different families of helical polymers such as poly(phenylacetylene)s (PPAs), polyacetylenes (PAs), poly(diphenylacetylene)s (PDPAs) —symmetric and non-symmetric—, poly(isocyanides) and poly(isocyanate)s among others.[22-32] Among these macromolecules, PPAs are a very interesting family of dynamic helical polymers where the helical sense and/or the elongation can selectively be tuned through the presence of external stimuli.[33-38]

The helical scaffold of PPAs or PDPAs can be built by defining four dihedral angles, ω_1, ω_2, ω_3 and ω_4 (Figure 1a), whose values can be extracted using a combination of structural techniques such as ECD, XRD, AFM, computational calculations, UV-vis, light irradiation studies, etc. Interestingly, while PPAs generate a helical scaffold consisting of two coaxial helices —internal helix (helix 1) described by the polyene backbone; external helix (helix 2) described by the pendants— (Figure 1a), the scaffold of a non-symmetric PDPA is made by three different helices —helix 1 described by the polyene backbone; helix 2 described by the substituents of the double bonds, i.e., the two phenyl groups; helix 3 generated when the polymer grows— (Figure 1b).

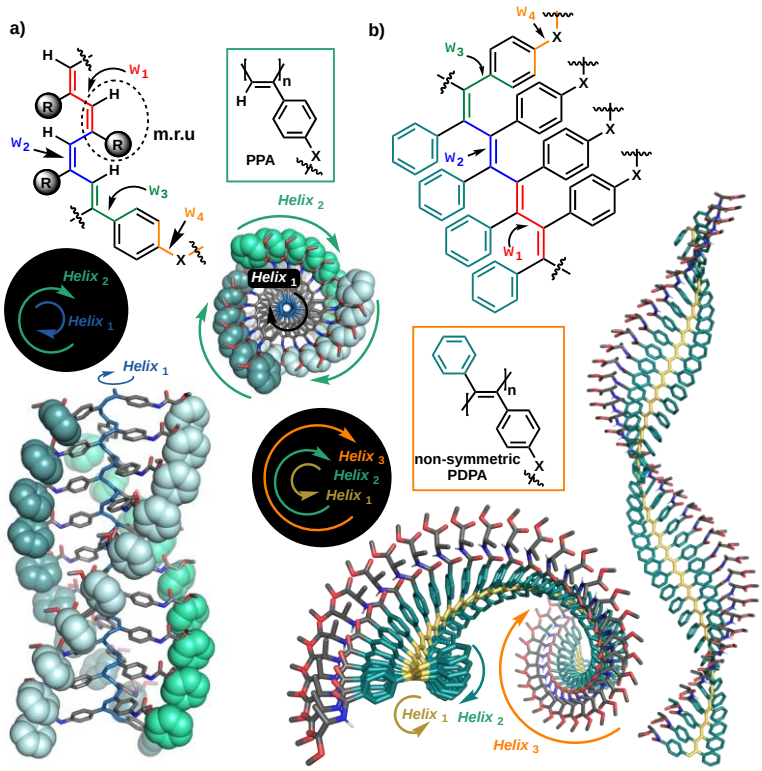

Figure 1. Schematic illustration of the main dihedral angles needed to build a 3D model of (a) PPAs and (b) PDPAs. The coaxial helices found in PPAs and PDPAs are highlighted.

Moreover, due to the presence of a more congested structure, the dynamic behavior of PDPAs is reduced compared to that of PPAs. This fact results in a greater chemical, thermal and photochemical stability of PDPAs. Additionally, the two aryl rings present in the conjugated double bonds provide the polymers with new properties such as fluorescence and circular polarized luminescence (CPL), which open up new applications for these materials.[39,40]

This complete replacement of the polyene backbone hydrogens with aryl rings in PDPAs renders the models used to determine the helical sense of a PPA, based on ECD data, useless for PDPAs. In PPAs, the first Cotton band of the ECD spectrum is usually attributed to ω_1,[41] and corresponds to the orientation of the internal helix, while in PDPAs the first Cotton band provides information about the orientation of the aryl rings within the helical scaffold (helix 2),[29] which is opposite to the helix described by the polyene backbone. Therefore, to elucidate the helical sense of a PPA or a PDPA, different models must be applied.

2. Results and Discussion

In literature, there are few examples where the helical sense of a dynamical helical polymer is inverted by changes on its polymerization degree.[42,43] However, herein we will

demonstrate through a combination of experimental and theoretical studies that the first Cotton band in the ECD trace of a PDPA is produced by the contributions of helix 1 and helix 2, which rotate in opposite directions and whose relative strengths will depend on the size of the polymer. Thus, while in short oligomers the first Cotton band in the ECD spectrum will be governed by helix 1, in larger polymers this Cotton band will be greatly affected by the orientation of helix 2.

To perform these studies, poly-(**1**-**3**) bearing the benzamide of *D*-alanine methyl ester (poly-**1**), the benzamide of *D*-valine methyl ester (poly-**2**) and the benzamide of *D*-leucine methyl ester (poly-**3**), in the *para* position of one of the aryl rings were used as model compounds (Figure 2a).

Table 1. Polymerization conditions of diphenylacetylene derivatives containing a pentafluorophenyl moiety[a]

no.	temp (ºC)	time (h)	yield (%)	M_w[b]	M_w/M_n[b]	DP
a	70	20	11	7500	1.2	19
b	70	24	26	9500	1.4	24
c	80	24	54	17100	1.8	44
d	100	48	61	39100	2.3	100
e	100	24	80	178700	1.3	460

[a] Carried out under nitrogen in toluene with WCl_6-Ph_4Sn as catalytic system; $[M]_0$ = 0.2 M, [cat] = 10 mM, $[Ph_4Sn]$ = 20 mM. [b] Estimated by GPC in THF based on a polystyrene calibration.

First, different batches of poly-PF5 were prepared by polymerization of perfluorophenyl 4-(phenylethynyl)benzoate with a mixture of WCl_6 and Ph_4Sn used as catalysts (Figure 2a). [29] By playing with the polymerization conditions (time and temperature) it was possible to generate poly-PF5 with different polymerization degrees that varies from 19 (oligomer size) to 460 (polymer form) (Table 1) as inferred from GPC studies (Table 1 and Figure 2b).[44,45] Next, the achiral Poly-PF5 was completely transformed into poly-**1**, poly-**2** and poly-**3** via a post-functionalization method. The fully derivatization of poly-PF5 was confirmed by comparing the integrals of the pendant proton peaks and the poly(diphenylacetylene) backbone at the ^{1}H-NMR spectra. Moreover, the complete post-functionalization was corroborated by ^{19}F-NMR, where no F signals appear in the ^{19}F-NMR spectra of poly-**1**, poly-**2** and poly-**3** (See SI).

Interestingly, ECD studies carried out for dilute solutions of poly-**1** with a DP ranging from 19 to 460, prepared in DMF and measured after thermal annealing at 80°C for 24h, show a strong relationship between ECD signature and polymerization degree (Figure 2c).

Thus, while oligomers with DP< 30 (entries a-b) —poly-(**1**$_a$-**1**$_b$)— do not exhibit ECD spectra in all the solvents tested, poly-**1**$_c$ with a DP= 44 (oligomer) shows a ECD (+) in DMF, while poly-(**1**$_d$-**1**$_e$) with DP= 100 and 460 respectively (polymer) show a ECD (-) in the same solvent (Figure 2c). This fact indicates that there is a minimum polymer length necessary to be folded with a certain screw sense excess. Moreover, by varying the polymer length, ECD traces with opposite sign are obtained. The same ECD sign/DP relationship were obtained for poly-**2** and poly-**3** (Figure 2d).

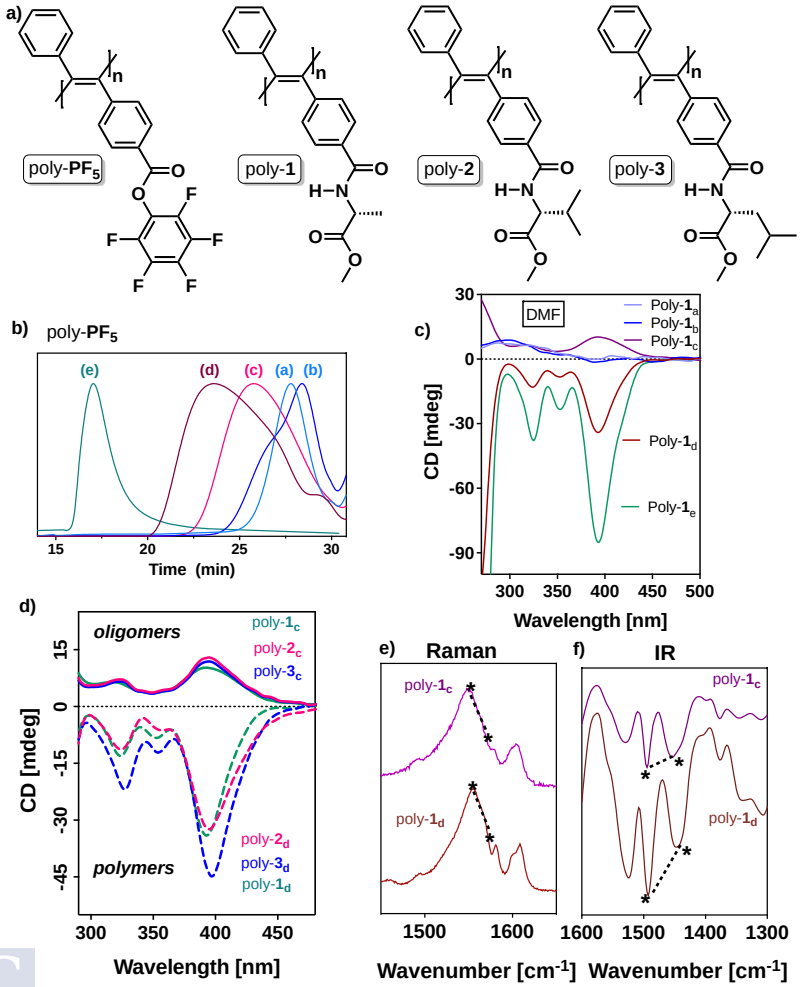

Figure 2. a) Structure of poly-PF$_5$ and poly-(1-3). b) GPC measurements of poly-PF$_{5(a-e)}$. c) CD spectra of poly-**1**$_{(a-e)}$ after thermal annealing at 80°C for 24 h. d) CD spectra of poly-(1-3)$_{(c-d)}$ after thermal annealing at 80°C for 24 h. f) Portion of the IR and Raman spectra of poly-1$_{(c-d)}$. [poly-(1-3)] = 0.5 mg/mL DMF.

To determine which structural parameter is related to this ECD trace/DP pattern, different structural studies were carried out. Thus, IR and Raman studies for poly-(**1**-**3**)$_{c\text{-}d}$ show the same stereoregularity (*E* configuration) in the double bonds at low and high DP —Raman bands ratio at ca.1585/1550 (cm^{-1}/cm^{-1}) < 1; IR bands ratio at ca.1500/1450 (cm^{-1}/cm^{-1}) > 1—, indicating that stereoregularity is not altered by the different polymerization conditions (Figure 2e-f).[23,29] In addition, 1D and 2D NMR studies (^{1}H-NMR, COSY and NOESY) indicate that poly-(**1-3**) have a defined head-to-tail regioregularity at different DPs (see SI).[29] These facts show that the variations in the ECD spectra are not caused by changes in the helical scaffold but by the different contributions of the helical motifs —helix 1 and 2—present in the PDPA scaffold when the polymer chain grows.

To further corroborate these hypotheses and to better understand the contribution of the different functional groups present in PDPAs with different DP to the ECD spectra, computational studies [TD-DFT(CAM-B3LYP)/3-21G][46-48] were performed for different oligomers (n= 8, 10, 12, 14, 16 m.r.u.) of a PDPA with *trans-transoidal* skeleton describing an internal *P* helix —ω_1= 165°, ω_2= 180°, ω_3= 110°— (Figure 3a).[49] The values of the dihedral angles employed to build the 3D models were obtained from previous studies.[29] In these models, the chiral substituents were removed to reduce the computational demands. In agreement to experimental results, it was found that the theoretical ECD spectrum of a PDPA varies with n. Thus, while the theoretical ECD spectrum of an n=8-mer shows a positive Cotton band at 300 nm, the theoretical ECD spectrum of an n=10-mer shows four alternating Cotton bands between 300 and 600 nm, the first being negative. Interestingly, for those oligomers with n>12, the ECD spectrua become negative in the same wavelength range (Figure 3a).

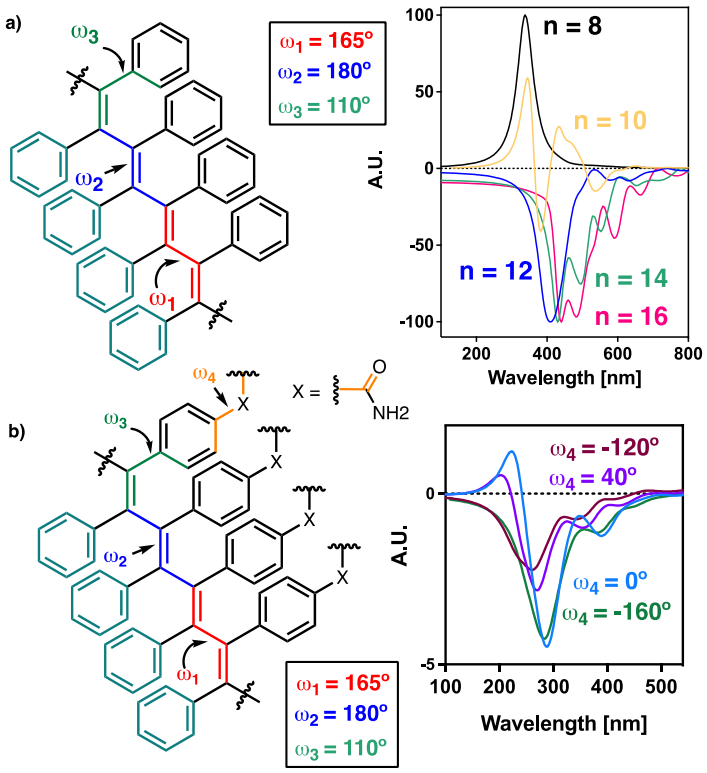

Figure 3. TD-DFT (CAM-B3LYP)/3-21G ECD spectra of (a) oligomers of different sizes and (b) for a 16-mer with different ω_4 values. Half width at half height equals (a) 28 nm and (b) 33 nm. Oligomer structures with ω_1= 165º, ω_2= 180º and ω3= 110º.

To determine if the pendant group interferes in the ECD spectrum of a PDPA, an amide group was introduced at the para position of one of the aryl rings oriented with different dihedral angles (ω4= 0°, 40º, -120º and -160º). TD-DFT(CAM-B3LYP)/3-21G calculations were performed on oligomers with sizes n=8, 10, 12, 14, 16 m.r.u. Theoretical ECD spectra show that the ECD traces are not affected by the orientation of this group (Figure 3b). For instance, in the case of the oligomer with n=8, a positive ECD spectrum was obtained independently of the value introduced for ω_4 (see SI), while in the case of the oligomer with n=16, a negative ECD trace was obtained in all cases (Figure 3b).

Thus, experimentally and theoretically, it is found that there is a direct relationship between the ECD spectra and the DP of a PDPA, an effect that was not observed experimentally or by theoretical calculations in previous reports for the PPAs.[41,49]

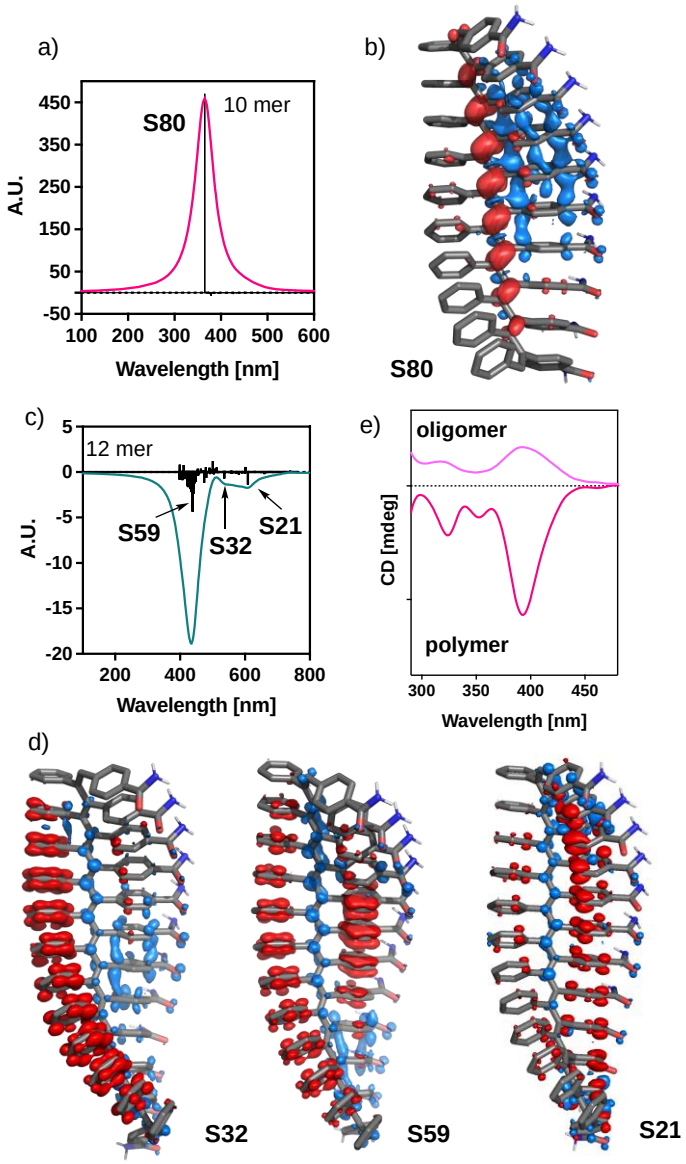

Figure 4. TD-DFT (CAM-B3LYP)/3-21G ECD spectra and the calculated electron density differences for the main transitions for a 10-mer (a-b) and a 12-mer (c-d). e) Experimental ECD spectra obtained for a short oligomer and a polymer like those already explained. Half width at half height equals 25 nm.

To better understand which electrons are involved in the different ECD signals, the electron density differences for the dominant transitions for the 10-mer (Figure 4a-b) and the 12-mer (Figure 4c-d) were calculated. Interestingly, in the 10-mer, the positive ECD spectrum is determined by electron transfer from the polyene backbone (helix 1) to the substituted phenyl ring, whereas, in the 12-mer, the negative ECD spectrum arises through electron transfer from phenyl rings of the PDPA (helix 2) to the main chain (see SI for details).

Hence, the ECD spectrum of a PDPA is governed by helix 1 (short oligomers) or helix 2 (polymers), depending on the DP of the PDPA, which produces opposite ECD signals for the same helical scaffold. For instance, a *P*/*M*/*M* (helix 1/helix 2/helix 3) helical scaffold will produce a positive ECD spectrum for short oligomers, while negative ECD spectra will be obtained for larger polymeric structures.

3. Conclusion

In conclusion, it has been demonstrated experimentally and theoretically that the sign of the ECD spectra of PDPAs depend on their length. Thus while short oligomers of poly-(1-3) produce positive ECD spectra in DMF, larger polymers generate negative ECD spectra. These opposite ECD traces are not related to opposite helical senses induced in the PDPA by polymer size, but rather are caused by the different contributions of the functional groups in polymers of different sizes. Thus, while in short oligomers, the ECD trace is dominated by the polyene backbone (helix 1), in larger polymers, the ECD trace is dominated by the helix described by the phenyl rings of the PDPA (helix 2). As it is known from previous studies, helix 1 and helix 2 rotate in opposite directions, and therefore the ECD traces generated by these two helices have opposite signs.[29]

As a result, a single scaffold will present two opposite ECD traces for different DP of the PDPA. Thus, on the one hand, a *P*/*M*/*M* (helix 1/helix 2/helix 3) will produce positive ECD spectra for short oligomers, while negative for larger polymeric structures. On the other hand, an *M*/*P*/*P* (helix 1/helix 2/helix 3) scaffold will give negative ECD spectra for short oligomers, while they will be positive for larger polymers.

4. References

[1] E. Yashima, K. Maeda, H. Iida, Y. Furusho, K. Nagai. *Chem. Rev.* **2009**, *109*, 6102-62111.

[2] M. Milton, R. Deng, A. Mann, C. Wang, D. Tang, M. Weck. *Acc. Chem. Res.*, **2021**, *54*, 2397-2408.

[3] E. Yashima, N. Ousaka, D. Taura, K. Shimomura, T. Ijai, K. Maeda. *Chem. Rev.* **2016**, *116*, 13752-13990.

[4] J. G. Rudick, V. Perce. *Acc. Chem. Res.* **2008**, *41*, 1641-1652.

[5] E. Yashima, K. Maeda, Y. Furusho. *Acc. Chem. Res.* **2008**, *41*, 1166-1180.

[6] N. Liu, L. Zhou, Z. Q. Wu. *Acc. Chem. Res.*, **2021**, *54*, 3953-3967.

[7] L. Zhou, X. H. Xu, Z. Q. Jiang, L. Xu, B.F. Chu, N. Liu, Z. Q. Wu. *Angew. Chem. Int. Ed.*, **2021**, *60*, 806-812.

[8] E. Anger, H. Iida, T. Yamaguchi, K. Hayashi, D. Kumano, J. Crassous, N. Vanthuyne, C. Roussel, E. Yashima. *Polym. Chem*. **2014**, *5*, 4909-4914.

[9] M. Ando, R. Ishidate, T. Ikai, K. Maeda, E. Yashima *J. Polym. Sci., Part A: Polym. Chem.* **2019**, 57, 2481-2490.

[10] C. Zhang, Y. Qiu, S. Bo, F. Wang, Y. Wang, L. Liu, Y. Zhou, H. Niu, H. Dong, T. Satoh. *J. Polym. Sci., Part A: Polym. Chem.* **2019**, *57*, 1024-1031.

[11] R. P. Megens, G. Roelfes. *Chem. Eur. J.* **2011**, *17*, 8514-8523.

[12] S. Ikeda, R. Takeda, T. Fujie, N. Ariki, Y. Nagata, M. Suginome. *Chem. Sci.* **2021**, *12*, 8811-8816.

[13] Y. Nagata, R. Takeda, M. Suginome. *ACS Cent. Sci.*, **2019**, *5*, 1235-1240.

[14] T. Ikai, M. Ando, M. Ito, R. Ishidate, N. Suzuki, K. Maeda, E. Yashima. *J. Am. Chem. Soc.*, **2021**, *143*, 12725-12735.

[15] R. Ishidate, T. Sato, T. Ikai, S. Kanoh, E. Yashima, K. Maeda. *Polym. Chem.*, **2019**, *10*, 6260-6268.

[16] D. Hirose, A. Isobe, E. Quiñoá, F. Freire, K. Maeda. *J. Am. Chem. Soc.* **2019**, *141*, 8592-8598.

[17] J. Shen, Y. Okamoto. *Chem. Rev*., **2016**, *116*, 1094-1138.

[18] K. Shimomura, T. Ikai, S. Kanoh, E. Yashima, K. Maeda. *Nat. Chem.* **2014**, *6*, 429-434.

[19] Y. Deng, M. Wang, Y. Zhuang, S. Liu, W. Huang, Q. Zhao. *Light Sci. Appl.* **2021**, *10*, 1–18.

[20] H. Tanaka, Y. Inoue, T. Mori. *ChemPhotoChem* **2018**, *2*, 386–402.

[21] S. Wang, D. Hu, X. Guan, S. Cai, G. Shi, Z. Shuai, J. Zhang, Q. Peng, X. Wan. *Angew.Chem. Int. Ed*. **2021**, *60*, 21918–21926.

[22] F. Rey-Tarrío, R. Rodríguez, E. Quiñoá, R. Riguera, F. Freire. *Angew. Chem. Int. Ed.* **2021**, *60*, 8095-8103.

[23] C. I. Simionescu, V. Percec. *Prog. Polym. Sci.*, **1982**, *8*, 133-214.

[24] A. Motoshige, Y. Mawatari, Y. Yoshida, R. Motoshige, M. Tabata. *Polym. Chem.* **2014**, 5, 971-978.

[25] Y. Yoshida, Y. Mawatari, A. Motoshige, R. Motoshige, T. Hiraoki, M. Wagner, K. Müllen, M. Tabata. *J. Am. Chem. Soc.* **2013**, 135, 4110-4116.

[26] A. Motoshige, Y. Mawatari, R. Motoshige, Y. Yoshida, M. Tabata. J. Polym. Sci., Part A: *Polym. Chem*. **2013**, *51*, 5177-5183.

[27] R. Rodriguez, E. Quinoa, R. Riguera, F. Freire. *J. Am. Chem. Soc*, **2016**, *138*, 9620-9628.

[28] K. Maeda, M. Nozaki, K. Hashimoto, K. Shimomura, D. Hirose, T. Nishimura, G. Watanabe, E. Yashima. *J. Am. Chem. Soc*. **2020**, *142*, 7668-7682.

[29] J. J. Tarrío, R. Rodríguez, B. Fernández, E. Quiñoá, F. Freire. *Angew. Chem. Int. Ed.*, **2022**, *61*, e202115070.

[30] S. Sueyoshi, T. Taniguchi, S. Tanaka, H. Asakawa, T. Nishimura, K. Maeda. *J. Am. Chem. Soc.*, **2021**, *143*, 16136-16146.

[31] A. Yurtsever, S. Das, T. Nishimura, R. Rodríguez, D. Hirose, K. Miyata, A. Sumino, T. Fukuma, K. Maeda. *Chem. Commun.*, **2021**, *57*, 12266-12269.

[32] K. Maeda, D. Hirose, M. Nozaki, Y. Shimizu, T. Mori, K. Yamanaka, K. Ogino, T. Nishimura, T. Taniguchi, M. Moro, E. Yashima. *Sci. Adv.*, **2021**, *7*, eabg5381.

[33] M. Núñez-Martínez, S. Arias, E. Quiñoá, R. Riguera, F. Freire. *Chem. Mater.* **2021**, *33*, 4805-4812.

[34] C. Zhao, S. Sun, W. L. Tong, M. C. W. Chan. *Macromolecules*, **2017**, *50*, 6896-6902.

[35] R. Rodríguez, E. Suarez-Picado, E. Quiñoá, R. Riguera, F. Freire. *Angew. Chem. Int. Ed.* **2020**, *59*, 8616-8622.

[36] M. Alzubi, S. Arias, R. Rodríguez, E. Quiñoá, R. Riguera, F. Freire. *Angew. Chem. Int. Ed.* **2020**, *59*, 13365-13369.

[37] E. Suarez-Picado, E. Quiñoá, R. Riguera, F. Freire. *Angew. Chem. Int. Ed.* **2020**, *59*, 4537-4543.

[38] M. Núñez-Martínez, S. Arias, J. Bergueiro, E. Quiñoá, R. Riguera, F. Freire. *Macromol. Rapid Commun*. **2021**, 2100616.

[39] L. E. MacKenzie, R. Pal. *Nat. Rev. Chem.* **2021**, *5*, 109-124.

[40] K. Dhbaibi, L. Abella, S. Meunier-Della-Gatta, T. Roisnel, N. Vanthuyne, B. Jamoussi, G. Pieters, B. Racine, E. Quesnel, J. Autschbach, J. Crassous, L. Favereau. *Chem. Sci*. **2021**, *12*, 5522-5533.

[41] B. Fernández, R. Rodríguez, A. Rizzo, E. Quiñoá, R. Riguera, F. Freire. *Angew. Chem. Int. Ed.* **2018**, *57*, 3666-3670.

[42] Y. Nagata, T. Nishikawa, K. Terao, H. Hasegawa, M. Suginome. *J. Polym. Sci., A, Polym. Chem.*, **2019**, *57*, 260-263.

[43] H. Onouchi, K. Okoshi, T. Kajitani, S. I. Sakurai, K. Nagai, J. Kumaki, K. Onitsuka, E. Yashima. *J. Am. Chem. Soc.*, **2008**, *130*, 229-236.

[44] X. A. Zhang, A. Qin, L. Tong, H. Zhao, Q. Zhao, J. Z. Sun, B. Z. Tang. *ACS Macro Letters*, **2012**, *1*, 75-79.

[45] W. Z. Yuan, A. Qin, J. W. Y. Lam, J. Sun, J., Y. Dong, M. Häussler, J. Liu, H. P. Xu, Q. Zheng, B. Z. Tang. *Macromolecules* **2007**, *40*, 3159-3166.

[46] E. Runge, E. K. U. Gross. *Phys. Rev. Lett.* **1984**, *52*, 997-1000.

[47] Y. Yanai, D. P. Tew, N. C. Handy. *Chem. Phys. Lett*. **2004**, *393*, 51-57.

[48] J. S. Binkley, J. A. Pople, W. J. Hehre. *J. Am. Chem. Soc.*, **1980**, *102*, 939-947.

[49] B. Fernández, R. Rodríguez, E. Quiñoá, R. Riguera, F. Freire. *ACS Omega*, **2019**, *4*, 5233-5240.

Chapter V

Dynamic *P*/*M* Memory Effect of the Macromolecular Helicity in Chiral Poly(diphenylacetylene)s: Kinetic and Thermodynamic Studies

Chapter V: Dynamic *P*/*M* Memory Effect of the Macromolecular Helicity in Chiral Poly(diphenylacetylene)s: Kinetic and Thermodynamic Studies

Abstract

Dynamic helical memory in chiral dissymmetric poly(diphenylacetylene)s is shown by using as model compound a PDPA that bears the benzamide of (*L*)-alanine methyl ester as pendant [poly-(*L*)-1]. By combining the conformational control at the pendant group and the high steric hindrance of the poly(diphenylacetylene) backbone it is possible to induced either a *P* or *M* helical sense in the polymer by using solvents with different donor character, which can be memorized by removing the solvent and dissolving it in another one where the opposite helical sense must be induced. ECD and CPL studies show how the chiroptical and emissive properties are memorized. Evolution experiments with time of the helix inversion process at different temperatures were done to determine the kinetic and thermodynamic parameters of the process.

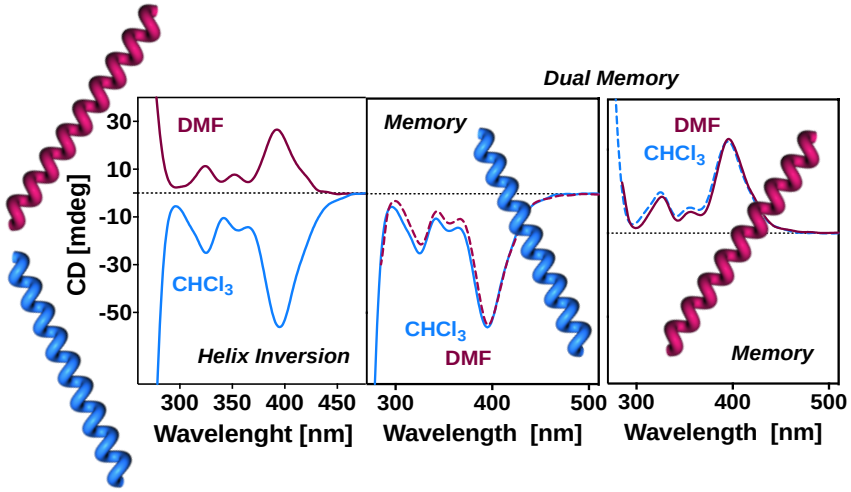

1. Introduction

Dynamic helical polymers play an important role in the chemistry of materials due to their application in different fields such as asymmetric catalysis,[1-6] chiral recognition,[7] sensing,[8-14] photoelectronic devices[15-17] or biological media.[20] This fact is related to the helical structure[21,22] adopted by the helical polymer —*P* or *M* helix, compressed/stretched—, which can be tuned by the presence of external stimuli, and to the functional groups present in the pendant that will be oriented in a certain position towards the helix. Thus, it is possible to do helix inversion, screw sense enhancement or stretching/compression of the helix through different mechanisms —supramolecular interactions,[23-30] solvent polarity,[31-33] sergeants and soldiers effect,[28,34] majority rules[28] or chiral-to chiral communication mechanisms[35-37]— that follow a cooperative effect. These changes in the helix in dynamic helical polymers are usually triggered by either playing with the conformational equilibrium of a chiral pendant or by stablishing a supramolecular interaction between achiral pendants and chiral molecules. In the later system, Yashima and coworkers found that, in some cases, when the chiral additive is removed from the solution, the dynamic helical polymer, i.e., a poly(phenylacetylene) bearing a carboxylic acid at the *para* position, maintain the helical structure induced by the chiral additive.[14] This phenomenon was denoted as "memory effect". They found that this phenomenon can be extrapolated to other polyacetylene derivatives, such as poly(biphenylacetylene)s (PBPA) and poly(diphenylacetylene)s. These systems were recently denoted as first-, second- and third generation of static helicity memory respectively, and their helix induction provoked by addition of a chiral additive can be storage after complete removal of the nonracemic guest.[38]

Herein, we want to go a step forward and explore the helical memory in chiral dynamic helical polymers, where the chiral group responsible of the induction of the helical sense is covalently linked to the polymer main chain. Our objective is to prepare a helical polymer that shows dynamic memory, where either *P* or *M* helical sense can be memorized in environmental conditions where the opposite helical sense should be induced. To perform these studies, we chose a poly(diphenylacetylene) (PDPAs) as dynamic helical polymer. This family of helical polymers have gained the attention of the scientific community lately due to properties associated to the

poly(diphenylacetylene) backbone such as chemical, photochemical and thermostabilities, and optical and chiroptical ones –CD, fluorescence emission, CPL–, which make PDPAs promising materials. At the beginning, these materials were considered as static, although recently two asymmetrically substituted PDPAs functionalized in one of the aryl rings with chiral amines[39-43] or amino acids[44] through amide bonds, were reported as the first examples of PDPAs with dynamic properties. In both cases, a solvent-dependent helix inversion is achieved based either on the polar/non-polar or the donor/non-donor character of the solvent. In these studies, the polymer adopts a preferred helical sense after thermal annealing at high temperatures (*e.g.*, 80°C during 24 h) in a specific solvent.[44-48]

2. Results and Discussion

One of these PDPAs, poly-(*L*)-**1**, a dissymmetric chiral poly(diphenylacetylene) that bears the benzamide of (*L*)-alanine methyl ester at one of the aryl rings of the diphenylacetylene was reported by our group.[44] We found that *M* or *P* helical senses can be induced in the polyene backbone of poly-(*L*)-**1** (helix 1) after thermal annealing (80°C/24 h) in donor (DMF, DMSO) and non-donor ($CHCl_3$, MeCN) solvents respectively (Figure 1a). This different screw sense excess obtained in donor and non-donor solvents is associated to a conformational change at the pendant group which was monitored by VCD studies. Thus, while in donor solvents, the carbonyls of the amide and ester groups are *synperyplanar* oriented (*syn* conformation), in non-donor solvents these two groups are a*ntiperiplanar* oriented (*anti* conformation) (Figure 1c). As a result, a chiroptical and circularly polarized luminescence (CPL) switch was obtained (Figure 1b).

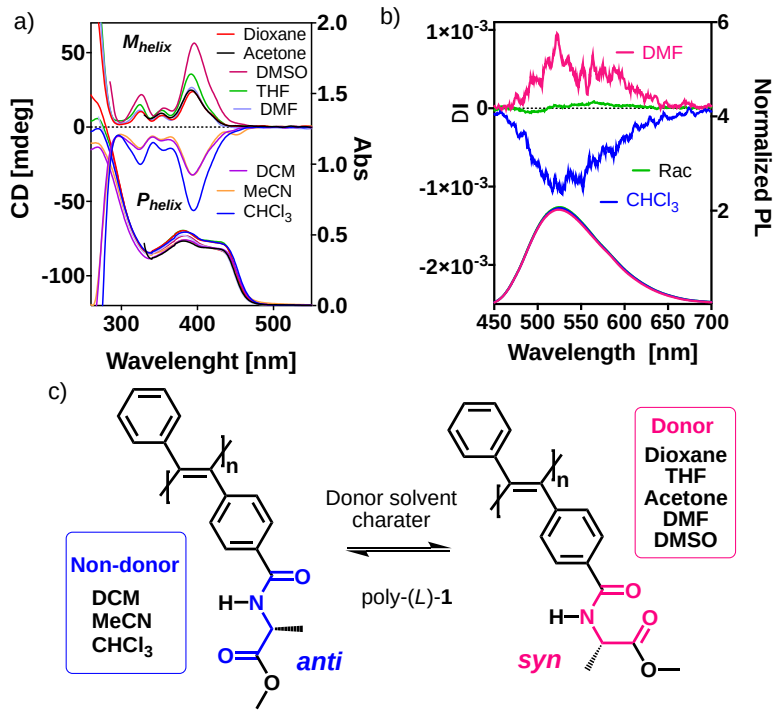

Figure 1. a) ECD and UV spectra of poly-(*L*)-**1** in different solvents (0.5 mg/mL, 1 mm path). b) CPL spectra of poly-(*L*)-w**1** (λ_{Exc} = 365 nm, 0.3 mg/mL). c) Schematic illustration of the solvent-triggered conformational change in the pendant group that promotes the helix inversion after a thermal annealing.

The large energy barrier between the two helical orientations (*P* and *M*) of poly-(*L*)-**1** is consequence of the intrinsic steric hindrance found in the PDPA backbone. The presence of two aryl rings at the double bonds of the conjugated polyene makes very difficult to switch from one helical sense to the other. Therefore, and taking advantage of this property, we decided to study the dynamic helical memory of poly-(*L*)-**1**. Accordingly, an *M* helical sense was first induced in poly-(*L*)-**1** after thermal annealing in a donor solvent (Figure 2a). Next, the solvent was removed under reduced pressure and finally it was dissolved again in a non-donor solvent (Figure 2a). Analogous experiments were also done in the opposite direction, 1) thermal annealing of poly-(*L*)-**1** in a non-donor solvent —*P* helix induction—, 2) solvent removal and 3) addition of a donor solvent (Figure 2a). ECD studies show that the helical sense induced through thermal annealing is memorized when dissolving the polymer at room temperature in a solvent with opposite donor character (Figure 2b). In addition, the CPL properties gained during the thermal annealing of the PDPA are retained once is redissolved in a solvent with different donor behavior (Figure 2c). This is, to the best of our knowledge, the first time that a dynamic memory effect is reported for a chiral helical polymer.

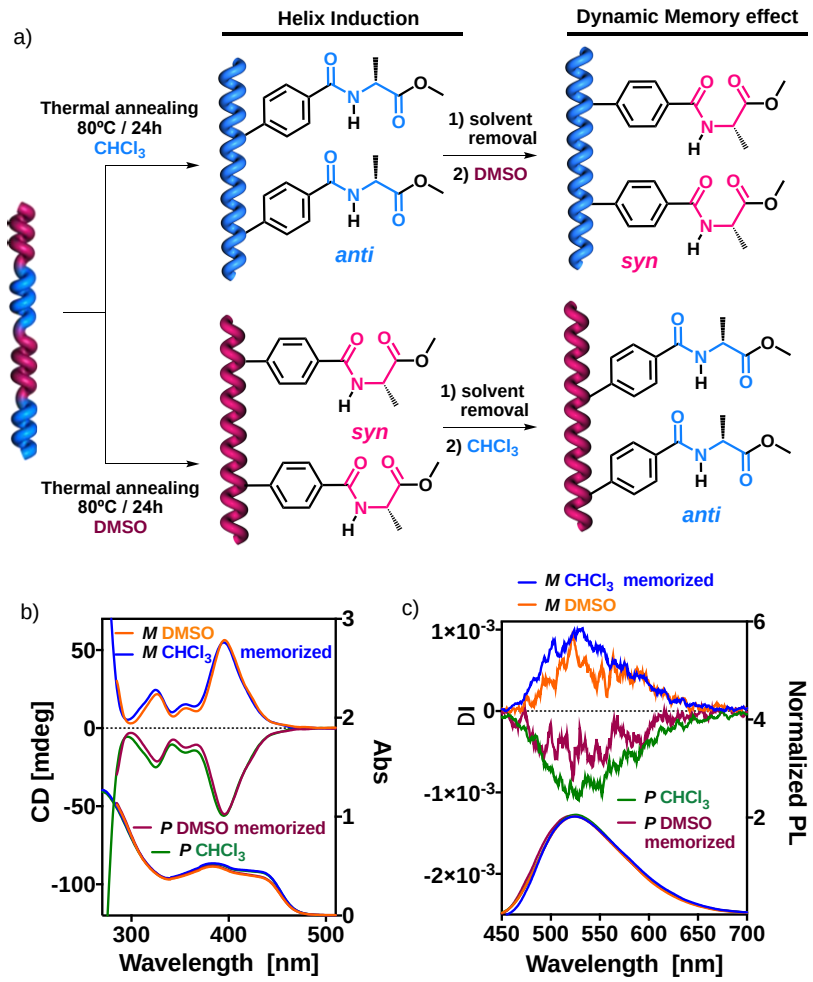

Figure 2. a) Schematic illustration of the *P*/*M* helix induction of poly-(*L*)-1 after thermal annealing and its dynamic memory effect. b) ECD and c) CPL studies showing the dynamic memory effect of poly-(*L*)-1. [poly-(*L*)-1] = 0.5 mg/mL.

Next, we proceed to analyze the *P*/*M* helical sense inversion through kinetic and thermodynamic studies. Thus, a memorized *P* helical structure obtained after thermal annealing of poly-(*L*)-1 in $CHCl_3$ followed by solvent removal was dissolved in DMF. The solution was heated up to 80°C and ECD measurements were done every 6 minutes during 948 min to study the evolution of a *P* memorized helix towards an *M* one induced by thermal annealing at 80°C in DMF (Figure 3b,c). It was found that a complete helix inversion of poly-(*L*)-1 in DMF is produced after 16 hours of thermal annealing at 80°C. By plotting the variation of the ECD at 393 nm vs time is possible to observe that follows and exponential grow that can be fitted to equation:

$$ECD=ECD_0 + (Plateau- ECD_0)*(1-exp(-K_{inv}*t))$$

Where ECD_0 is the value of the ECD signal when time is zero and Plateau is the ECD value at infinite times. In this case, the equation obtained is:

$$ECD=-46.02 + (76.81)*(1-exp(-0.002834*t))$$

From this equation, a kinetical constant from *P* to *M* helix inversion (k_{inv}) for poly-(*L*)-**1** in DMF at 80°C, $k_{inv}= 2.83\cdot10^{-3}$ min^{-1} ($k_{inv}= 4.72\cdot10^{-5}$ s^{-1}) was obtained. Similar studies were carried out at different temperatures: 70, 90 and 100°C. The kinetical constant from *P* to *M* helix inversion decreases at 70°C when compared to that obtained at 80°C ($k_{inv\ (80°C)}= 4.72\cdot10^{-5}$ s^{-1}, $k_{inv\ (70°C)}= 2.6\cdot10^{-5}$ s^{-1}). On the contrary, this constant increases when the experiment is performed at higher temperature ($k_{inv\ (90°C)}= 9.76\cdot10^{-5}$ s^{-1}, $k_{inv\ (100°C)}= 1.73\cdot10^{-4}$ s^{-1}). The value of the k_{inv} at different temperatures was used to calculate the activation energy barrier (E_a) of the helical inversion by plotting $ln(k_{inv})$ vs T^{-1} K^{-1} (Figure 3d). In this case, the activation energy barrier to produce a *P* to *M* helix inversion of poly-(*L*)-**1** is $E_a= 16.38$ kcal mol^{-1}. In addition, by applying the Eyring equation —$ln(k_{inv}/T)$ vs T^{-1} K^{-1}—, the thermodynamic parameters $\Delta H^{\ddagger}$ and $\Delta S^{\ddagger}$ for the helical inversion were calculated. In this case, $\Delta H^{\ddagger}$=15.6 kcal mol^{-1} and $\Delta S^{\ddagger}$=-34.5 cal K^{-1} mol^{-1}, (Figure 3e).

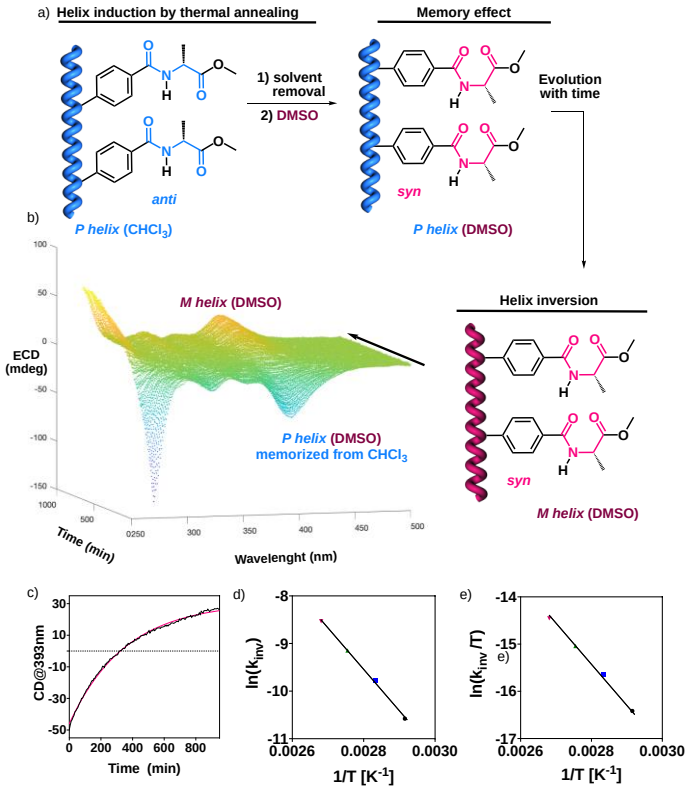

Figure 3. a) Schematic illustration of the helical inversion produced with time from a memorized helix of poly-(L)-**1**. (b-c) Time dependent ECD studies for a DMF solution of poly-(L)-**1** at 80°C pre-

annealed in $CHCl_3$. d) Arrhenius plot of $\ln(k_{inv})$ obtained from the slope of c) versus T^{-1} K^{-1}. e) Eyring plot of $\ln(k_{inv}/T)$ vs T^{-1} K^{-1}.

Analogous studies were carried out for poly-(*L*)-**1** when a memorized *M* helix evolves towards a *P* helix by thermal annealing at 80°C of poly-(*L*)-**1** in 1,1,2,2-tetrachloroethane (TCE) (see SI). From these studies, it was possible to obtain a similar kinetical constant of inversion ($k_{inv} = 4.83 \cdot 10^{-5}$ s^{-1}) demonstrating the reversibility of the process.

The evolution of the memorized ECD spectra for poly-(*L*)-**1** in $CHCl_3$ and DMF and further dissolved in DMF and $CHCl_3$, respectively, were also monitored at rt and lower temperatures (i.e., 4°C and -20°C). These studies showed that, at low temperatures, a longer-lasted memory effect is obtained. For instance, while a decrease of 20% is observed after 2 days at rt, at 4° and -20°C a decrease in the ECD trace of 4% and 2% is found.

3. Conclusions

In conclusion, in this work it is demonstrated, through an elegant example, that chiral PDPAs show a dynamic chiral effect associated to their intrinsic steric properties. To verify this, an asymmetric PDPA bearing the benzamide of *L*-alanine methyl ester at one of the aryl rings was prepared [poly-(*L*)-1]. This polymer can adopt either *P* or *M* helical senses after thermal annealing in $CHCl_3$ and DMF, respectively. Remarkably, it was found that the helical structure obtained after thermal annealing is memorized after solvent removal followed by redissolution in another solvent that promotes the opposite helical sense. For instance, the *P* helical structure adopted by poly-(*L*)-1 after thermal annealing in $CHCl_3$ after solvent evaporation followed by redissolution in DMF. The memory effect is temperature dependent and is maintained at lower temperatures. Interestingly, not only the helical structure is memorized, but also other properties associated to the helical scaffold such as CPL emission. This is the first time to our knowledge that a chiral dynamic helical polymer shows memory effect, and where the two helical senses obtained for a given polymer can be tested for potential applications in the same solvent, *e.g.*, *P* or *M* helices can be obtained in both $CHCl_3$ and DMF. Hence, the two *P* and *M* helical structures can be obtained in a certain solvent, although just one is favored. This fact opens a new horizon in the application of this materials.

4. References

1) Ando, M.; Ishidate, R.; Ikai, T.; Maeda, K.; Yashima, E. *J. Polym. Sci., Part A: Polym. Chem.* **2019**, 57, 2481-2490.

2) Zhang, C.; Qiu, Y.; Bo, S.; Wang, F.; Wang, Y.; Liu, L.; Zhou, Y.; Niu, H.; Dong, H.; Satoh, T. *J. Polym. Sci., Part A: Polym. Chem.* **2019**, *57*, 1024-1031.

3) Megens, R. P.; Roelfes, G. *Chem. Eur. J.* **2011**, *17*, 8514-8523.

4) Ikeda, S.; Takeda, R.; Fujie, T.; Ariki, N.; Nagata, Y.; Suginome, M. *Chem. Sci.* **2021**, *12*, 8811-8816.

5) Nagata, Y.; Takeda, R.; Suginome, M. *ACS Cent. Sci.*, **2019**, *5*, 1235-1240.

6) Ikai, T.; Ando, M.; Ito, M.; Ishidate, R.; Suzuki, N.; Maeda, K.; Yashima, E. *J. Am. Chem. Soc.*, **2021**, *143*, 12725-12735.

7) Anger, E.; Iida, H.;Yamaguchi, T.; Hayashi, K.; Kumano, D.; Crassous, J.; Vanthuyne, N.; Roussel, C.; Yashima, E. *Polym. Chem*. **2014**, *5*, 4909-4914.

8) Ishidate, R.; Markvoort, A. J.; Maeda, K.; Yashima, E. *J. Am. Chem. Soc.*, **2019**, *141*, 7605-7614.

9) Maeda, K.; Hirose, D.; Okoshi, N.; Shimomura, K.; Wada, Y.; Ikai, T.; Kanoh, S.; Yashima, E. *J. Am. Chem. Soc.*, **2018**, *140*, 3270-3276.

10) Sakai, R.; Barasa, E. B.; Sakai, N.; Sato, S. I.; Satoh, T.; Kakuchi, T. *Macromolecules*, **2012**, *45*, 8221-8227.

11) Yashima, E.; Maeda, K. *Macromolecules*, **2008**, *41*, 3-12.

12) Maeda, K.; Yashima, E. *Supramolecular chirality*, **2006**, 47-88.

13) Nonokawa, R.; Yashima, E. *J. Am. Chem. Soc.*, **2003**, *125*, 1278-1283.

14) Yashima, E.; Maeda, K.; Okamoto, Y. *Nature*, **1999**, *399*, 449-451.

15) Ando, M.; Ishidate, R.; Ikai, T.; Maeda, K.; Yashima, E. *J. Polym. Sci. A Polym. Chem.*, **2019**, *57*, 2481-2490.

16) Gao, Y.; Guo, F.; Cao, P.; Liu, J.; Li, D.; Wu, J.; Wang, N.; Su, Y.; Zhao, Y. *ACS nano*, **2020**, *14*, 3442-3450.

17) Park, H. L.; Jun, J.; Kim, M. H.; Lee, S. H. *Org. Electron.*, **2022**, *100*, 106385.

18) Zheng, Z. G.; Lu, Y. Q.; Li, Q. *Adv. Mater.*, **2020**, *32*, 1905318.

19) Sa, C.; Xu, X.; Wu, X.; Chen, J.; Zuo, C.; Fang, X. *J. Mater. Chem. C*, **2019**, *7*, 13097-13103.

20) Leigh, T.; Fernandez-Trillo, P. *Nat. Rev. Chem.*, **2020**, *4*, 291-310.

21) Yashima, E.; Ousaka, N.; Taura, D.; Shimomura, K.; Ikai, T.; Maeda, K. *Chem. Rev.* **2016**, *116*, 13752-13990.

22) Yashima, E.; Maeda, K.; Iida, H.; Furusho, Y.; Nagai, K. *Chem. Rev.*, **2009**, *109*, 6102-6211.

23) Kim, K. Y.; Kim, J.; Moon, C. J.; Liu, J.; Lee, S. S.; Choi, M. Y.; Feng, C.; Jung, J. H. *Angew. Chem. Int. Ed*, **2019**, *58*, 11709-11714.

24) Guan, X.; Wang, S.; Shi, G.; Zhang, J.; Wan, X. *Macromolecules*, **2021**, *54*, 4592-4600.

25) Qiao, J.; Lin, S.; Li, J.; Tian, J.; Guo, J. *Chem. Commun.*, **2019**, *55*, 14590-14593.

26) Ishidate, R.; Sato, T.; Ikai, T.; Kanoh, S.; Yashima, E.; Maeda, K. *Polym. Chem.*, **2019**, *10*, 6260-6268.

28) Ishidate, R.; Markvoort, A. J., Maeda, K.; Yashima, E. *J. Am. Chem. Soc.*, **2019**, *141*, 7605-7614.

29) Shimomura, K.; Ikai, T.; Kanoh, S.; Yashima, E.; Maeda, K. *Nat. Chem.* **2014**, *6*, 429-434.

30) Leiras, S.; Suárez-Picado, E.; Quiñoá, E.; Riguera, R.; Freire, F. *Giant* **2021**, *7*, 100068.

31) Leiras, S.; Freire, F.; Seco, J. M.; Quiñoá, E.; Riguera, R. *Chem. Sci.* **2013**, *4*, 2735-2743

32) Rodríguez, R.; Quiñoá, E.; Riguera, R.; Freire, F. *Small,* **2019**, *15*, 1970070

33) Rodríguez, R.; Suárez-Picado, E.; Quiñoá, E.; Riguera, R.; Freire, F. *Angew. Chem. Int. Ed.* **2020**, *59*, 8616-8622.

34) Bergueiro, J.; Freire, F.; Wendler, E. P.; Seco, J. M.; Quiñoá, E.; Riguera, R. *Chem. Sci.*, **2014**, *5*, 2170-2176.

35) Cobos, K.; Rodríguez, R.; Quiñoá, E.; Riguera, R.; Freire, F. *Angew. Chem. Int. Ed.*, **2020**, *59*, 23724-23730.

36) Alzubi, M.; Arias, S.; Rodríguez, R.; Quiñoá, E.; Riguera, R.; Freire, F. *Angew. Chem. Int. Ed.* **2020**, *59*, 13365-13369.

37) Cobos, K.; Quiñoá, E.; Riguera, R.; Freire, F. *J. Am. Chem. Soc.* **2018**, *140*, 12239–12246.

38) Yashima, E.; Maeda, K. *Bull. Chem. Soc. Jpn.* **2021**, *94*, 2637-2661.

39) Maeda, K.; Nozaki, M.; Hashimoto, K.; Shimomura, K.; Hirose, D.; Nishimura, T.; Watanabe, G.; Yashima, E. *J. Am. Chem. Soc*. **2020**, *142*, 7668-7682.

40) Hirose, D.; Nozaki, M.; Maruta, M.; Maeda, K. *Chirality*, **2022**, *34*, 597–608.

41) Sueyoshi, S.; Taniguchi, T.; Tanaka, S.; Asakawa, H.; Nishimura, T.; Maeda, K. *J. Am. Chem. Soc.*, **2021**, *143*, 16136-16146.

42) Yurtsever, A.; Das, S.; Nishimura, T.; Rodríguez, R.; Hirose, D.; Miyata, K.; Sumino, A.; Fukuma, T.; Maeda, K. *Chem. Commun.*, **2021**, *57*, 12266-12269.

43) Maeda, K.; Hirose, D.; Nozaki, M.; Shimizu, Y.; Mori, T.; Yamanaka, K.; Ogino, K.; Nishimura, T.; Taniguchi, T.; Moro, M; Yashima, E. *Sci. Adv.*, **2021**, *7*, eabg5381.

44) Tarrío, J. J.; Rodríguez, R.; Fernández, B.; Quiñoá, E.; Freire, F. *Angew. Chem. Int. Ed.*, **2022**, *61*, e202115070.

45) Seo, K. U.; Jin, Y. J.; Kim, H.; Sakaguchi, T.; Kwak, G. *Macromolecules*, **2018**, *51*, 34-41.

46) Jim, C. K. W.; Lam, J. W. Y.; Leung, C. W. T.; Qin, A.; Mahtab, F.; Tang, B. Z. *Macromolecules*, **2011**, *44*, 2427–2437.

47) Kim, H.; Seo, K. U.; Jin, Y. J.; Lee, C. L.; Teraguchi, M.; Kaneko, T.; Aoki, T.; Kwak, G. *ACS Macro Lett.* **2016**, *5*, 622−625.

48) Zhang, X. A.; Qin, A.; Tong, L.; Zhao, H.; Zhao, Q.; Sun, J. Z., Tang, B. Z. *ACS Macro Lett.*, **2012**, *1*, 75-79.

Chapter VI

Complex Aggregation Pathways in Covalent Helical Polymers: Consecutive Mechanism and Kinetically Trapped Aggregates in PDPA/M^{n+} Complexes

Chapter VI: Complex Aggregation Pathways in Covalent Helical Polymers: Consecutive Mechanism and Kinetically Trapped Aggregates in PDPA/M^{n+} Complexes

Abstract

Stable *M* and *P* nanospheres with opposite circularly polarized luminescence (CPL) can be obtained from a single helical polymer/metal complex under the same environmental conditions. This fact is possible due to the employment of a poly(diphenylacetylene) with dynamic memory effect as helical polymer. The high energy barrier of the helix inversion process in these polymers makes possible to isolate Kinetically trapped (Agg_1) and thermodynamic aggregates (Agg_2) with opposite chirality. These aggregates consist on stable and low polydisperse nanospheres, which can be dispersed in solution in either *M* or *P* chiralities for days or months.

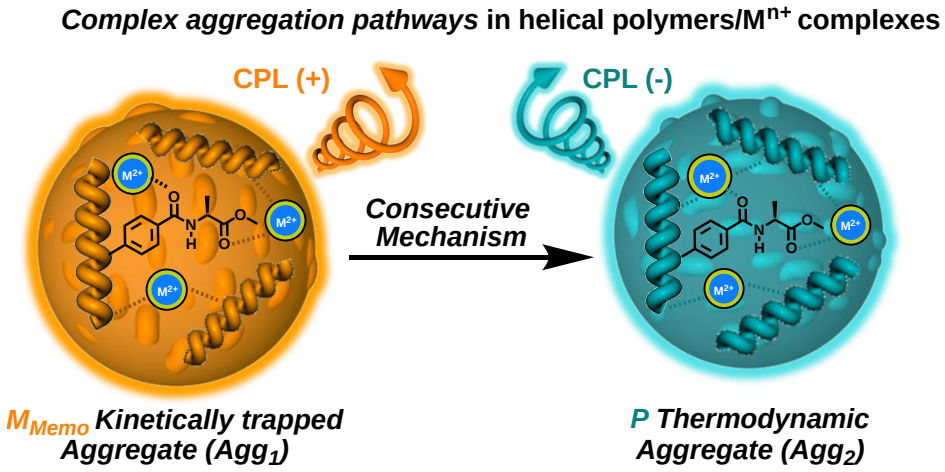

1. Introduction

Nanomaterial chemistry is a research field that involves the design, development and application of new materials at the nanoscale, which have different properties compared to the bulk state.[1] Incorporation of chirality to nanomaterials provide them with interesting properties associated to it such as stereo complexation, circularly polarized emission (CPL), sensing,[2-5] chiral recognition,[6-8] separation[9-11] or catalysis.[12-17] The preparation of chiral nanomaterials has been explored using different approaches (*e.g.*, self-assembly of monomers, metal organic frameworks (MOFs), or metal-polymer complexes) depending on the building blocks used.

Dynamic helical polymers are promising materials that fulfill both essential features — nanomaterial and chirality— for being applied as chiral nanomaterials. Moreover, the dynamic behavior of the polymer makes possible to prepare, from a single polymer, nanostructures with different chirality at the surface that can be tuned by external stimuli.[18-22] For instance, during the last decade, dynamic chiral nanostructures such as nanospheres, nanotubes or nanotoroids were generated from the combination of poly(phenylacetylene)s (PPAs) and metal ions to yield helical polymer-metal complexes (HPMCs).[23-25] In these systems, the PPA is used as dynamic chiral source, while the metal ion is used as crosslinking agent. The high aggregation tendency of HPMCs in organic solvents results in a poor stability of the dispersed nanostructures. Additionally, PPAs are light-sensitive, and a photochemical electrocyclization of the polyene backbone can occur under light exposure breaking down the material.[22]

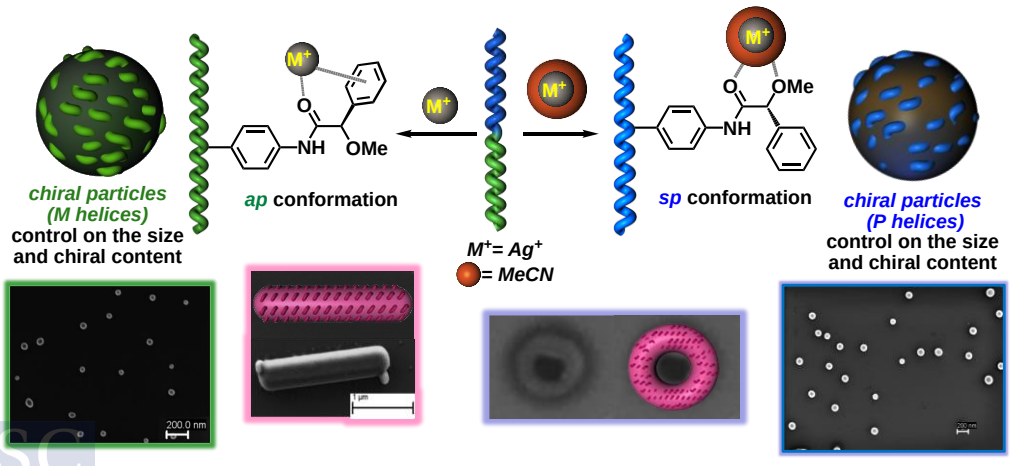

Figure 1. Schematic illustration of different methodologies to prepare PPA polymeric particles based on the nanostructuration of helical polymer-metal complexes.

In this work, our goal is to surpass the problems of stability associated to PPA/M^{n+} complexes and to prepare stable dynamic chiral polymeric particles which can be stored,

dispersed in solution, for months using a PDPA.[26,27] Moreover, we will explore the formation of smart nanomaterials whose induced chirality can be memorized once the external stimulus is removed. In this case, we are interested in the generation of nanomaterials with dynamic memory effect, which will lead to the formation of complex aggregation pathways of covalent polymers. Thus, to perform these studies, we will use a chiral PDPA that shows a kinetically controlled dynamic helical behavior. Therefore, the two *P*/*M* screw senses can be induced in the PDPA by playing with the conformational composition of the pendant group at high temperature.[28] Moreover, the induced screw sense excess can be kinetically trapped at low temperatures once the external stimulus is removed. On the other hand, different metal perchlorates [$LiClO_4$ and $Ba(ClO_4)_2$] will be used as crosslinking agents to assemble the PDPAs into the desired nanostructures in solvents where the polymer is completely dissolved, such as $CHCl_3$ or DCE. Additionally, the use of chiral PDPAs that show dynamic memory effect will allow us to analyze the evolution of the aggregates over time, which will evolve towards other aggregates through a complex aggregation mechanism (Agg_1 to Agg_2). Thus, during these studies, we will analyze the formation of kinetically trapped aggregates (Agg_1) and their evolution towards thermodynamic ones (Agg_2), which could follow a consecutive mechanism through a gradual helix inversion of the PDPA within the aggregate.

2. Results and Discussion

To carry out these studies, an asymmetric PDPA that bears the 4-benzamide of alanine methyl ester as pendant group in one of the aryl rings was chosen as model compound (poly-(*L*)-**1**) (see SI for synthetic details and characterization data). This polymer can adopt either *M* or *P* screw sense excess at the polyene backbone (helix 1) after a thermal annealing (i.e., 80°C/24h) in donor (DMF, DMSO, THF, Dioxane, Acetone) and non-donor solvents ($CHCl_3$, CH_2Cl_2, MeCN) respectively (Figure 2).

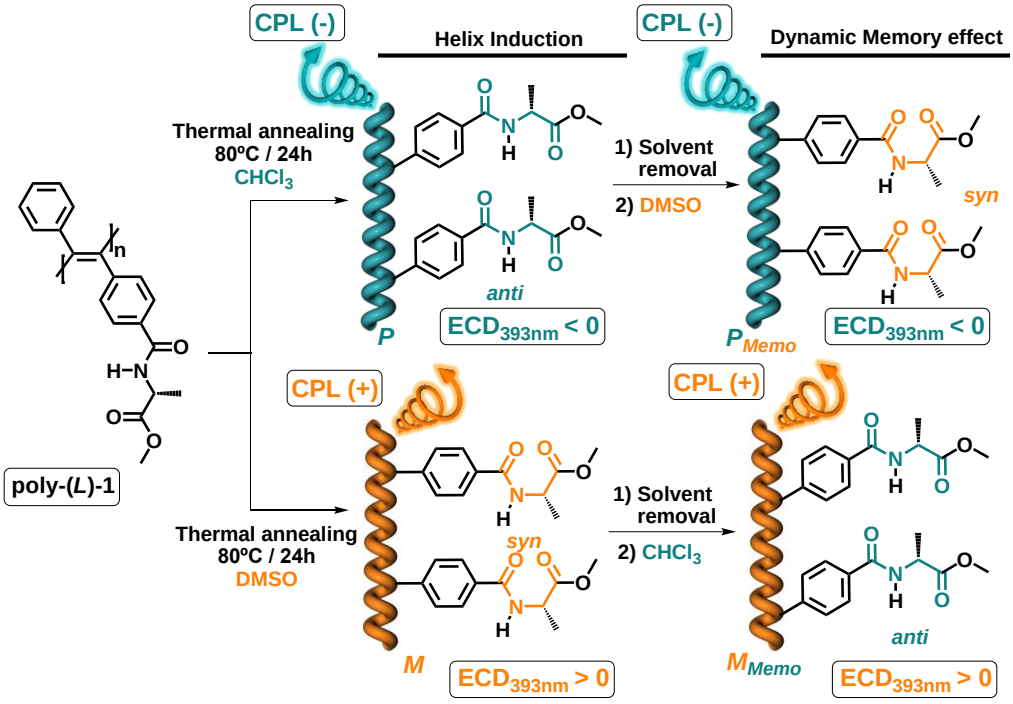

Figure 2. Chemical structure of poly-(*L*)-1 and helical induction towards *P* and *M* helical senses after thermal annealing in non-donor and donor solvents respectively. The dynamic memory effect produced after solvent removal and redissolution is also illustrated.

The different helical senses adopted by poly-(*L*)-**1** in donor and non-donor solvents is attributed to a conformational change at the pendant group as inferred from vibrational circular dichroism studies (VCD).[28] Thus, while in donor solvents, the two carbonyl groups in the pendant (amide and ester) are *synperyplanar* oriented (*syn* conformation), in non-donor solvents these two carbonyls are a*ntiperiplanar* oriented (*anti* conformation) (Figure 2). As a result, a chiroptical and a circularly polarized luminescence (CPL) switch based on the donor solvent character was obtained. Interestingly, the helical sense adopted by poly-(*L*)-**1** after thermal annealing can be memorized, remaining unaltered after solvent removal and redissolving it in a solvent with opposite donor character (Figure 2).

Hence, poly-(*L*)-**1** (0.5 mg/mL) was preannealed in DCE and THF at 80°C for 24h to induce either a P_{helix} (DCE, ECD_{393}<0) and an M_{helix} (THF, ECD_{393}>0) in the PDPA (Figure 3). The solvent was removed and the helical sense memorized in the solid state. Preoriented poly-(*L*)-**1** into *P* and *M* helices was re-dissolved in DCE, being the helical structure memorized after dissolvint it as proven by ECD studies (Figure 3b). Next, metal perchlorate salts —$LiClO_4$ and $Ba(ClO_4)_2$— dissolved in MeOH (10mg/mL) were added to different vials containg solutions of *P* or *M* poly-(*L*)-**1** (0.5mg/mL DCE) in 1/2 mol/mol polymer/metal ratio. ECD studies of these helical polymer metal complexes showed that during the first 7 days, the preannealed *P* and *M* helical senses induced in poly-(*L*)-**1** are retained after complexation with the metal ions, similarly to

what happens in the absence of metal ions but afer the addition of 200 ml of MeOH (See Figure 3b and SI). As expected, the P_{helix} (ECD_{393}<0) favoured in DCE is slightly enhanced over time in poly-(*L*)-**1**/$Li^+$and poly-(*L*)-**1**/Ba^{2+} metal complexes, while the disfavoured P_{helix} in DCE diminishes.

Interestingly, DLS and surface electron microscopy (SEM) studies show the formation of aggregates right after the formation of the HPMC. Moreover, from these studies it is found that while poly-(*L*)-**1**/Li^+ complexes produce polydisperse particles, poly-(*L*)-**1**/Ba^{2+} complexes produce low polydisperse nanospheres, whose size and polydispersion index (PDI) do not vary over time (See Figure 3 for poly-(*L*)-**1**/Ba^{2+} and SI for poly-(*L*)-**1**/Li^+).

IR studies were also done to analyze the different coordinations of the metal ions to the pendant group, which allowed us to explain the different polydispersion found in poly-(*L*)-**1**/Li^+ and poly-(*L*)-**1**/Ba^{2+} complexes (Figure S15). Interestingly, while Li^+ ions coordinate the carbonyl of the ester group, Ba^{2+} ions coordinate both carbonyls of amide and ester separately. Therefore, in poly-(*L*)-**1**/Li^+ complexes, the metal ion is placed towards the outer part of the helix, while in the case of poly-(*L*)-**1**/Ba^{2+} complexes, the metal ion is distributted between two different positions at the PDPA helical scaffold (inner and outer part). As a result, the metal ion is more prompt to aggregate in poly-(*L*)-**1**/Li^+ than in poly-(*L*)-**1**/Ba^{2+} complexes, being more difficult to control the polydispersity of the resulting nanostructures.

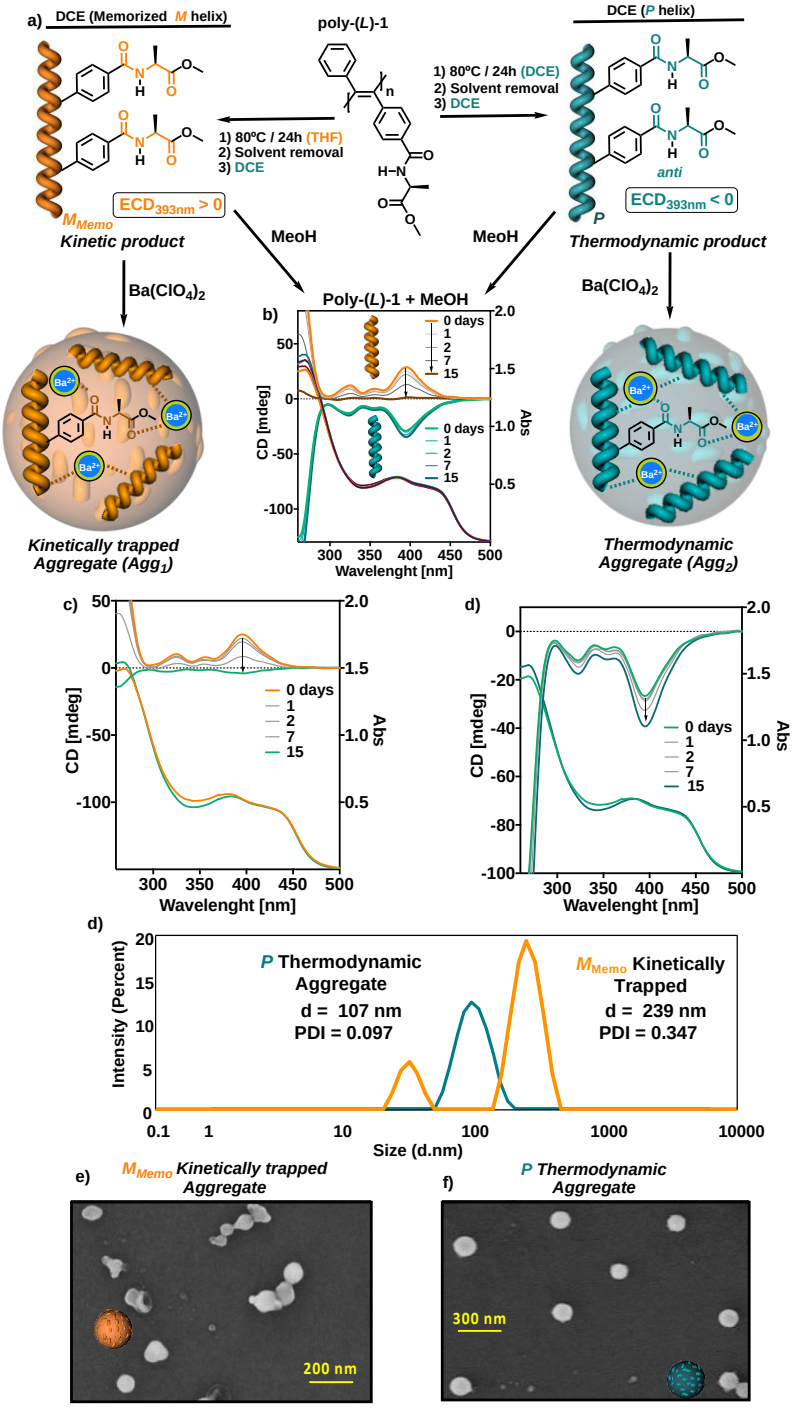

Figure 3. (a) Schematic illustration of the evolution over time of the pre-induced *M* and *P* helical structures of poly-(*L*)-1 and poly-(*L*)-1/Ba^{2+} complex. Time dependent ECD studies of the pre-induced *P* and *M* helical structures of (b) poly-(*L*)-1 and (c, d) poly-(*L*)-1/Ba^{2+} complex. SEM and DLS studies of (e) the kinetically trapped and (f) thermodynamic aggregates.

Time dependent ECD, DLS and SEM studies show that while *P* aggregates (Agg_2, ECD_{393}<0) of poly-(*L*)-**1**/Ba^{2+} remain stable in DCE for more than 6 months, the *M* aggregates (ECD_{393}>0) do not. In this case, a consecutive aggregation pathway is observed, where a *P* aggregate (Agg_1) is transformed into an *M* aggregate (Agg_2) over time. Moreover, the CPL

activity of the aggregates obtained through this consecutive process is also different in Agg_1 and in Agg_2, being attributted therefore to the opposite helical sense adopted by the PDPA [*M* nanospheres, CPL(+); *P* nanospheres, CPL(-)].

Taking into account the different kinetics associated to the helix inversion effect of PDPAs and the nanostructuration of the poly-(*L*)-**1**/Ba^{2+} metal complex, kinetically trapped (Agg_1, *M* nanospheres) and thermodynamic (Agg_2, *P* nanospheres) aggregates with opposite chirality can be isolated from poly-(*L*)-**1**/Ba^{2+} complexes at different moments, showing different emissive properties atending to the helical sense adopted by poly-(*L*)-**1**.

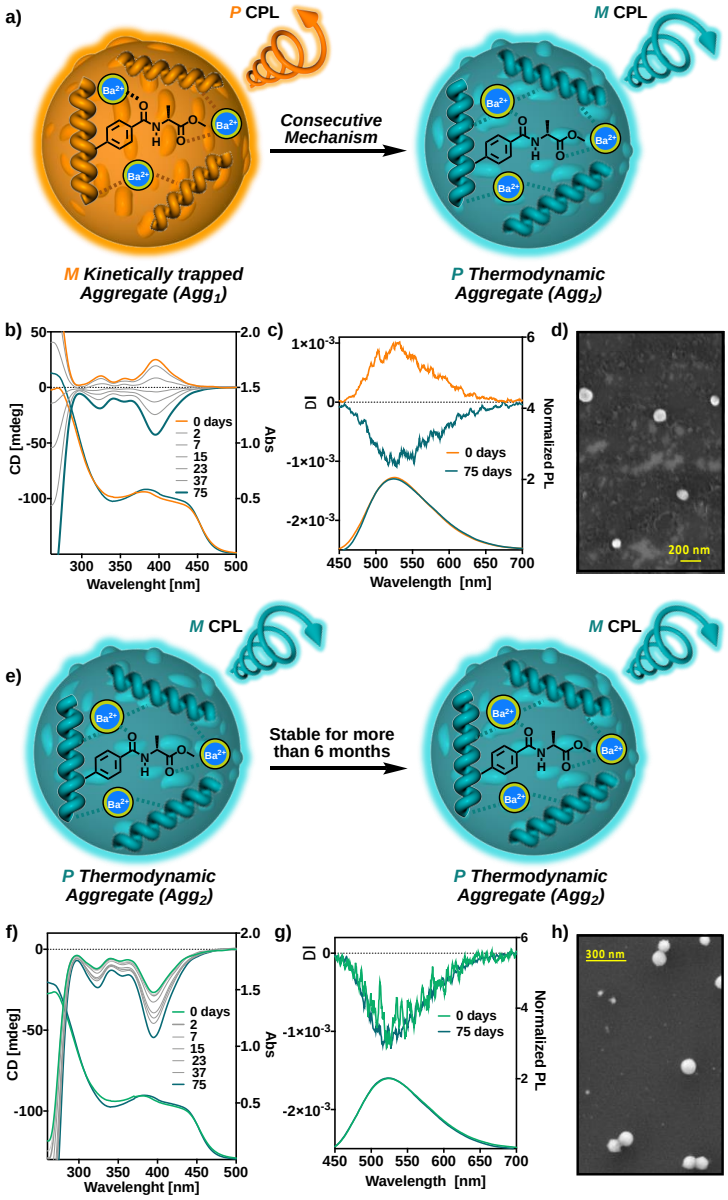

Figure 4. Schematic illustration of the evolution over time of the pre-induced (a) *M* and (e) *P* poly-(*L*)-**1**/Ba^{2+} complexes. Time dependent ECD studies of the pre-induced (b) *M* and (f) *P* helical structures of

poly-(*L*)-**1**/Ba^{2+}. (c) and (g) Time dependent CPL monitoring of the emission through evolution of the aggregates. SEM studies of (d) kinetically trapped and (h) thermodynamic aggregates after 6 months.

3. Conclusion

In conclusion, we have demontrated that *P* or *M* macroscopically chiral nanospheres can be obtained from a PDPA/$M(ClO_4)_n$ system through complex aggregation pathways. In this case, *P* or *M* macroscopically chiral nanospheres are obtained under the same experimental conditions for a PDPA/$M(ClO_4)_n$ complex. This fact is possible due to the large energy barrier of the helix inversion process in PDPAs. Thus, a kinetic aggregate (Agg_1) can be trapped for days or even moths at low temperatures, which can evolve towards a thermodynamic aggregate (Agg2) through a consecutive aggregation process. Interestingly, other properties associated to the chiral content of the aggregate, such as the circularly polarized luminescence, change once the helix of the PDPA is inverted within the aggregate. This findings open a new horizon in the development of nanomaterials whose chiroptical properties can be kinetically trapped, allowing to test them for potential applications in either *P* or *M* macroscopic chiralities without altering the experimental conditions in which the experiments are performed.

4. References

1. Chaikittisilp, W.; Yamauchi, Y.; Ariga, K. *Adv. Mater.*, **2022**, 2107212.

2. Wang, S.; Hu, D.; Guan, X.; Cai, S.; Shi, G.; Shuai, Z.; Zhang, J.; Peng, Q.; Wan, X. *Angew. Chem. Int. Ed*., **2021**, *60*, 21918–21926.

3. Maeda, K.; Hirose, D.; Nozaki, M.; Shimizu, Y.; Mori, T.; Yamanaka, K.; Ogino, K.; Nishimura, T.; Taniguchi, T.; Moro, M.; Yashima, E. Helical springs as a color indicator for determining chirality and enantiomeric excess. *Sci. Adv.*, **2021**, *7*, eabg5381.

4. Leiras, S.; Suárez-Picado, E.; Quiñoá, E.; Riguera, R.; Freire, F. *Giant*, **2021**, *7*, 100068.

5. Jin, Y. J.; Kwak, G. *Polym. Rev.*, **2017**, *57*, 175-199.

6. Anger, E.; Iida, H.; Yamaguchi, T.; Hayashi, K.; Kumano, D.; Crassous, J.; Vanthuyne, N.; Roussel, C.; Yashima, E. *Polym. Chem*. **2014**, *5*, 4909-4914.

7. Maeda, K.; Maruta, M.; Shimomura, K.; Ikai, T.; Kanoh, S. *Chem. Lett.* **2016**, *45*, 1063–1065.

8. Maeda, K.; Maruta, M.; Sakai, Y.; Ikai, T.; Kanoh, S. *Molecules*, **2016**, *21*, 1487-1500.

9. Shen, J.; Okamoto, Y. *Chem. Rev.*, **2016**, *116*, 1094-1138.

10. Shimomura, K.; Ikai, T.; Kanoh, S.; Yashima, E.; Maeda, K. *Nat. Chem.* **2014**, *6*, 429-434.

11. Hirose, D.; Ogino, K.; Uematsu, K.; Maeda, K. *J. Chromatogr. A*, **2022**, 463164.

12. Yamamoto, T.; Murakami, R.; Komatsu, S.; Suginome, M. *J. Am. Chem. Soc.* **2018**, *140*, 3867-3870.

13. Ando, M.; Ishidate, R.; Ikai, T.; Maeda, K.; Yashima, E. *J. Polym. Sci., Part A: Polym. Chem.* **2019**, 57, 2481-2490.

14. Zhang, C.; Qiu, Y.; Bo, S.; Wang, F.; Wang, Y.; Liu, L.; Zhou, Y.; Niu, H.; Dong, H.; Satoh, T. *J. Polym. Sci., Part A: Polym. Chem.* **2019**, *57*, 1024-1031.

15. Megens, R. P.; Roelfes, G. *Chem. Eur. J.* **2011**, *17*, 8514-8523.

16. Ikeda, S.; Takeda, R.; Fujie, T.; Ariki, N.; Nagata, Y.; Suginome. *Chem. Sci.* **2021**, *12*, 8811-8816.

17. Nagata, Y.; Takeda, R.; Suginome, M. *ACS Cent. Sci.*, **2019**, *5*, 1235-1240.

18. Nuñez-Martínez, M.; Arias, S.; Quiñoá, E.; Riguera R.; Freire, F. *Chem. Mater.* **2021**, *33*, 4805-4812.

19. Rodríguez, R.; Suarez-Picado, E.; Quiñoá, E.; Riguera, R.; Freire, F. *Angew. Chem. Int. Ed.* **2020**, *59*, 8616-8622.

20. Alzubi, M.; Arias, S.; Rodríguez, R.; Quiñoá, E.; Riguera, R.; Freire, F. *Angew. Chem. Int. Ed.* **2020**, *59*, 13365-13369.

21. Hirose, D.; Isobe, A.; Quiñoá, E.; Freire, F.; Maeda, K. *J. Am. Chem. Soc.* **2019**, *141*, 8592-8598.

22. Rey-Tarrío, F.; Rodríguez, R.; Quiñoá, E.; Riguera, R.; Freire, F. *Angew. Chem. Int. Ed.* **2021**, *60*, 8095-8103.

23. Arias, S., Núñez-Martínez, M., Quiñoá, E., Riguera, R., Freire, F. *Polym. Chem.*, **2017**, *8*, 3740-3745.

24. Arias, S.; Núñez-Martínez, M.; Quiñoá, E.; Riguera, R.; Freire, F. *Small,* **2017,***13, 1602398.*

25. Rodríguez, R.; Arias, S.; Quiñoá, E.; Riguera, R.; Freire, F. *Nanoscale,* **2017**, *9*, 17752-17757.

26. Zhang, Y.; Wu, Y.; Xu, R.; Deng, J. *Polym. Chem.*, **2019**, *10*, 2290-2297.

27. Kim, H.; Jin, Y. J.; Kim, B. S. I.; Aoki, T.; Kwak, G. *Macromolecules*, **2015**, *48*, 4754-4757.

28. Tarrío, J. J.; Rodríguez, R.; Fernández, B.; Quiñoá, E.; Freire, F. *Angew. Chem. Int. Ed.*, **2022**, *61*, e202115070.

Chapter VII

Evaluation of Substitution Effects in the Structure, Optical and Chiroptical Properties of Chiral Poly(diphenylacetylene)s

Chapter VII: Evaluation of Substitution Effects in the Structure, Optical and Chiroptical Properties of Chiral Poly(diphenylacetylene)s

Abstract

Chiral asymmetrically substituted PDPAs allow the possibility of playing with the aromatic substitution pattern to modulate their helical scaffold and dynamic helical properties. Thus, by placing the chiral pendant group in a *meta*- position and therefore close to the backbone, it is possible to generate a well folded helix with a poorer dynamic helical behavior when compared to the *para*-counterpart. The difference in the intramolecular π-stacking and the helical conformation adopted make important variations in the chiroptical properties, as well as in the structure and self-assembly ability.

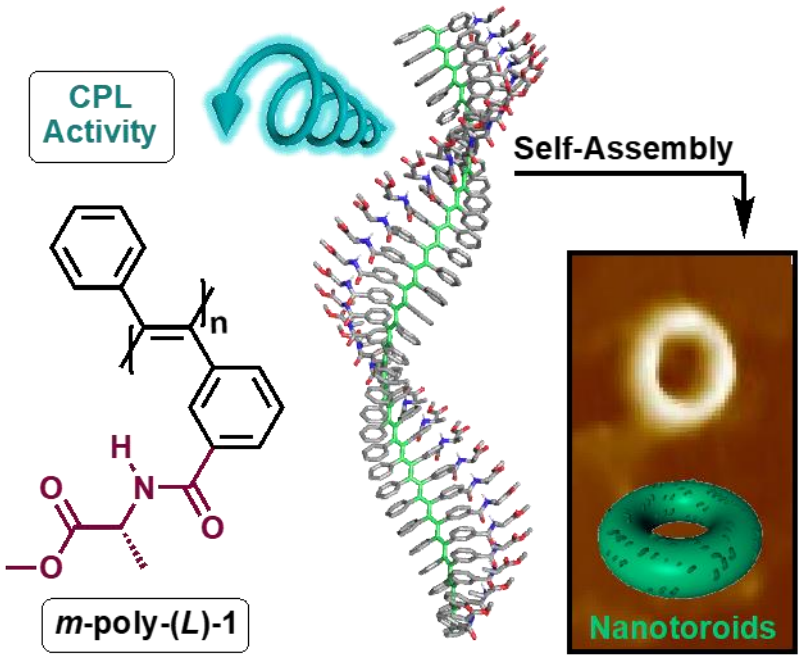

1. Introduction

Conjugated polymers (CPs) have been extensively studied since the last century for their properties and possible applications.[1-4] Molecular engineering and the rational design of monomers permit to create CPs with specific properties to be applied as functional materials in different fields such as organic light-emitting devices (OLEDs)[5] or organic thin film transistors (OTFTs).[6] CPs based on acetylenic monomers allow the creation of a large library of compounds due to the high reactivity of the monomers and the robustness of the polymerization reaction. As a result, poly(acetylene)s with different opto-electronic and photophysical properties can be generated by introducing pendant substituents with different bulkiness,[7] symmetries or electron donating/withdrawing abilities.[8,9] This is related to the modulation of the HOMO/LUMO energy levels and them band gaps, which produce variations in the fluorescence emission, color tuning and conductivity among others. In this sense, helical poly(phenylacetylene)s (PPAs)[10-16] and poly(diphenylacetylene)s (PDPAs)[17-26], two families of PAs, produce helical polymers with different properties such as thermal and photo stabilities, stimuli responsive properties, memory effect and luminescence. The main difference between these two families of polymer is the substitution pattern at the polyene backbone. Thus, while in PPAs the double bonds have an aryl ring, in PDPAs the two carbons of the double bonds are substituted with aryl rings. This different substitution pattern in the polyene backbone results in a more congested main chain in PDPAs when compared to PPAs, which results in a large stability of the polymer, a reduced dynamic behavior, and the presence of circularly polarized luminescence properties. The poor dynamic behavior of PDPAs caused them to be considered static, although recently, our group and Maeda´s showed that is possible to create PDPAs with stimuli responsive properties, which can vary their helical sense by applying different external stimuli such as solvents with different donor or polar parameters.[18,22]

In literature, there is just one example dealing with *meta*-substituted non-symmetric PDPAs.[23] In this work, Prof. Kwak and collaborators prepared two achiral *meta*- and *para* substituted PDPAs bearing a trimethylsilyl group as pendant. Interestingly, they found that, while it is possible to induce a helical sense in the *para*-PDPA by dissolving it into a chiral solvent such as (*R*)- or (*S*)-limonene, in the *meta*-substituted PDPA the helix induction does not take place. This result, in combination with the null helical induction effect found by Yashima *et al*. in achiral *meta*-

substituted-PPAs, led the scientific community not to pay attention to this family of *meta*-substituted helical polymers. Thus, to the best of our knowledge, no CD active chiral or achiral *meta* substituted PDPAs have been reported to date.

In our group, it was found that *meta*-substituted PPAs can adopt a screw sense excess when a chiral pendant is used.[27-30] Interestingly, it was also found that the dynamic behavior in PPAs decreases dramatically by placing the pendant group close to the backbone.[28] With all this information on hand, we decided to prepare a non-symmetric PDPA that bears a chiral pendant in the *meta*-position and to check how the structure and properties vary in relation to its *para*-substituted counterpart.

2. Results and Discussion

To perform these studies, we have chosen as model compounds *meta*- and *para*-substituted PDPAs bearing the benzamide of (*L*)-alanine-methyl ester as pendant (*p*-poly-(*L*)-**1** and *m*-poly-(*L*)-**1**) (Scheme 1). These polymers were prepared using a post-functionalization procedure described by Prof. B. Z. tang and coworkers.[26] Thus, achiral monomers bearing an activated ester in *para*- and *meta*-positions, *p*-M-$\mathbf{PF_5}$ and *m*-M-$\mathbf{PF_5}$, were prepared and further polymerized with a mixture of WCl_6-Ph_4Sn as catalyst (see Scheme 1 and Table 1).

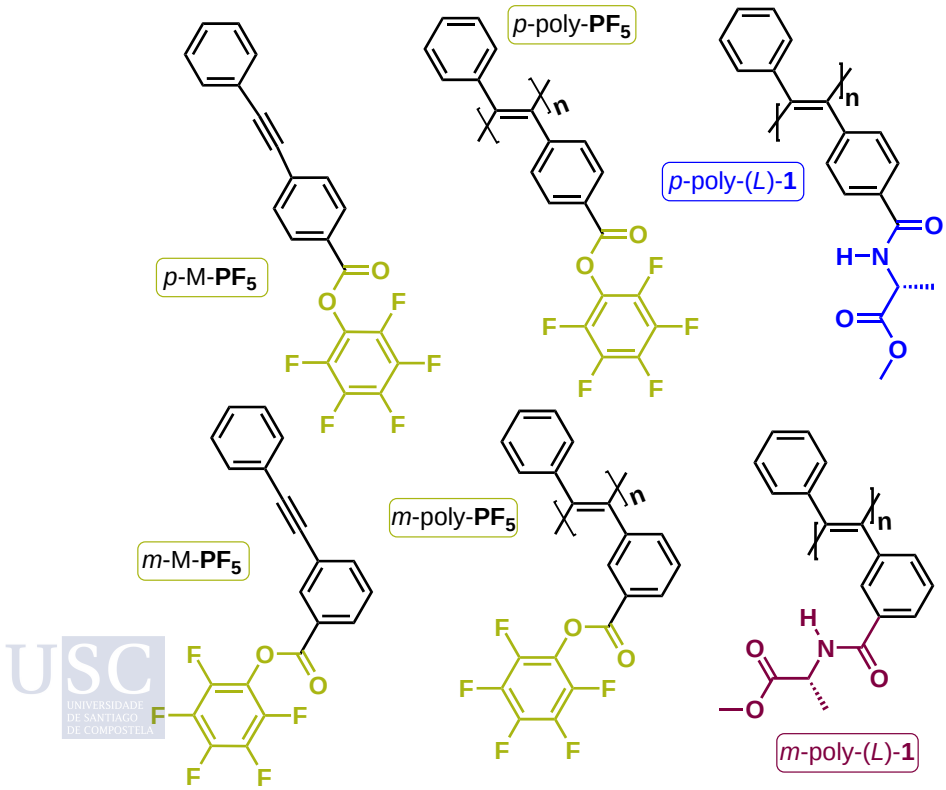

Scheme 1. Chemical structure of monomers and polymers.

The resulting *p*-poly-**PF_5** and *m*-poly-**PF_5** were fully transformed into *p*-poly-(*L*)-**1** and *m*-poly-(*L*)-**1** via post-functionalization with (*L*)-alanine methyl ester as inferred from ^{19}F-NMR studies (see SI). The number average molar mass (M_n) and molar mass dispersity (M_w/M_n) of *p*-poly-(*L*)-**1** and *m*-poly-(*L*)-**1** were determined by gel permeation chromatography (GPC) using THF as eluent and polystyrene narrow standards (PSS) as calibrants. The M_n and M_w/M_n values obtained for *p*-poly-(*L*)-**1** and *m*-poly-(*L*)-**1** were 1.3 x 10^5, 1.3 and 1.5 x 10^4, 1.5, respectively (Table 1). These values correspond to polymers with a DP of 438 and 58. In PDPAs, the ECD trace depends on the polymerization degree, being dominated by the transitions of the polyene backbone in oligomers and by the poly(diphenylacetylene) backbone in long polymers. ECD studies of *p*-poly-(*L*)-**1** and *m*-poly-(*L*)-**1** after thermal annealing (i.e., 0.5 mg/mL at 80ºC for 24h) in different solvents such as $CHCl_3$, DCE, THF, acetone, MeCN, DMF, DMSO and dioxane, show a strong helical induction in both *para*- and *meta*- substituted PDPAs —*p*-poly-(*L*)-**1** and *m*-poly-(*L*)-**1**— with maximum g_{abs} values in DMSO of 5.3x10^{-3} and 6.3x10^{-3} respectively, which are quite similar and indicate a similar folding degree (Figure 1a,b).

Table 1. Polymerization of diphenylacetylene derivatives containing a pentafluorophenyl moiety in *p*- and *m*- positions[a]

Polymer	temp (ºC)	Time (h)	yield (%)	M_w[b]	M_w/M_n
p-poly-PF_5	100	24	80	170000	1.3
m-poly- PF_5	100	24	71	22500	1.5

[a] Carried out under nitrogen in toluene with WCl_6-Ph_4Sn as catalytic system; $[M]_0$ = 0.2 M, [cat] = 10 mM, [Ph_4Sn] = 20 mM. [b] Estimated by GPC in THF based on a polystyrene calibration.

This is a very important finding because *meta*-substituted chiral PDPAs produce well folded helical polymers not achieved until date. Interestingly, from these studies, it is found that while *p*-poly-(*L*)-**1** produces an $ECD_{390} > 0$ in donor solvents and an $ECD_{390} < 0$ in non-donor solvents (Figure 1a), *m*-poly-(*L*)-**1** generates $ECD_{390} > 0$ in all the solvents (Figure 1b). This fact indicates that the dynamic behavior of *m*-poly-(*L*)-**1** is limited due to the steric hindrance emerged by placing the pendant group closer to the poly(diphenylacetylene) backbone.

Next, photoluminescence (PL) studies were carried out for *p*-poly-(*L*)-**1** and *m*-poly-(*L*)-**1** (*p*-poly-(*L*)-**1**: F_{PL} = 0.57 in DMSO, 0.26 in $CHCl_3$; *m*-poly-(*L*)-**1**: F_{PL} = 0.58 in DMSO, 0.25 in $CHCl_3$) obtaining similar emission abilities for both polymers, which differ from the results obtained for other *meta*-substituted PDPAs found in literature.[31] This difference can be attributed to the different folding degree adopted by chiral (this work) and achiral (literature) *meta*-substituted

PDPAs. Considering the emissive properties of *p*-poly-(*L*)-**1** and *m*-poly-(*L*)-**1,** circularly polarized light (CPL) emission studies were carried out for both polymers**.** The CPL emission was gauged by the dissymmetric factor defined as $|g_{lum}| = 2(I_L - I_R)/(I_L + I_R)$, being I_L and I_R the left- and right-handed luminescent emissions respectively. Interestingly, in both cases, a maximum g_{lum} value of ca. $+/-1x10^{-3}$ at 520 nm was obtained, whose sign is in accordance with the ECD sign of the PDPA (Figure 1c,d).

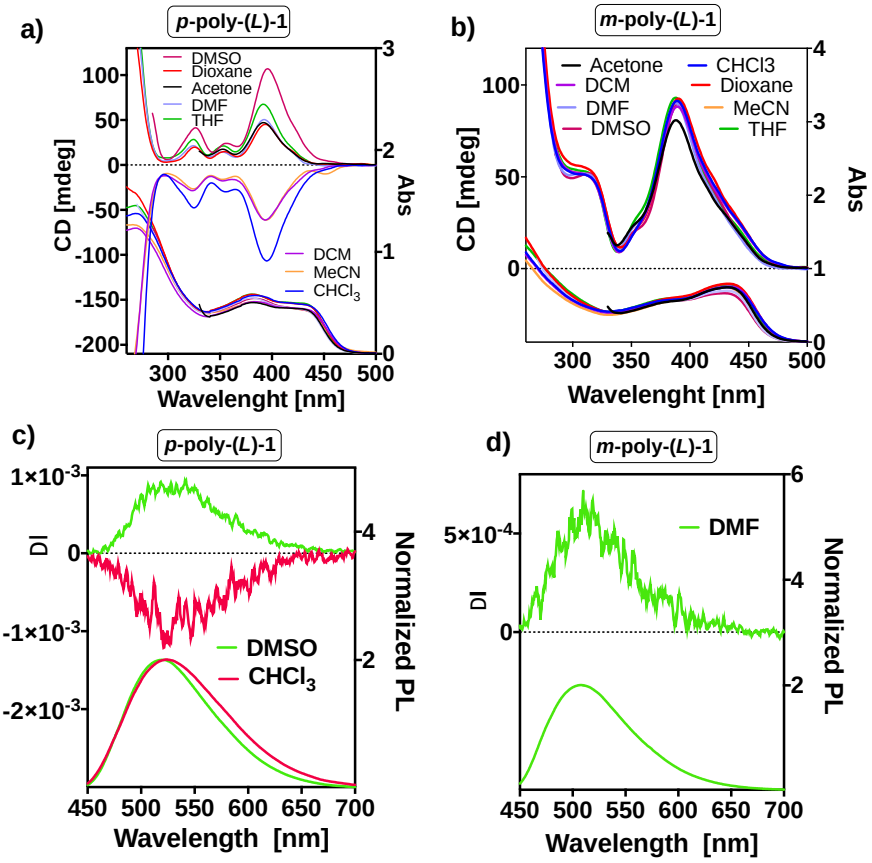

Figure 1. ECD and UV spectra of (a) *p*-poly-(*L*)-**1**, (b) *m*-poly-(*L*)-**1.** CPL spectra of (c) *p*-poly-(*L*)-**1**, (d) *m*-poly-(*L*)-**1** (λ_{Exc} = 365 nm). [c= 0.3 mg/mL].

Finally, structural studies such as IR, Raman and NMR were carried out to determine the stereo- and regioregularities of the polyene backbone in *m*-poly-(*L*)-**1**. In a previous work, asymmetrically substituted *para*-PDPAs were described as *trans-transoidal* polymers, due to a positive relation of the Raman and the IR bands at 1550 and 1585 cm^{-1} ($I_{1550}/ I_{1585} > 0$), and 1500 and 1450 cm^{-1} ($I_{1500}/ I_{1450} > 0$) respectively[22,32]. The same pattern was observed here for *m*-poly-(*L*)-**1**, indicating a stereoregular *trans-transoidal* polyene backbone (Figure 2a-b). Moreover, the regioregularity of *m*-poly-(*L*)-**1** was analyzed by 2D-NMR experiments such as NOESY. No NOE cross-peaks are found between H_a, the *para*- aromatic proton of the non-substituted phenyl ring and the protons of the alanine residue, which confirms a head to tail regioregularity (Figure 2c).

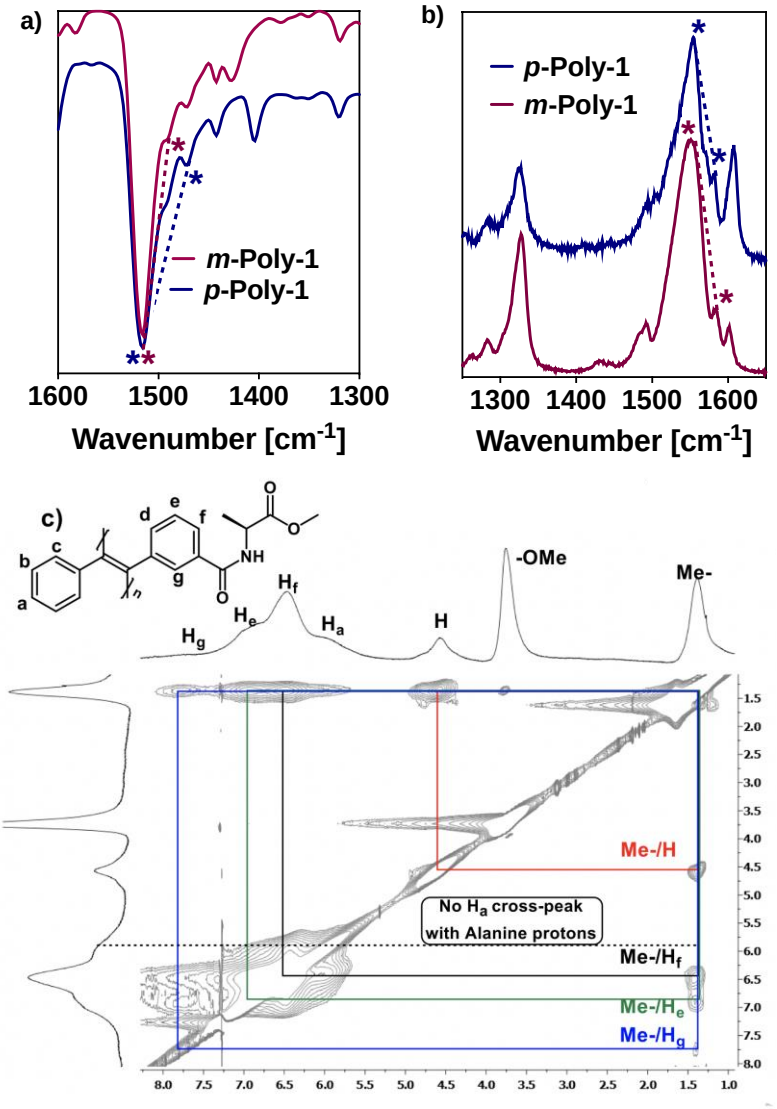

Figure 2. Partial a) IR and (b) Raman spectra of *m*-poly-(*L*)-**1** showing the 1300-1600 cm^{-1} region. c) NOESY spectrum of *m*-poly-(*L*)-**1** in $CDCl_3$.

AFM studies were carried out to build an approximated 3D-structure for *m*-poly-(*L*)-**1**. Thus, 5ml of a dilute solution of *m*-poly-(*L*)-**1,** annealed at 80°C for 24h in DMF or $CHCl_3$, were spin coated onto freshly exfoliated highly oriented pyrolytic graphite (HOPG) and left it under a solvent atmosphere for 2-3 hours. High resolution AFM images show in both solvents the presence of nanotoroidal structures resulting from the self-assembly of the *m*-poly-(*L*)-**1** polymer chains (Figure 3a,b). These nanotoroids appear in a bimodal manner having average heights of 30 and 15 nm and internal and external diameters of 565 and 30 nm, respectively (Figure 3c). The presence of the same nanostructures in solvents with different donor and polar characters such as DMF or $CHCl_3$ indicates the high tendency of this material to aggregate into nanotoroidal structures, never observed in PDPAs, PPAs or PAs to date.

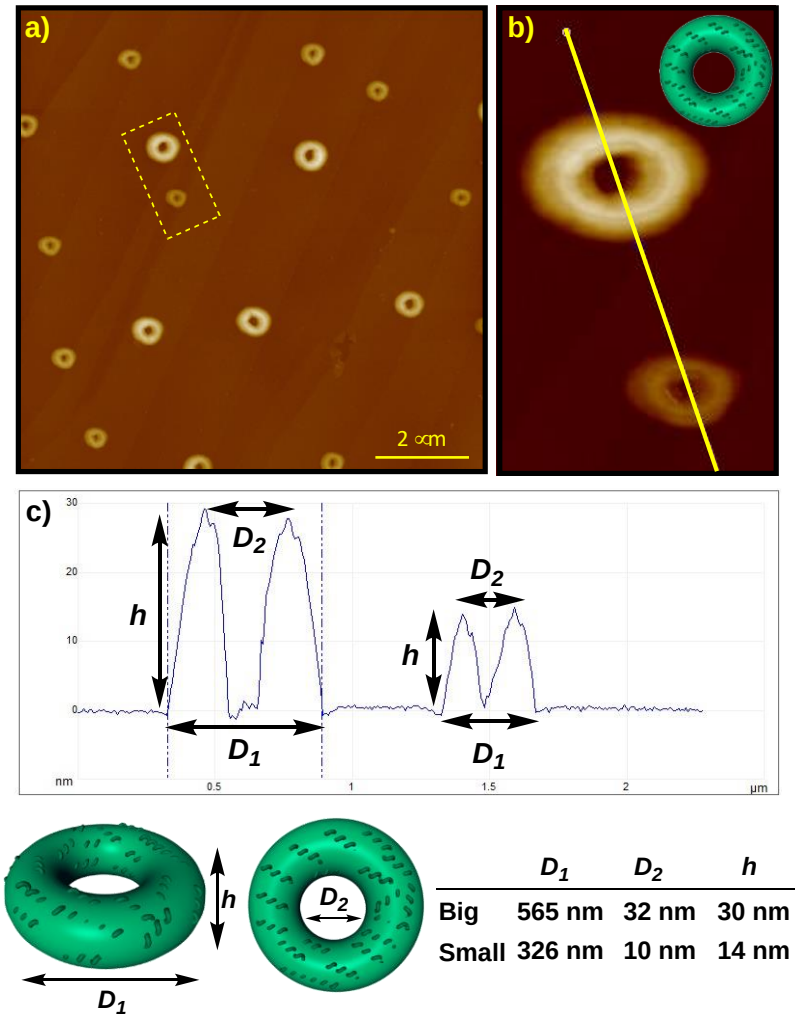

	D_1	D_2	h
Big	565 nm	32 nm	30 nm
Small	326 nm	10 nm	14 nm

Figure 3. a) High resolution AFM images showing self-assembled toroidal nanostructures from *m*-poly-(*L*)-**1** (HOPG as substrate). b) Magnification of the area highlighted in picture a) and c) height profile in picture a) ($CHCl_3$ solution spin coated onto HOPG).

Comparison of the UV-vis spectra of *p*-poly-(*L*)-**1** and *m*-poly-(*L*)-**1** shows a coincidence in the maxima and an increase in intensity of the UV band at 430 nm which is related to longitudinal couplings between polymeric chains.[22,33,34] Taking this into account, we built a helical structure where the double bonds are *M* oriented (helix 1, w_1= -165°) and the orientation of consecutive diphenylacetylene m.r.u. (helix 2) and the whole scaffold (helix 3) are *P* oriented ($M_1/P_2/P_3$). Thus, the macromolecular structure is described by the angles w_1= -165°, w_2= 180° and w_3= 40°.

As a result of this structure, and in the same way as what happens for *p*-poly-(*L*)-**1**,[22] the sign of the first Cotton band is ruled by helices 2 and 3, and not just by the orientation of the polyene backbone. Therefore, a first positive Cotton band at 400 nm indicates a helical structure with a *M*/*P*/*P* (helix 1/helix 2/helix 3) orientation. On the contrary, if the asymmetric PDPA shows a $CD_{400} < 0$, then the polymer adopts a *P*/*M*/*M* (helix 1/helix 2/helix 3) orientation.

Computational studies [TD-DFT(CAM-B3LYP)/3-21G] of ECD spectra were performed with this structure. A good match between experimental and theoretical ECD spectra of the proposed structure was obtained (Figure 4c), which allowed us to create a 3D model of the helical structure of *m*-poly-(*L*)-**1** (Figure 4d).

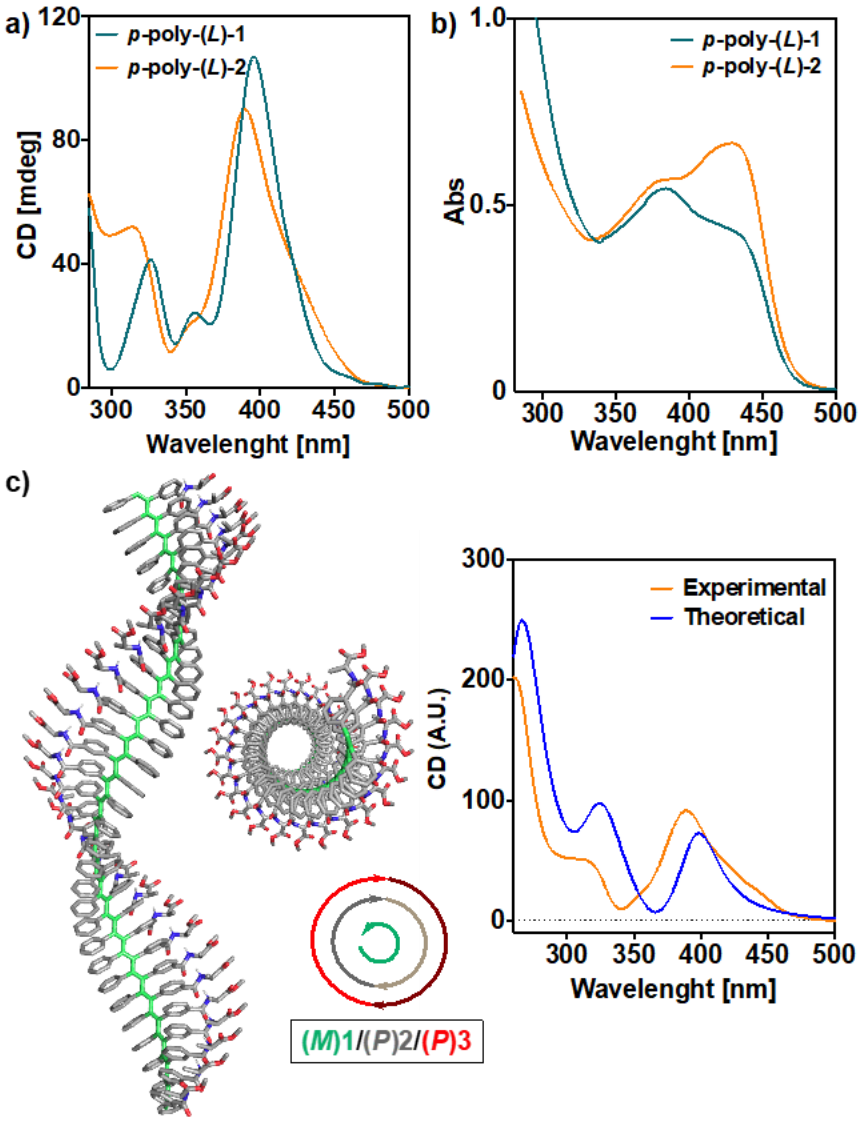

Figure 4. Comparison of the a) ECD and b) UV-vis spectra for *p*-poly-(*L*)-**1** and *m*-poly-(*L*)-**1**. c) 3D model of *m*-poly-(*L*)-**1** and comparison between theoretical and experimental ECD spectra obtained for *m*-poly-(*L*)-**1**.

The dynamic behavior of asymmetric PDPAs is drastically reduced by changing the aromatic substitution pattern from *para* to *meta*. As the main goal of this work is to create different chiral helical materials and to compare their properties, a library of several *para*- and *meta*-substituted PDPAs were prepared, and their chiroptical properties analyzed. Thus, *p*- and *m*-poly-(*L*)-(**2-6**) bearing the *para*- and *meta*-benzamide of (*L*)-methionine methyl ester [poly-(*L*)-**2**], (*L*)-valine methyl ester [poly-(*L*)-**3**], (*L*)-leucine methyl ester [poly-(*L*)-**4**], (*L*)-isoleucine

methyl ester [poly-(*L*)-**5**] and (*L*)-phenylalanine methyl ester [poly-(*L*)-**6**] as pendant groups were prepared following the same procedure to synthetize *m*-poly-(*L*)-**1** (see SI for experimental and characterization details).

ECD and CPL studies of *p*- and *m*-poly-(*L*)-(**1-6**) after thermal annealing (i.e., 0.5 mg/mL at 80°C for 24h) in different solvents such as $CHCl_3$, DCM, THF, acetone, MeCN, DMF, DMSO and dioxane, show different behaviors for the polymers. In the case of *para*- polymers, *p*-Poly-(*L*)-(**1,2,4**) show a dynamic behavior that distinguishes the solvents by donor character; *p*-Poly-(*L*)-(**5,6**) are sensitive to MeCN and DCE, respectively, presenting an opposite CD spectra to the other solvents; and *p*-Poly-(*L*)-**3** presents a static behavior. On the other hand, static behaviors for most of the *meta*-substituted polymers were found —*m*-poly-(*L*)-(**1,3-6**)—. Interestingly, in the special case of *m*-poly-(*L*)-**2**, a dynamic helical behavior was obtained inducing *P*/*M*/*M* (helix 1/helix 2/helix 3) orientation —$CD_{400} < 0$— in dioxane and *M*/*P*/*P* orientation —$CD_{400} > 0$— in the other solvents (see SI).

3. Conclusion

In conclusion, it was demonstrated through different examples that chiral *meta*-substituted PDPAs produce helical structures with similar chiroptical and circularly polarized emissive properties as those found in *para*-PDPAs. Moreover, although the secondary structure is quite similar, *meta*-substituted PDPAs showed a huge tendency to self-assembly in annular arrangements. Interestingly, the location of the pendant group, closer to the polyene backbone in *meta*-PDPAs, generates a more congested structure that inhibits the helical inversion in most cases. In the case of *m*-poly-(*L*)-2, this inversion is allowed in dioxane, being the first dynamic *meta*-substituted PDPA synthetized. In our group, more studies are being carried out on the activation energy barrier for helical inversion and the dynamic memory effect in this polymer that will allow us to explore the different effects of the substitution pattern on helicity for potential application of these materials in fields such as chiral stationary phases, chiral recognition ability, chiral ligands in asymmetric synthesis, among others.

4. References

1) Qiu, Z.; Hammer, B. A.; Muellen, K. *Prog. Polym. Sci.*, **2020**, *100*, 101179.

2) Dai, C.; Liu, B. *Energy Environ. Sci.*, **2020**, *13*, 24-52.

3) Zhao, C.; Chen, Z.; Shi, R.; Yang, X.; Zhang, T. *Adv. Mater.*, **2020**, *32*, 1907296.

4) Fratini, S.; Nikolka, M.; Salleo, A.; Schweicher, G.; Sirringhaus, H. *Nat. Mater.*, **2020**, *19*, 491-502.

5) Hong, G.; Gan, X.; Leonhardt, C.; Zhang, Z.; Seibert, J.; Busch, J. M.; Bräse, S.. *Adv. Mater.*, **2021**, *33*, 2005630.

6) Cavallari, M. R.; Pastrana, L. M.; Sosa, C. D. F.; Marquina, A. M. R.; Izquierdo, J. E. E.; Fonseca, F. J.; de Amorim, C. A.; Paterno, L. G.; Kymissis, I. *Materials*, **2021**, *14*, 3.

7) Masuda, T. *J. Polym. Sci., Part A-1: Polym. Chem.*, **2007**, *45*, 165-180.

8) Szyszkowska, M.; Czaplewski, C.; Wiczk, W. *J. Mol. Struct.*, **2017**, *1138*, 81-89.

9) Szyszkowska, M.; Bylińska, I.; Wiczk, W. *J. Photochem. Photobiol. A*, **2016**, *326*, 76-88.

10) Núñez-Martínez, M.; Arias, S.; Quiñoá, E.; Riguera, R.; Freire, F. *Chem. Mater.* **2021**, *33*, 4805-4812.

11) Zhao, C.; Sun, S.; Tong, W. L.; Chan, M. C. W. *Macromolecules*, **2017**, *50*, 6896-6902.

12) Rodríguez, R.; Suarez-Picado, E.; Quiñoá, E.; Riguera, R.; Freire, F. *Angew. Chem. Int. Ed.* **2020**, *59*, 8616-8622.

13) Alzubi, M.; Arias, S.; Rodríguez, R.; Quiñoá, E.; Riguera, R.; Freire, F. *Angew. Chem. Int. Ed.* **2020**, *59*, 13365-13369.

14) Suarez-Picado, E.; Quiñoá, E.; Riguera, R.; Freire, F. *Angew. Chem. Int. Ed.* **2020**, *59*, 4537-4543.

15) Núñez-Martínez, M.; Arias, S.; Bergueiro, J.; Quiñoá, E.; Riguera, R.; Freire, F. *Macromol. Rapid Commun*. **2021**, 2100616.

16) Rey-Tarrío, F.; Rodríguez, R.; Quiñoá, E.; Riguera, R.; Freire, F. *Angew. Chem. Int. Ed.* **2021**, *60*, 8095-8103.

17) Maeda, K.; Nozaki, M.; Hashimoto, K.; Shimomura, K.; Hirose, D.; Nishimura, T.; Watanabe, G.; Yashima, E. *J. Am. Chem. Soc*. **2020**, *142*, 7668-7682.

18) Hirose, D.; Nozaki, M.; Maruta, M.; Maeda, K. *Chirality*, **2022**, *34*, 597–608.

19) Sueyoshi, S.; Taniguchi, T.; Tanaka, S.; Asakawa, H.; Nishimura, T.; Maeda, K. *J. Am. Chem. Soc.*, **2021**, *143*, 16136-16146.

20) Yurtsever, A.; Das, S.; Nishimura, T.; Rodríguez, R.; Hirose, D.; Miyata, K.; Sumino, A.; Fukuma, T.; Maeda, K. *Chem. Commun.*, **2021**, *57*, 12266-12269.

21) Maeda, K.; Hirose, D.; Nozaki, M.; Shimizu, Y.; Mori, T.; Yamanaka, K.; Ogino, K.; Nishimura, T.; Taniguchi, T.; Moro, M; Yashima, E. *Sci. Adv.*, **2021**, *7*, eabg5381.

22) Tarrío, J. J.; Rodríguez, R.; Fernández, B.; Quiñoá, E.; Freire, F. *Angew. Chem. Int. Ed.*, **2022**, *61*, e202115070.

23) Seo, K. U.; Jin, Y. J.; Kim, H.; Sakaguchi, T.; Kwak, G. *Macromolecules*, **2018**, *51*, 34-41.

24) Jim, C. K. W.; Lam, J. W. Y.; Leung, C. W. T.; Qin, A.; Mahtab, F.; Tang, B. Z. *Macromolecules*, **2011**, *44*, 2427–2437.

25) Kim, H.; Seo, K. U.; Jin, Y. J.; Lee, C. L.; Teraguchi, M.; Kaneko, T.; Aoki, T.; Kwak, G. *ACS Macro Lett.* **2016**, *5*, 622−625.

26) Zhang, X. A.; Qin, A.; Tong, L.; Zhao, H.; Zhao, Q.; Sun, J. Z., Tang, B. Z. *ACS Macro Lett.*, **2012**, *1*, 75-79.

27) Rodríguez, R.; Arias, S.; Quiñoá, E.; Riguera, R.; Freire, F. *Nanoscale*, **2017**, *9*, 17752-17757.

28) Rodriguez, R.; Quinoa, E.; Riguera, R.; Freire, F. *J. Am. Chem. Soc.*, **2016**, *138*, 9620-9628.

29) Arias, S.; Rodríguez, R.; Quiñoá, E.; Riguera, R.; Freire, F. *J. Am. Chem. Soc.*, **2018**, *140*, 667-674.

30) Cobos, K.; Rodriguez, R.; Domarco, O.; Fernandez, B.; Quiñoá, E.; Riguera, R.; Freire, F. *Macromolecules*, **2020**, *53*, 3182-3193.

31) Lee, W. E.; Oh, C. J.; Park, G. T.; Kim, J. W.; Choi, H. J.; Sakaguchi, T.; Fujiki, M.; Nakao, A.; Shinohara, K.; Kwak, G. *Chem. Commun.*, **2010**, *46*, 6491-6493.

32) Simionescu, C. I.; Percec, V.; Dumitrescu, S. *J. Polym. Sci. A: Polym. Chem.*, **1977**, *15*, 2497-2509.

33) Kim, S. I.; Jin, Y. J.; Lee, W. E.; Yu, R.; Park, S. J.; Kim, H. J.; Song, K.; Kwak, G. *Adv. Mater. Interfaces*, **2014**, *1*, 1300029.

34) Lee, D.; Kim, H.; Suzuki, N.; Fujiki, M.; Lee, C. L.; Lee, W. E.; Kwak, G. *Chem. Commun.*, **2012**, *48*, 9275-9277.

Chapter VIII

Resume

Resume

Nos últimas décadas, a comunidade científica prestou unha gran interese no desenrolo de novos materiais capaces de emular as propiedades e funcións de diversas biomoléculas. Exemplos das moléculas de estudo son os polisacáridos, proteínas ou o mesmo ADN. En este tipo de moléculas está presente a estrutura helicoidal como principal patrón estrutural. Ditas hélices son as responsables de gran parte das funcións que desenrolan nos organismos e das súas propiedades. Por elo, no afán por conseguir imitar ditos patróns e polo tanto, as súas propiedades, xurdiron diferentes polímeros helicoidais sintéticos.

Aínda que existe unha gran variedade deste tipo de materiais polimeríceos, cobrou unha especial relevancia a familia dos poli(acetileno)s (PAs). Dentro da ampla familia que compoñen os PAs, especialmente nos últimos anos tomaron unha importante relevancia os poli(fenilacetileno)s (PPAs). Estes materiais derivados do PA, son unha familia de polímeros helicoidais altamente dinámicos moi interesantes xa que a súa estrutura secundaria pode ser modulada (sentido de xiro e/ou elongación) mediante a aplicación de estímulos externos como poden ser as variacións de polaridade do medio, cambios de temperatura, a adición de ións metálicos, ou o cambio de pH, entre outros. Este control sobre a estrutura secundaria fai que posúan potenciais aplicacións en campos tan diferentes como o seu uso como sensores, a catálise asimétrica ou a preparación de fases estacionarias quirais para HPLC.

Máis recentemente, e para abordar as problemáticas que impiden o uso dos PPAs como materiais (tales como escasa estabilidade térmica ou fotoquímica), xorde a familia dos poli(difenilacetileno)s (PDPAs). Esta tese de doutoramento titulada *Poly(diphenylacetylene)s: Design, Synthesis and Application*, posúe cinco capítulos no que se estudará a síntese e caracterización de varios poli(difenilacetileno)s, así como o estudo de diversas propiedades opto-electrónicas que posúen estes.

A continuación farase un breve resumo dos resultados mais relevantes de cada capítulo:

Captítulo III. Poli(difenilacetileno)s Disimétricos Quirais: Elucidación da Estrutura Secundaria e Luminescencia Dinámica.

A enxeñaría molecular permítenos o deseño e desenrolo de novos materiais con certa estrutura e propiedades específicas relacionadas con ela. A creación de novos materiais sintéticos capaces de emular certas propiedades de biomoléculas naturais preséntase como un importante desafío, o cal debe ser abordado dende os seus inicios con unha clara relación establecida entre estrutura/función. Isto permite no futuro modificar a vontade certos parámetros ou motivos estruturais para modificar as propiedades ou funcións do material.

Aínda que na literatura pódese encontrar varios traballos que abordan a síntese de poli(difenilacetileno)s, desgraciadamente case na súa totalidade omiten facer referencia ao estudo da estrutura secundaria dos polímeros, ou preséntanse estudos moi preliminares e contrapostos. Isto é signo do alto grao de dificultade que presenta o análise estrutural de macromoléculas.

Tendo esta información en conta, neste primeiro capítulo abordouse a síntese dun PDPA aquiral xa descrito previamente que posúe un éster activado, ideal para realizar funcionalizacións despois da polimerización. Trala polimerización, utilizouse un derivado metil éster do aminoácido alanina para introducir un centro quiral ao polímero. Un amplo estudo de diversos polímeros coñecidos, xunto con estes PDPAs, permitíronnos mediante as técnicas de IR e Raman asignar como *trans-transoide* a configuración dos dobres enlaces que forman o esqueleto do polímero.

Outra grande problemática que presentas os PDPAs asimetricamente substituídos é a rexio isomería. Debido as múltiples combinacións (cabeza-cabeza, cabeza-cola e cola-cola) nas que se poden introducir as unidades monoméricas de repetición (m.r.u.) ao polímero en crecemento, esperaríase obter complexos espectros de RMN. Tendo en conta isto, empregando técnicas de RMN bidimensionais (COSY e NOESY) e R-X, conseguiuse explicar que unha das combinación é a que prevalece sobre as outras, sendo materias con unha rexio isomería definida como cabeza-cola. Unha vez solventada a problemática da estrutura primaria do polímero, grazas a elaboración dun cristal 2D de polímero púidose observar mediante AFM varias cadeas helicoidais, o que nos permitiu obter importantes parámetros estruturais como son o paso de hélice, o sentido de xiro e ángulos de empaquetamento. Con todo este cúmulo de información estrutural, deseñamos un modelo computacional en 3D do polímero e fixéronse cálculos teóricos con dita estrutura para observar se reproducía axeitadamente os espectros de ECD e UV-Vis.

Unha vez feita a completa elucidación da estrutura secundaria do polímero, observamos que a conxestión provocada pola presenza de dous aneis aromáticos converten aos PDPAs en polímeros menos dinámicos que os PPAs. Para que os polímeros adquiran unha estrutura helicoidal é necesario realizar un tratamento a alta temperatura (por exemplo, 80ºC durante 24h) unha vez disoltos. Empregando esta metodoloxía puidemos observar un comportamento dinámico por primeira vez en PDPAs, onde o polímero presenta diferente sentido de xiro en función da habilidade dadora do disolvente. Este dinamismo non foi visto só por Dicroísmo Circular, se non tamén por Luminescencia Circularmente Polarizada (CPL), creando así un dos poucos conmutadores de CPL creados ata agora. Ademais, estudos de Dicroísmo Circular

Vibracional (VCD) amosaron que o cambio de helicidade ven promovido por un cambio conformacional do *pendant* onde os carbonilos da alanina están presentes en conformación *sinperiplanar* en disolventes dadores e en *antiperiplanar* en disolventes non dadores.

Por último, fixéronse estudos de agregación empregando o método de nanoprecipitación observando a formación de nanoesferas por microscopía electrónica de barrido (SEM) e súper hélices por AFM. O empaquetamento de diferentes cadeas polimeríceas supón a aparición dun novo Cotton no espectro de CD a lonxitudes de ondas maiores debido a conxugación.

Capítulo IV. O Grao de Polimerización Determina Drasticamente as Propiedades Quirópticas de Poli(difenilacetileno)s Asimétricos e Dinámicos

No primeiro capítulo desta tese de doutoramento, fíxose unha primeira síntese e caracterización estrutural completa de un PDPA funcionalizado co éster metílico da alanina. Cálculos computacionais preliminares do modelo xerado arroxaban diferentes resultados en función do tamaño da estrutura empregada para os cálculos.

Ademais, a información coñecida previamente sobre CD en PPAs non se pode aplicar aos PDPAs, xa que os primeiros están formados por dúas hélices coaxiais mentres que os segundos están formados por tres. Mentres que nos PPAs o CD está determinado pola orientación do esqueleto poliénico, no primeiro capítulo observamos que en PDPAs o CD ven determinado pola orientación da hélice externa. Así, un polímero con un CD positivo estaría formado por unha estrutura *M/P/P* (hélice 1/hélice 2/ hélice 3), mentres que un CD negativo sería producido por unha estrutura de tipo *P/M/M*.

Non obstante, a análise das transicións dos espectros teóricos de CD amosaron como resultado a participación en todo o espectro dos aneis aromáticos e do esqueleto poliénico. Nas estruturas calculadas de maior tamaño observouse como a orientación dos aneis aromáticos é a que predominaba no espectro de CD, mentres que nas estruturas de menor tamaño, foron as transicións gobernadas polo polieno as mandatarias.

Por isto, baseándose en diferentes condicións de síntese reportadas en bibliografía, obtivéronse polímeros de diferente tamaño (diferente grao de polimerización), caracterizados por GPC, que se funcionalizaron seguindo a metodoloxía explicada no primeiro capítulo. En este caso, empregáronse os derivados metil éster da alanina, valina e leucina. Nos tres casos observouse como existe un tamaño mínimo necesario para o pregamento da hélice, e a partir de dito tamaño existe unha pequena marxe onde os espectros de CD dan un signo oposto ao esperado.

Tras unha exhaustiva caracterización estrutural empregando as técnicas descritas no capítulo un, observamos que o responsable deste cambio das propiedades quirópticas non é un camiño diferente de polimerización cara estruturas diferentes, se non a diferente contribución ao espectro de CD dos grupos funcionais presentes no polímero. Así, para oligómeros con baixo grao de polimerización, obsérvase un CD provocado pola orientación da parte interna do polímero (dobres enlaces), mentres que para polímeros (grao de polimerización superior a cen) as transición que provocan o espectro de CD veñen gobernadas pola orientación dos aneis aromáticos.

Capítulo V. Efecto Memoria Dinámico P/M da Helicidade Macromolecular en Poli(difenilacetileno)s Quirais: Estudos Cinéticos e Termodinámicos

No primeiro capítulo describiuse como o cambio conformacional no *pendant* provoca o cambio de sentido de xiro da hélice polimerícea mediante estudos de VCD e ECD. En este capítulo afondamos no control da estrutura helicoidal aproveitando a alta rixidez destes polímeros.

O efecto memoria da helicidade macromolecular é unha propiedade moi interesante presente en algúns sistemas helicoidais dinámicos. Así, en bibliografía describíronse ata tres xeracións diferentes de efecto memoria. En todas elas consistiu no uso de sustancias quirais (por exemplo, aminas) para xerar unha estrutura helicoidal definida mediante interaccións supramoleculares en un polímero con grupos carboxílicos libres como *pendant*. Logo, substituíase dito auxiliar quiral por outro aquiral e a estrutura helicoidal mantíñase invariábel. Na terceira xeración, baseada no emprego de PDPAs conseguiu manterse a estrutura helicoidal eliminando o indutor quiral sen ser necesario reemplazalo por unha molécula aquiral. Esto sen dúbida foi froito da estrutura tan ríxida que posúen estes polímeros.

En este capítulo nós vamos un paso máis alá no estudo do efecto memoria e deixamos de lado as interaccións supramoleculares para dar lugar a un efecto memoria en polímeros onde o indutor quiral está unido covalentemente.

Unha vez máis, traballando co PDPA derivado co éster metílico da alanina, observamos como é necesario realizar un tratamento térmico a alta temperatura para que o polímero adquira unha estrutura helicoidal. Así, por exemplo, disolvendo o polímero en THF e quentando a 80^{o}C durante 24h como resultado obsérvase un CD positivo. Ao evaporar o THF e redisolver o polímero en $CHCl_3$ púidose observar como o CD non variaba resultando en un efecto memoria da helicidade macromolecular. Non é ata pasados varios días a temperatura ambiente, ou varias horas quentando a alta temperatura, que se consegue a inversión

helicoidal e polo tanto un CD negativo. Esta memoria da helicidade non se observou só por CD, se non tamén en diferentes medidas de CPL. Como a temperatura ambiente a inversión helicoidal é moi lenta, decidimos realizar estudos a baixa temperatura logrando aumentar a semanas e incluso meses o efecto memoria.

Po último, fíxose un estudo cinético e termodinámico da inversión helicoidal a diferentes temperaturas logrando calcular as constantes cinéticas de inversión, enerxía de activación, así como a variación de entalpía e entropía de activación do proceso. Para isto fíxose uso das ecuacións de Arrhenius e Eyring.

Capítulo VI. Vías de Agregación Complexas en Polímeros Helicoidais Covalentes: Mecanismo Consecutivo e Agregados Cinéticamente Atrapados nun Complexo PDPA/M^{n+}

A química dos nanomateriais é un campo de investigación que implica o deseño, desenvolvemento e aplicación de novos materiais na escala nanoscópica, onde as propiedades do material difiren en comparación coas do estado masivo. Ademais, a incorporación da quiralidade aos nanomateriais proporciónalles propiedades interesantes asociadas a dita quiralide como poden ser emisión de CPL, recoñecemento quiral, ou catálise.

Os polímeros helicoidales dinámicos son materiais prometedores que cumpren as dúas características esenciais (nanomateriais e quiralidade) para ser aplicados como nanomateriais quirais. Ademais, o comportamento dinámico do polímero fai posible preparar a partir dun só polímero, nanoestruturas con diferente quiralidade na superficie. Por exemplo, durante a última década xeráronse nanoestruturas quirais dinámicas como nanoesferas, nanotubos ou nanotoroides a partir da combinación de poli(fenilacetileno)s (PPA) e ións metálicos para producir complexos de polímero helicoidal-metal (HPMC). Nestes sistemas, o ión metálico úsase como axente de entrecruzamento. A alta tendencia á agregación do HPMC en disolventes orgánicos resulta nunha escasa estabilidade das nanoestruturas dispersas. Ademais, os PPA son sensibles á luz, onde se produce unha electrociclización fotoquímica do esqueleto poliénico baixo a exposición á luz que acaba ca ruptura do material.

Neste capítulo, o noso obxectivo é superar os problemas de estabilidade asociados aos complexos PPA/M^{n+} e preparar partículas poliméricas quirais dinámicas estables que poidan almacenarse dispersas en disolución durante meses. Ademais, exploramos a formación de nanomateriais intelixentes cuxa quiralidade inducida pode ser memorizada unha vez que se elimina o estímulo externo. Neste caso, estamos interesados na xeración de nanomateriais con efecto memoria dinámica, que dan lugar á formación de vías complexas de agregación de polímeros covalentes.

Así, para realizar estes estudos empregamos un PDPA quiral funcionalizado co éster metílico da alanina que mostra un comportamento helicoidal dinámico controlado cinéticamente. Polo tanto, os dous sentidos de xiro *P/M* poden ser inducidos no PDPA xogando coa composición conformacional do grupo *pendant*. Como explicamos no capítulo anterior, o sentido de xiro inducido pode quedar atrapado cinéticamente se non se aplica un tratamento térmico a alta temperatura unha vez disolto. Por outra banda, empregáronse diferentes sales de perclorato metálico [$LiClO_4$ e $Ba(ClO_4)_2$] como axentes de entrecruzamento para ensamblar o PDPA en nanoestruturas esféricas en disolventes onde o polímero está completamente disolto como $CHCl_3$ ou DCE. Ademais, o uso dun PDPAs quiral que posúe un efecto memoria dinámico permitiunos analizar a evolución do agregado co tempo, que evoluciona dende un agregado cinético cara a outro termodinámico mediante un mecanismo complexo de agregación (Agg_1 a Agg_2). Así, durante o proceso de cambio do agregado cinético ao termodinámico, prodúcese unha inversión gradual da hélice do PDPA que forma o agregado mediante un mecanismo consecutivo de inversión.

Curiosamente, os estudos de DLS e microscopía electrónica de barrido (SEM) mostraron a formación de agregados polidispersos cando se utiliza Li^+ como axente de entrecruzamento, mentres que os complexos con Ba^{2+} producen nanosferas de baixa polidispersión (PDI), cuxo tamaño e PDI non varían co tempo.

Estudos de IR amosaron que a coordinación dos ións metálicos co grupo *pendant* prodúcese coa parte externa (carbonilo do éster) no caso do Li^+, mentres que no caso do Ba^{2+} coordínase tanto a parte interna como a externa (ambos carbonilos). Os estudos de CD, DLS e SEM co tempo mostraron que mentres os agregados termodinámicos (Agg_2, $ECD_{393}<0$) permanecen estables en DCE durante máis de 6 meses, mentres que os agregados cinéticos (Agg_1, $ECD_{393}>0$) non. Ademais, os espectros de CPL dos agregados obtidos tamén son diferentes, sendo CPL(+) en Agg_1 e CPL(-) para o Agg_2.

Capítulo VII. Avaliación dos Efectos de Substitución na Estrutura, Propiedades Ópticas e Quirópticas dos Poli(difenilacetileno)s Quirais

Os polímeros conxugados foron amplamente estudados dende o século pasado polas súas propiedades e posibles aplicacións. O deseño racional dos monómeros permiten crear polímeros con propiedades específicas para ser aplicadas como materiais funcionais en diferentes campos como os dispositivos emisores de luz orgánicos (OLED) ou os transistores orgánicos (OTFTs). Os polímeros conxugados baseados en monómeros acetilénicos permiten a creación dunha gran biblioteca de compostos debido á alta reactividade dos monómeros e a capacidade para incluír grupos funcionais. Como resultado, pódense xerar poli(acetileno)s con

diferentes propiedades optoelectrónicas e fotofísicas. Isto está relacionado coa modulación dos niveis de enerxía HOMO/LUMO e a súa diferencia de enerxía, que producen variacións na emisión de fluorescencia, axuste da cor e a condutividade entre outras. Neste sentido, os poli(difenilacetileno)s (PDPA)s arroxan interesantes propiedades quirópticas, emisoras, así como unha gran estabilidade e resposta a estímulos. Por outra banda, tendo en conta a alta barreira enerxética da inversión da hélice nos PDPA, outra interesante propiedade que posúen é o efecto memoria dinámico da helicidade macromolecular.

Tendo en conta o anterior, propuxémonos esclarecer que ocorre coas propiedades quirópticas e ópticas dos PDPA ao cambiar o patrón de substitución dunha posición *para*- a *meta*-. Debido a que o *pendant* se atopa máis cerca do esqueleto poliénico, cabe esperar que o dinamismo do material diminúa.

Na literatura, só existe un exemplo que trata a síntese de un PDPA *meta*- substituído. Neste traballo compáranse dous PDPA aquirais substituídos en posición *para*- e *meta*-, respectivamente, con un grupo trimetilsililo. Curiosamente, descubriron que, aínda que é posible inducir un sentido helicoidal no *para*- substituído disolvéndoo nun disolvente quiral como (*R*)- ou (*S*)-limoneno, no PDPA *meta*- substituído a indución de helicidade non ten lugar. Este resultado, xunto ca nula indución de helicidade atopada por Yashima *et al*. nos PPA aquirais *meta*- substituídos, fixo que a comunidade científica non preste atención a esta familia de polímeros helicoidais.

Seguindo a metodoloxía sintética explicada en capítulos previos, abordouse a síntese dun PDPA aquiral que posúe un éster activado en posición *meta*. Unha vez obtido dito polímero, funcionalizouse con diferentes derivados de aminoácidos metil éster. Os derivados de aminoácidos empregados foron: alanina, valina, leucina, isoleucina, fenilalanina e metionina. No caso dos cinco primeiros, estudos de CD arroxaron como resultado polímeros estáticos que tan só adquiren un sentido de xiro (CD positivo) en tódolos disolventes empregados (DCE, $CHCl_3$, MeCN, THF, Dioxano, Acetona, DMF e DMSO). No caso da metionina, logrouse obter ambos sentidos de xiro *P/M* dando lugar a o primeiro PDPA dinámico *meta*-substituído. Este carácter dinámico foi observado mediante CD e CPL. Ademais, os mesmos polímeros foron sintetizados en *para* observando diferentes grados de dinamismo entre eles.

Outra importante parte deste traballo foi a caracterización da estrutura destes novos polímeros. Seguindo a metodoloxía do primeiro capítulo e aplicando diferentes técnicas como IR, Raman e RMN púidose esclarecer a estéreo isomería *trans-transoide* e a rexio isomería *cabeza-rabo* das unidades monoméricas de repetición que conforman o polímero. Ademais, estudos de AFM arroxaron a alta tendencia destes polímeros a agregar en forma de toroides.

Chapter IX

Conclusions

Conclusions

This thesis is focused on the synthesis and characterization of novel materials based on poly(diphenylacetilene)s (PDPAs). PDPAs were described as a family of static helical polymers where the helical structure is acquired after a thermal annealing at high temperature (i.e., 80ºC during 24h), but the structural parameters (helical sense and/or elongation) cannot be tuned by external stimuli. This is due to the congested structure because of the presence of two aryl rings attached to the polyenic backbone.

Throughout the different chapters, it was described the synthesis and structural elucidation of new dynamic asymmetrically substituted PDPAs. This finding open new possibilities of applications for these materials. Moreover, the properties derived from the dynamism of these materials are also studied.

Following, the main conclusions for each chapter are summarized below.

***Chapter III*. Dissymmetric Chiral Poly(diphenylacetylene)s: Secondary Structure Elucidation and Dynamic Luminescence**

In this chapter, the combination of data collected from different structural techniques allowed us to build an approximated structure for an asymmetric PDPA prepared by polymerization with WCl_6/Ph_4Sn of a diphenyl acetylene monomer substituted with an active pentafluorophenyl ester (PFP) group. This polymer was further transformed into a chiral polymer by a post-functionalization reaction that incorporates *L*-alanine methyl ester into the pendants.

To elucidate the secondary structure of the polymer, Raman and IR spectroscopies were used to discern between *Z* and *E* configurations of the double bonds. In this case, the polymer adopts mainly a *trans* configuration of the double bonds. 1D and 2D-NMR experiments helped us to elucidate the regioregularity of the polymer, indicating a preferred head-to-tail polymerization reaction.

AFM studies provided useful information related to different helical structural parameters such as helical pitch, packing angle and the orientation of the external helix described by the pendant groups. The use of molecular modelling, together with the constrains provided by the results of IR, Raman, NMR and AFM studies allowed us to build an approximate secondary structure for this polymer. Thus, poly-(*S*)-**2** adopts a preferred *trans-transoidal* helical scaffold that is formed by three different helices. Helix 1, described by the orientation between conjugated double bonds; helix 2,

described by the pendant groups; and helix 3, described by a twisting degree of the whole polymer chain and observed when the polymer grows.

Computational studies on the model compound result in a theoretical ECD spectrum that resembles the experimental one and that allows us to demonstrate that in an asymmetric PDPA, the sign of the first Cotton band is ruled by helices 2 and 3, and not just by the orientation of the polyene backbone. Moreover, the present study also made it possible to explain why in different aggregation states, such as superhelices or nanospheres, a new ECD band appears because of a longitudinal coupling between polymer chains.

Additionally, this work reveals the dynamic behavior of poly-(*S*)-**2** and shows how *P* or *M* helical senses can be induced by conformational changes at the pendant groups using external stimuli such as solvent donor ability, fact corroborated by a combination of VCD experiments and theoretical calculations. Finally, associated to this dynamic helical behavior, a dynamic circular polarized luminescence switch with a $|g_{lum}|$ = +/- $1x10^{-3}$ was obtained for poly-(*S*)-**2**, where a CPL (+) is produced by a *M*/*P*/*P* (helix 1/helix 2/helix 3) arrangement generated in donor solvents, while a CPL (-) is ascribed to a *P*/*M*/*M* (helix 1/helix 2/helix 3) helical orientation produced when poly-(*S*)-**2** is annealed in non-donor solvents.

The elucidation of the three-dimensional structure of a PDPA opens a new horizon in the development of functional materials due to the possibility of establishing structure/function relationships that can result in an improvement of the functionality of the polymer through a directed tuning of its secondary structure.

Chapter IV. **The Degree of Polymerization Drastically Determines the Chiroptical Properties of Dynamic Asymmetric Poly(diphenylacetylene)s**

In this chapter, it has been demonstrated experimentally and theoretically that the sign of the ECD spectra of PDPAs depend on their length. Thus while short oligomers of polymers dervied with different metyl ester amino acids derivatives produce positive ECD spectra in DMF, larger polymers generate negative ECD spectra. These opposite ECD traces are not related to opposite helical senses induced in the PDPA by polymer size, but rather are caused by the different contributions of the functional groups in polymers of different sizes. Thus, while in short oligomers, the ECD trace is dominated by the polyene backbone (helix 1), in larger polymers, the ECD trace is dominated by the helix described by the phenyl rings of the PDPA (helix 2). As it is

known from previous studies, helix 1 and helix 2 rotate in opposite directions, and therefore the ECD traces generated by these two helices have opposite signs.

As a result, a single scaffold will present two opposite ECD traces for different degree of polymerization of the PDPA. Thus, on the one hand, a *P*/*M*/*M* (helix 1/helix 2/helix 3) will produce positive ECD spectra for short oligomers, while negative for larger polymeric structures. On the other hand, an *M*/*P*/*P* (helix 1/helix 2/helix 3) scaffold will give negative ECD spectra for short oligomers, while they will be positive for larger polymers.

Chapter V. **Dynamic P/M Memory Effect of the Macromolecular Helicity in Chiral Poly(diphenylacetylene)s: Kinetic and Thermodynamic Studies**

In this chapter, it was demonstrated through an elegant example that chiral poly(diphenylacetylene)s show a dynamic memory effect associated to the intrinsic steric properties of PDPAs. To show this, an asymmetric PDPA bearing the benzamide of *L*-alanine methyl ester at one of the aryl rings was prepared.

This polymer can adopt either a *P* or *M* helical sense after thermal annealing in $CHCl_3$ and DMF, respectively. Interestingly, it was found that the helical structure obtained after thermal annealing is memorized by solvent removal and redissolving it in another solvent that promotes opposite helical sense. For instance, the *P* helical structure adopted by the polymer after thermal annealing in CHCl3 after solvent evaporation and redissolving it in DMF.

The memory effect is temperature dependent, being long-lasted at lower temperatures. Interestingly not only the helical structure is memorized, other properties associated to the helical scaffold such as CPL emission is also memorized. This is the first time at our knowledge that a chiral dynamic helical polymer show memory effect, and where the two helical senses obtained for a certain polymer can be tested for potential applications in the same solvent, i.e. a *P* or *M* helix can be obtained either in CHCl3 or DMF. Hence, the two *P* and *M* helical structures can be obtained in a certain solvent, although just one is favored. This fact opens a new horizon in the application of these materials.

Chapter VI. **Complex Aggregation Pathways in Covalent Helical Polymers: Consecutive Mechanism and Kinetically Trapped Aggregates in a PDPA/M^{n+} complexes**

In this chapter, we have demontrated that *P* or *M* macroscopically chiral nanospheres can be obtained from a PDPA/$M(ClO_4)_n$ system through complex aggregation pathways. In this case, *P* or *M* macroscopically chiral nanospheres are obtained under the same environmental conditions for a PDPA/$M(ClO_4)_n$ complex. This fact is possible due to the large energy barrier of

the helix inversion process in PDPAs. Thus, a kinetic aggregate (Agg_1) can be trapped for days or even moths at low temperatures, which can evolve towards a thermodynamic aggregate (Agg_2) through a consecutive aggregation process.

Interestingly, other properties associated to the chiral content of the aggregate, such as the circularly polarized emission change once the helix of the PDPA is inverted within the aggregate. These findings open a new horizon in the development of nanomaterials whose chiroptical properties can be kinetically trapped, allowing to test the material for potential applications either into the *P* or *M* macroscopic chirality without altering the environmental conditions to perform the experiment.

Chapter VII. **Evaluation of Substitution Effects in the Structure, Optical and Chiroptical Properties of Chiral Poly(diphenylacetylene)s**

In the last chapter, it was demonstrated through different examples that chiral *meta*-substituted PDPAs produces helical structures with similar chiroptical and circularly polarized emissive properties found for *para*-PDPAs. Moreover, although the secondary structure is quite similar, *meta*-substituted PDPAs showed a huge tendency to self-assembly in annular arrangements. Interestingly, the location of the pendant group closer to the polyene backbone in *meta*-PDPAs generates a more congested structure that inhibits the helical inversion in most cases. In the case of a *m*-PDPA derived with methionine methyl ester, this inversion is allowed in Dioxane, being the first dynamic *meta*-substituted PDPA synthetized.

In our group, more studies are being carried out on the activation energy barrier for helical inversion and the dynamic memory effect in this polymer that will allow us to explore the different effect of the substitution pattern on helicity for potential application of these materials in fields such as chiral stationary phases, chiral recognition ability, chiral ligands in asymmetric synthesis, among others.

Chapter X

Experimental Sections and Methodology

Experimental Section Chapter III

1. Materials and methods

CD measurements were done in a Jasco-720. The amounts of polymer used for CD measurements were 0.5 mg/mL in DCM, $CHCl_3$, THF, Acetone, MeCN, Dioxane, DMF and DMSO.

UV spectra were registered in a Jasco V-630. The amounts of polymer used for UV measurements were 0.5 mg/mL in DCM, $CHCl_3$, THF, Acetone, MeCN, Dioxane, DMF and DMSO.

G_{abs} was calculated using the following equation G_{abs}= CD/(UV*3300), where CD is the value of circular dichroism at a given wavelength and UV is the absorption at a given wavelength.

IR studies were carried out in a FTIR Varian 670 equipped with an ATR (GladiATR model) with diamond crystal of PIKE Technologies.

Raman spectra were performed in a Renishaw confocal Raman spectrometer (Invia Reflex model), equipped with two lasers (diode laser 785 nm and Ar laser 514 nm).

GPC studies were carried out in a Waters Alliance equipped with Phenomenex GPC columns. The amount of polymer used for GPC measurements was 0.5 mg/mL.

AFM measurements were performed in a MultiMode V Scanning Probe Microscope (Veeco Instruments) in air at rt with standard silicon cantilevers and super-sharp cantilevers in tapping mode using 12 µm and 1 µm scanners. Nanoscope processing software and WSxM 4.0 Beta 1.0 [4] (Nanotec Electronica, S.L.) were used for image analysis.

For molecular modeling we used Spartan 14 (MMFF94). As a molecular visualization system, we used PyMOL. The additional methodology used in the computational study is detailed in the Computational Details section.

CPL spectra were recorded on a Jasco CPL-300 at a scanning rate of 100nm/min over an average of 5 scans, using a 10 mm quartz cell.

VCD spectra were recorded in a Jasco FVS-6000 over an average of 6000 scans using a cell equipped with BaF_2 lens and a Teflon spacer generating a 150 µm path length.

2. Synthesis of monomers

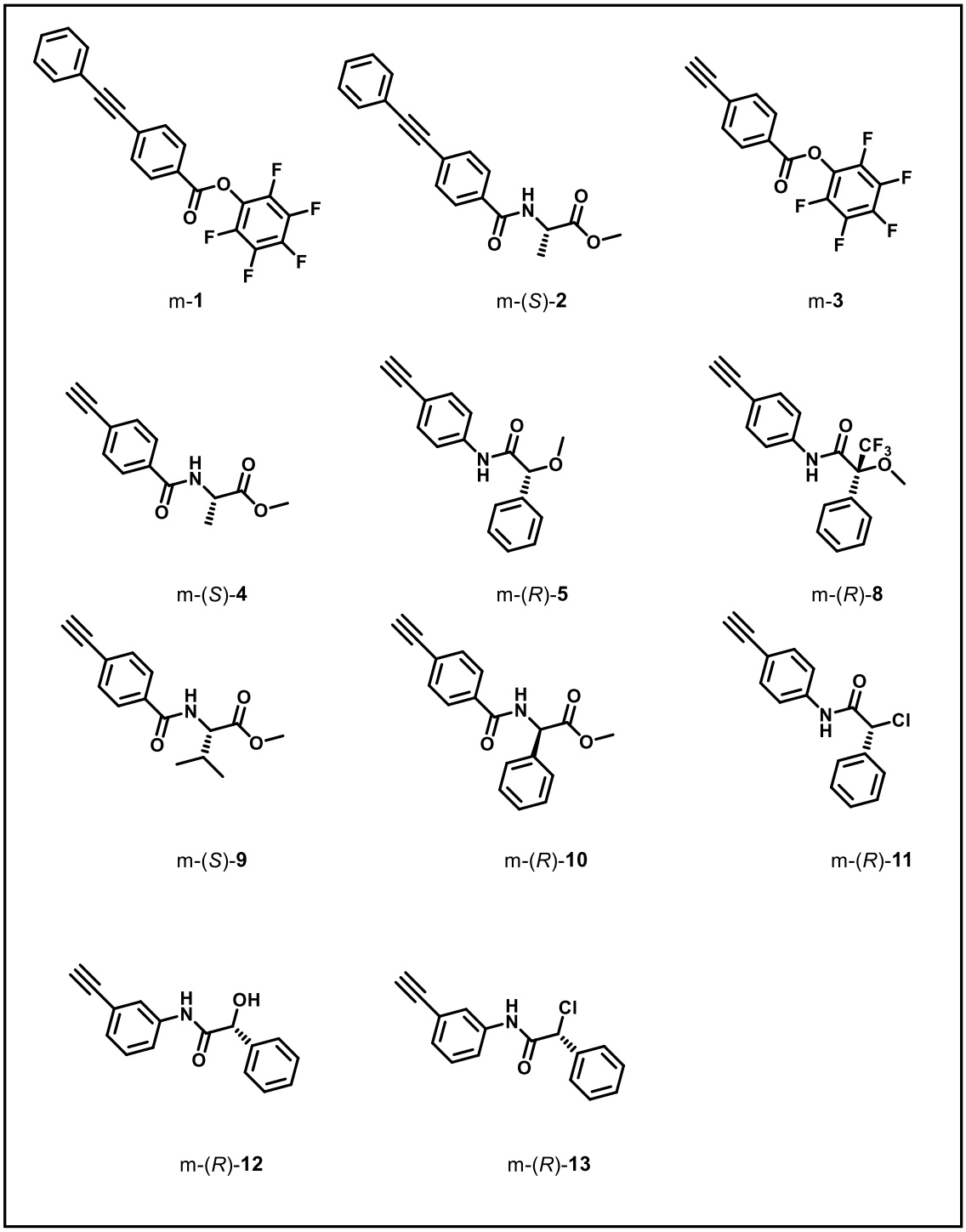

Figure S1: Compounds m-**1**, m-(*S*)-**2**, m-**3**, m-(S)-**4**, m-(*R*)-**5**, m-(*R*)-**8**, m-(*S*)-**9**, m-(*S*)-**10**, m-(*R*)-**11**, m-(*R*)-**12** and m-(*R*)-**13** were prepared following the experimental procedure depicted below.

M-**3**, m-(*R*)-**5**, m-(*R*)-**8**, m-(*R*)-**10** were prepared according to Ref. **S1**, **S3**, **S4** and **S5** respectively. M-(S)-**4** and m-(*S*)-**9** were prepared according to Ref. **S2**. M-(*R*)-**11**, m-(*R*)-**12** and m-(*R*)-**13** were prepared according to Ref. **S6.**

For preparation of m-**1** and m-(*S*)-**2** see experimental details below.

Perfluorophenyl 4-iodobenzoate

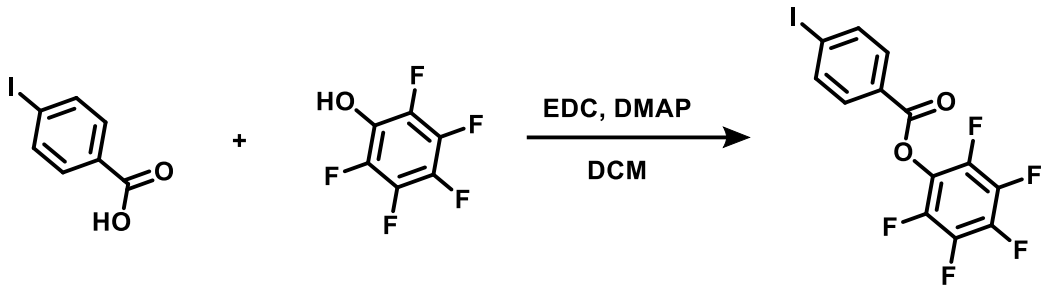

1 **2** **3**

4-iodobenzoic acid (**1**, 2.96 g, 11.94 mmol), EDC (2.40 g, 12.48 mmol), DMAP (0.073 g, 0.6 mmol) and 100 mL dry DCM were added into a 250 mL flask. After activation, pentafluorophenol (**2**, 2.00 g, 10.86 mmol) was added. The mixture was stirred at rt for 12 h and a white precipitate was formed. Then, the solid was filtrated and washed with hexane. After concentration in a rotary evaporator, the crude product was purified by silica gel column chromatography (40-63 mesh) using a mixture of hexane and ethyl acetate (95:5 by volume) as eluent. After evaporation of solvents in a rotary evaporator, a white solid was obtained in 75% yield.

^{1}H NMR (300MHz, $CDCl_3$) δ (ppm): 8.11 - 7.71 (4H, dd)

^{19}F NMR (282.3 MHz, $CHCl_3$) δ (ppm): -152.6, -157.7, -162.2

^{13}C NMR (75MHz, $CDCl_3$) δ (ppm): 162.2, 138.3, 131.8, 126.3, 103.1

HRMS (ESI) m/z calcd for $C_{13}H_5F_5IO_2$ $[M+H]^+$: 414.9246, found: 414.9249, see Figure S28.

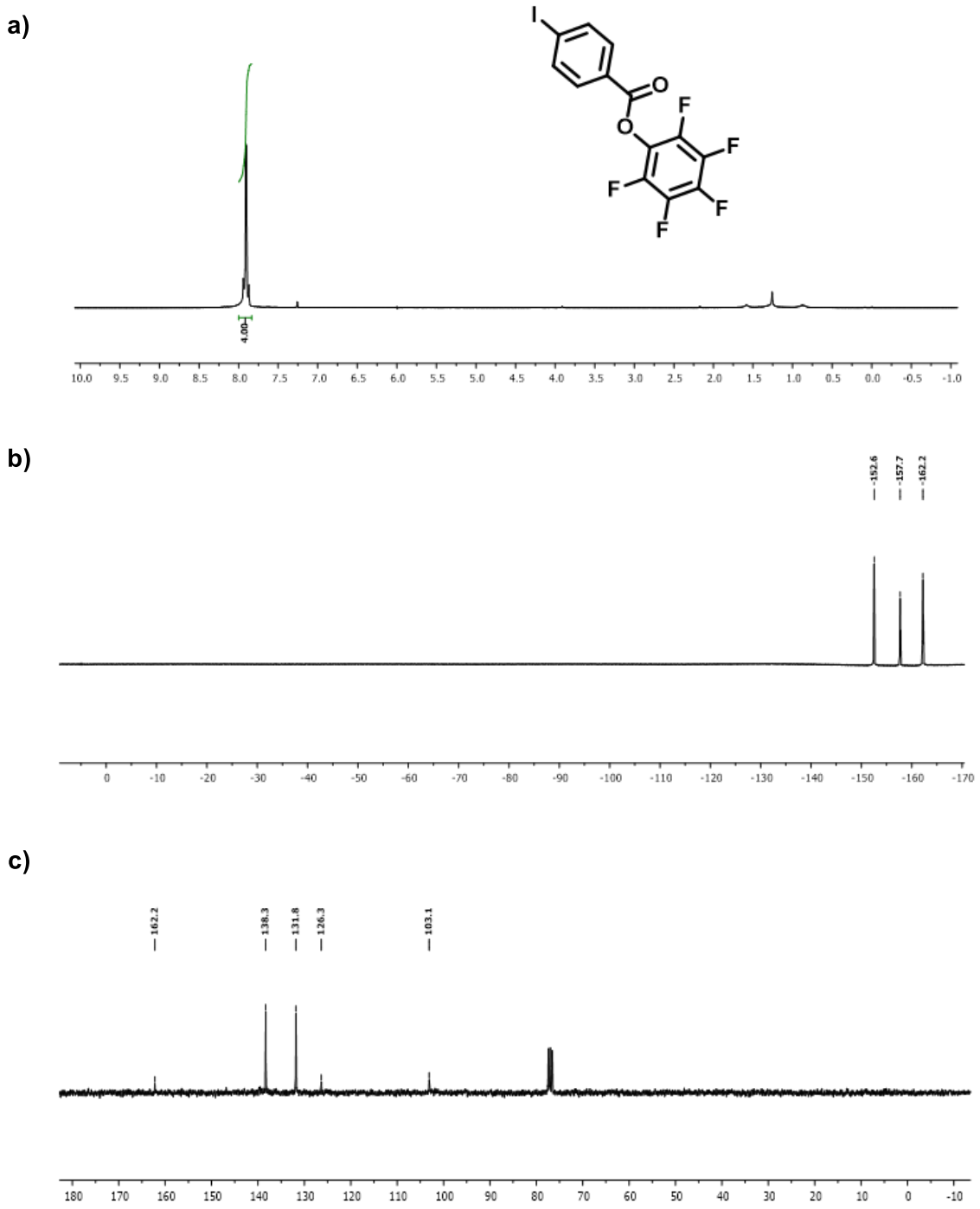

Figure S2. a) ^{1}H, b) ^{19}F and c) ^{13}C NMR spectra of **3** (perfluorophenyl 4-iodobenzoate).

Perfluorophenyl 4-(phenylethynyl)benzoate

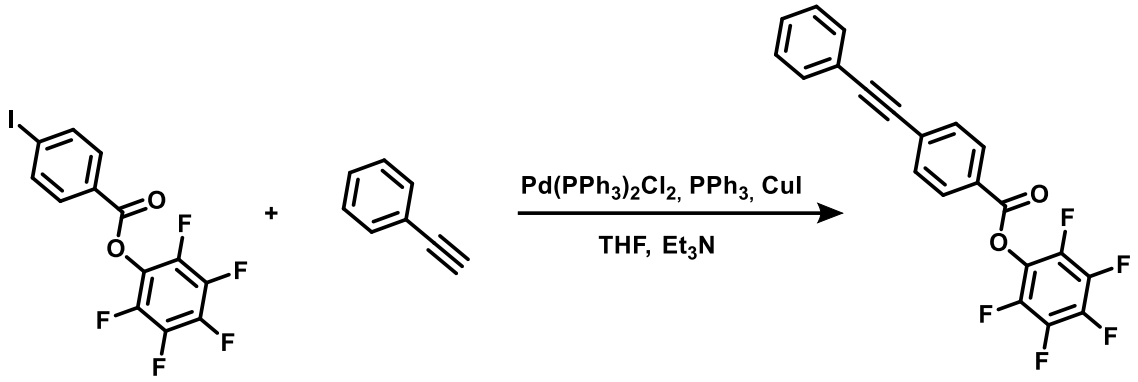

3 **4** **M-1**

Perfluorophenyl 4-iodobenzoate (**3**, 3.94 g, 9.51 mmol), $PdCl_2(PPh_3)_2$ (333 mg, 0.475 mmol), CuI (181 mg, 0.951 mmol), PPh_3 (249 mg, 0.951 mmol) were added to 50 mL of THF and 6.6 mL of Et_3N (47.55 mmol) under nitrogen. After the catalysts was completely dissolved, phenylacetylene (1.5 mL, 14.2 mmol) was injected into the flask and the mixture was stirred at rt for 24 h. The solid was removed by filtration and washed with diethyl ether. The filtrate was then concentrated in a rotary evaporator. The crude product was purified by silica gel column chromatography (40-63 mesh) using a mixture of hexane and ethyl acetate (95:5 by volume) as eluent. **M-1** was obtained as a white solid in 80% yield.

^{1}H NMR (300MHz, $CDCl_3$, δ, TMS, ppm): 8.18 (2H, d), 7.68 (2H, d), 7.57 (2H, m), 7.39 (3H, m).

^{19}F NMR (282.3 MHz, $CHCl_3$) δ (ppm): -152.5, -157.8, -162.3

^{13}C NMR 75 MHz, $CDCl_3$, δ, TMS, ppm): 162.1, 139.6, 136.3, 131.9, 131.8, 130.6, 130.0, 129.0, 128.5, 126.0, 122.4, 93.8, 88.2

HRMS (ESI) m/z calcd for $C_{21}H_{10}F_5O_2$ $[M+H]^+$: 389.0595, found: 389.0595, see Figure S29.

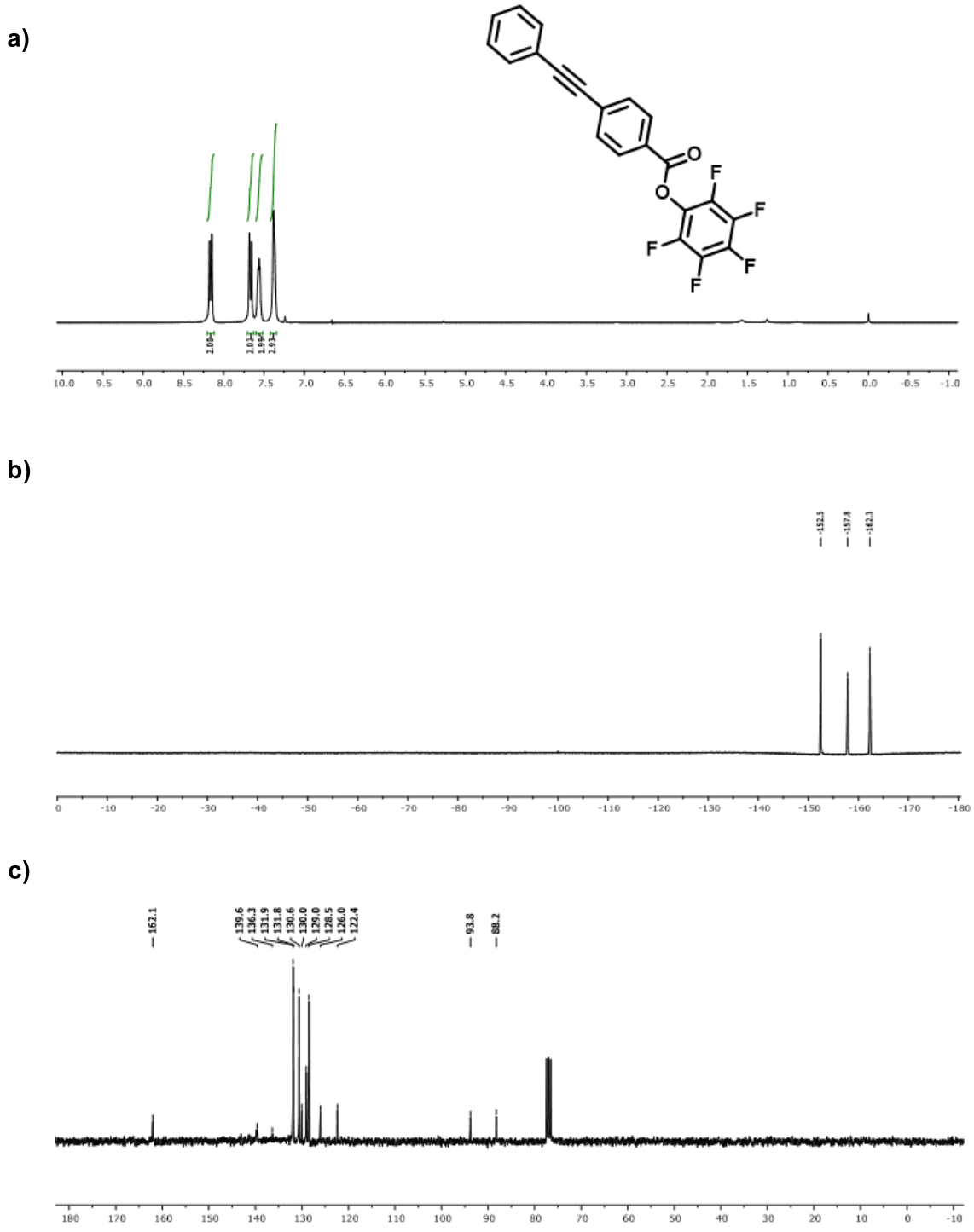

Figure S3. a) ^{1}H, b) ^{19}F and c) ^{13}C NMR spectra of m-1.

Methyl (4-(phenylethynyl)benzoyl)-*L*-alaninate

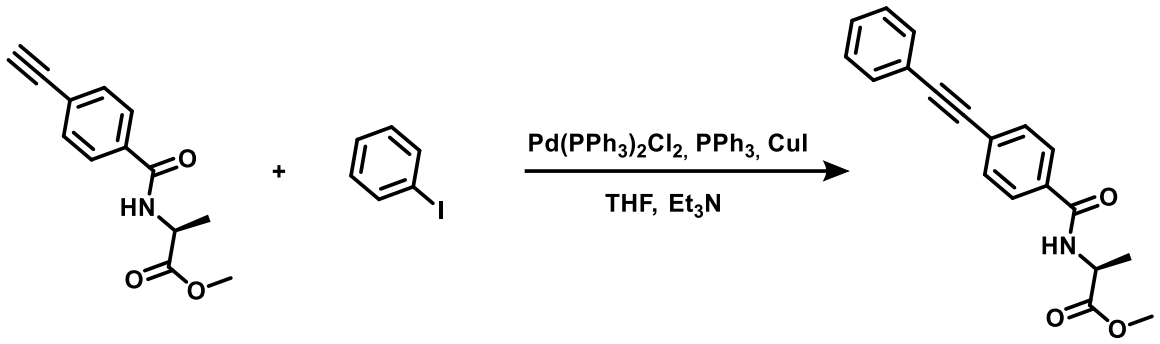

m-(*S*)-4 5 m-(*S*)-2

Iodobenzene (**5**, 0.150 mL, 1.34 mmol), $PdCl_2(PPh_3)_2$ (47 mg, 0.067 mmol), CuI (25.5 mg, 0.134 mmol), PPh_3 (35.1 mg, 0.134 mmol) were added to 15 mL of THF and 1 mL of Et_3N (6.7 mmol) under nitrogen. After the catalysts was completely dissolved, m-(*S*)-**4** (371 mg, 1.608 mmol) was added into the flask and the mixture was stirred at rt for 24 h. The solid was removed by filtration and washed with diethyl ether. The filtrate was then concentrated in a rotary evaporator. The crude product was purified by silica gel column chromatography (40-63 mesh) using a mixture of hexane and ethyl acetate (7:3 by volume) as eluent. m-(*S*)-**2** was obtained as a white solid in 83% yield.

^{1}H NMR (300MHz, $CDCl_3$, δ, TMS, ppm): 7.79 (2H, d), 7.51 (4H, m), 7.28 (3H, m), 7.08 (1H, d), 4.77 (1H, m), 3.75 (3H, s), 1.51 (3H, d).

^{13}C NMR 75 MHz, $CDCl_3$, δ, TMS, ppm): 174.0, 166.5, 133.4, 132.0, 131.9, 129.0, 128.7, 127.5, 127.1, 123.0, 92.2, 88.9, 52.9, 48.9, 18.7

HRMS (ESI) m/z calcd for $C_{19}H_{18}NO_3$ $[M+H]^+$: 308,1281, found: 308.1292, see Figure S30.

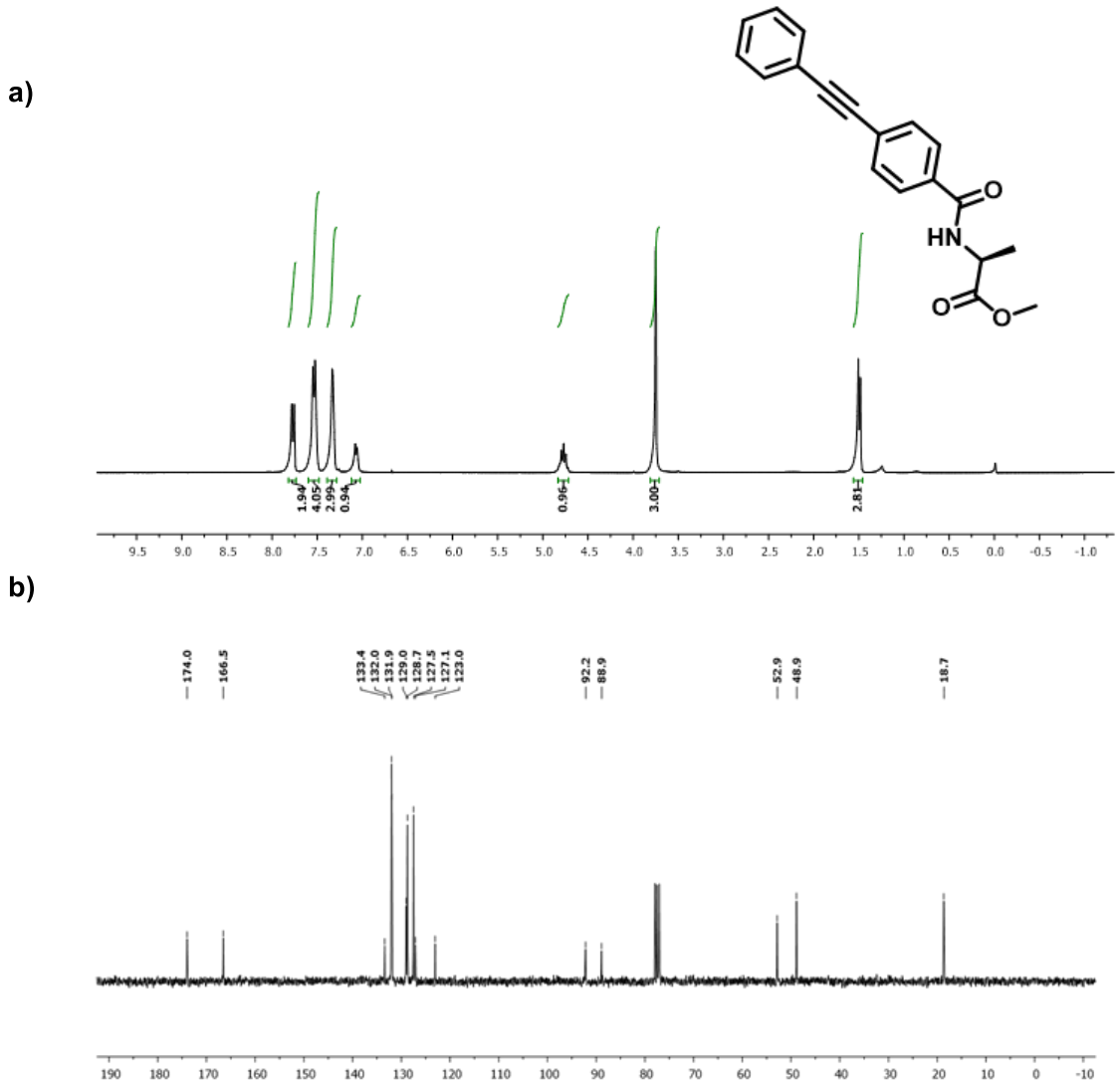

Figure S4. a) ^{1}H and b) ^{13}C NMR spectra of m-(*S*)-**2**.

3. Crystallographic Data

For X-ray analysis, crystals of monomer m-(*S*)-**2** were grown by slow evaporation from a 1:1 mixture of dichloromethane/hexane.

Computing details

Data collection: Bruker *APEX3* software; cell refinement: *SAINT* V8.40A (Bruker Nano, Inc., 2019); data reduction: *SAINT* V8.40A (Bruker Nano, Inc., 2019); program(s) used to solve structure: *SHELXT* 2014/5 (Sheldrick, 2014); program(s) used to refine structure: *SHELXL2018*/3 (Sheldrick, 2018); molecular graphics: shelXle (C.B. Huebschle, rev 958).

*Crystal data for m-(S)-**2***

Crystal data

$C_{19}H_{17}NO_3$	$F(000) = 648$
$M_r = 307.33$	$D_x = 1.244$ Mg m^{-3}
Monoclinic, $P2_1$	Cu $K\alpha$ radiation, $\lambda = 1.54178$ Å
$a = 10.0443$ (2) Å	Cell parameters from 9697 reflections
$b = 16.9854$ (3) Å	$\theta = 4.6$–$80.2°$
$c = 10.3162$ (2) Å	$\mu = 0.68$ mm^{-1}
$\beta = 111.1992$ (9)°	$T = 100$ K
$V = 1640.91$ (5) Å^3	Needle, colourless
$Z = 4$	0.28 × 0.10 × 0.03 mm

Data collection

Bruker D8 VENTURE PHOTON-III 14 diffractometer	$T_{min} = 0.92$, $T_{max} = 0.98$
Radiation source: microfocus sealed tube, Incoatec IμS 3.0	57991 measured reflections
Multilayer mirror monochromator	7020 independent reflections
Detector resolution: 7.3910 pixels mm^{-1}	6709 reflections with $I > 2\sigma(I)$
φ or ω oscillation scans	$R_{int} = 0.039$
Absorption correction: multi-scan *SADABS2016*/2 - Bruker AXS area detector scaling and absorption correction	$\theta_{max} = 80.5°$, $\theta_{min} = 4.6°$
	$h = -12 \rightarrow 12$
	$k = -21 \rightarrow 21$
	$l = -13 \rightarrow 12$

Refinement

Refinement on F^2	$R[F^2 > 2\sigma(F^2)] = 0.028$
Least-squares matrix: full	$wR(F^2) = 0.068$
$S = 1.04$	$w = 1/[\sigma^2(F_o^2) + (0.0304P)^2 + 0.3028P]$ where $P = (F_o^2 + 2F_c^2)/3$
7020 reflections	$(\Delta/\sigma)_{max} < 0.001$
425 parameters	$\Delta\rho_{max} = 0.17$ e Å^{-3}
1 restraint	$\Delta\rho_{min} = -0.16$ e Å^{-3}
Primary atom site location: dual	Absolute structure: Flack x determined using 3072 quotients [(I+)-(I-)]/[(I+)+(I-)] (Parsons, Flack and Wagner, Acta Cryst. B69 (2013) 249-259).
Secondary atom site location: difference Fourier map	Absolute structure parameter: −0.06 (5)
Hydrogen site location: mixed	
H atoms treated by a mixture of independent and constrained refinement	

Special details

Geometry. All e.s.d.'s (except the e.s.d. in the dihedral angle between two l.s. planes) are estimated using the full covariance matrix. The cell e.s.d.'s are taken into account individually in the estimation of e.s.d.'s in distances, angles and torsion angles; correlations between e.s.d.'s in cell parameters are only used when they are defined by crystal symmetry. An approximate (isotropic) treatment of cell e.s.d.'s is used for estimating e.s.d.'s involving l.s. planes.

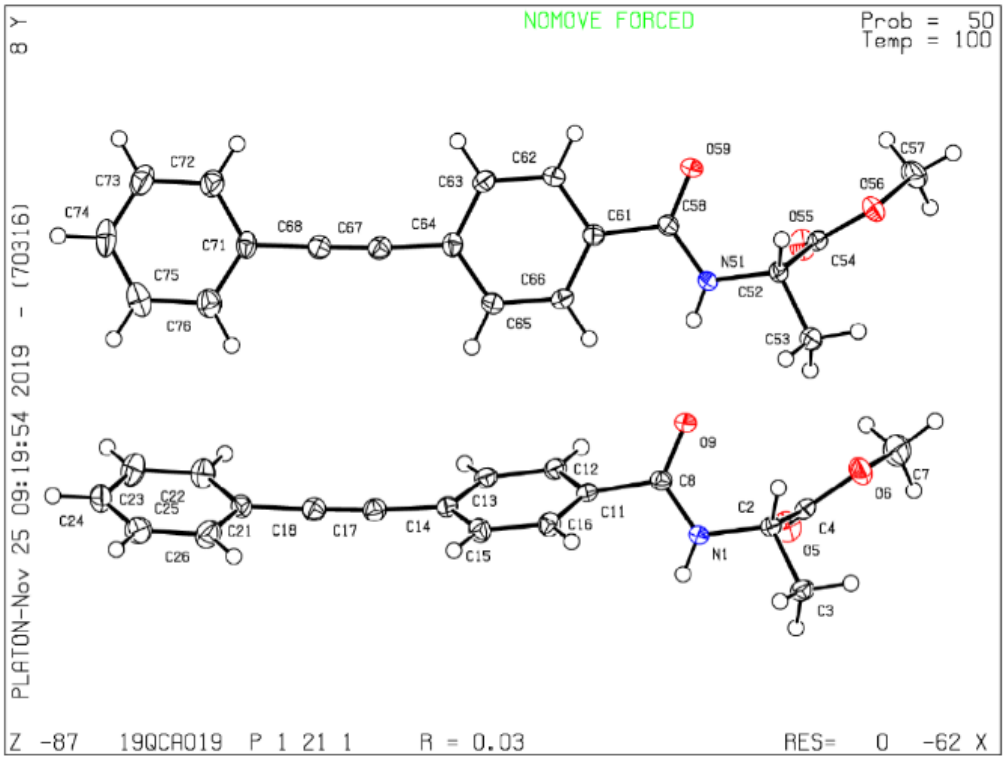

Figure S5. Crystal data and ORTEP view of the asymmetric unit content for m-(*S*)-**2**.

4. Synthesis of Polymers

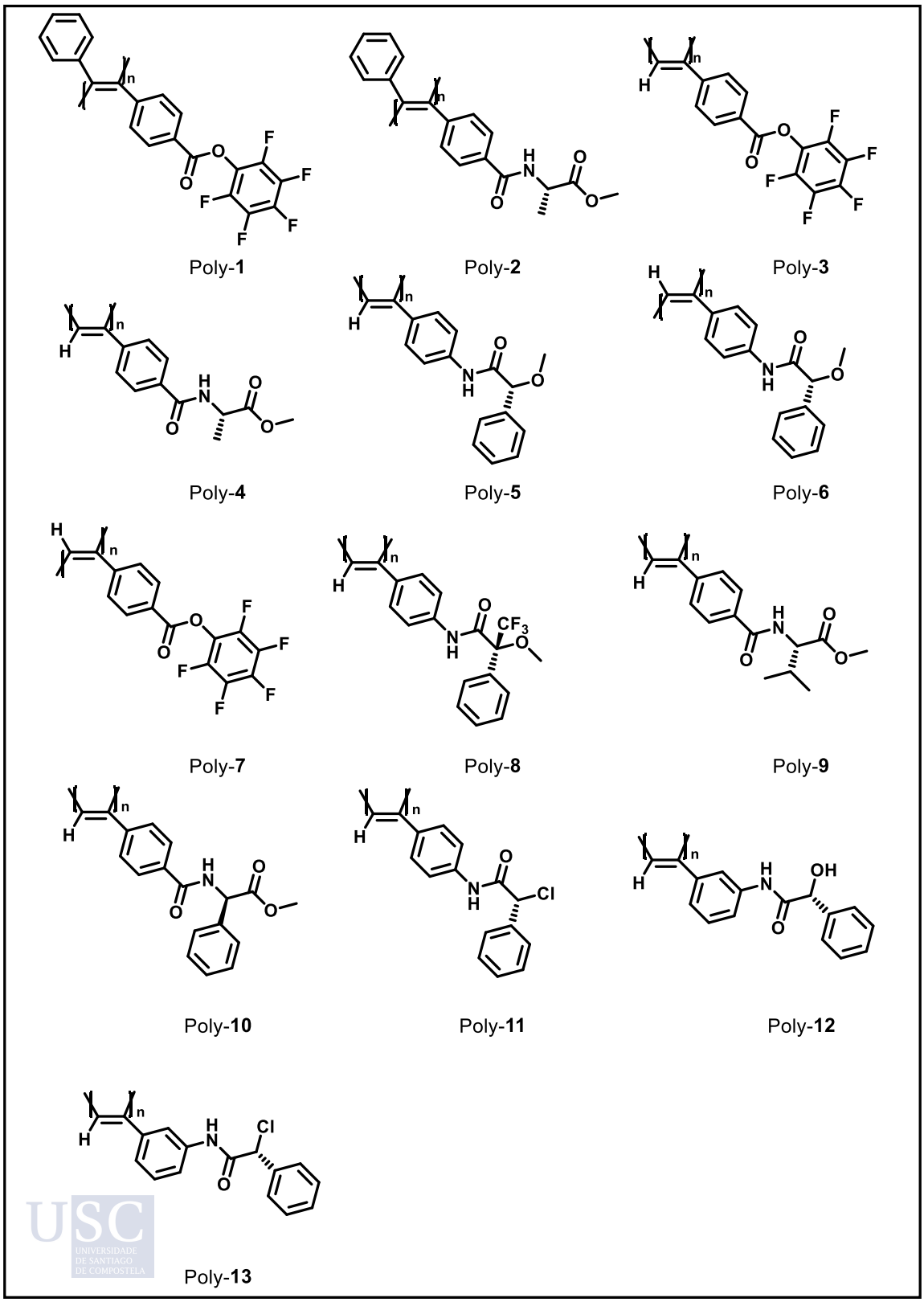

Figure S6: Structure of the polymers synthesized in this work.

It should be noted that Poly-**2** and Poly-**6** cannot be polymerized directly. To obtain Poly-**2**, a post-polymerization coupling of Poly-**1** is needed. To obtain Poly-**6**, it is necessary to add a solution of Au^{3+} salt in MeOH to Poly-**5**.

The general procedures to obtain *cis* and *trans* polymers are described below.

Cis Polymerization Reaction

The reaction flask (sealed ampoule) was dried under vacuum and argon flushed three times before the monomer was added as a solid. Then, the flask was evacuated on a vacuum line and flushed with dry argon (three times). Dry THF was added with a syringe and the triethylamine dropwise. A solution of rhodium norbornadiene chloride dimer, $[Rh(nbd)Cl]_2$, in THF was added at 30 °C. The reaction mixture was stirred at 30 °C for 6 h. Then, the resulting polymer was diluted in CH_2Cl_2 and precipitated in a large amount of methanol, centrifuged (twice), reprecipitated in hexane and centrifuged again.

Table S1: Polymerization conditions of the corresponding polymers

Polymer	**Monomer Mass (mg)**	**THF (mL)**	**$[Rh(nbd)Cl]_2$ (mg)**	**Et_3N (µL)**	**Yield (%)**
Poly-**3**	100	1.0	1.0	5	91
Poly-**4**	100	1.0	1.0	5	88
Poly-**5**	100	1.0	1.0	5	93
Poly-**8**	100	1.0	1.0	5	92
Poly-**9**	100	1.0	1.0	5	90
Poly-**10**	100	1.0	1.0	5	89
Poly-**11**	100	1.0	1.0	5	87
Poly-**12**	100	1.0	1.0	5	90
Poly-**13**	100	1.0	1.0	5	92

Trans Polymerization Reaction

The polymerization reaction was carried out under a nitrogen atmosphere using standard Schlenk technique, unless otherwise specified. A typical procedure for the polymerization of M-**1** is given below as an example.

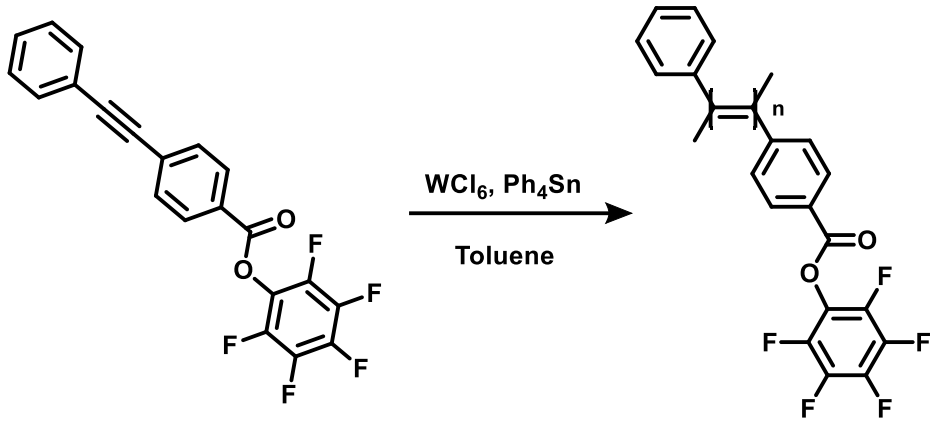

M-1 **P-1**

20.4 mg of WCl_6 and 44.0 mg of Ph_4Sn were added into a baked 10 mL Schlenk tube with a stopcock in the side arm. The tube was evacuated under vacuum and then flushed with dry nitrogen three times through the side arm. Freshly distilled toluene (1 mL) was injected into the tube to dissolve the mixture of catalysts and then, the catalyst solution was aged at 100 °C for 10 min. The monomer solution was prepared in another tube by dissolving 200 mg of **M-1** in 1.6 mL of toluene and was transferred to the catalyst solution using a hypodermic syringe. The reaction mixture was stirred at 100 °C for 24 h. The solution was cooled to rt, diluted with CH_2Cl_2 and then precipitated in a large amount of methanol. The precipitate was allowed to stand overnight and then collected by filtration. The polymer was washed with methanol and hexane and dried under vacuum at room temperature to a constant weight. **P-1** was obtained as a brown solid in 52% yield.

^{1}H-NMR (300MHz, $CDCl_3$), δ (TMS, ppm): 7.39, 6.75, 6.60, 6.28, 6.06.

^{19}F NMR (282.3MHz, $CDCl_3$), δ (TMS, ppm): -153.3, -157.6, -163.0.

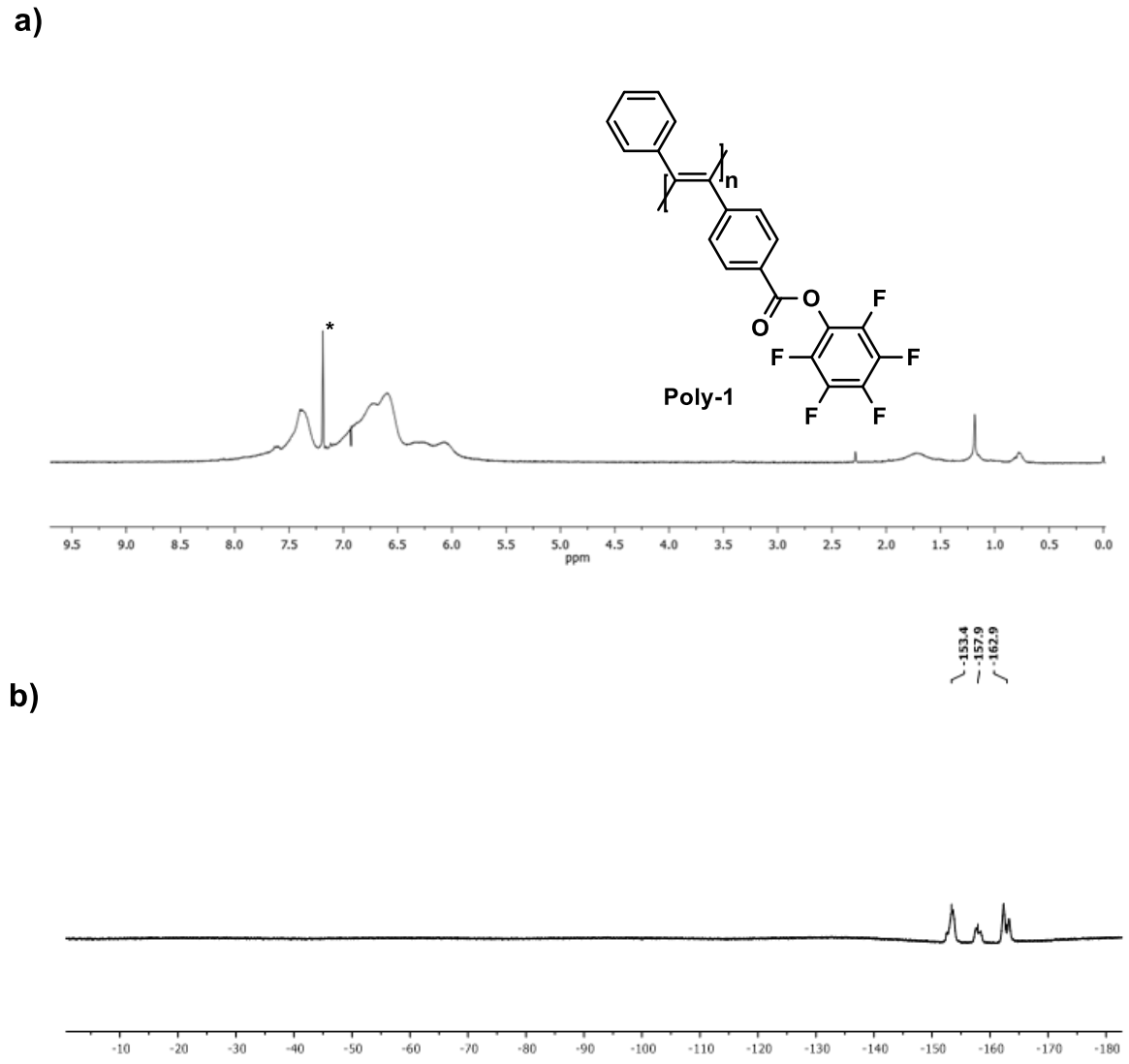

Figure S7. a) ^{1}H and b) ^{19}F NMR spectra of Poly-**1**.

Post-polymerization Coupling

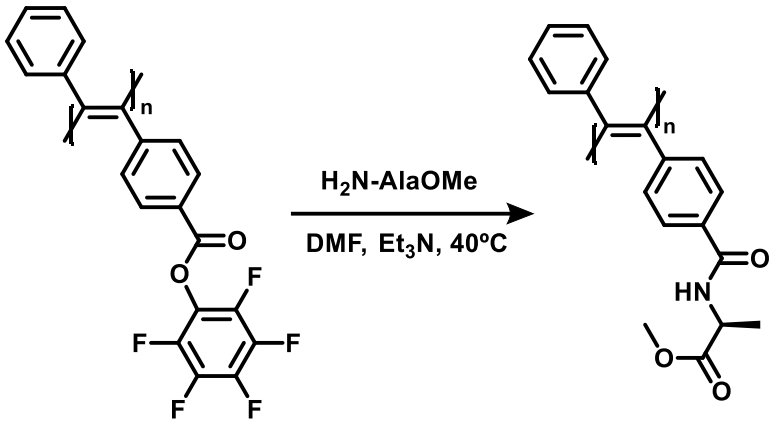

P-1 **P-(*S*)-2**

20 mg (0.052 mmol) P-**1**, 9.4 mg (0.067 mmol) L-alanine methyl ester hydrochloride and 2 mL dry DMF with a drop of TEA were added into a 10 mL reaction tube with magnetic stirring bar under nitrogen. The reaction solution was stirred for 12 h at 40 °C. Next, the solution mixture was added dropwise to 300 mL methanol through a cotton filter under vigilant stirring. The precipitate was kept still overnight and then filtered. The obtained polymer was washed with methanol and hexane several times and dried at rt to a constant weight. **P-(*S*)-2** was obtained as a yellow solid in 95 % yield.

^{1}H NMR (300 MHz, $CDCl_3$), δ (TMS, ppm): 7.25, 6.92, 6.63, 6.53, 6.12, 4.69, 3.73, 1.48.

^{19}F NMR (282.3 MHz, $CDCl_3$), δ (TMS, ppm): no signals.

$[\alpha]_D$= -141 (10 mg mL^{-1}, $CHCl_3$ after annealing)

$[\alpha]_D$= +58 (10 mg mL^{-1}, DMF after annealing)

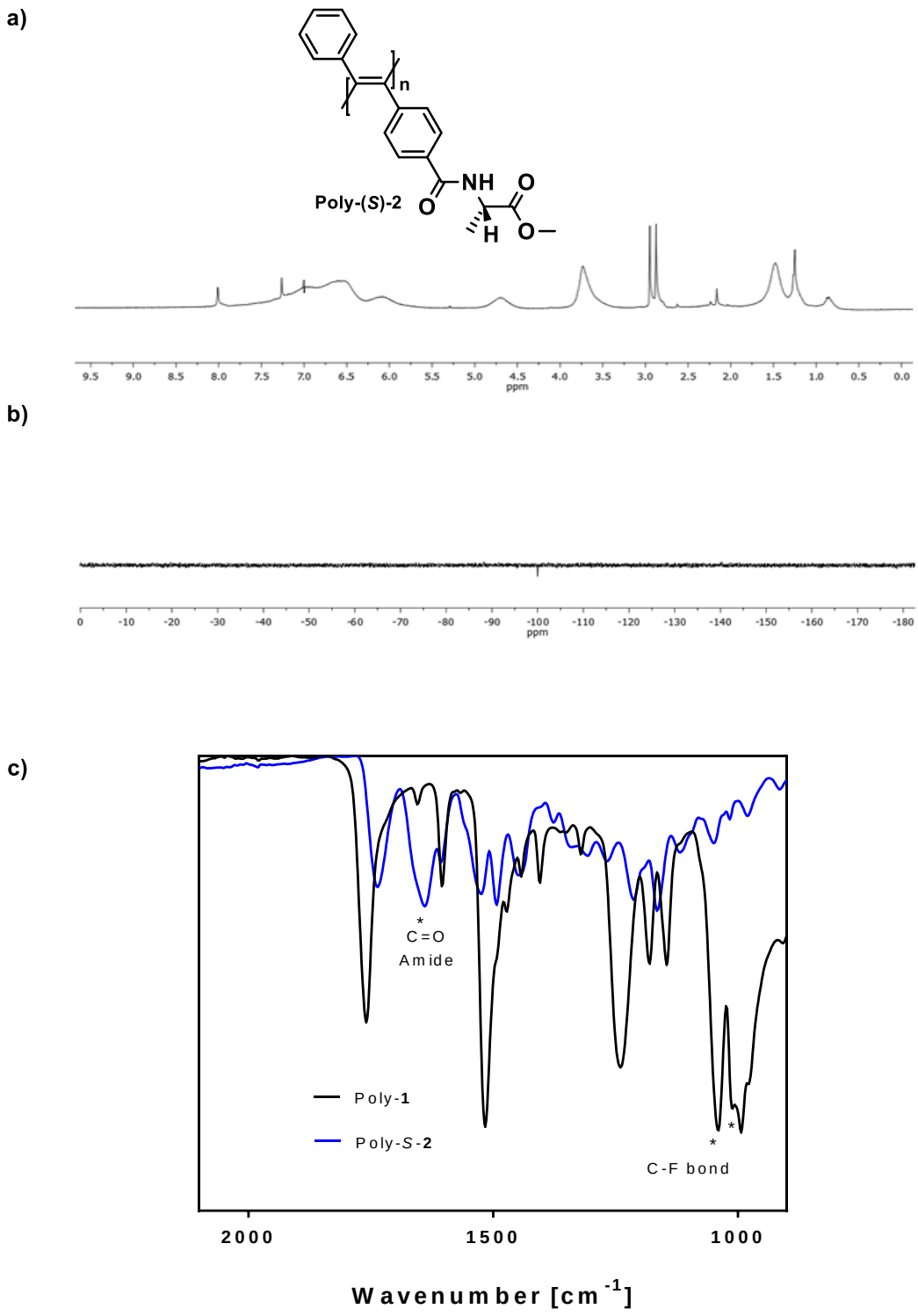

Figure S8. a) ^{1}H, b) ^{19}F of Poly-*S*-**2** and c) IR comparative of Poly-**1** and Poly-*S*-**2**.

5. NMR, Raman and IR studies of the polymers

The *cis* stereoregularity of the polymers was determined by ^{1}H-NMR spectroscopy, where the vinyl proton resonates at 6.0-5.8 ppm; Raman, where the peak at 1570-1585 cm^{-1} is assigned to C=C bond stretching in the *cis* poly(acetylene); IR, where the ratio between $I_{1500}/I_{1450} \approx 1$ is ascribed to *cis* configuration of different poly(acetylene)s and poly(phenylacetylene)s.

The trans stereoregularity cannot be determined by ^{1}H-NMR in poly(diphenylacetylene)s due to the absence of vinyl protons. Nevertheless, comparing the poly(phenylacetylene)s synthesized in both configurations —*cis* (poly-**3**, poly-**5**) and *trans* (poly-**7**, poly-**6**)— we can observe broader signals in the *trans* polymers and a shifting to 6.5-6-8 ppm of the vinyl proton as explained in Ref. **S8**.

In Raman studies, the C=C bond stretching in the *trans* polymers shows an intensive peak at 1550 cm^{-1} and a decrease in the band at 1570-1585 cm^{-1} assigned to *cis* polymers.

IR experiments show a > 1 ratio between I_{1500}/I_{1450} that is ascribed to a *trans* configuration of different poly(acetylene)s and poly(phenylacetylene)s.

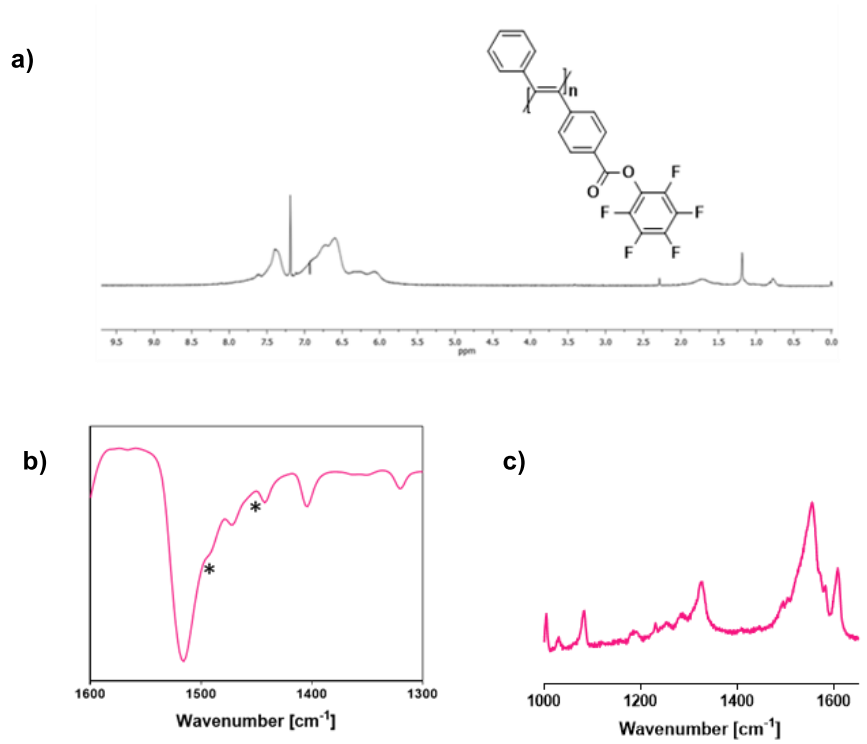

Figure S9. a) ^{1}H, b) IR and c) Raman spectra of *trans* Poly-**1**

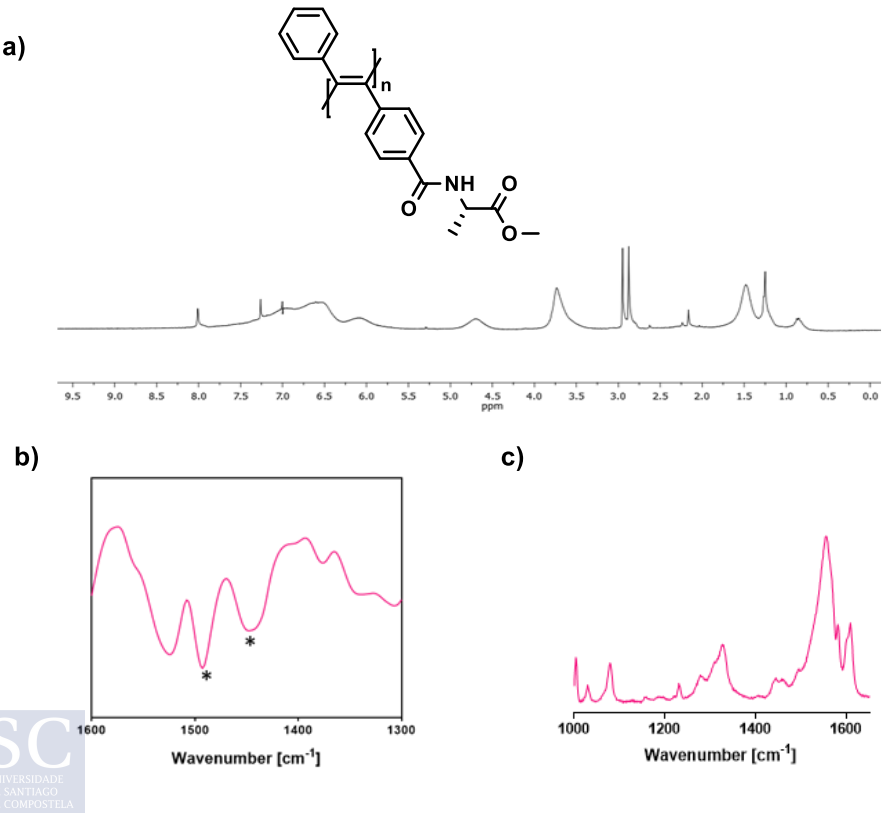

Figure S10. a) ^{1}H, b) IR and c) Raman spectra of *trans* Poly-**2**

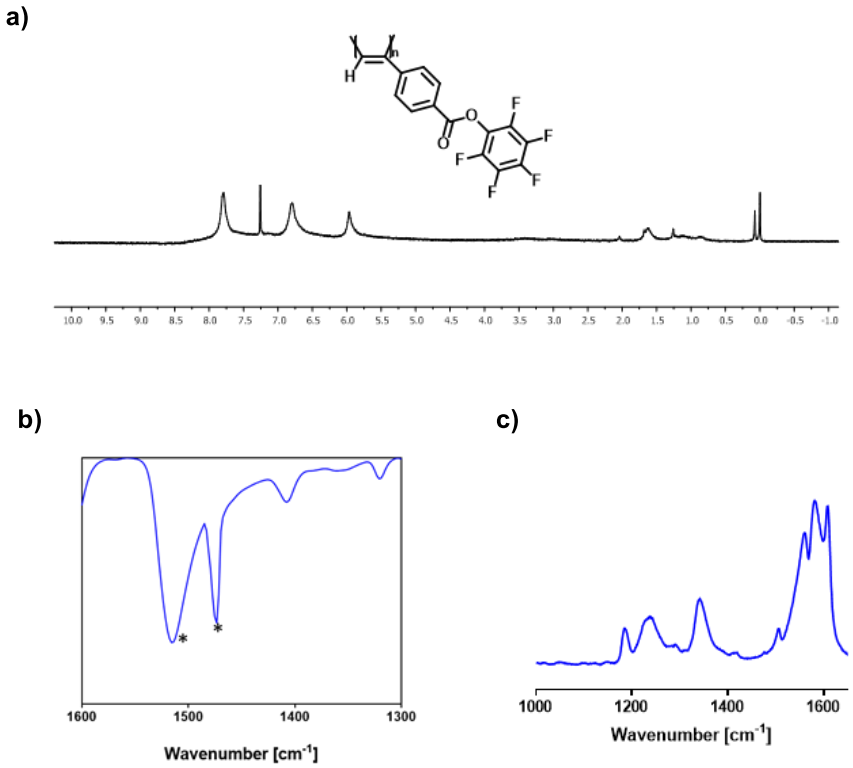

Figure S11. a) ^{1}H, b) IR and c) Raman spectra of *cis* Poly-**3**.

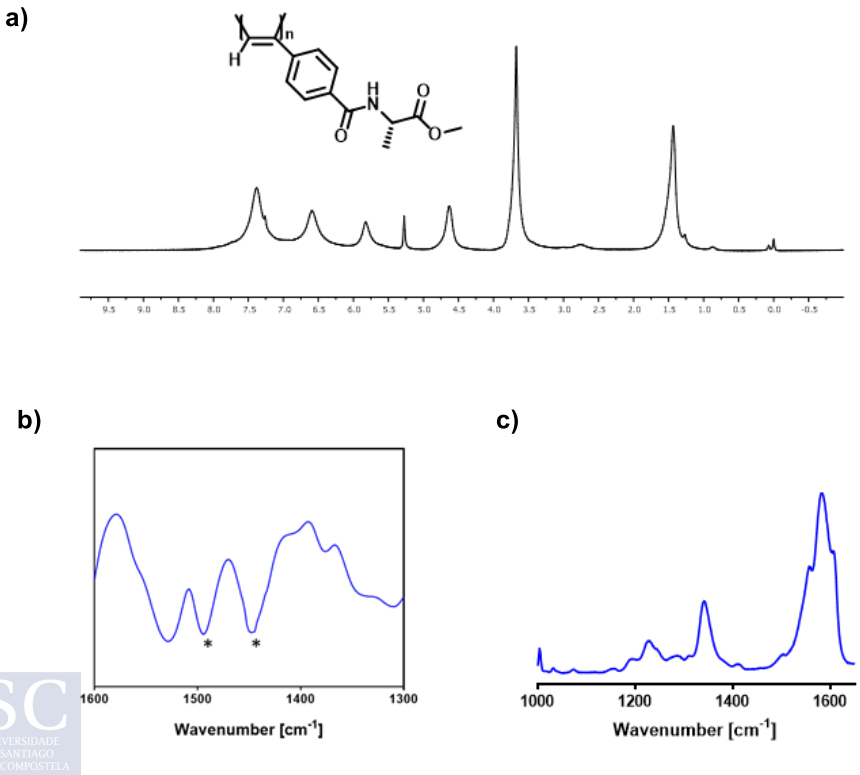

Figure S12. a) ^{1}H, b) IR and c) Raman spectra of *cis* Poly-**4**.

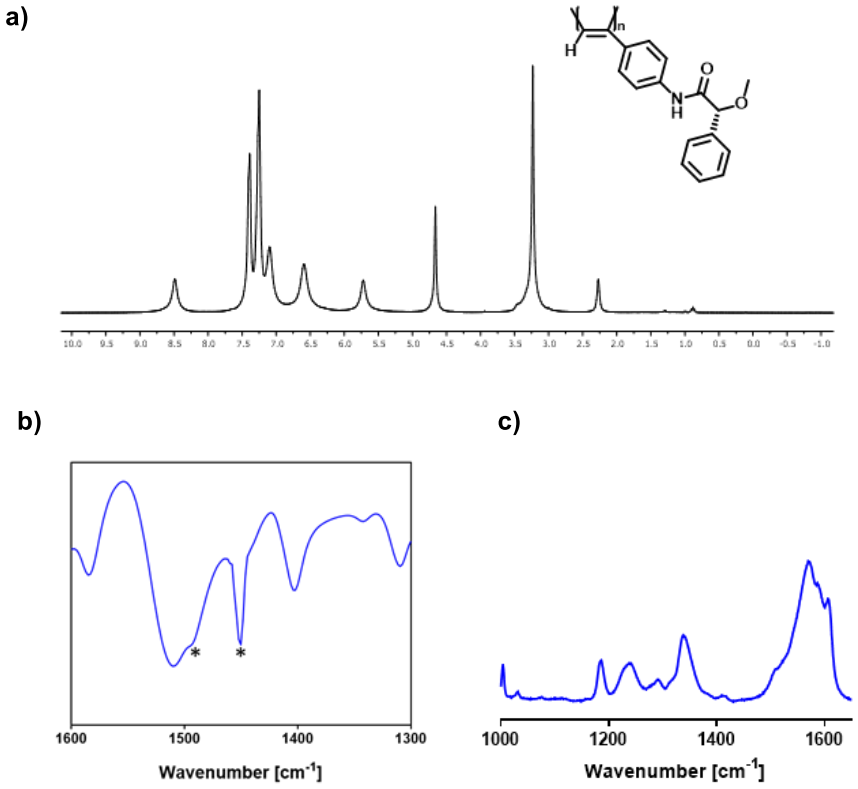

Figure S13. a) ^{1}H, b) IR and c) Raman spectra of *cis* Poly-**5**.

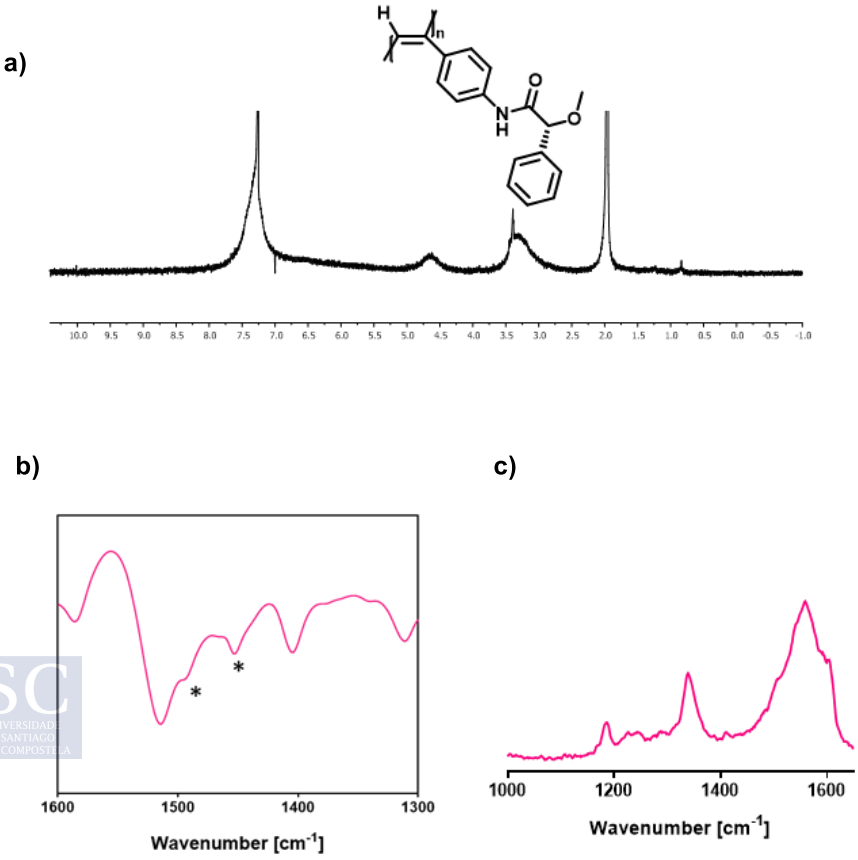

Figure S14. a) ^{1}H, b) IR and c) Raman spectra of *trans* Poly-**6**.

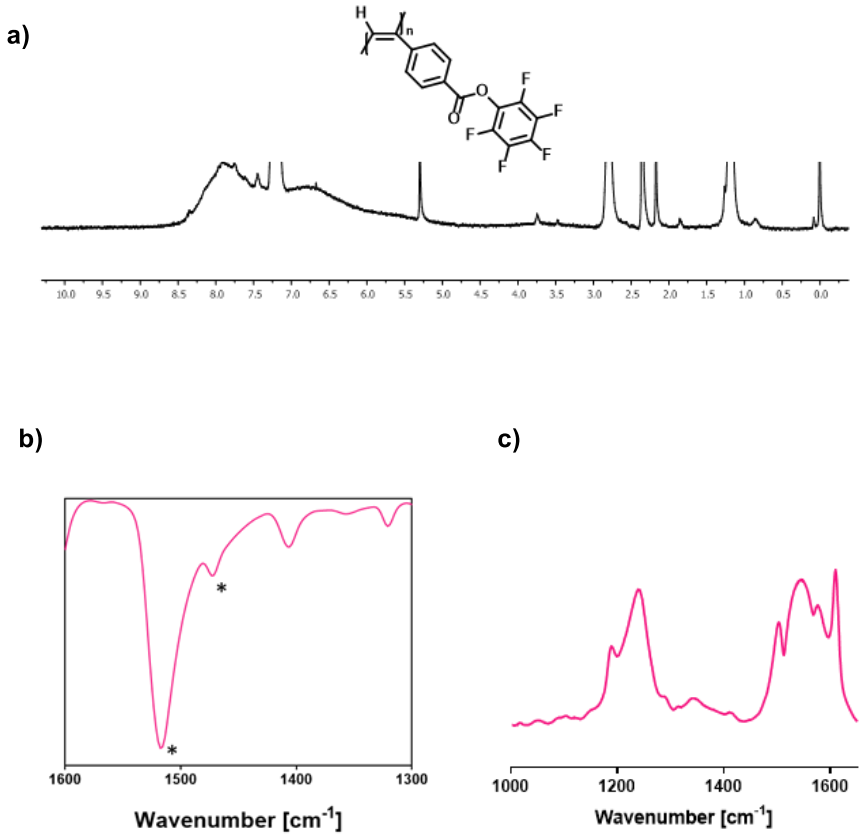

Figure S15. a) ^{1}H, b) IR and c) Raman spectra of *trans* Poly-**7**.

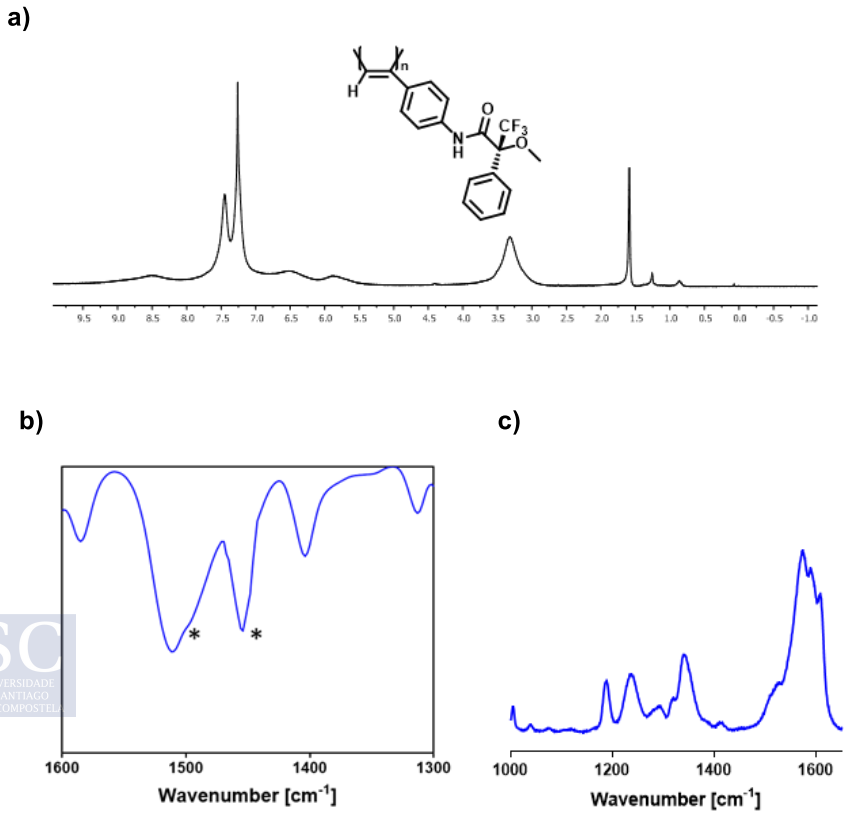

Figure S16. a) ^{1}H, b) IR and c) Raman spectra of *cis* Poly-**8**.

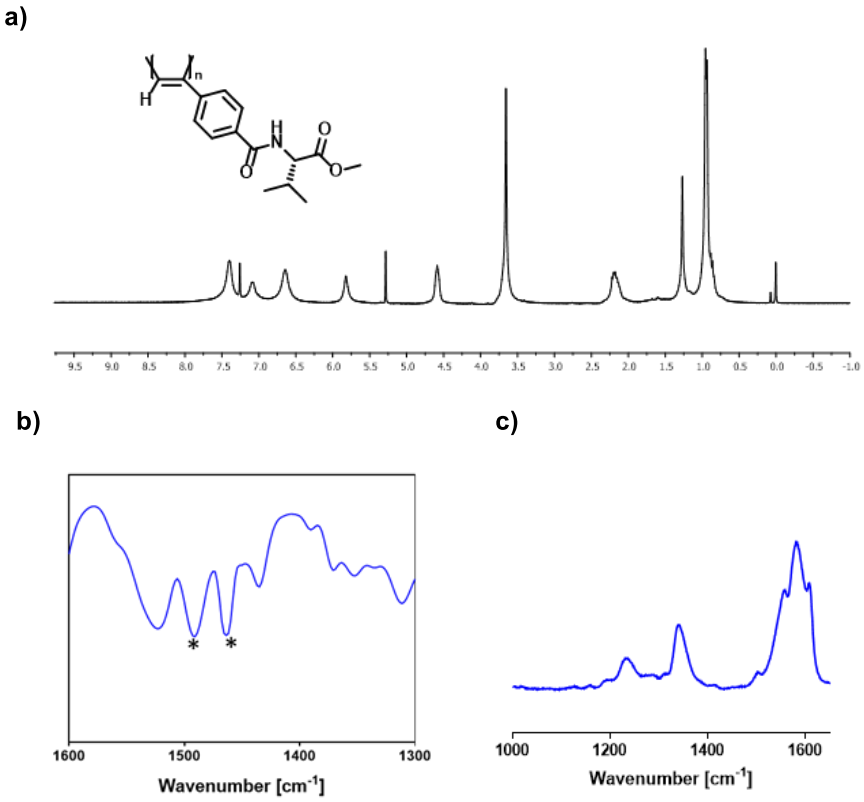

Figure S17. a) ^{1}H, b) IR and c) Raman spectra of *cis* Poly-**9**.

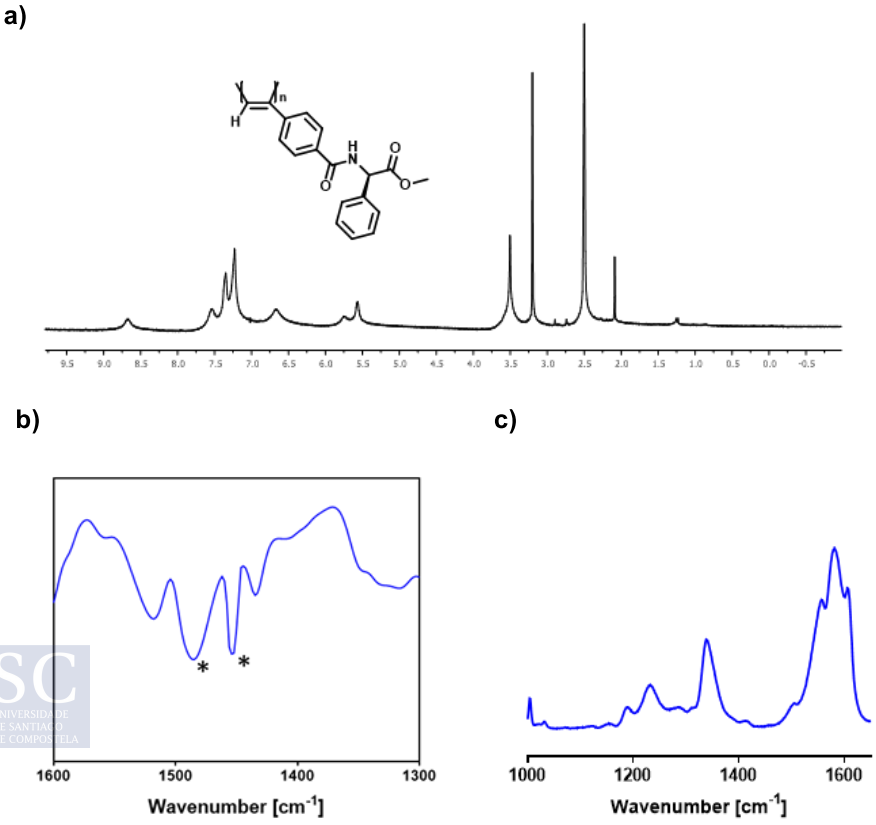

Figure S18. a) ^{1}H, b) IR and c) Raman spectra of *cis* Poly-**10**.

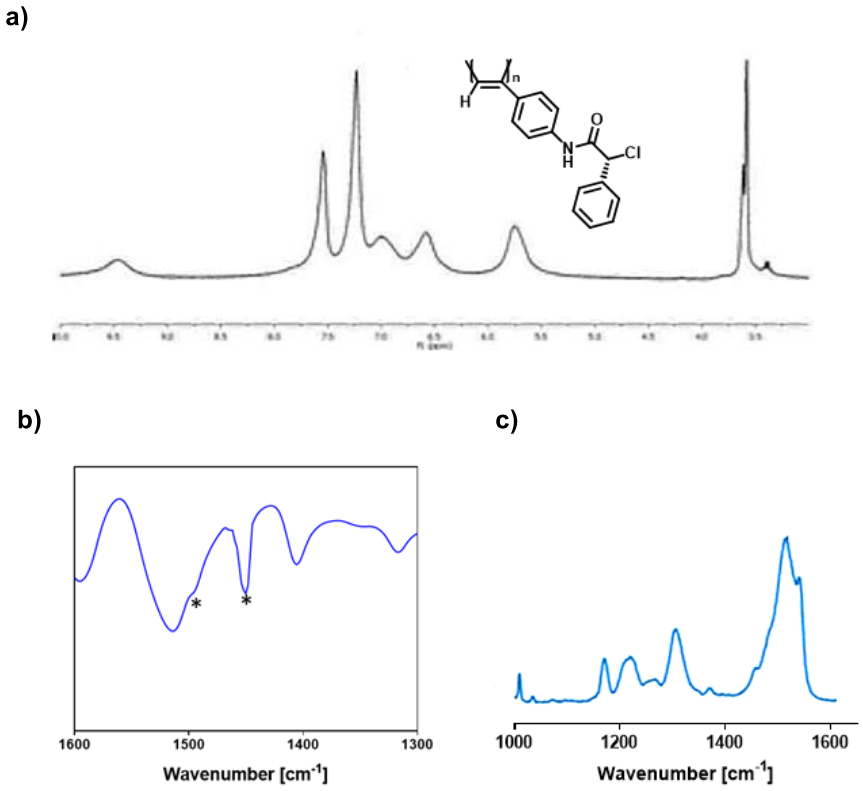

Figure S19. a) ^{1}H, b) IR and c) Raman spectra of *cis* Poly-**11**.

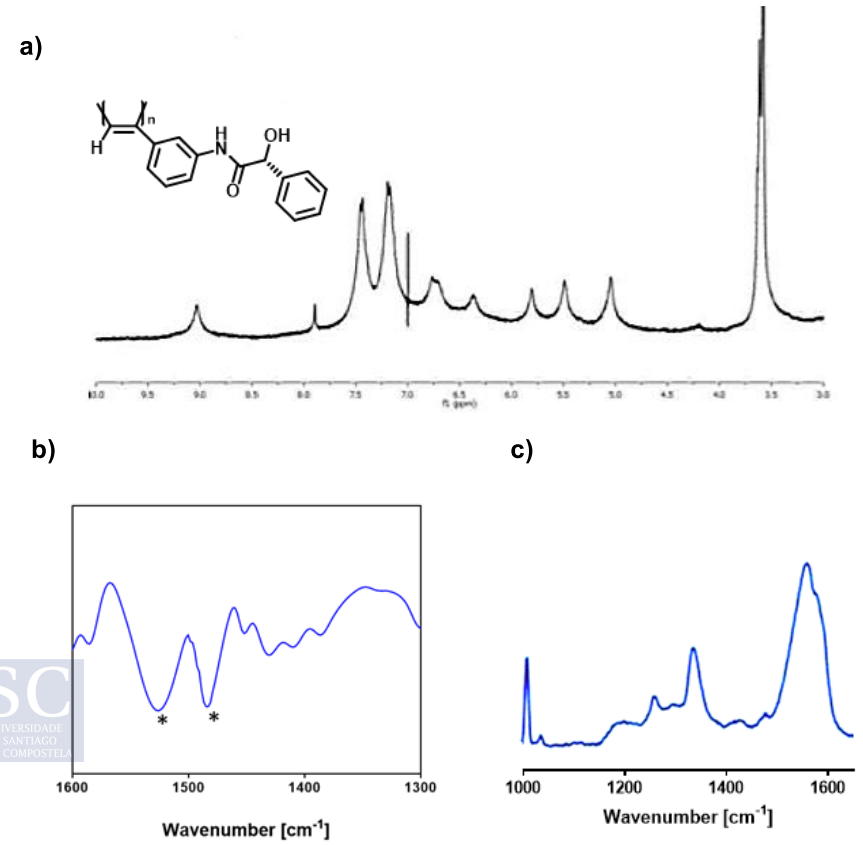

Figure S20. a) ^{1}H, b) IR and c) Raman spectra of *cis* Poly-**12**.

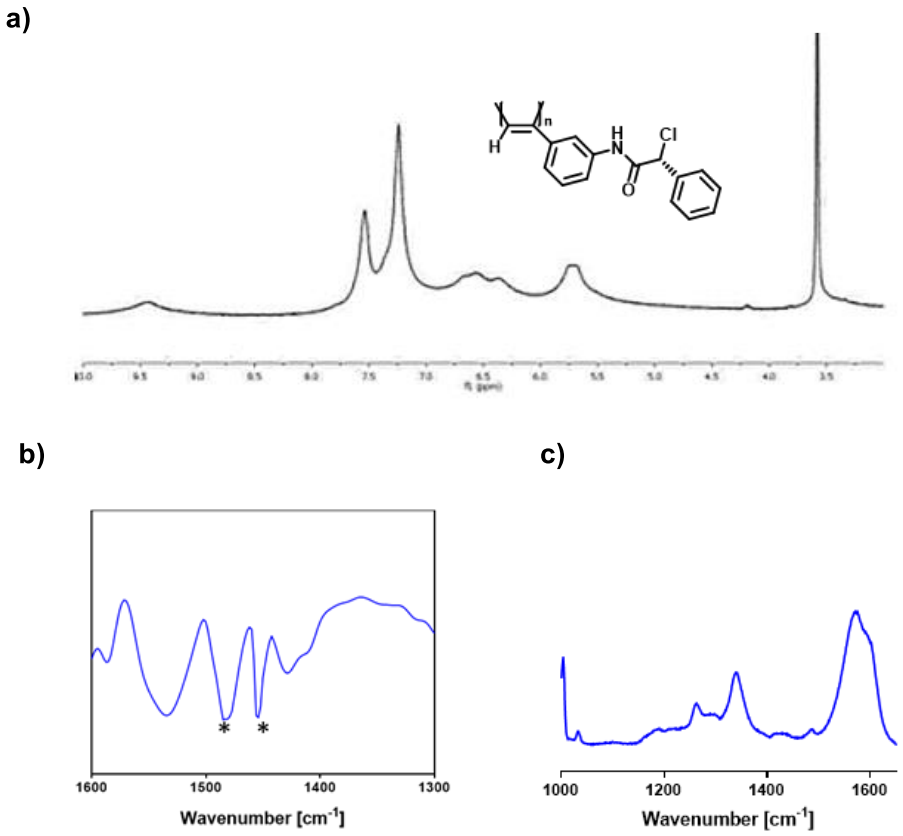

Figure S21. a) ^{1}H, b) IR and c) Raman spectra of *cis* Poly-**13**.

6. COSY Experiment of Poly-2 in $CHCl_3$

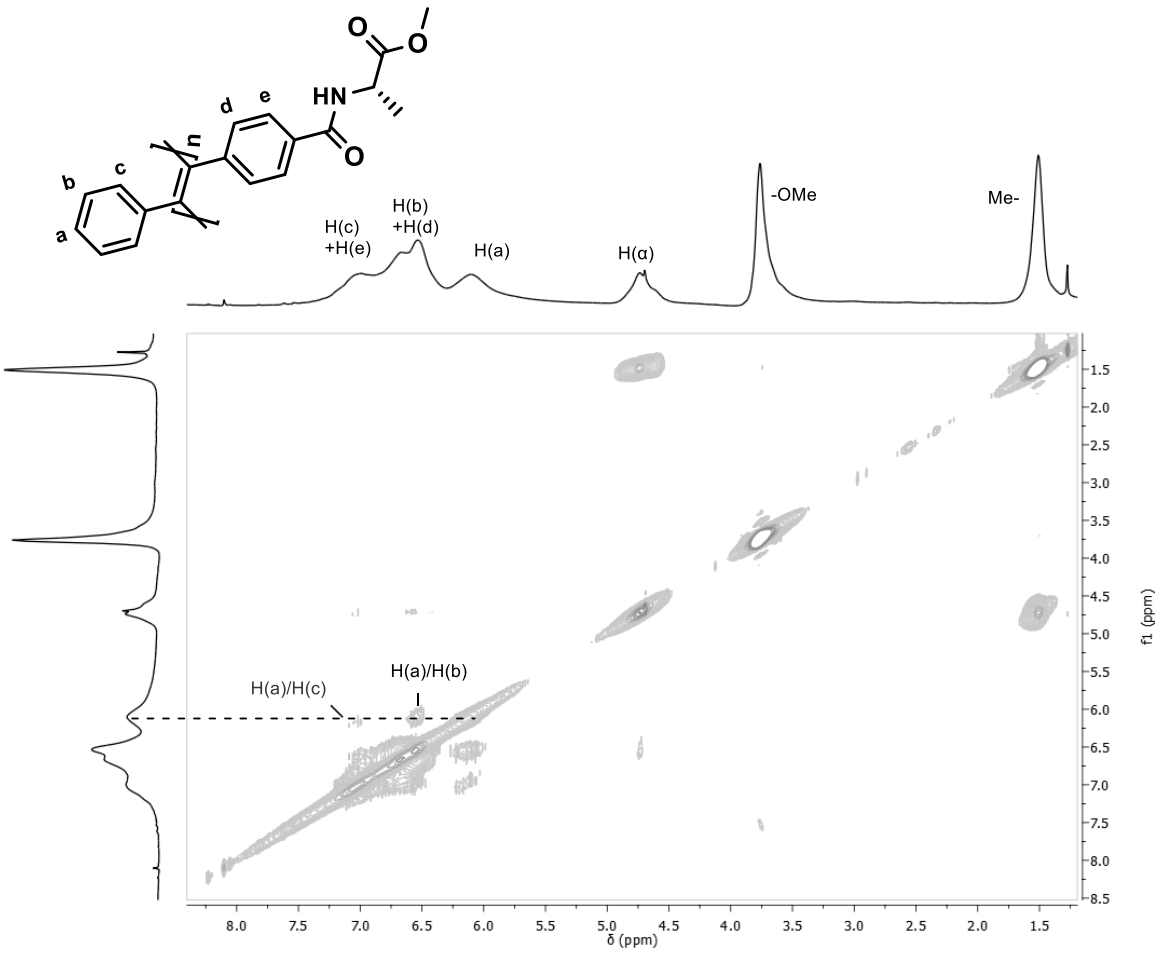

Figure S22. ^{1}H-COSY spectrum of poly-**2** in $CHCl_3$.

7. NOESY Experiments of Poly-2 in different solvents

To evaluate the regioregularity of Poly-**2**, different NOESY experiments were performed. Spectra in $CHCl_3$, THF and DMSO measured at 100 ms are shown below.

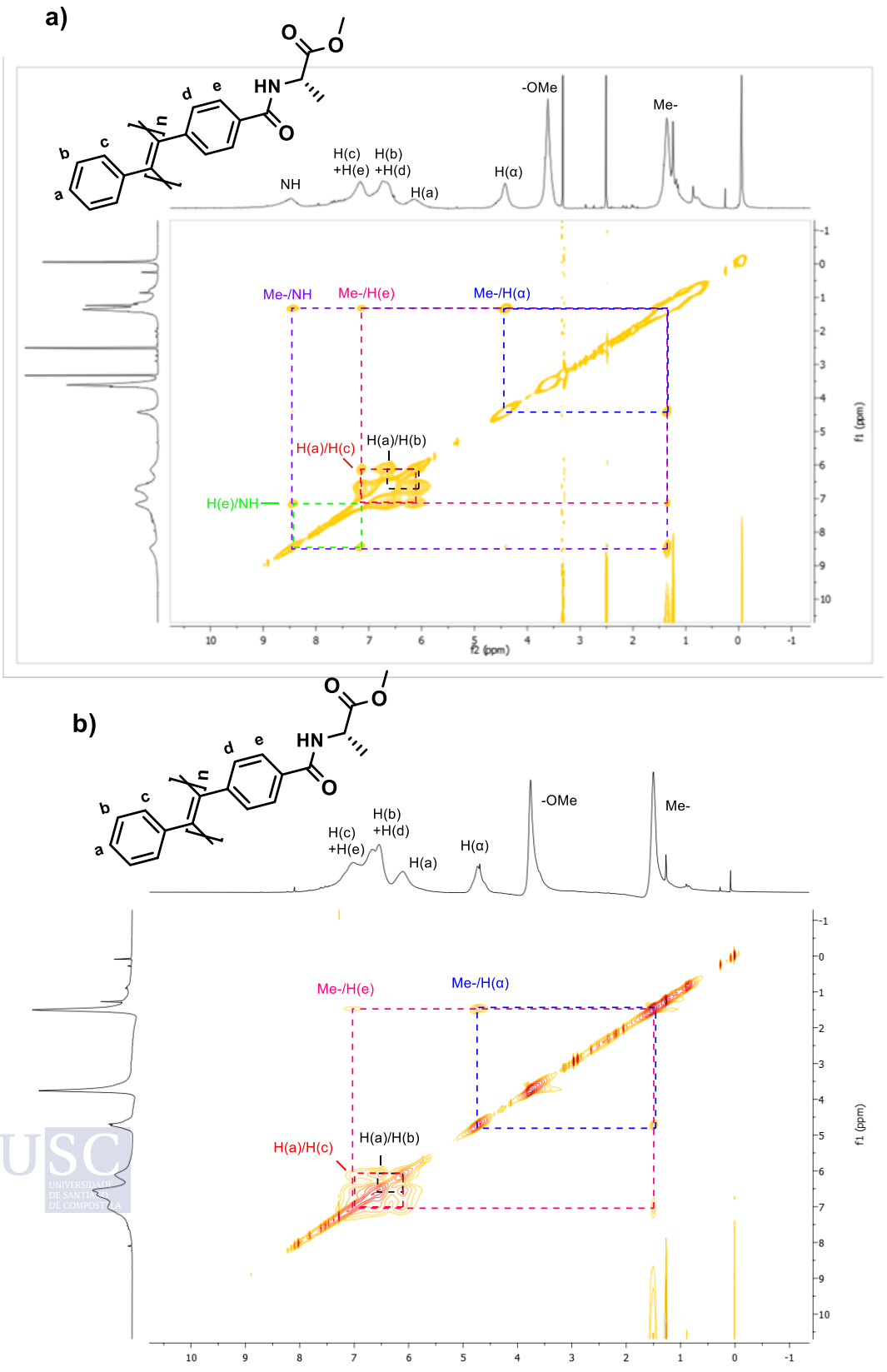

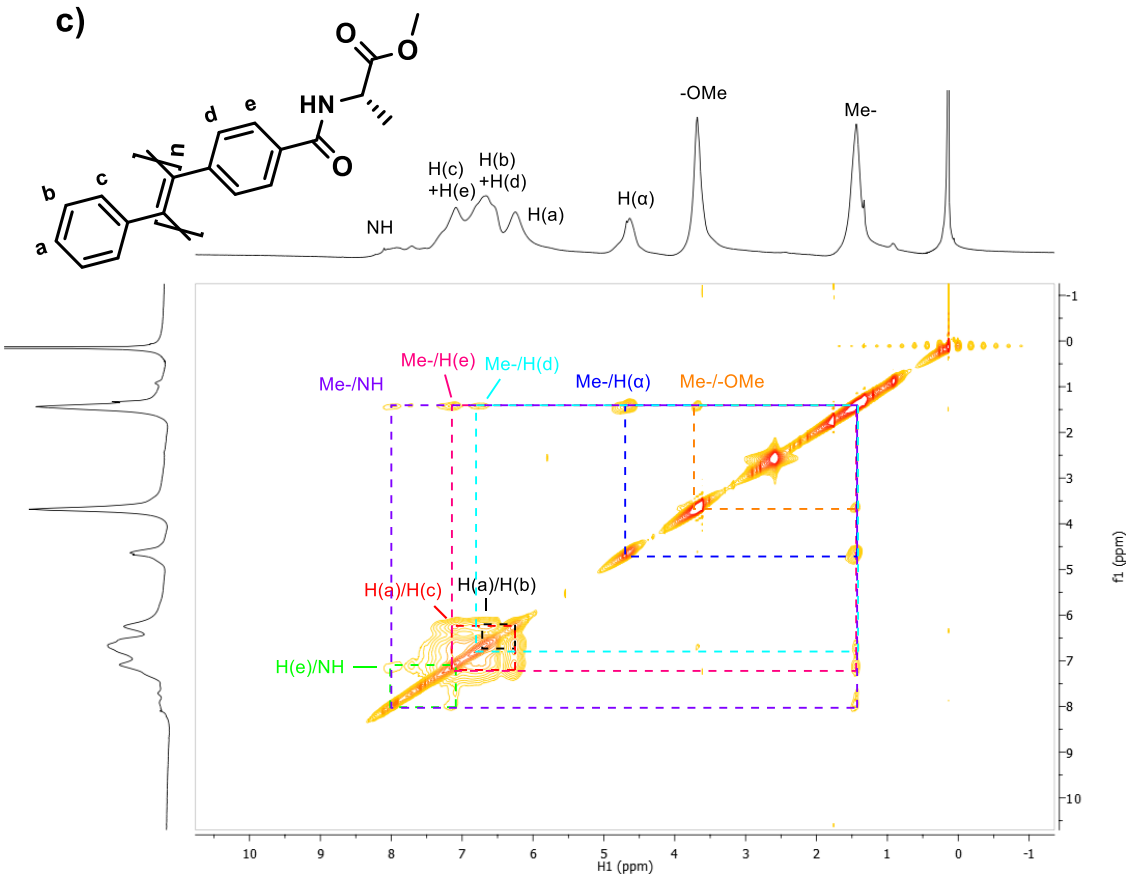

Figure S23. ^{1}H-NOESY spectra of poly-**2** in a) DMSO, b) $CHCl_3$ and c) THF.

8. Atomic Force Microscopy (AFM) measurements

All AFM measurements were performed at CACTI (Vigo University, Spain) in a MultiMode V Scanning Probe Microscope (Veeco Instruments) in air at rt with standard silicon cantilevers and super-sharp cantilevers in tapping mode using 12 µm and 1 µm scanners. Nanoscope processing software and WSxM 4.0 Beta 1.0 [4] (Nanotec Electronica, S.L.) were used for image analysis.

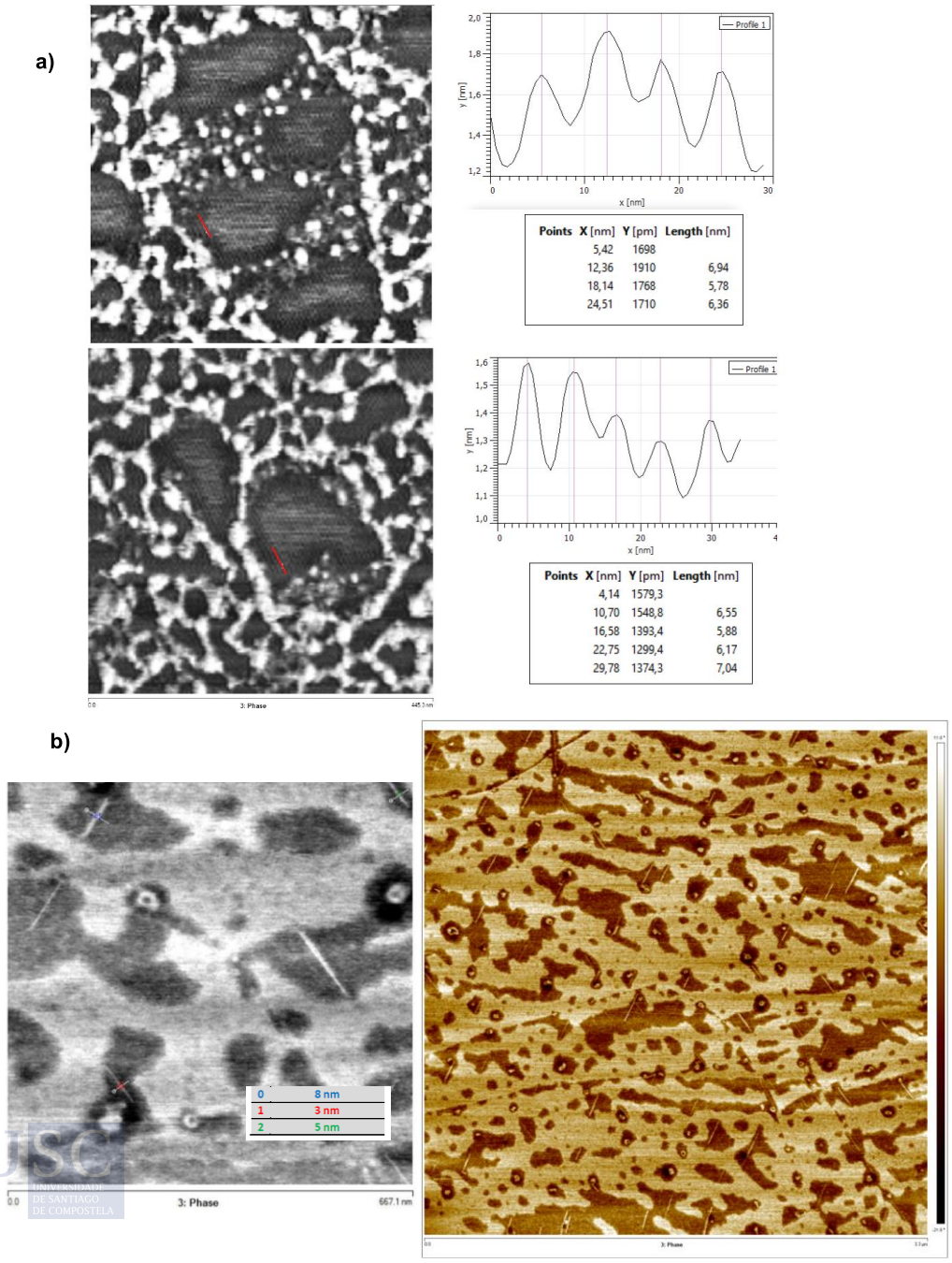

Figure S24: **a)** AFM images of individual right-handed helices of a Poly-(*S*)-**2** solution in DMF. **b)** AFM images of a Poly-(*S*)-**2** solution in MeCN showing bundles of helices forming left-handed superhelices.

9. Modelling *Z* Structures

3D models of Poly-*S*-**2** with Z configuration of double bonds —in a head to tail regioregularity— with different dihedral angles between conjugated double bonds were built to look for a helical structure that fit the parameters obtained from AFM. For those structures that match the experimental data, the pendat groups were too close, with distances between atoms lower than 1.2 Å (Figure S25a). For those structures where distances above 2 Å between pendant groups, the helical parameters do not match the experimental ones (Figure S25b). Moreover, in all the structures, the para proton of the unsubstituted phenyl ring is very close to the alanine pendant group of other m.r.u, and strong NOE must be observed, which is not present in the NOESY spectra.

a) ω_1=165 ω_3=160

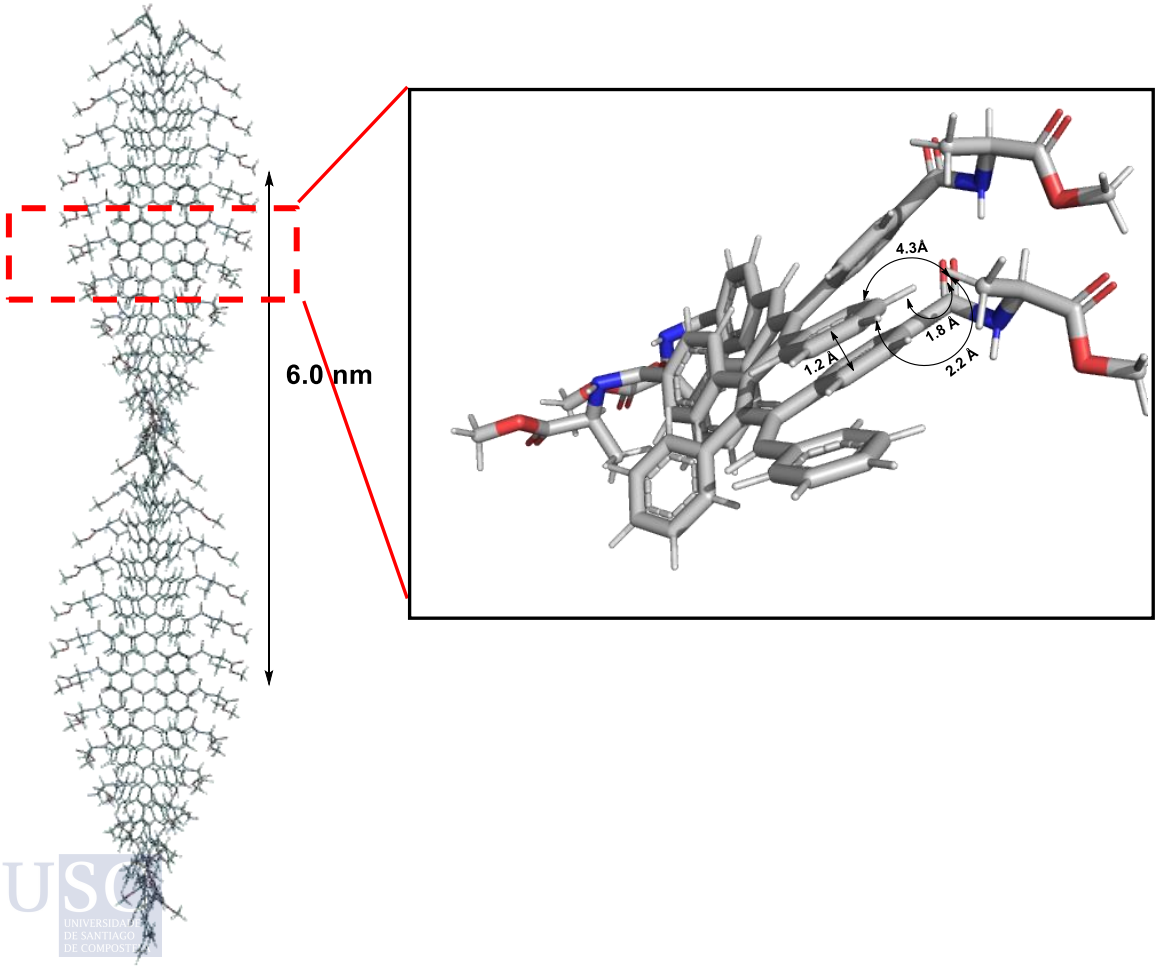

b) ω_1=150 ω_3=150

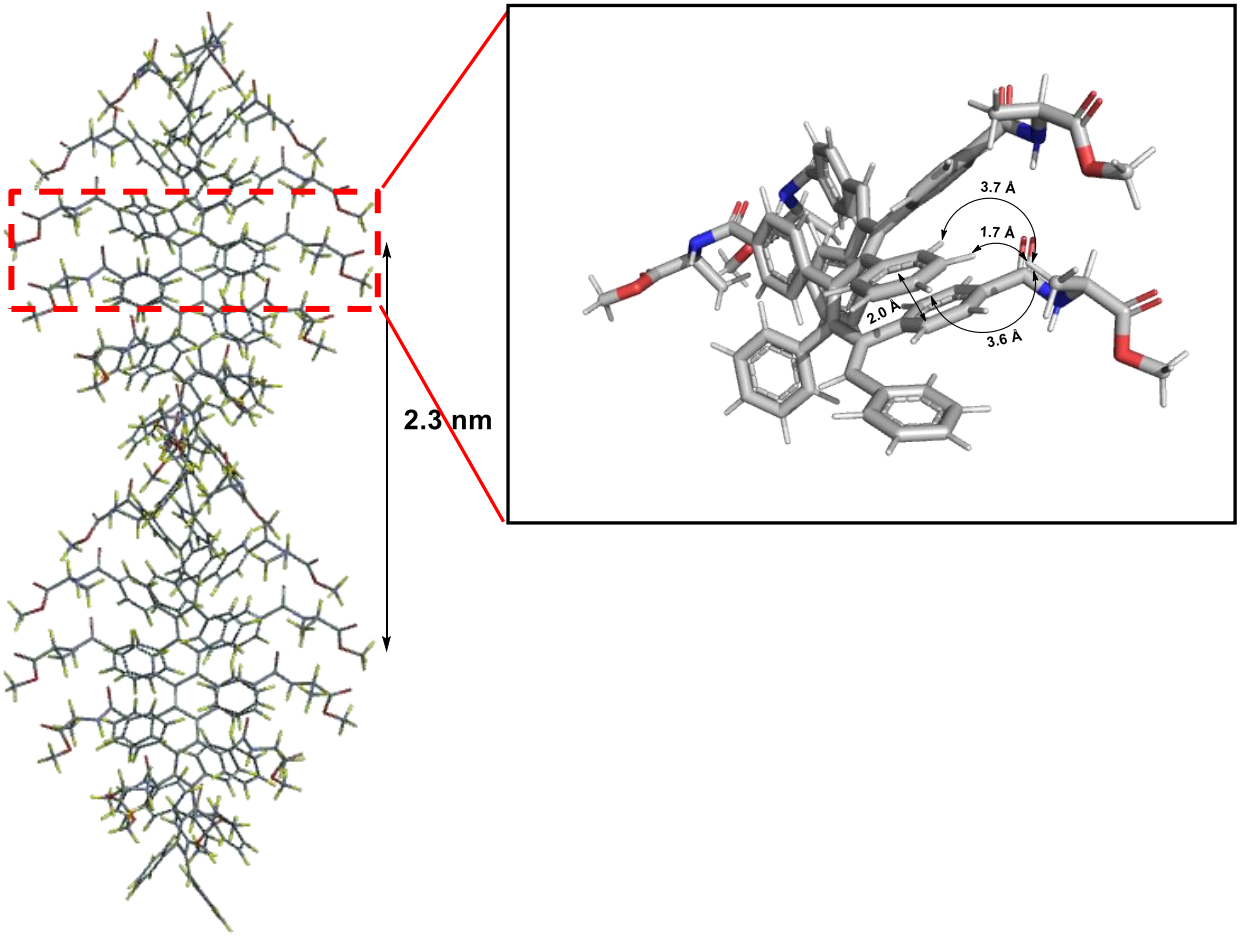

Figure S25: a) Model of *cis-transoidal* helix with ω_1=165 ω_3=160 and b) Model of *cis-transoidal* helix with ω_1=150 ω_3=150 showing the helical pitch and the distances that are incompatible with the lack of interaction in bidimensional NMR spectra.

10. CD studies of Poly-2

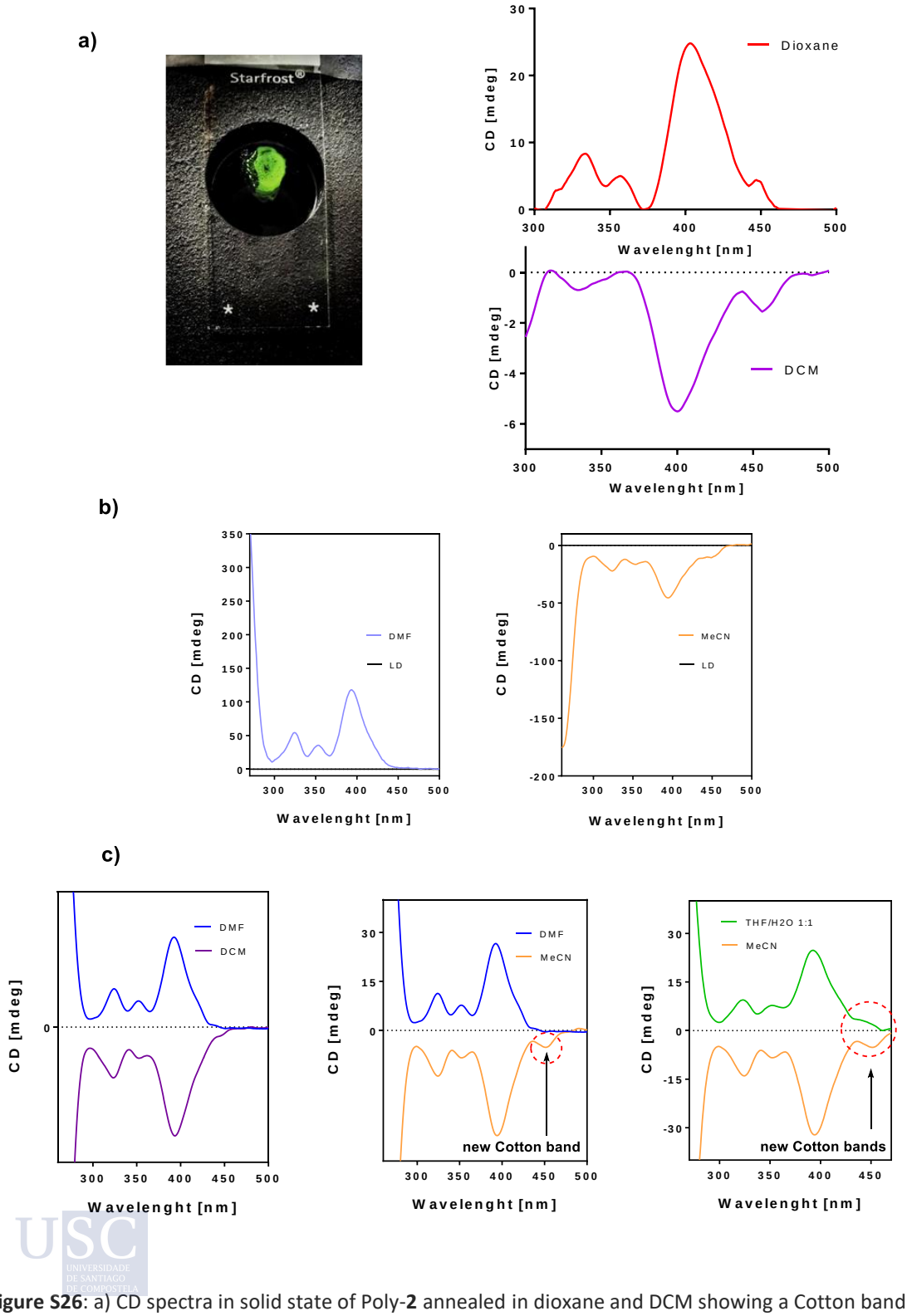

Figure S26: a) CD spectra in solid state of Poly-**2** annealed in dioxane and DCM showing a Cotton band at 450 nm. b) CD spectra of a solution of Poly-**2** in MeCN and DMF showing not LD. c) Comparison of the ECD spectra of *poly-(S)-2* in DMF/DCM, DMF/ MeCN and THF-H_2O/MeCN.

11. Computational Details

Considering the difficulties to carry out theoretical calculations on large polymers, we resorted to the use of a reduced-size representative oligomer with 20 monomer repeating units. The input structure used for the ECD calculations was adjusted according to the results obtained from structural techniques such as Raman, IR and AFM. A 3D structure 20-mer oligomer, with ω_1, ω_2 and ω_3 dihedral angles equal to -165º, 180º and 40º respectively, was obtained and submitted for ECD calculations (see Figure 4d in manuscript for dihedral angle definitions).

The choice of the methodology used to carry out the ECD and UV calculations was determined by the size of the polymers under investigation. Considering this, time-dependent density functional theory (TD-DFT, Ref. **S9**) was the only option available, and we used it together with the CAM-B3LYP density functional (Ref. **S10**) and the 3-21G basis set (Ref. **S11**). We included 80 excitation energies in the calculation. This combination of density functional and basis set was selected based on density functional and basis set selection studies carried out in previous work, where it provided ECD and UV spectra for polyphenylacetylenes (PPAs) in an efficient way in terms of computational cost and reproducibility of the experimental spectra (Refs. **S12** and **S13**). The use of larger bases results prohibitive in the case of the considered polymers. For a more efficient correlation between the theoretical and the experimental results, and taking into account the known differences of DFT in getting accurate ECD spectra, we adjusted the theoretical 20-mer spectrum with a correlation factor obtained from comparison (between theory and experiment) of the wavelength and intensity at the maximum corresponding to the first Cotton effect. In this way, we evaluated a correction factor for lambda as the difference between the theoretical and experimental wavelengths, and we shifted the rest of the theoretical spectrum accordingly. Regarding the intensity, from the above comparison we rescaled the theoretical values in order to get the experimental intensity at the first Cotton effect band. To plot the ECD spectrum we selected a full width at half height (FWHM) of 43 nm and employed lorentzian curves.

Transition density differences were obtained for the main transitions in the UV-Vis and ECD spectra for a 12-mer oligomer at the TD-DFT(CAM-B3LYP)/3-21G level. An isovalue of 0.00035 was selected to plot the density differences, red color was chosen for negative sign and blue for positive. The 12-mer ECD and UV-Vis spectra were evaluated using the same methodology and the corresponding intensities and wavelengths were corrected following the above ideas for correlation between theory and experiment. Additionally, in Figure 5, in order

to better visualize the bar spectra, their intensities were multiplied by a factor 2.4 times larger than that used for the ECD curves.

For carrying out the theoretical VCD study, we started with a conformational analysis of the monomer to obtain the most stable conformers. For these, we evaluated the VCDs using density functional theory (DFT) together with the rCAM-B3LYP functional (Ref. **S14**) and the cc-pVTZ basis set (Ref. **S15**). The theoretical spectra were compared to the experimental ones in order to identify the conformers that determine the VCDs in the different solvents.

The UV-Vis and ECD spectra were evaluated with the ORCA program (Ref. **S16**) and the VCD with the Gaussian-16 program (Ref. **S17**). To plot the spectra, we used the GABEDIT program (Ref. **S18**) and for the density differences Avogadro (Ref. **S19**). No solvent effects were included in the calculations.

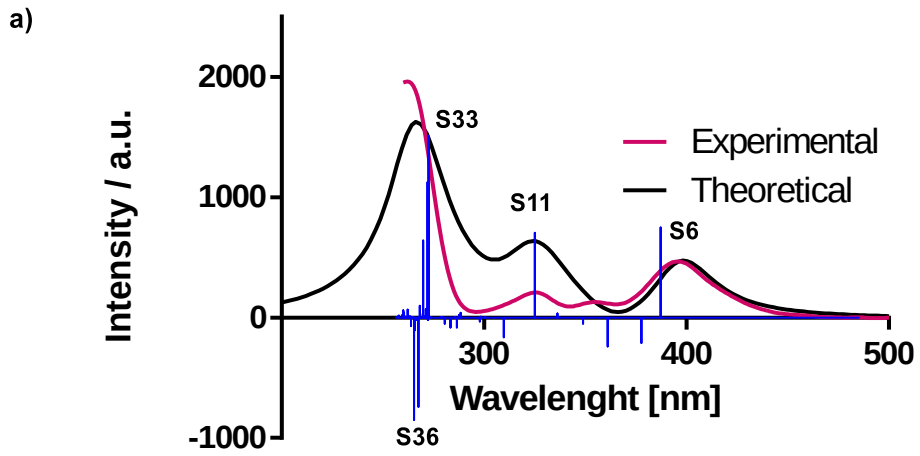

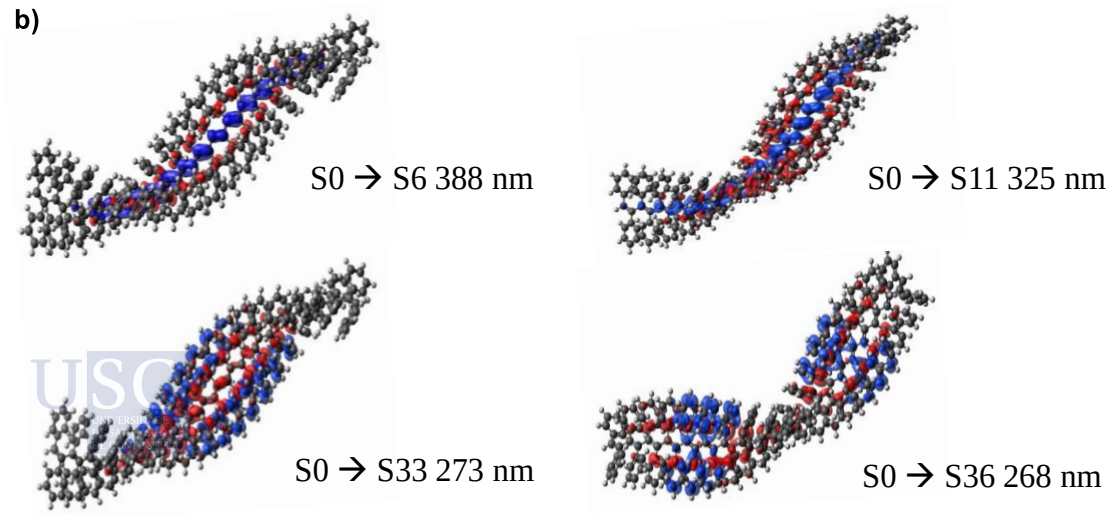

Figure S27: **a)** Theoretical and experimental ECD comparison for the 20-mer indicating the main transitions. **b)** TD-DFT (CAM-B3LYP)/3-21G S0 → S6, S0 → S11, S0 → S33, and S0 → S36 electron density differences for the 20-mer.

12. Mass Spectrometry

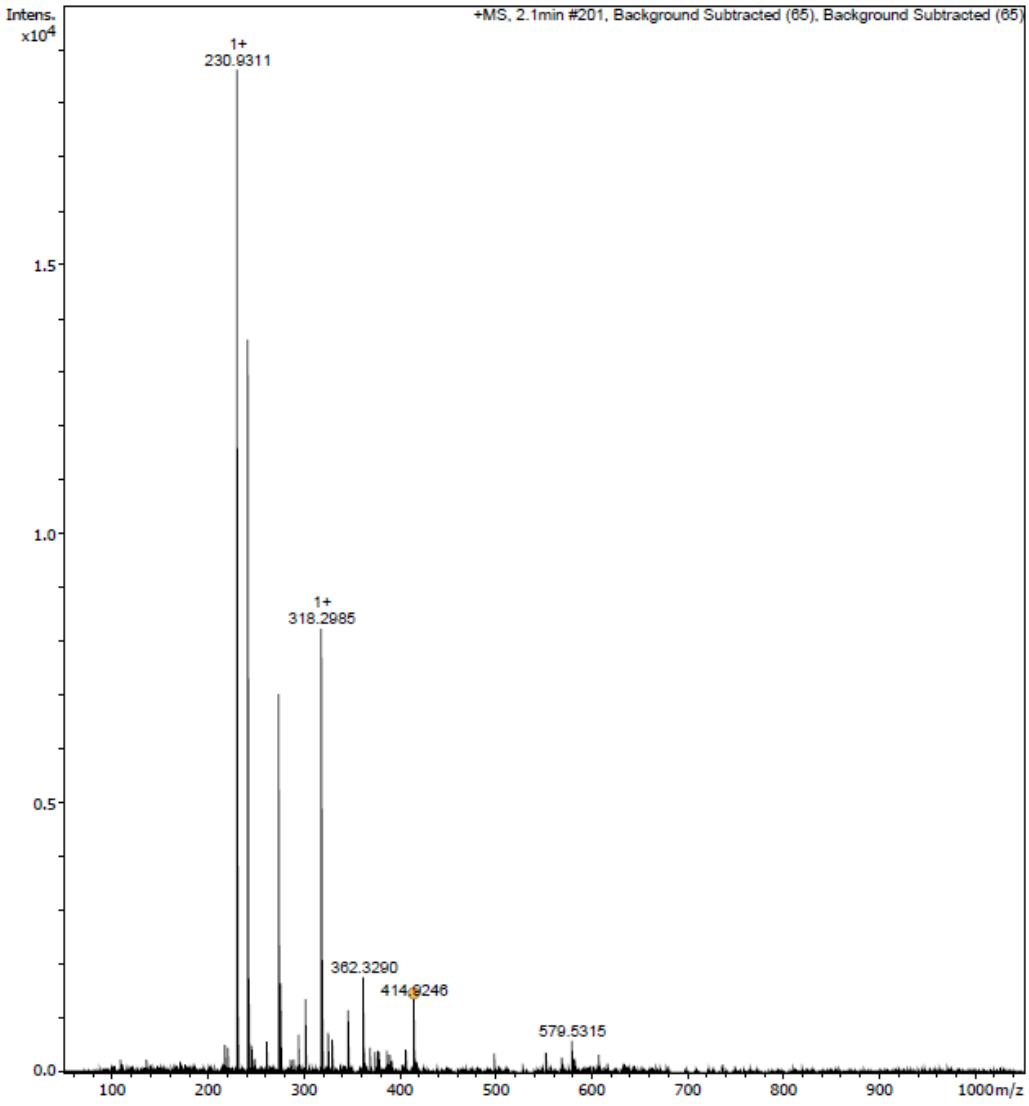

Figure S28: Mass spectrum of perfluorophenyl 4-iodobenzoate.

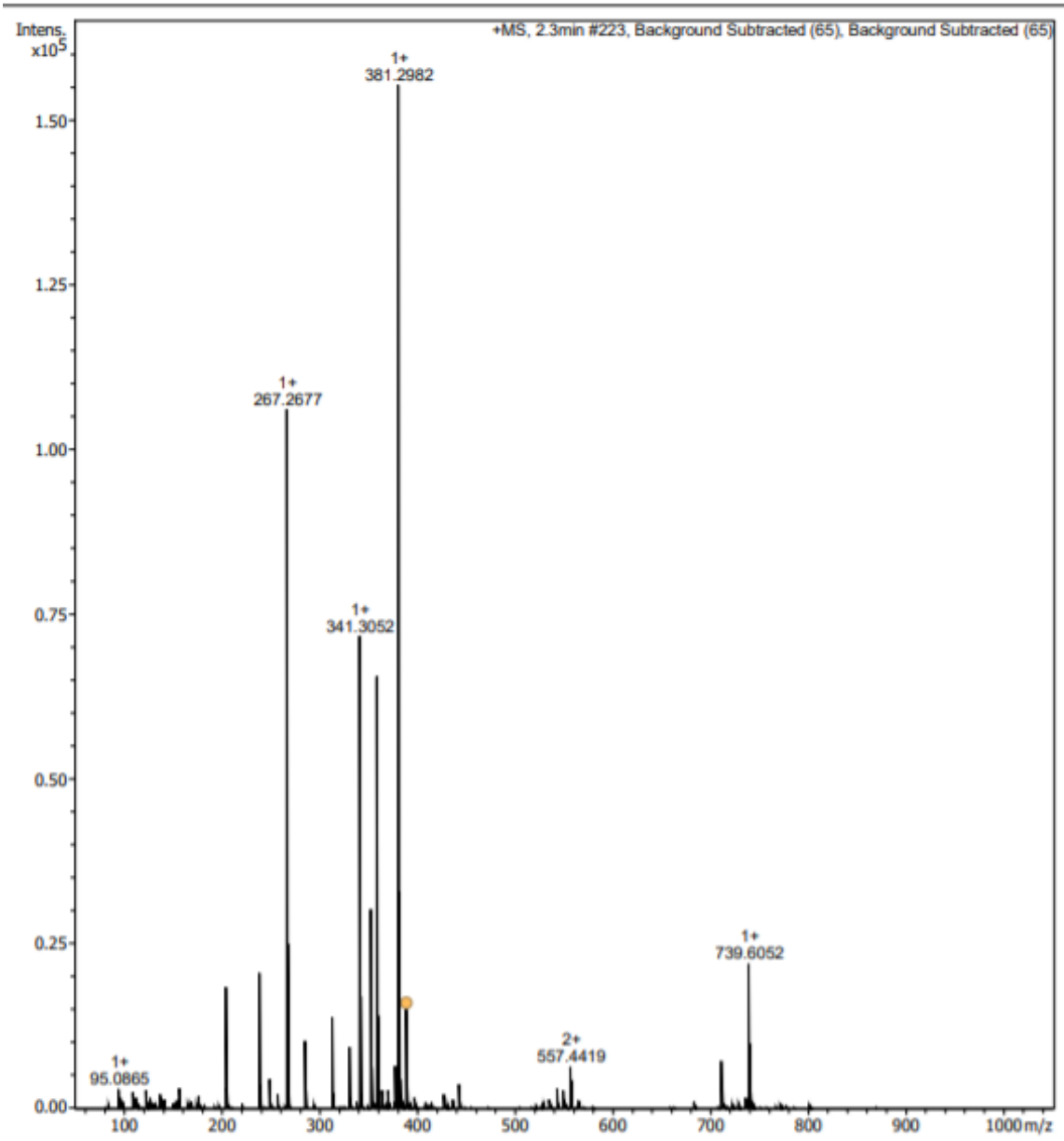

Figure S29: Mass spectrum of perfluorophenyl 4-(phenylethynyl)benzoate

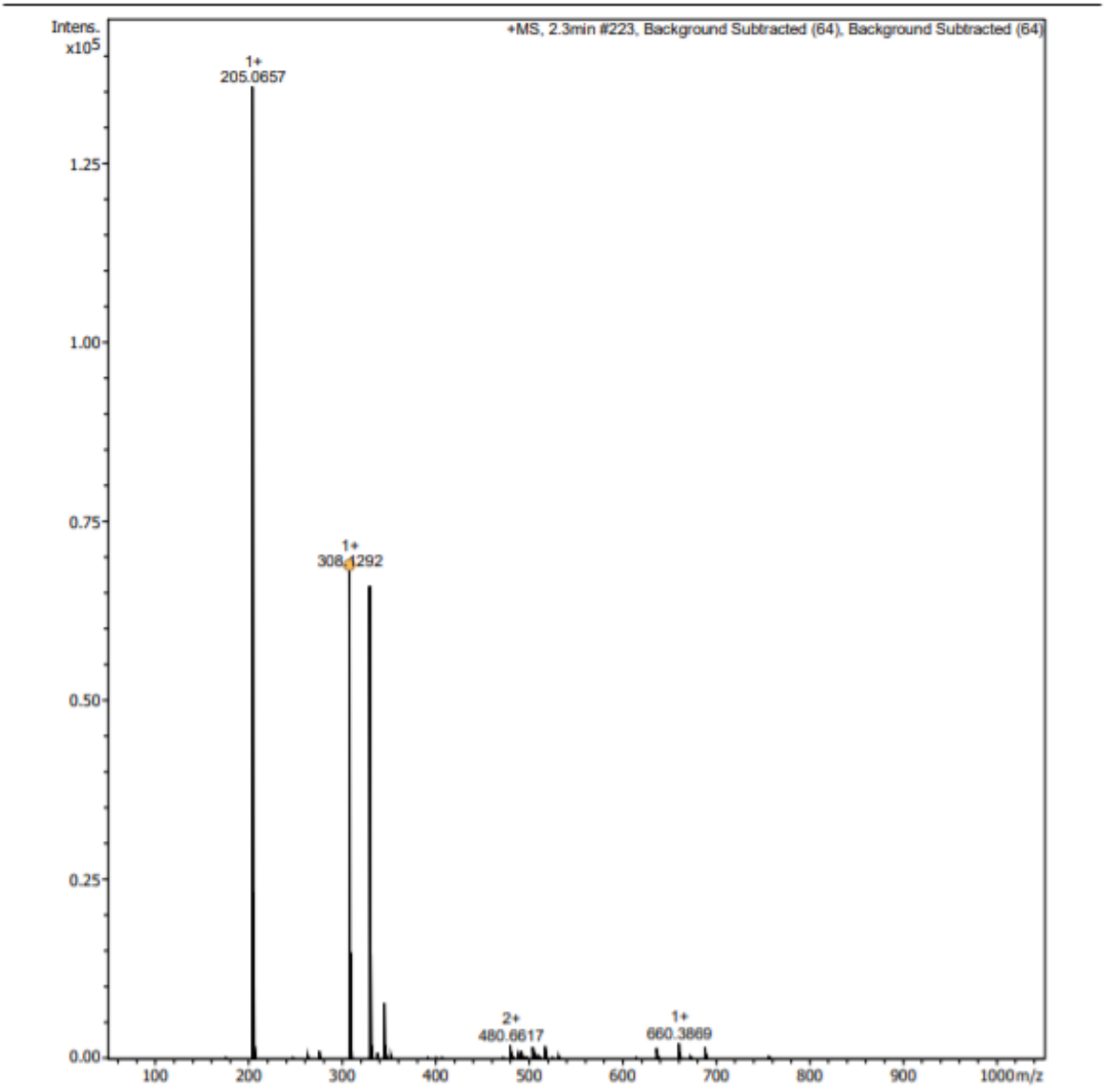

Figure S30: Mass spectrum of methyl (4-(phenylethynyl)benzoyl)-L-alaninate.

13. Supporting References

S1. A. C. Pauly, P. Theato, P. *Polymer Chemistry*. **2012**, *3*, 1769-1782.

S2. S. Arias, M. Núñez-Martínez, E. Quiñoá, R. Riguera, F. Freire, *Polym. Chem*., **2017**, *8*, 3740-3745.

S3. F. Freire, J. M. Seco, E. Quiñoá, R. Riguera, *Angew. Chem. Int. Ed*. **2011,** *50*, 11692-11696.

S4. S. Leiras, F. Freire, J. M. Seco, E. Quiñoá, R. Riguera, *Chemical Science*. **2013**, *4*, 2735-2743.

S5. I. Louzao, J. M. Seco, E. Quiñoá, R. Riguera, *Angewandte Chemie*. **2010**, *122*, 1472-1475.

S6. K. Cobos, R. Rodríguez, O. Domarco, B. Fernandez, E. Quiñoá, R. Riguera, F. Freire, *Macromolecules*. **2020**, *53*, 3182-3193.

S7. X. A. Zhang, A. Qin, L. Tong, H. Zhao, Q. Zhao, J. Z. Sun, B. Z. Tang, *ACS Macro Letters*. **2012**, *1*, 75-79.

S8. C. I. SIMIONESCU, V. PERCEC, *Journal of Polymer Science: Polymer Chemistry Edition*. **1980**, *18*, 147-155.

S9. E. Runge, E. K. U. Gross, *Phys. Rev. Lett*. **1984**, *52*, 997-1000.

S10. Y. Yanai, D. P. Tew, N. C. A. Handy, *Chem. Phys. Lett.* **2005**, *393*, 51-57.

S11. J. S. Binkley, J. A. Pople, W. J. Hehre, *J. Am. Chem. Soc.* **1980**, *102*, 939-947.

S12. B. Fernández, R. Rodríguez, A. Rizzo, E. Quiñoá, R. Riguera, F. Freire, *Angew. Chem. Int. Ed*. **2018**, *57*, 3666-3670.

S13. Z. Fernández, B. Fernández, E. Quiñoá, F. Freire, *Angew. Chem. Int. Ed.* **2021**, https://doi.org/10.1002/anie.202100162.

S14. A. J. Cohen, P. Mori-Sánchez, W. Yang, J. Chem. Phys. **2007,** *126*, 191109.

S15. T. H. Dunning, *J. Chem. Phys*. **1989**, *90*, 1007–1023.

S16. F. Neese, *WIREs Comput Mol Sci*. **2012**, *2*, 73-78.

S17. Gaussian 16, Revision C.01, Frisch, M. J.; Trucks, G. W.; Schlegel, H. B.; Scuseria, G. E.; Robb, M. A.; Cheeseman, J. R.; Scalmani, G.; Barone, V.; Petersson, G. A.; Nakatsuji, H.; Li, X.; Caricato, M.; Marenich, A. V.; Bloino, J.; Janesko, B. G.; Gomperts, R.; Mennucci, B.; Hratchian, H. P.; Ortiz, J. V.; Izmaylov, A. F.; Sonnenberg, J. L.; Williams-Young, D.; Ding, F.; Lipparini, F.; Egidi, F.; Goings, J.; Peng, B.; Petrone, A.; Henderson, T.; Ranasinghe, D.; Zakrzewski, V. G.; Gao, J.; Rega, N.; Zheng, G.; Liang, W.; Hada, M.; Ehara, M.; Toyota, K.; Fukuda, R.; Hasegawa, J.; Ishida, M.; Nakajima, T.; Honda, Y.; Kitao, O.; Nakai, H.; Vreven, T.; Throssell, K.;

Montgomery, J. A., Jr.; Peralta, J. E.; Ogliaro, F.; Bearpark, M. J.; Heyd, J. J.; Brothers, E. N.; Kudin, K. N.; Staroverov, V. N.; Keith, T. A.; Kobayashi, R.; Normand, J.; Raghavachari, K.; Rendell, A. P.; Burant, J. C.; Iyengar, S. S.; Tomasi, J.; Cossi, M.; Millam, J. M.; Klene, M.; Adamo, C.; Cammi, R.; Ochterski, J. W.; Martin, R. L.; Morokuma, K.; Farkas, O.; Foresman, J. B.; Fox, D. J. Gaussian, Inc., Wallingford CT, **2016**.

S18. A. R. Allouche, *J. Comput. Chem.* **2011**, *32*, 174-182.

S19. M. D. Hanwell, D. E. Curtis, D. C. Lonie, T. Vandermeersch, E. Zurek, G. R. Hutchison, *Journal of Cheminformatics* **2012**, *4*, 17.

Expertimental Section Chapter IV

1. Materials and methods

CD measurements were done in a Jasco-720. The amounts of polymer used for CD measurements were 0.5 mg/mL in DMF and $CHCl_3$.

IR studies were carried out in a FTIR Varian 670 equipped with an ATR (GladiATR model) with diamond crystal of PIKE Technologies.

Raman spectra were performed in a Renishaw confocal Raman spectrometer (Invia Reflex model), equipped with two lasers (diode laser 785 nm and Ar laser 514 nm).

GPC studies were carried out in a Waters Alliance equipped with Phenomenex GPC columns. The amount of polymer used for GPC measurements was 0.5 mg/mL.

For molecular modeling we used Spartan 14 (MMFF94). As a molecular visualization system, we used PyMOL. The additional methodology used in the computational study is detailed in the Computational Details section.

2. Synthesis of Monomer and Polymers

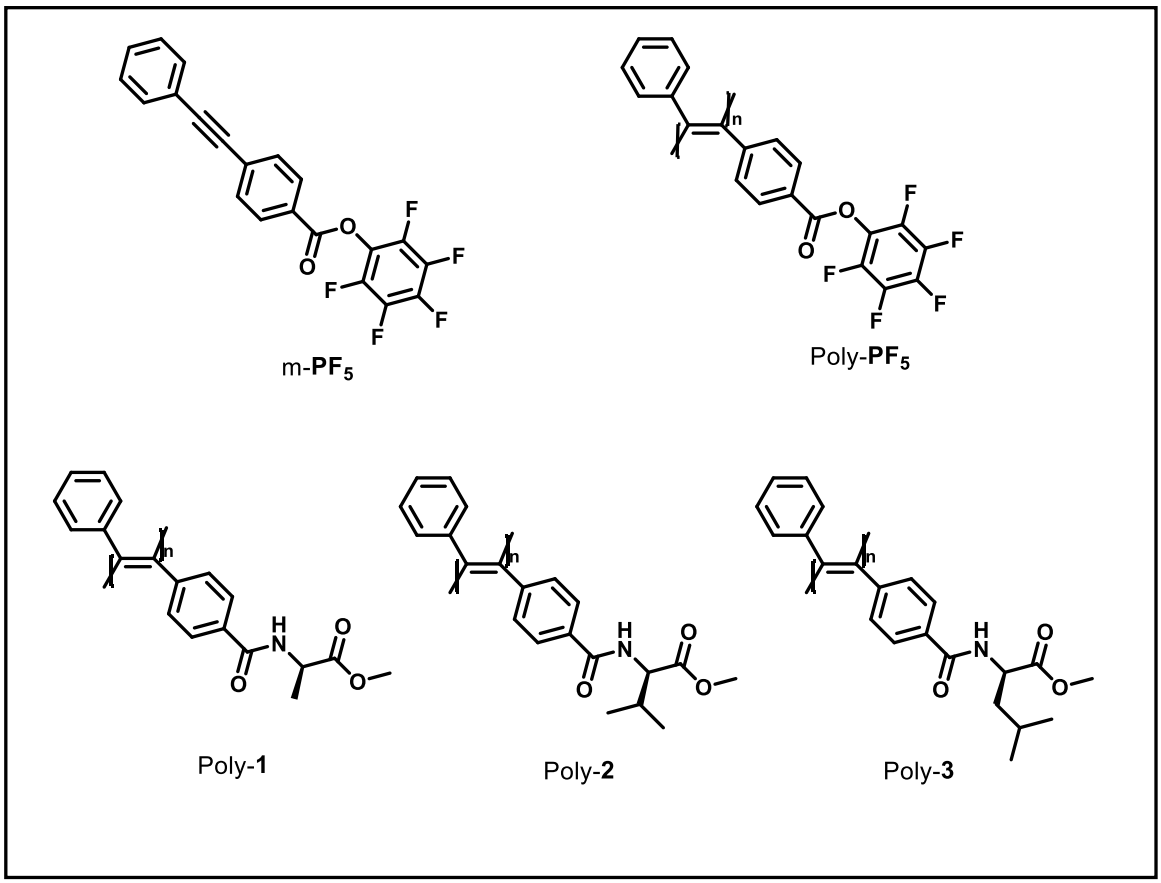

Figure S1: Structure of compounds m-$\mathbf{PF_5}$, Poly-$\mathbf{PF_5}$ poly-**1**, poly-**2**, poly-**3**.

For preparation of m-$\mathbf{PF_5}$ and its polymerization, as well as the post-polymerization couplings procedure, see SI of Ref. **S1**.

3. NMR, Raman and IR studies of the polymers

The comparative NMR, IR and Raman spectra of short and large polymers showing the same structure pattern are shown below.

In Raman studies, the C=C bond stretching in the *trans* polymers shows an intensive peak at 1550 cm^{-1} and a decrease in the band at 1570-1585 cm^{-1} assigned to *cis* polymers.

IR experiments show a > 1 ratio between I_{1500}/I_{1450} that is ascribed to a *trans* configuration of different poly(acetylene)s and poly(phenylacetylene)s [Ref. **S2**].

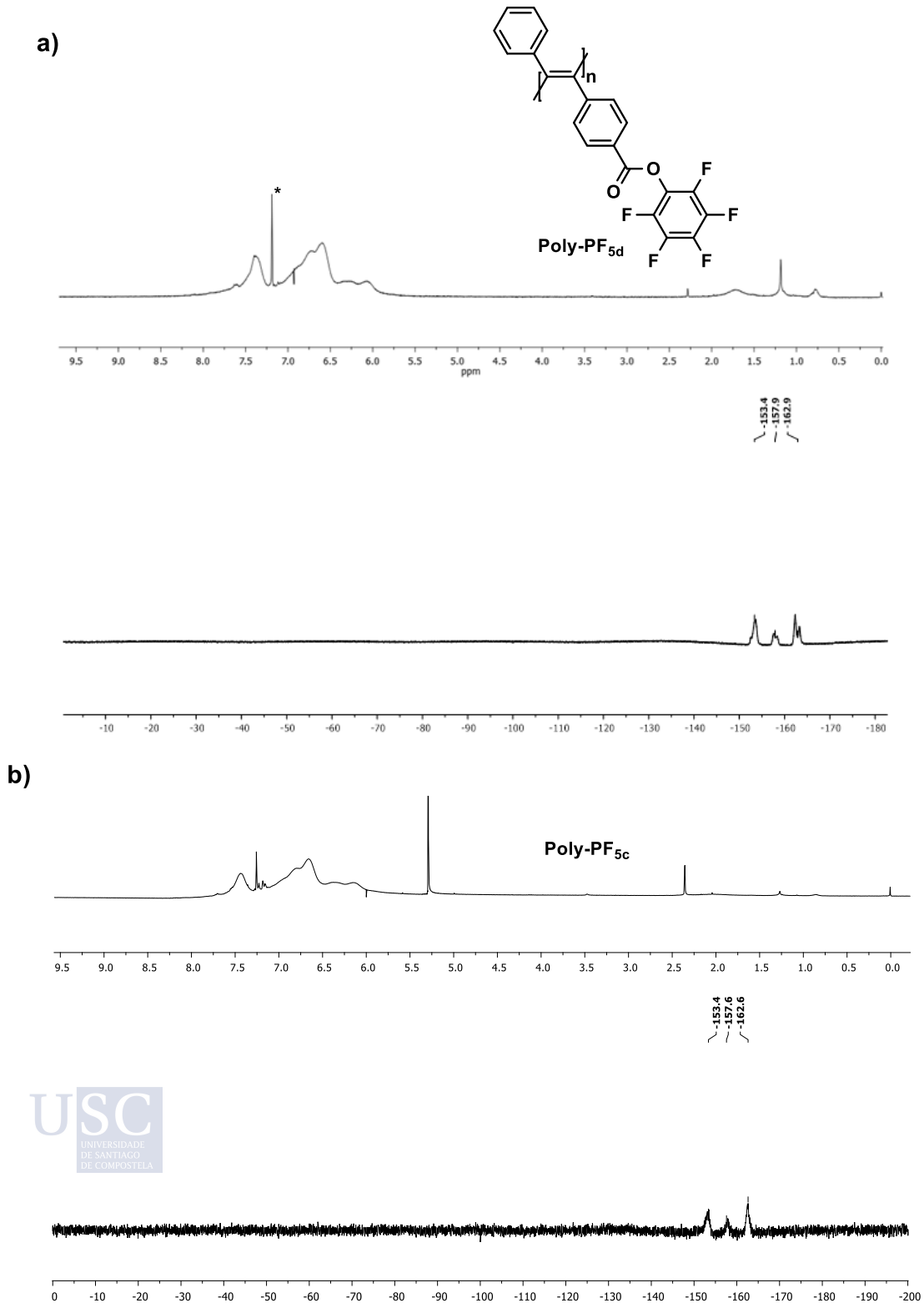

Figure S2. ^{1}H-NMR and ^{19}F-NMR spectra in $CDCl_3$ of a) Poly-**PF$_{5d}$** and b) Poly-**PF$_{5c}$**.

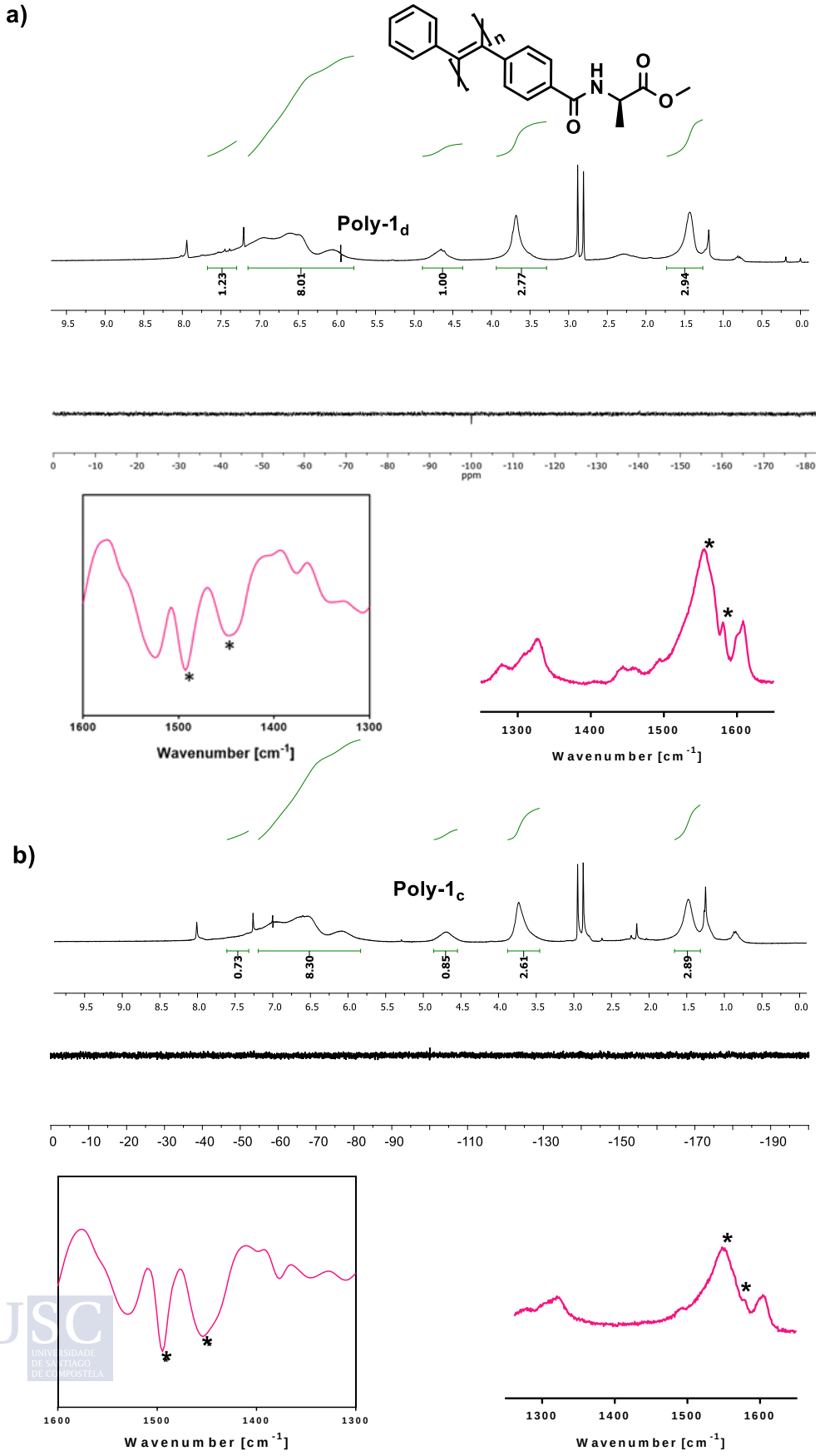

Figure S3. ^{1}H-NMR and ^{19}F-NMR spectra in $CDCl_3$, IR and Raman spectra of a) Poly-**1**$_d$ and b) Poly-**1**$_c$.

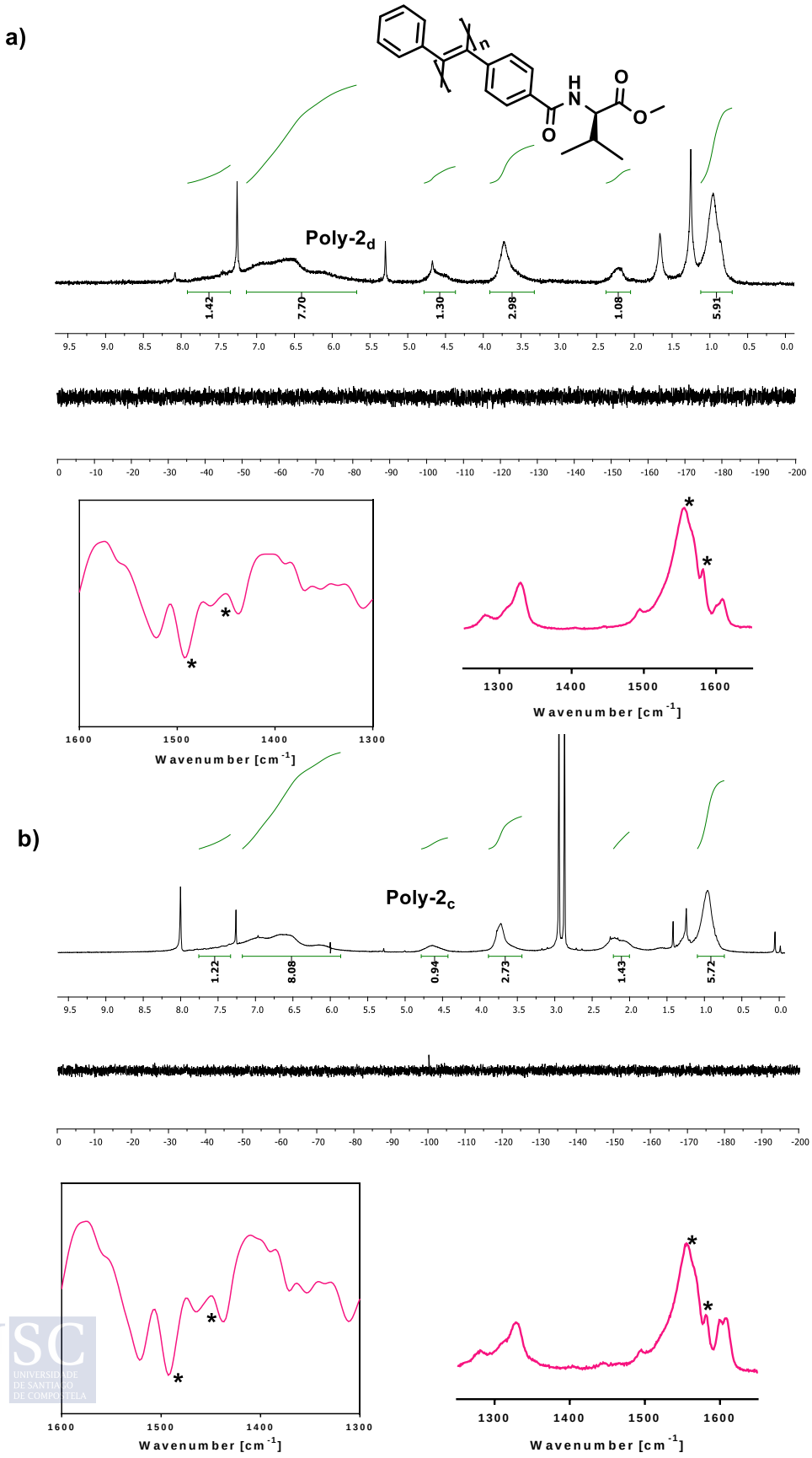

Figure S4. ^{1}H-NMR and ^{19}F-NMR spectra in $CDCl_3$, IR and Raman spectra of a) Poly-**2**$_d$ and b) Poly-**2**$_c$.

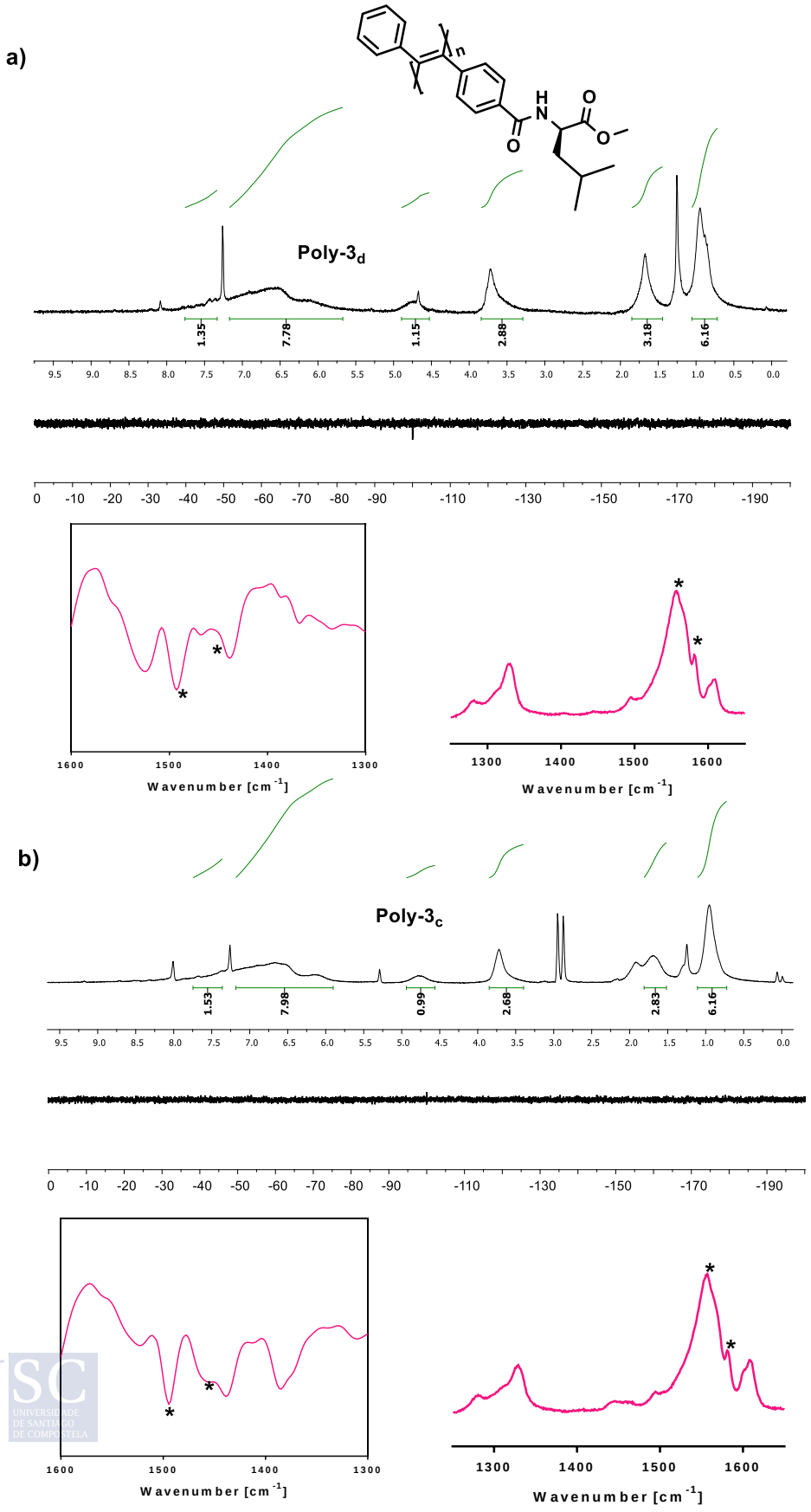

Figure S5. ^{1}H-NMR and ^{19}F-NMR spectra in $CDCl_3$, IR and Raman spectra of a) Poly-**3**$_d$ and b) Poly-**3**$_c$.

4. CD Measurements

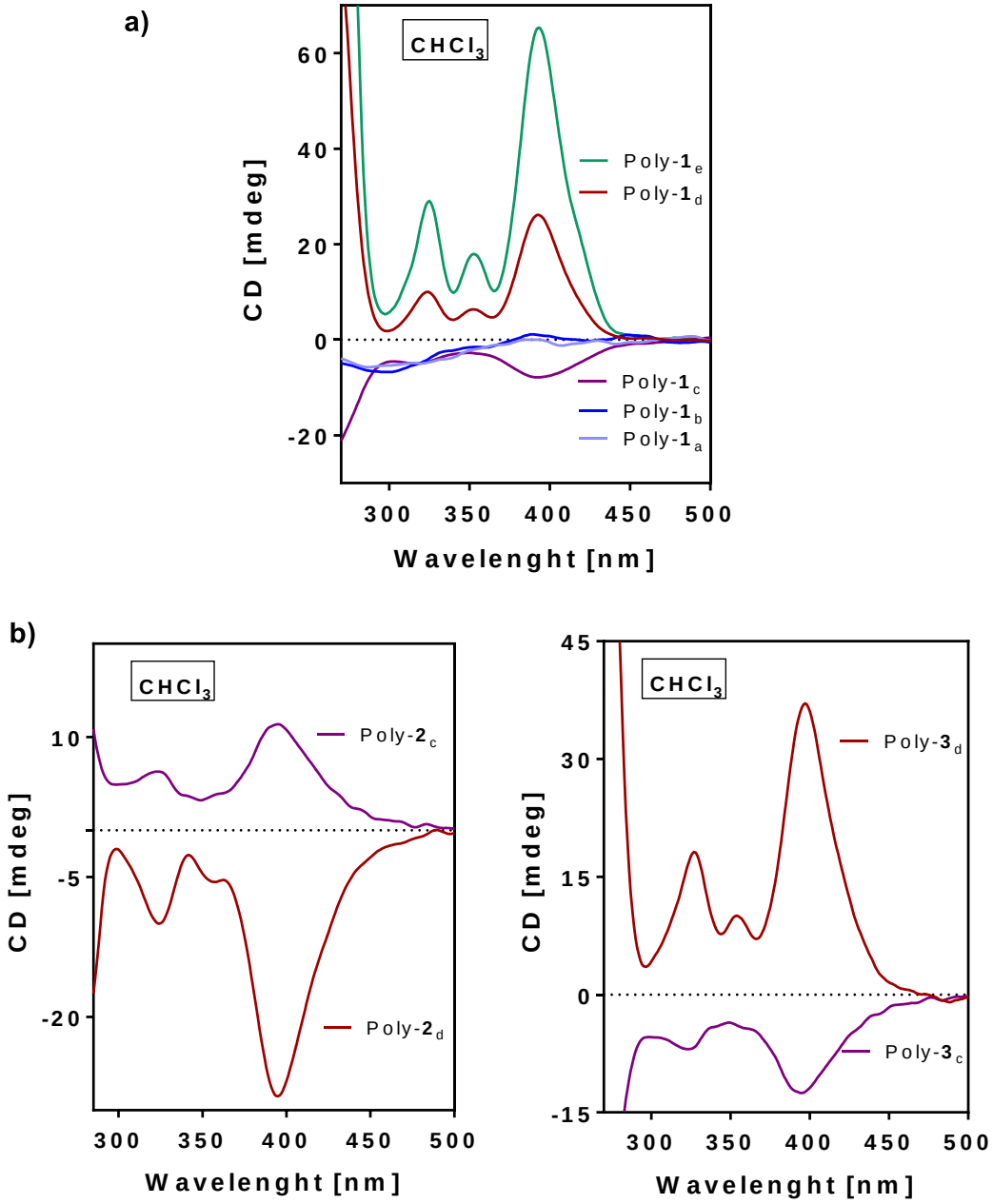

Figure S6: a) 0,5 mg/mL solutions of poly-**1**$_{a\text{-}e}$ in $CHCl_3$ after thermal annealing at 80 ºC during 24 h. b) 0,5 mg/mL solutions of poly-**2**$_{c,d}$ and poly-**3**$_{c,d}$ in $CHCl_3$ after thermal annealing at 80 ºC during 24 h.

Notice that Poly-**2** presents the same CD spectra in DMF (Figure 2d in manuscript) and $CHCl_3$.

5. Computational Details

Considering the difficulties to carry out theoretical calculations on large polymers, we resorted to the use of a reduced-size representative oligomer with 8 to 16 monomer repeating units.

The input structures used for the ECD calculations were adjusted according to the results obtained from structural techniques such as Raman, IR and AFM [Ref **S1a**]. Different 12-mer structures changing ω_1 and ω_3 dihedral angles and with $\omega_2 = 180º$ were calculated (see Figure 1b in the manuscript for dihedral angle definitions). From these results we selected the 12-mer defined by $\omega_1 = 165º$ and $\omega_3 = 110º$ due to its lower energy (Table S1) and the better agreement with the experimental CD.

Table S1. DFT(CAM-B3LYP)/3-21G electronic energies of the 12-mers. Angles are given in degrees

12-mer (ω_1-ω_3)	Energy (a.u.)
165-110	-6434.0798114
165-140	-6432.7030308
170-110	-6433.7370503
170-135	-6432.2250039

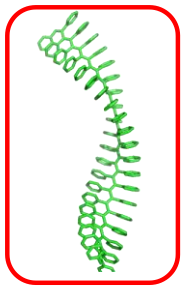

$\omega_1 = 165º, \omega_3 = 110º$

$\omega_1 = 165º, \omega_3 = 140º$

$\omega_1 = 170º, \omega_3 = 110º$

$\omega_1 = 170º, \omega_3 = 135º$

Figure S7: Different 20-mer structures calculated varying the ω_1 and ω_3 dihedral angles.

Methodology Applied

The choice of the methodology used to carry out the ECD calculations was determined by the size of the polymers under investigation. Considering this, time-dependent density functional theory (TD-DFT, Ref. **S3**) was the most efficient choice available, and we used it together with the CAM-B3LYP density functional (Ref. **S4**) and the 3-21G basis set (Ref. **S5**). We included 80 excitation energies in the calculations. This combination of density functional and basis set was selected based on density functional and basis set selection studies carried out in previous work, where it provided ECD and UV spectra for polyphenylacetylenes (PPAs) in an efficient way in terms of computational cost and reproducibility of the experimental spectra (Refs. **S6** and **S7**). The use of larger bases results prohibitive in the case of the considered polymers. Moreover, gas phase theoretical optimizations of the initial structures provided oligomers with a pitch that did not agree with the experimental AFM results.

The energies and ECD spectra were evaluated with the ORCA program (Ref. **S8**). To plot the spectra we used the GABEDIT program (Ref. **S9**) and for the density differences Avogadro (Ref. **S10**). For the ECD spectra we included 80 excitation energies in the calculations and employed lorentzian curves for the spectra. An isovalue of 0.003 was used to get the transition density differences. No solvent effects were included in the calculations.

Correlation between the Electronic Transfer and the Sign of the Transition Band

A tendency in the origin of the electron transfer and the sign of the corresponding transition band in the spectra can be observed. Thus, for a short oligomer with n = 8, electron transfer starts on the polyenic skeleton, whereas when the oligomer is larger (n = 12) electron transfer takes places mainly from the phenyl rings. In the intermediate cases, for instance when n = 10, a different behavior is observed. Here, both contributions are almost equally important showing an alternated spectrum that resembles those of PPAs.

We report in Figure S8 the main transitions involved in the different spectral bands for the spectra of the n = 8, 10 and 12 oligomers. In going from the 10- to the 12-mer the change in sign in the positive bands at around 350 and 450 nm can be attributed to excitations with larger negative intensity in the 12-mer spectrum, like those to the 44^{th} and the 58^{th} states.

To analyse these results further, we evaluated the electron density differences for the corresponding main excitations. The calculated electron density differences indicate that electron transfer from the phenyl substituents to the main skeleton takes place upon excitation in the 10-mer and the 12-mer, but the opposite trend occurs in the case of the 8-mer.

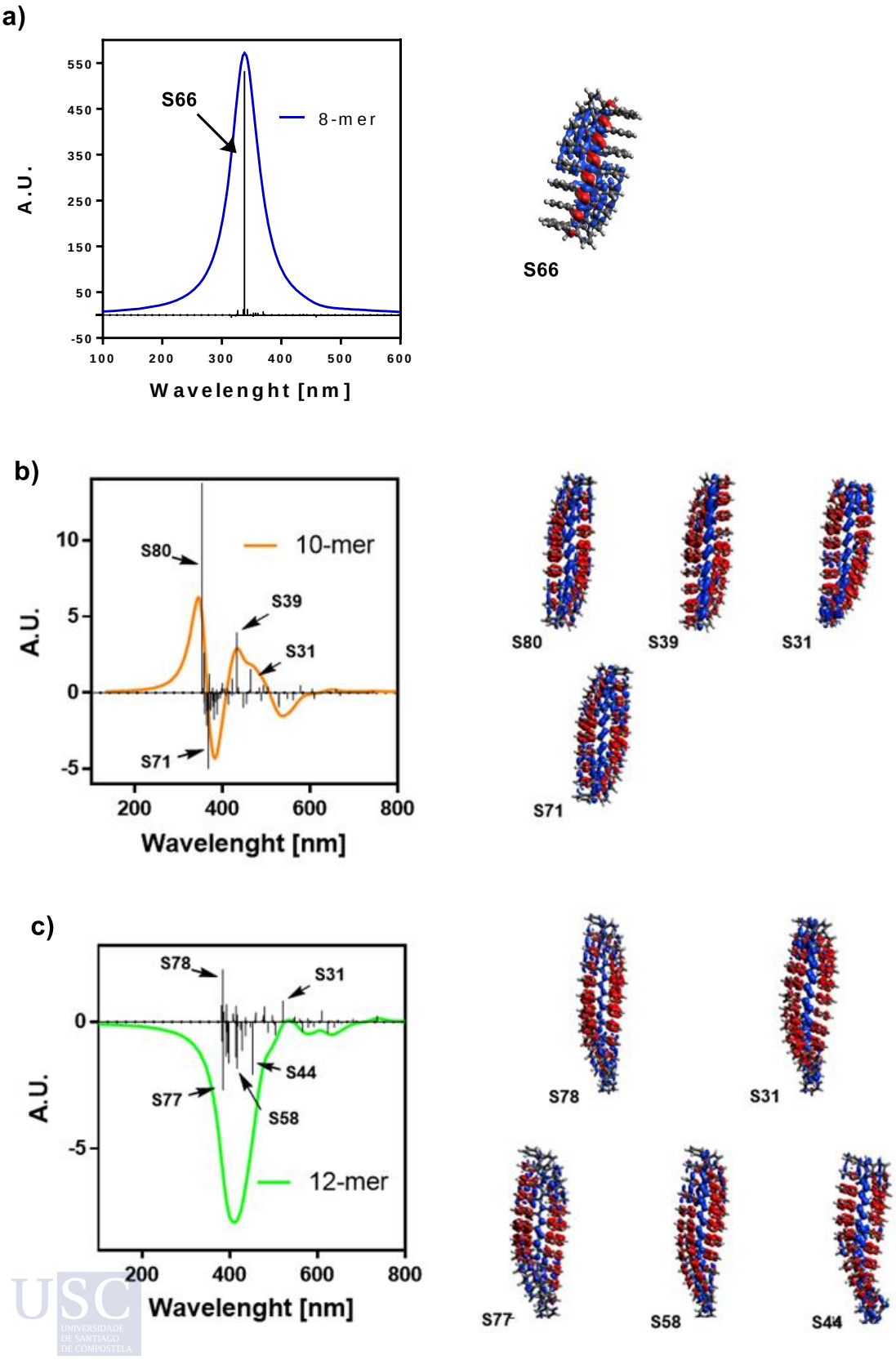

Figure S8: TD-DFT (CAM-B3LYP)/3-21G ECD spectra and electron density differences for the a) 8-mer b) 10-mer and c) 12-mer oligomers with ω1 (ω3)= 165 (110) degrees, showing the excited states (xth in Sx) that participate in the principal transitions within the main bands. Half width at half height equals 28 nm. No correction factors are included in the spectra. (red color negative and blue positive, isovalue

equals 0.0003).

Influence of the ω_4 variation

Table S2. DFT(CAM-B3LYP)/3-21G electronic energies of 16-mers ω_1= 165º, ω_2= 180º and w3= 110º. Angles are given in degrees.

16-mer (ω_4)	Energy (a.u.)
-160	-11261.3811695
-120	-11260.4477777
0	-11261.3534380
40	-11261.1576255

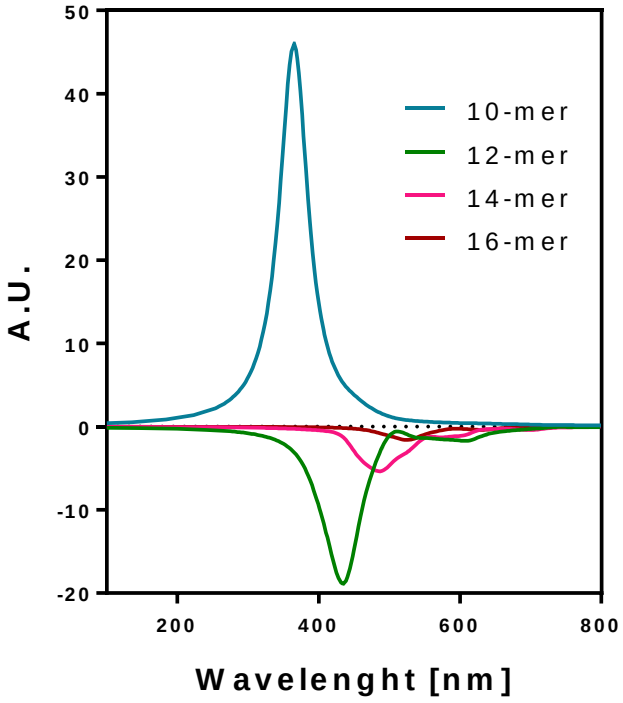

Figure S9: TD-DFT (CAM-B3LYP)/3-21G ECD spectra for the 10-,12-,14- and 16-mer with ω_1 (ω_3) ω_4 = 165 (110) -160 degrees. Half width at half height equals 25 nm. Intensities have been divided by a factor of 10 for the 10-mer.

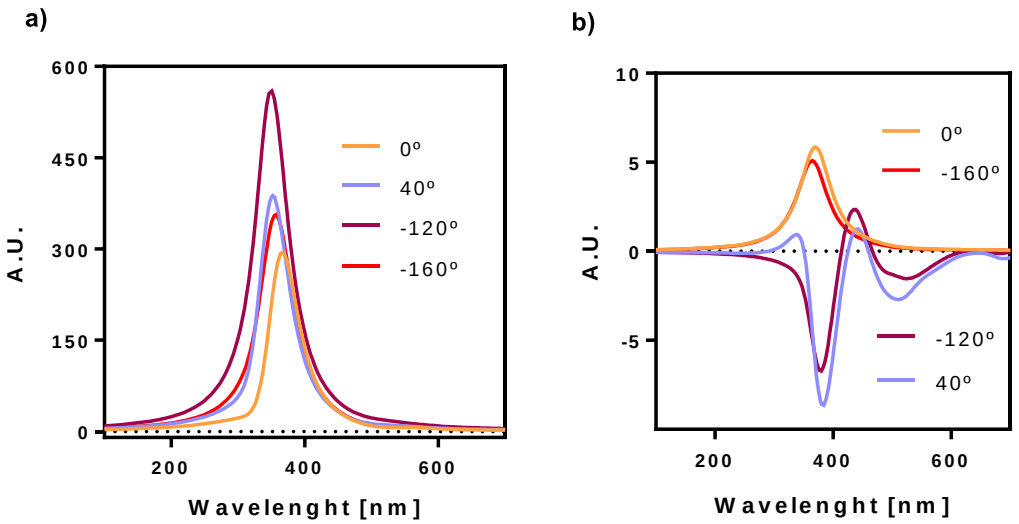

Figure S10: TD-DFT (CAM-B3LYP)/3-21G ECD spectra for the a) 8-mer and b) 10-mer with ω_1 (ω_3) = 165 (110) degrees changing ω_4. Half width at half height equals 25 nm.

PA and PPA calculations

We evaluated the corresponding ECDs for n= 8, 10, 12, 14, 16, 18, 20 and 100 for trans PA and for n= 8, 10, 12, 14, 16, 18, 20 and 25 for trans PPA.

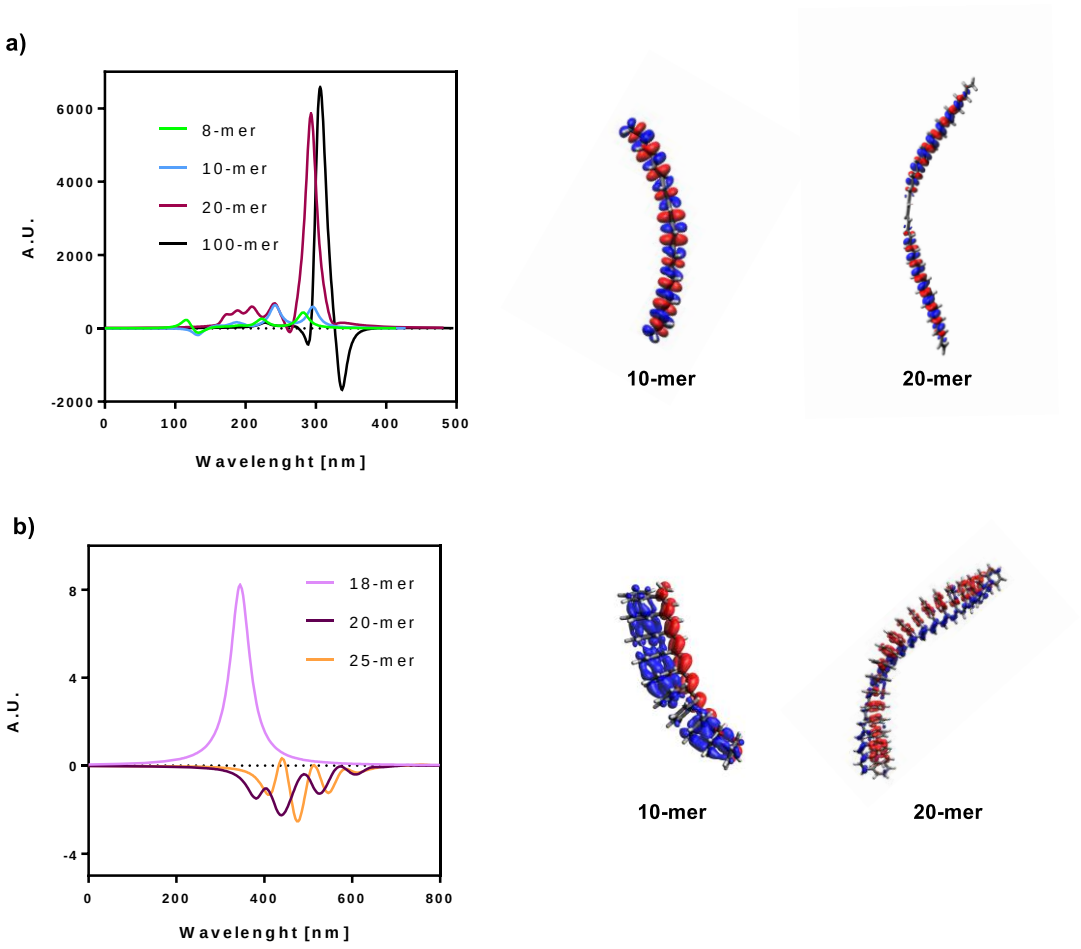

Figure S11. TD-DFT (CAM-B3LYP)/3-21G ECD spectra for the a) 8-,10-, 20- and 100-mer *trans* PA with ω_1 = 165 degrees and b) for the 18-, 20- and 25-mer *trans* PPA with ω_1 (ω_3)= 165 (110) degrees. Half width at half height equals 10 nm for *trans* PA and 27 nm for *trans* PPA. Intensities have been divided by a factor of 100 for the 18-mer PPA and by a factor of 10 for 100-mer PA.

6. Supporting References

S1. a) Tarrío, J. J.; Rodríguez, R.; Fernández, B.; Quiñoá, E.; Freire, F. Dissymmetric Chiral Poly (diphenylacetylene) s: Secondary Structure Elucidation and Dynamic Luminescence. *Angew. Chem. Int. Ed.*, **2022**, *61*, e202115070. b) Zhang, X. A.; Qin, A.; Tong, L.; Zhao, H.; Zhao, Q.; Sun, J. Z., Tang, B. Z. Synthesis of functional disubstituted polyacetylenes bearing highly polar functionalities via activated ester strategy. *ACS Macro Letters*, **2012**, *1*, 75-79.

S2. Simionescu, C. I.; Percec, V. Progress in Polyacetylene Chemistry. *Prog. Polym. Sci.*, **1982**, *8*, 133-214.

S3. Runge, E.; Gross, E. K. U. Density-Functional Theory for Time-Dependent Systems. *Phys. Rev. Lett.* **1984**, *52*, 997-1000.

S4. Yanai, T.; Tew, D. P.; Handy, N. C. A new hybrid exchange–correlation functional using the Coulomb-attenuating method (CAM-B3LYP). *Chem. Phys. Lett.*, **2004**, *393*, 51-57**.**

S5. Binkley, J. S.; Pople, J. A.; Hehre, W. J. Self-consistent molecular orbital methods. 21. Small split-valence basis sets for first-row elements. *J. Am. Chem. Soc.*, **1980**,*102*, 939-947.

S6. Fernández, B.; Rodríguez, R.; Rizzo, A.; Quiñoá, E.; Riguera, R.; Freire, F. Predicting the Helical sense of Poly(phenylacetylene)s from their Electron Circular Dichroism Spectra. *Angew. Chem. Int. Ed.* **2018**, *57*, 3666-3670.

S7. Fernández, Z.; Fernández, B.; Quiñoá, E.; Freire, F. The Competitive Aggregation Pathway of an Asymmetric Chiral Oligo (p-phenyleneethynylene) Towards the Formation of Individual P and M Supramolecular Helical Polymers. *Angew. Chem. Int. Ed.*, **2021**, *60*, 9919-9924.

S8. Neese, F. The ORCA program system. *WIREs Comput Mol Sci*. **2012**, *2*, 73-78.

S9. Gaussian 16, Revision C.01, Frisch, M. J.; Trucks, G. W.; Schlegel, H. B.; Scuseria, G. E.; Robb, M. A.; Cheeseman, J. R.; Scalmani, G.; Barone, V.; Petersson, G. A.; Nakatsuji, H.; Li, X.; Caricato, M.; Marenich, A. V.; Bloino, J.; Janesko, B. G.; Gomperts, R.; Mennucci, B.; Hratchian, H. P.; Ortiz, J. V.; Izmaylov, A. F.; Sonnenberg, J. L.; Williams-Young, D.; Ding, F.; Lipparini, F.; Egidi, F.; Goings, J.; Peng, B.; Petrone, A.; Henderson, T.; Ranasinghe, D.; Zakrzewski, V. G.; Gao, J.; Rega, N.; Zheng, G.; Liang, W.; Hada, M.; Ehara, M.; Toyota, K.; Fukuda, R.; Hasegawa, J.; Ishida, M.; Nakajima, T.; Honda, Y.; Kitao, O.; Nakai, H.; Vreven, T.; Throssell, K.; Montgomery, J. A., Jr.; Peralta, J. E.; Ogliaro, F.; Bearpark, M. J.; Heyd, J. J.; Brothers, E. N.; Kudin, K. N.; Staroverov, V. N.; Keith, T. A.; Kobayashi, R.; Normand, J.; Raghavachari, K.; Rendell, A. P.; Burant, J. C.; Iyengar, S. S.; Tomasi, J.; Cossi, M.; Millam, J. M.; Klene, M.; Adamo, C.; Cammi, R.; Ochterski, J. W.; Martin, R. L.; Morokuma, K.; Farkas, O.; Foresman, J. B.; Fox, D.

J. Gaussian, Inc., Wallingford CT, **2016**.

S10. Allouche, A. R. Gabedit—A graphical user interface for computational chemistry softwares. *J. Comput. Chem.* **2011**, *32*, 174-182.

S11. Hanwell, M. D.; Curtis, D. E.; Lonie, D. C.; Vandermeersch, T.; Zurek, E.; Hutchison, G. R. Avogadro: an advanced semantic chemical editor, visualization, and analysis platform. *Journal of Cheminformatics* **2012**, *4*, 17.

Experimental Section Chapter V

1. Materials and methods

CD measurements were done in a Jasco-720. The amounts of polymer used for CD measurements were 0.5 mg/mL in DCM, 1,2-DCE, 1,1,2,2-TCE, $CHCl_3$, THF, Acetone, MeCN, Dioxane, DMF and DMSO.

UV spectra were registered in a Jasco V-630. The amounts of polymer used for UV measurements were 0.5 mg/mL in DCM, 1,2-DCE, 1,1,2,2-TCE, $CHCl_3$, THF, Acetone, MeCN, Dioxane, DMF and DMSO.

GPC studies were carried out in a Waters Alliance equipped with Phenomenex GPC columns. The amount of polymer used for GPC measurements was 0.5 mg/mL.

CPL spectra were recorded on a Jasco CPL-300 at a scanning rate of 100nm/min over an average of 5 scans, using a 10 mm quartz cell.

2. Synthesis of monomer

The synthesis of M-**1** was made following the steps depicted in the SI of Ref. **S1**.

Perfluorophenyl 4-iodobenzoate

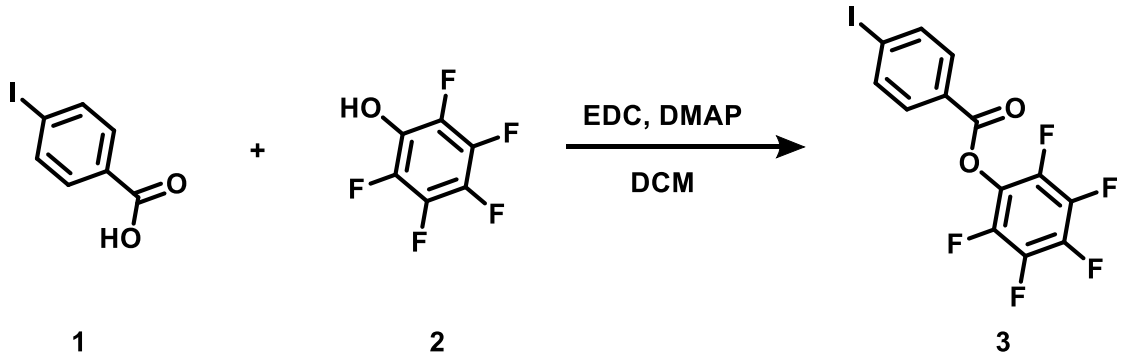

1 **2** **3**

4-iodobenzoic acid (**1**, 2.96 g, 11.94 mmol), EDC (2.40 g, 12.48 mmol), DMAP (0.073 g, 0.6 mmol) and 100 mL dry DCM were added into a 250 mL flask. After activation, pentafluorophenol (**2**, 2.00 g, 10.86 mmol) was added. The mixture was stirred at rt for 12 h and a white precipitate was formed. Then, the solid was filtrated and washed with hexane. After concentration in a rotary evaporator, the crude product was purified by silica gel column chromatography (40-63 mesh) using a mixture of hexane and ethyl acetate (95:5 by volume) as

eluent. After evaporation of solvents in a rotary evaporator, a white solid was obtained in 75% yield.

^{1}H NMR (300MHz, $CDCl_3$) δ (ppm): 8.11 - 7.71 (4H, dd)

^{19}F NMR (282.3 MHz, $CHCl_3$) δ (ppm): -152.6, -157.7, -162.2

^{13}C NMR (75MHz, $CDCl_3$) δ (ppm): 162.2, 138.3, 131.8, 126.3, 103.1

HRMS (ESI) m/z calcd for $C_{13}H_5F_5IO_2$ $[M+H]^+$: 414.9246, found: 414.9249.

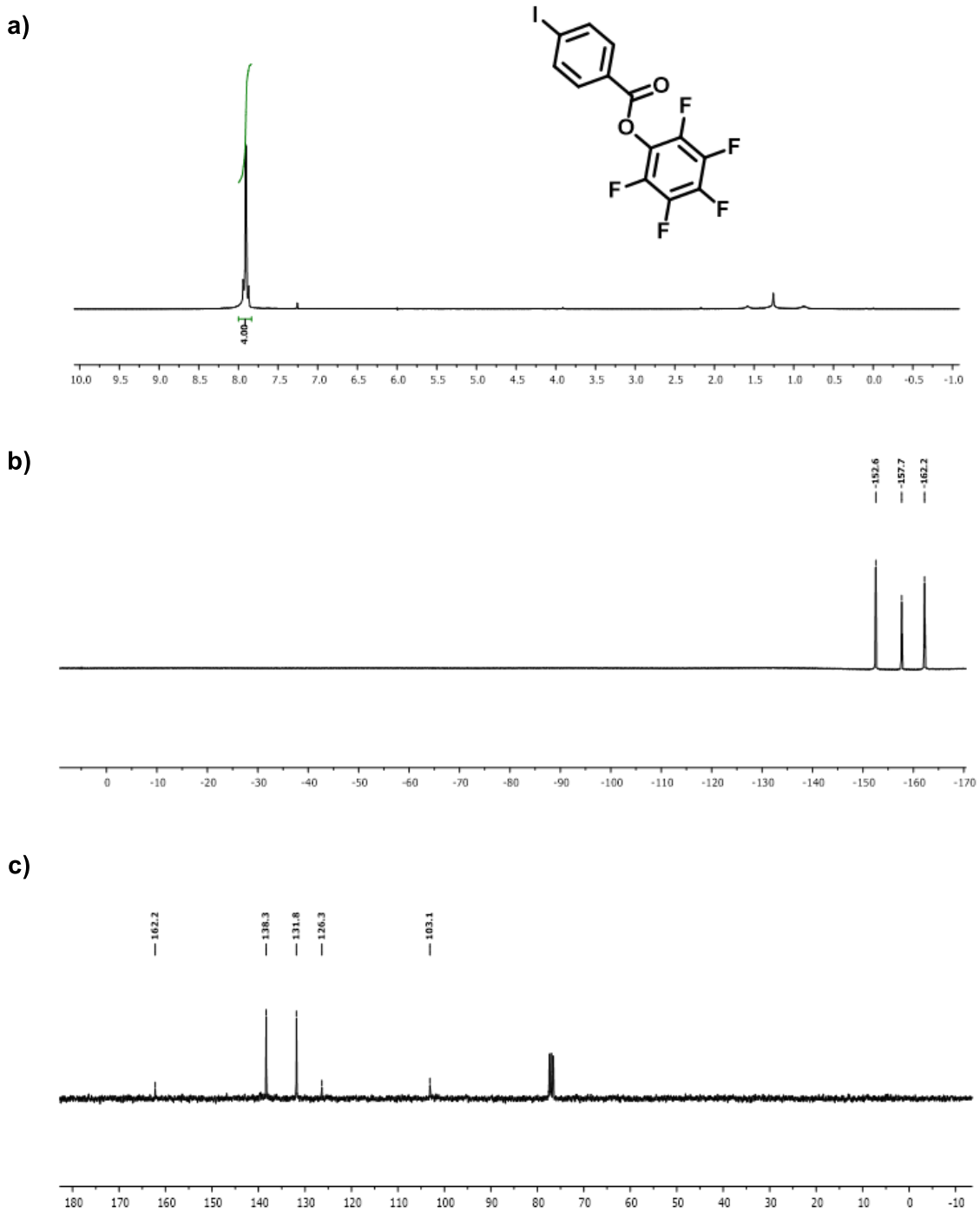

Figure S1. a) ^{1}H, b) ^{19}F and c) ^{13}C NMR spectra of **3** (perfluorophenyl 4-iodobenzoate).

Perfluorophenyl 4-(phenylethynyl)benzoate

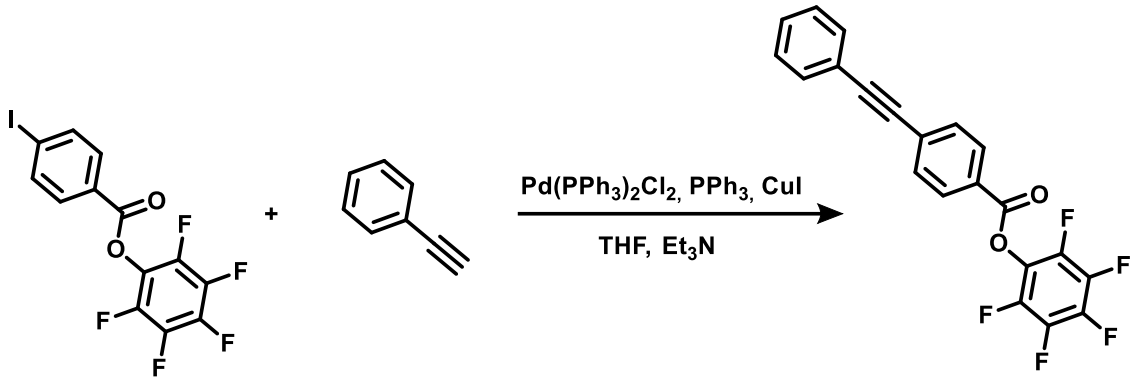

3 **4** **M-1**

Perfluorophenyl 4-iodobenzoate (**3**, 3.94 g, 9.51 mmol), $PdCl_2(PPh_3)_2$ (333 mg, 0.475 mmol), CuI (181 mg, 0.951 mmol), PPh_3 (249 mg, 0.951 mmol) were added to 50 mL of THF and 6.6 mL of Et_3N (47.55 mmol) under nitrogen. After the catalysts was completely dissolved, phenylacetylene (1.5 mL, 14.2 mmol) was injected into the flask and the mixture was stirred at rt for 24 h. The solid was removed by filtration and washed with diethyl ether. The filtrate was then concentrated in a rotary evaporator. The crude product was purified by silica gel column chromatography (40-63 mesh) using a mixture of hexane and ethyl acetate (95:5 by volume) as eluent. **M-1** was obtained as a white solid in 80% yield.

1H NMR (300MHz, $CDCl_3$, δ, TMS, ppm): 8.18 (2H, d), 7.68 (2H, d), 7.57 (2H, m), 7.39 (3H, m).

^{19}F NMR (282.3 MHz, $CHCl_3$) δ (ppm): -152.5, -157.8, -162.3

^{13}C NMR 75 MHz, $CDCl_3$, δ, TMS, ppm): 162.1, 139.6, 136.3, 131.9, 131.8, 130.6, 130.0, 129.0, 128.5, 126.0, 122.4, 93.8, 88.2

HRMS (ESI) m/z calcd for $C_{21}H_{10}F_5O_2$ $[M+H]^+$: 389.0595, found: 389.0595.

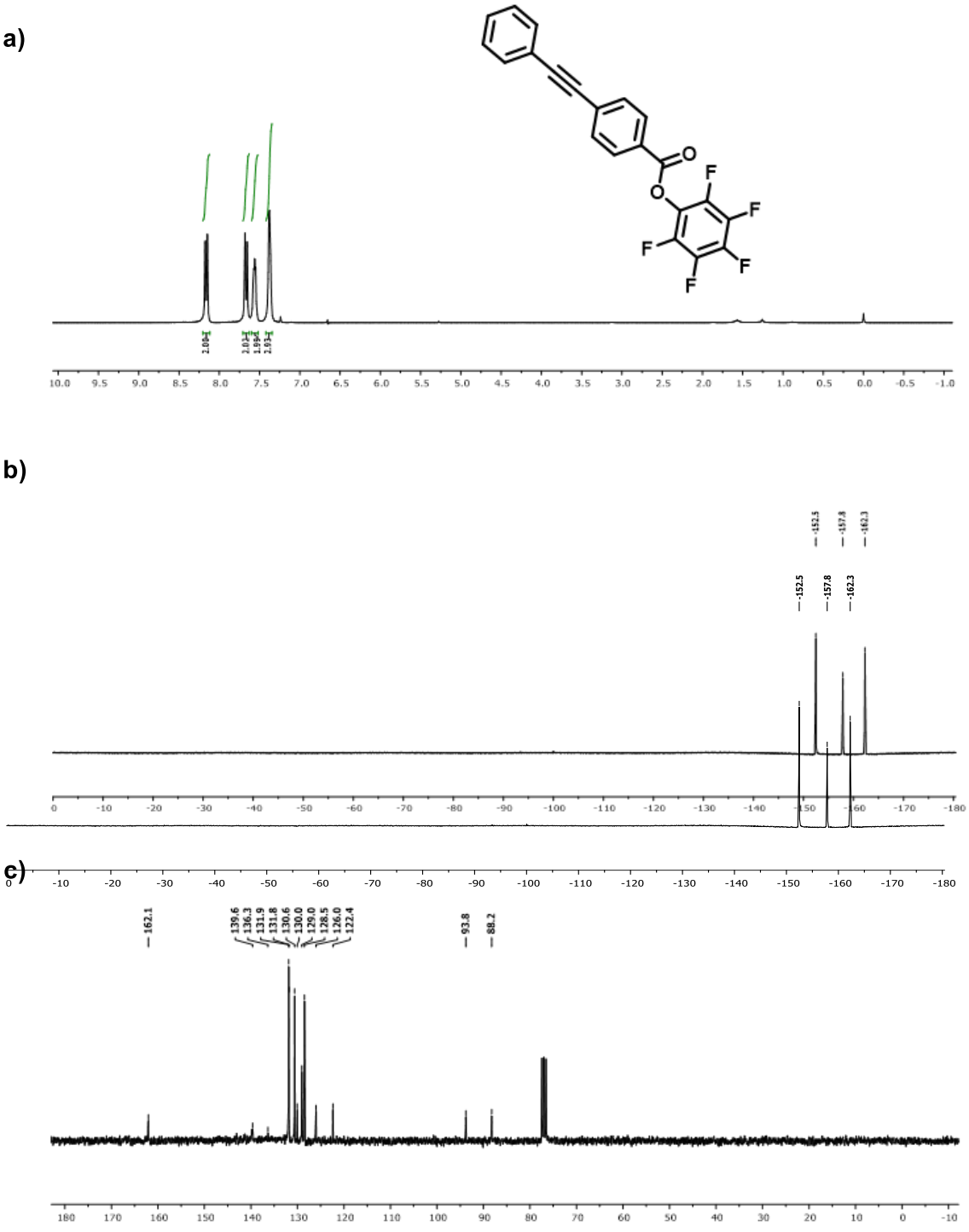

Figure S2. a) ^{1}H, b) ^{19}F and c) ^{13}C NMR spectra of m-**1**.

3. Synthesis of Polymers

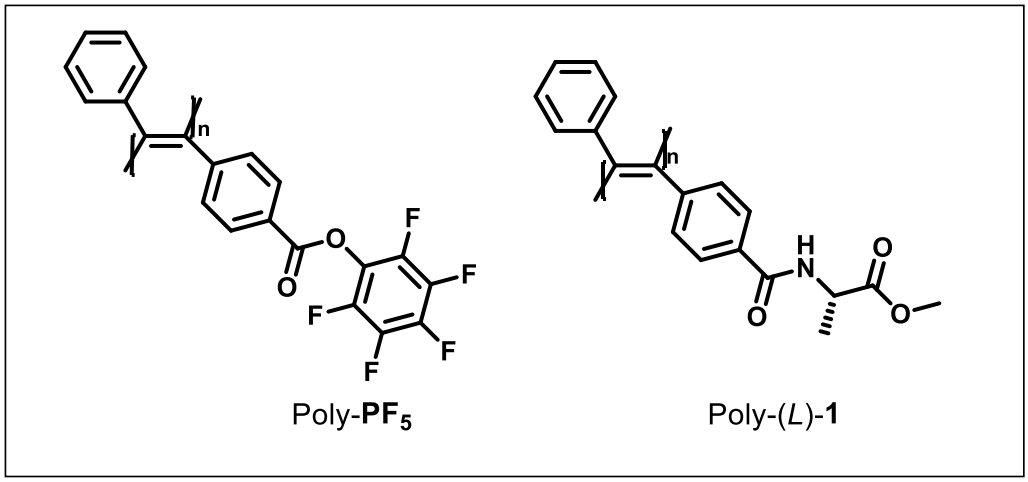

Figure S3: Structure of the polymers synthesized in this work.

Trans Polymerization Reaction

The polymerization reaction was carried out under a nitrogen atmosphere using standard Schlenk technique, unless otherwise specified. A typical procedure for the polymerization of M-**1** is given below as an example following the conditions of Ref. **S1**.

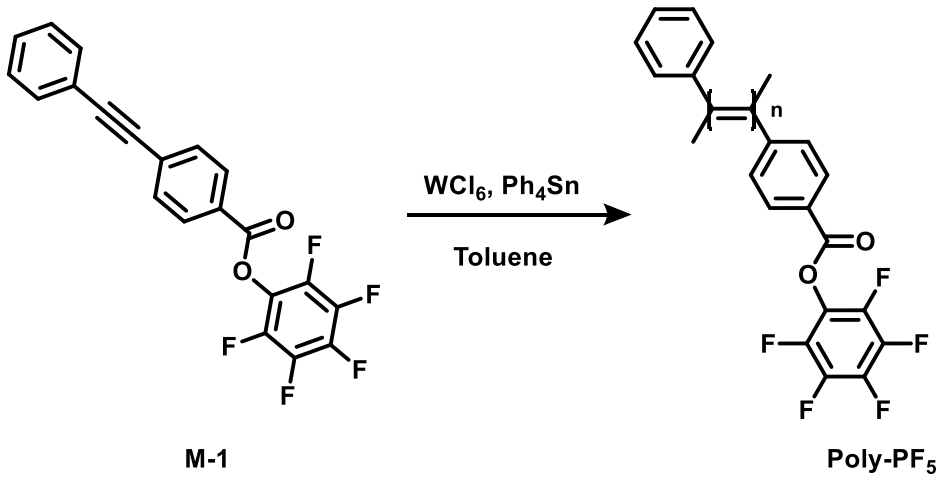

20.4 mg of WCl_6 and 44.0 mg of Ph_4Sn were added into a baked 10 mL Schlenk tube with a stopcock in the side arm. The tube was evacuated under vacuum and then flushed with dry nitrogen three times through the side arm. Freshly distilled toluene (1 mL) was injected into the tube to dissolve the mixture of catalysts and then, the catalyst solution was aged at 100 °C for 10 min. The monomer solution was prepared in another tube by dissolving 200 mg of **m-1** in 1.6 mL of toluene and was transferred to the catalyst solution using a hypodermic syringe. The reaction mixture was stirred at 100 °C for 24 h. The solution was cooled to rt, diluted with

CH_2Cl_2 and then precipitated in a large amount of methanol. The precipitate was allowed to stand overnight and then collected by filtration. The polymer was washed with methanol and hexane and dried under vacuum at room temperature to a constant weight. Poly-**PF_5** was obtained as a brown solid in 52% yield.

^{1}H-NMR (300MHz, $CDCl_3$), δ (TMS, ppm): 7.39, 6.75, 6.60, 6.28, 6.06.

^{19}F NMR (282.3MHz, $CDCl_3$), δ (TMS, ppm): -153.3, -157.6, -163.0.

Post-polymerization Coupling

The post-polymerization reaction was carried out using standard peptide coupling conditions. A typical procedure for the coupling of alanine methyl ester is given below as an example following the conditions of Ref. **S1**.

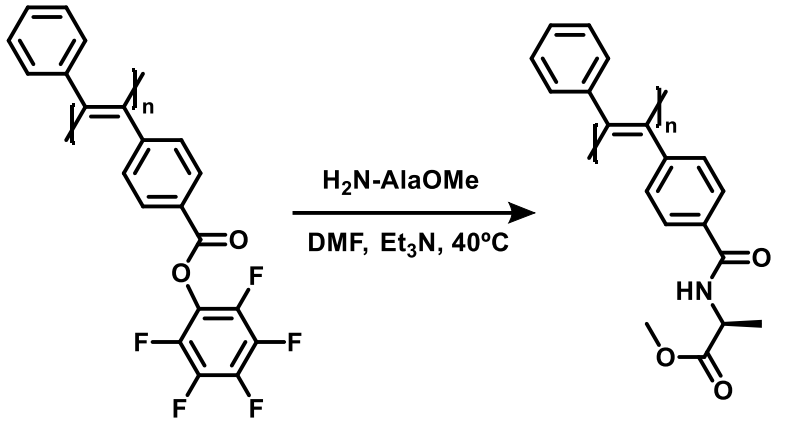

Poly-PF_5 **Poly-(*L*)-1**

20 mg (0.052 mmol) Poly-**PF_5**, 9.4 mg (0.067 mmol) L-alanine methyl ester hydrochloride and 2 mL dry DMF with a drop of TEA were added into a 10 mL reaction tube with magnetic stirring bar under nitrogen. The reaction solution was stirred for 12 h at 40 °C. Next, the solution mixture was added dropwise to 300 mL methanol through a cotton filter under vigilant stirring. The precipitate was kept still overnight and then filtered. The obtained polymer was washed with methanol and hexane several times and dried at rt to a constant weight. Poly-(*L*)-**-1** was obtained as a yellow solid in 95 % yield.

^{1}H NMR (300 MHz, $CDCl_3$), δ (TMS, ppm): 7.25, 6.92, 6.63, 6.53, 6.12, 4.69, 3.73, 1.48.

^{19}F NMR (282.3 MHz, $CDCl_3$), δ (TMS, ppm): no signals.

4. ^{1}H and ^{19}F NMR experiments of the polymers

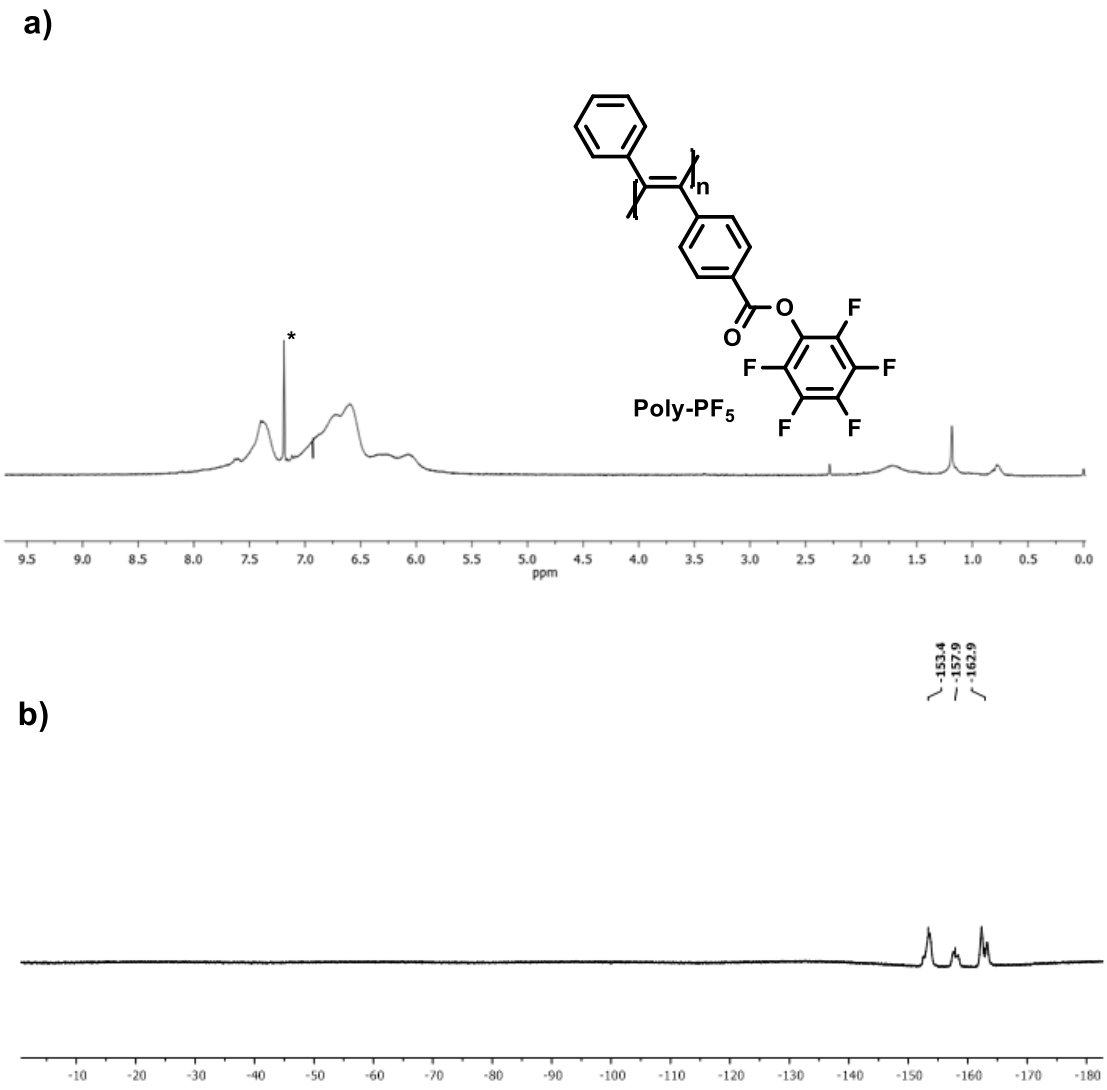

Figure S4. a) ^{1}H-NMR and b) ^{19}F-NMR spectra of Poly-**PF$_5$**.

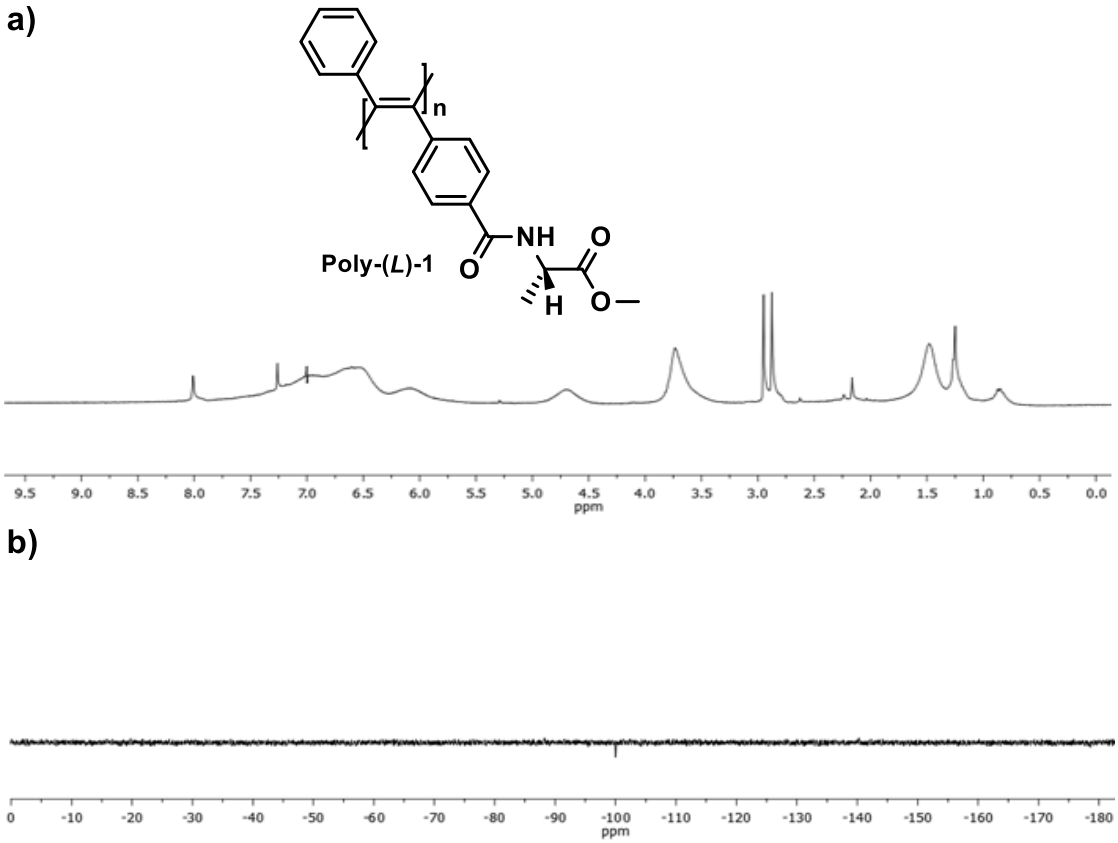

Figure S5. a) ^{1}H-NMR and b) ^{19}F-NMR spectra of Poly-(*L*)-**1**.

5. Size and solvent effects on the CD spectra of poly-(*L*)-1

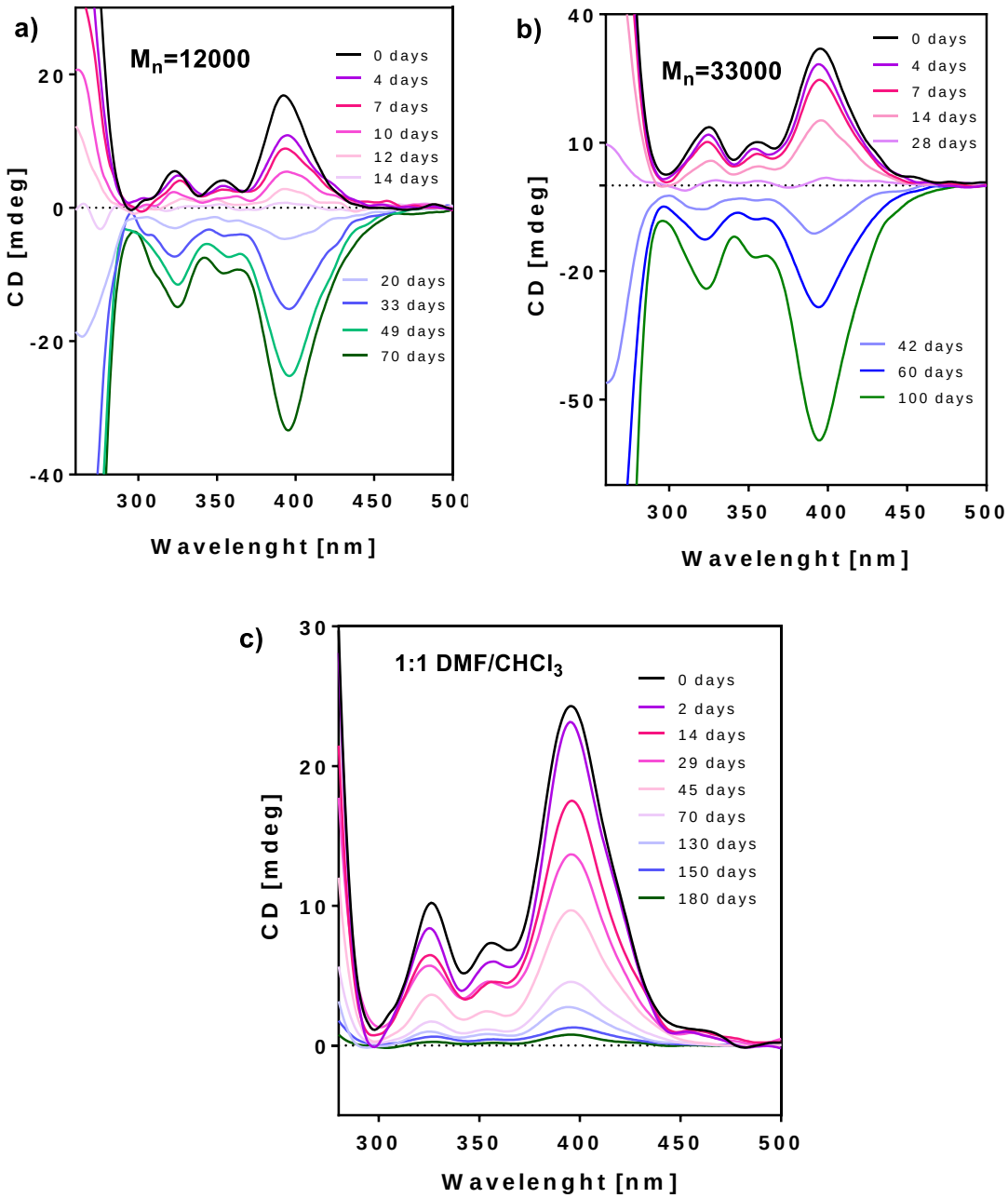

Figure S6: Variation of CD spectra of solutions of Poly-(*L*)-**1** in $CHCl_3$ (0.5 mg/mL) pre-annealed in DMF with a polymer size of a) 12000 M_n and b) 33000 M_n. c) Decrease of a solution 1:1 in DMF/$CHCl_3$ of Poly-**2** pre-annealed in DMF.

6. CD studies of Poly-(*L*)-1 at high temperatures

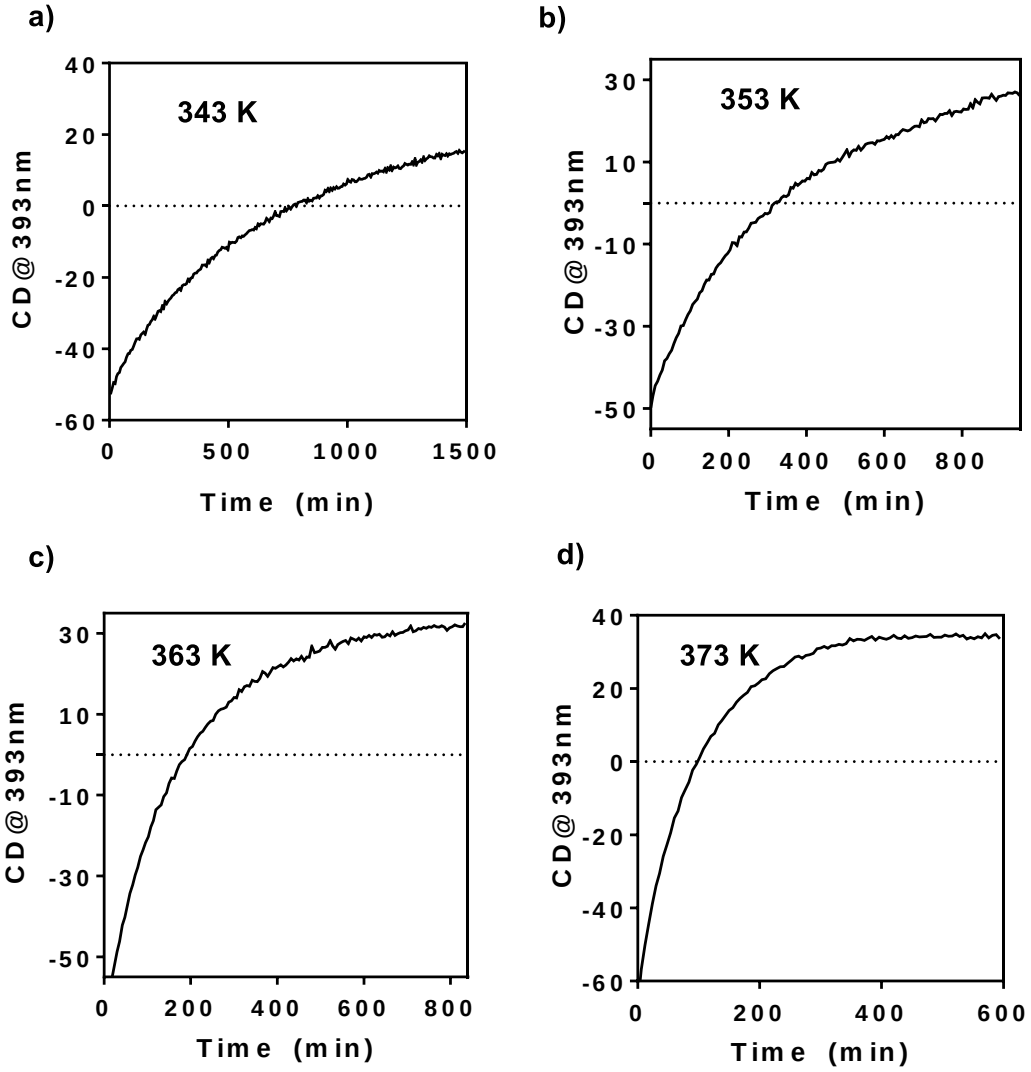

Figure S7: Evolution of CD signal at 393 nm of Poly-(*L*)-**1** pre-annealed in $CHCl_3$ during a thermal annealing in DMF (0,5 mg/mL) at: a) 70°C, b) 80°C, c) 90°C and d) 100°C.

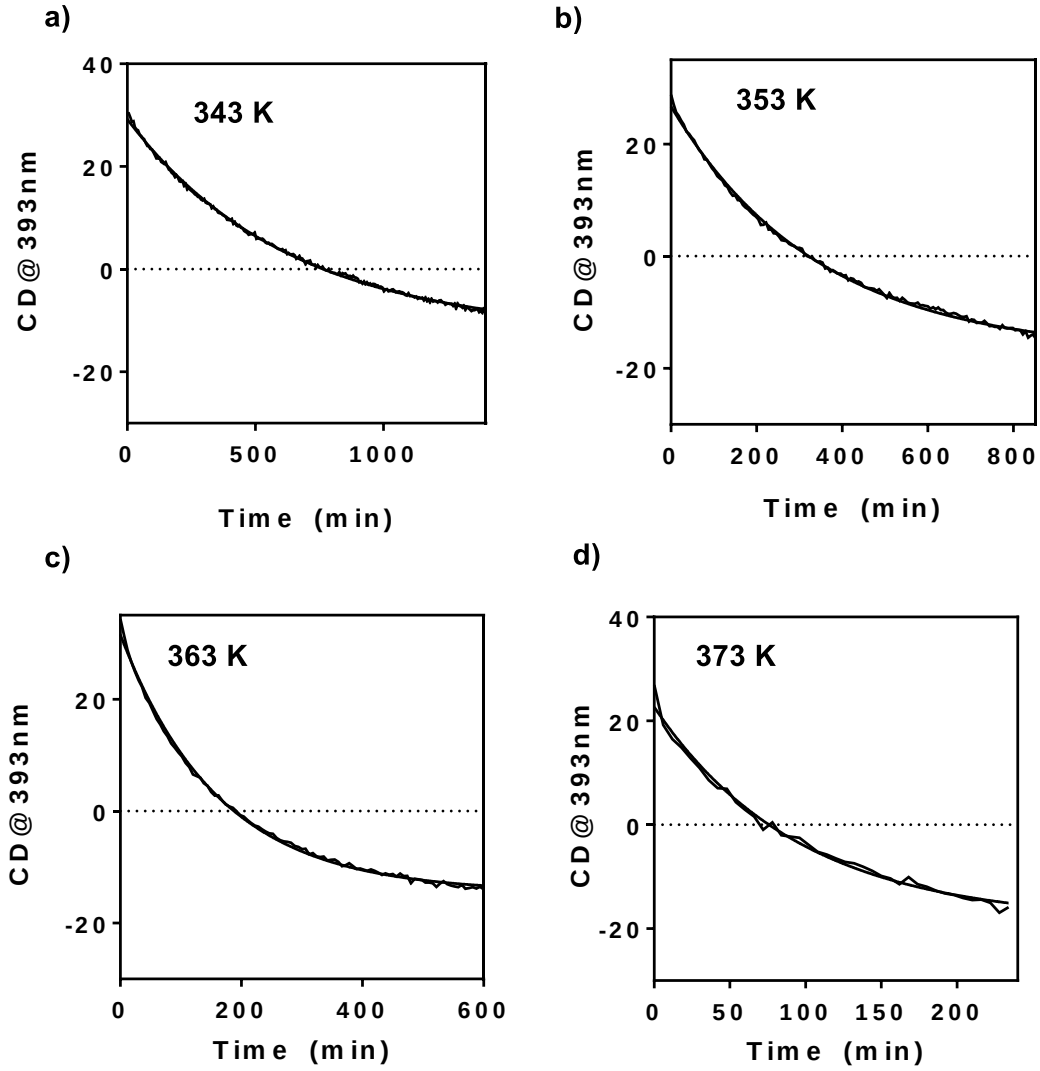

Figure S8: Evolution of CD signal at 393 nm of Poly-(*L*)-**1** pre-annealed in DMF during a thermal annealing in 1,1,2,2-TCE (0,5 mg/mL) at: a) 70ºC, b) 80ºC, c) 90ºC and d) 100ºC.

7. CD studies of poly-(*L*)-1 at low temperatures

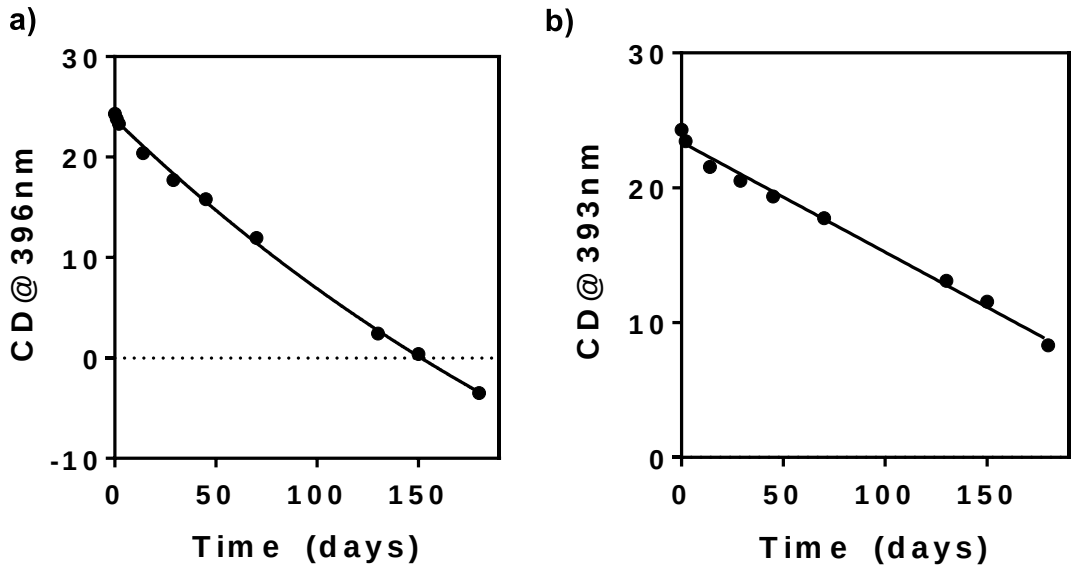

Figure S9: Evolution of CD signal at 393 nm of poly-**2** solution in $CHCl_3$ pre-annealed in DMF at a) 4ºC and b) -20ºC.

8. Equations

By plotting the variation of the ECD at 393 nm vs time is possible to observe that follows and exponential grow that can be fitted to the following equation:

$$ECD=ECD_0 + (Plateau- ECD_0)*(1-exp(-k_{inv}*t))$$

Where ECD_0 is the value of the ECD signal when time is zero and Plateau is the ECD value at infinite times. This equation is the result of considering the whole inversion process. Nevertheless, the inversion process can be separated in two steps with a first racemization process (Figure S10c).

In this way, the first step follows a pseudo-first order kinetics where the k_{rac} can be obtained representing the $\ln(CD/CD_0)$ vs time for each temperature in the shortest times where the evolution of the CD follows a first-order kinetic process. After this, k_{inv} is the double assuming that both helices have the same energy. See Ref. **S2** and **S3** for further information. In both cases, the k_{inv} calculated are the same.

R value used is 8.314 $J\cdot K^{-1}\cdot mol^{-1}$, $k_B = 1.381 \times 10^{-23}$ $J\cdot K^{-1}$ and $h = 6.626 \times 10^{-34}$ $J\cdot s^{-1}$. More details about the equations are given bellow in Figure S10.

a) **Arrhenius Equation**

$$k = A \cdot e^{\frac{-E_a}{RT}}$$

- k = rate constant
- A = pre-exponential factor
- E_a = Activation Energy
- R = Universal gas constant
- T = Absolute Temperature

b) **Eyring Equation**

$$\ln\frac{k}{T} = \frac{-\Delta H^{\ddagger}}{R}\cdot\frac{1}{T} + \ln\frac{k_B}{h} + \frac{-\Delta S^{\ddagger}}{R}$$

- k = rate constant
- T = Absolute Temperature
- $\Delta H^{\ddagger}$ = Enthalpy of activation
- R = Universal gas constant
- k_B = Boltzmann constant
- h = Planck constant
- $\Delta S^{\ddagger}$ = Entropy of activation

c)

Enantiomeric Equilibrium

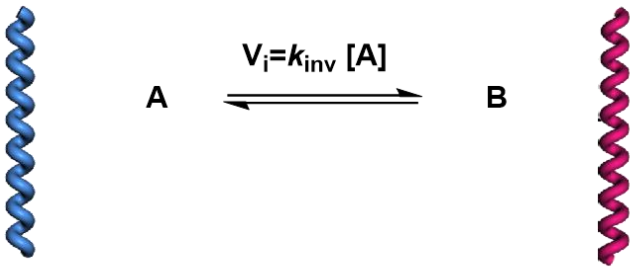

Racemization Equilibrium

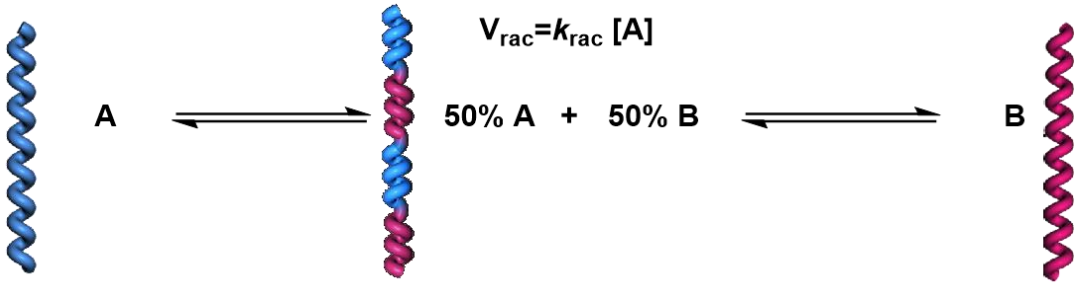

$V_{rac}=2V_i$ ⟶ k_{rac} [A] = 2 k_{inv} [A] ⟶ $k_{rac}/2 = k_{inv}$

Figure S10: a) Arrhenius equation, b) Eyring equation and c) schematic illustration of the racemization and inversion processes.

9. K_{rac} Equations

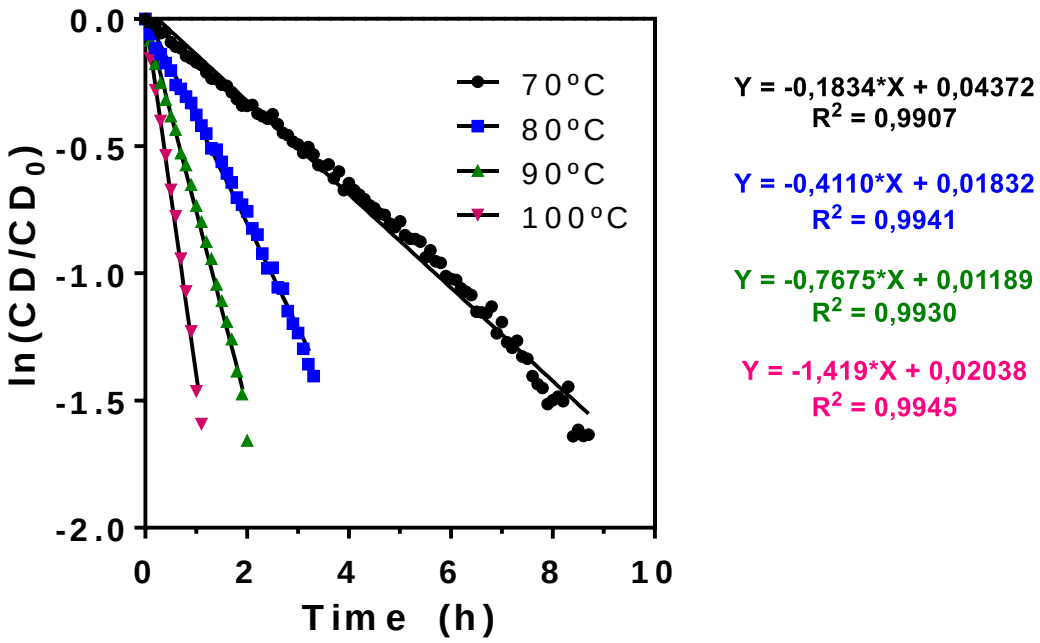

Figure S11: Evolution of CD signal at 393 nm of Poly-(*L*)-**1** pre-annealed in $CHCl_3$ during a thermal annealing in DMF (0,5 mg/mL) at: a) 70ºC, b) 80ºC, c) 90ºC and d) 100ºC.

10. Supporting References

S1. Tarrío, J. J.; Rodríguez, R.; Fernández, B.; Quiñoá, E.; Freire, F. Dissymmetric Chiral Poly (diphenylacetylene) s: Secondary Structure Elucidation and Dynamic Luminescence. *Angew. Chem. Int. Ed.*, **2022**, *61*, e202115070.

S2. Jensen, F. Activation energies and the Arrhenius equation. *Qual. Reliab. Eng. Int.*, **1985**, *1*, 13-17.

S3. Shimizu, Y.; Shoji, Y.; Hashizume, D.; Nagata, Y.; Fukushima, T. Sensing the chirality of various organic solvents by helically arranged π-blades. *Chem. Commun.*, **2018**, *54*, 12314-12317.

Experimental Section Chapter VI

1. Materials and Methods

CD measurements were done in a Jasco-720. The amounts of polymer used for CD measurements were 0.5 mg/mL in 1,2-DCE and THF.

UV spectra were registered in a Jasco V-630. The amounts of polymer used for UV measurements were 0.5 mg/mL in 1,2-DCE and THF.

The normalized CD was calculated as I_{CD}/I_{UV}, where the I_{CD} is the value of circular dichroism at a given wavelength and I_{UV} is the absorption at a given wavelength.

IR studies were carried out in a FTIR Varian 670 equipped with an ATR (GladiATR model) with diamond crystal of PIKE Technologies.

Raman spectra were performed in a Renishaw confocal Raman spectrometer (Invia Reflex model), equipped with two lasers (diode laser 785 nm and Ar laser 514 nm).

GPC studies were carried out in a Waters Alliance equipped with Phenomenex GPC columns. The amount of polymer used for GPC measurements was 0.5 mg/mL.

For molecular modeling we used Spartan 14 (MMFF94). As a molecular visualization system, we used PyMOL. The additional methodology used in the computational study is detailed in the Computational Details section.

CPL spectra were recorded on a Jasco CPL-300 at a scanning rate of 100nm/min over an average of 5 scans, using a 10 mm quartz cell.

SEM measurements were performed on a LEO-435VP electron microscope equipped with an energy dispersive X-ray (EDX) spectrometer

DLS studies were performed on a Nano-ZS 90 (Malvern) equipped with a He-Ne laser (l = 633 nm) under scattering angle of 173°. The samples were maintained at the designed temperature for 5 min before testing.

Fluorescence measurements were carried out on a Cary Eclipse model Varian Fluorescence Spectrophotometer. l of excitation was 365 nm and the concentration employed was 0.4 mM for all the solutions.

2. Synthesis of monomer and polymers

The synthesis of M-**1**, Poly-**PF_5** and Poly-(*L*)-**1** was made following the steps depicted in the SI of Ref. **S1**.

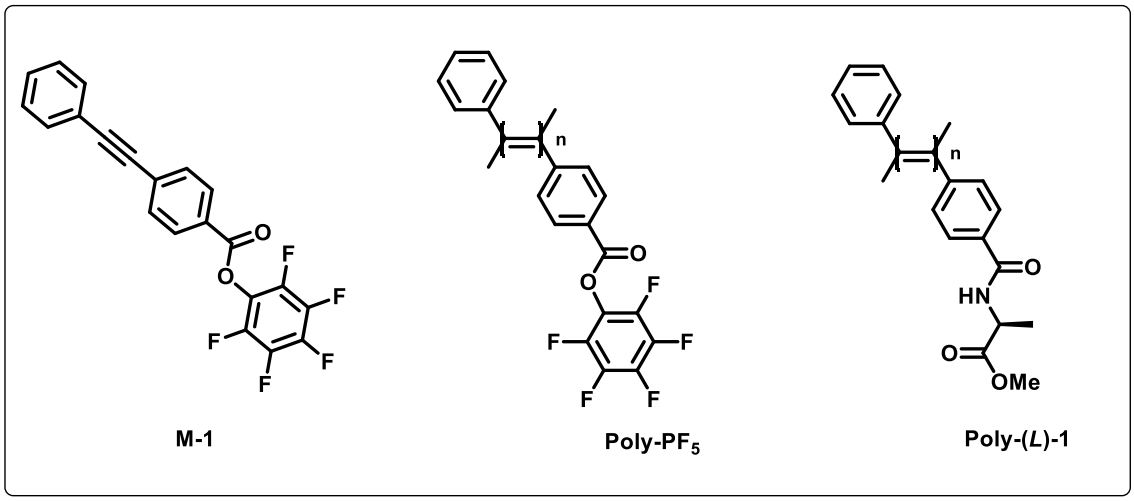

Figure S1. Structure of the monomer and polymers synthetized in this work.

3. Characterization of monomer and polymers

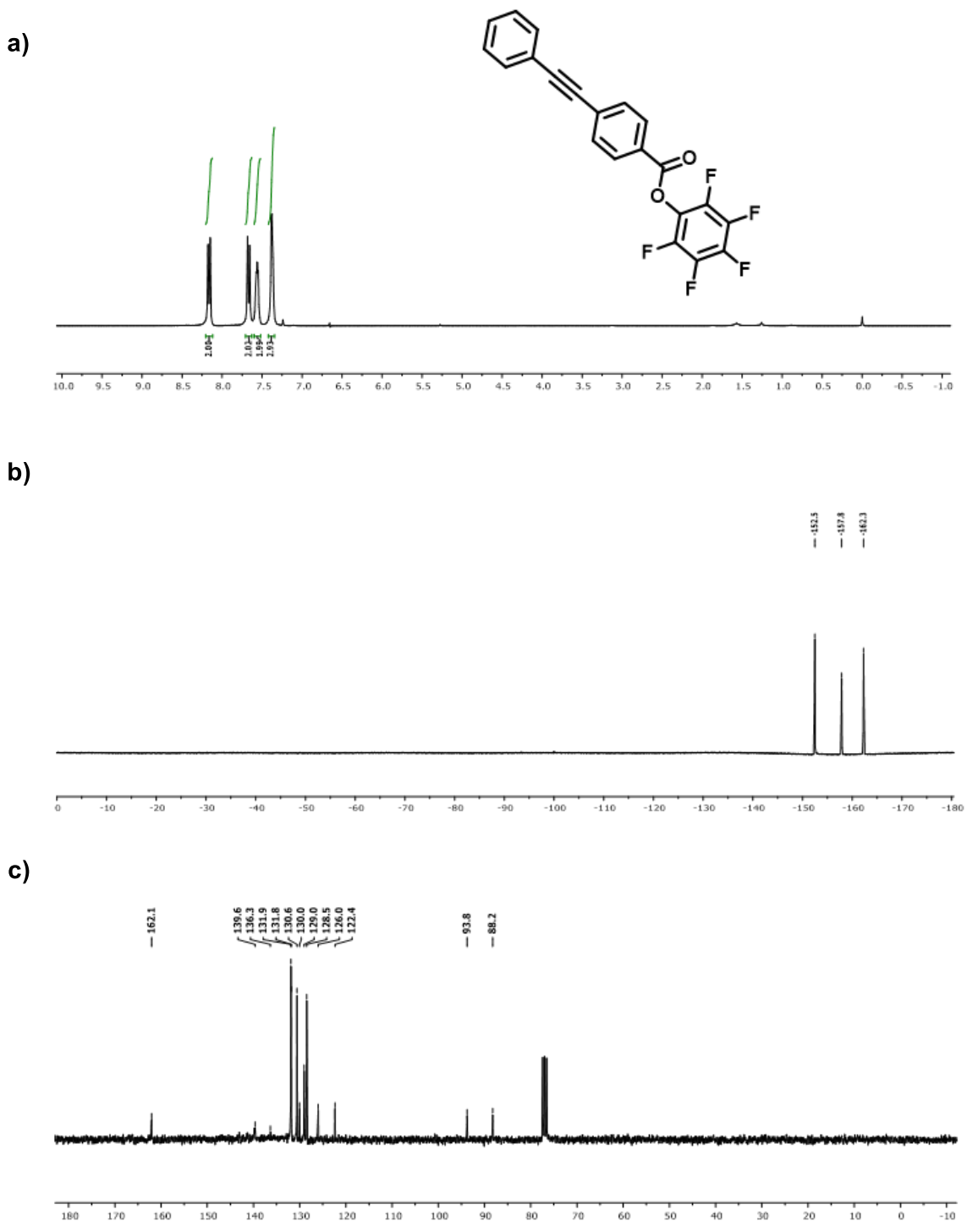

Figure S2. a) ^{1}H, b) ^{19}F and c) ^{13}C NMR spectra of m-**1**.

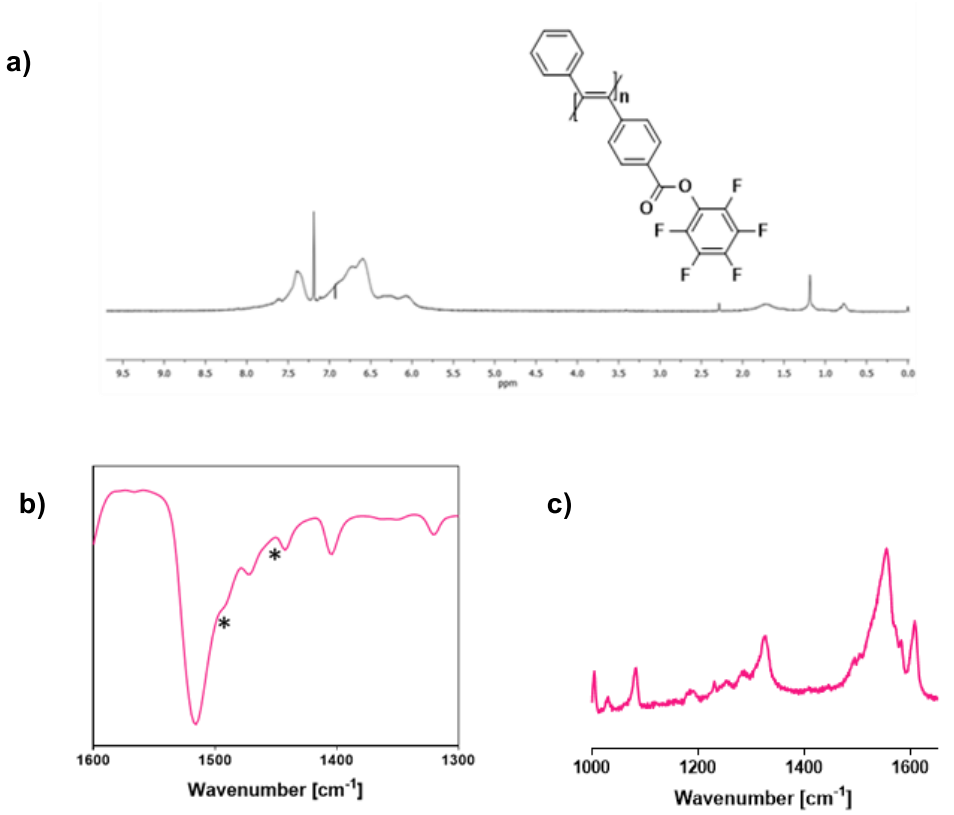

Figure S3. a) ^{1}H, b) IR and c) Raman spectra of Poly-**PF$_5$**

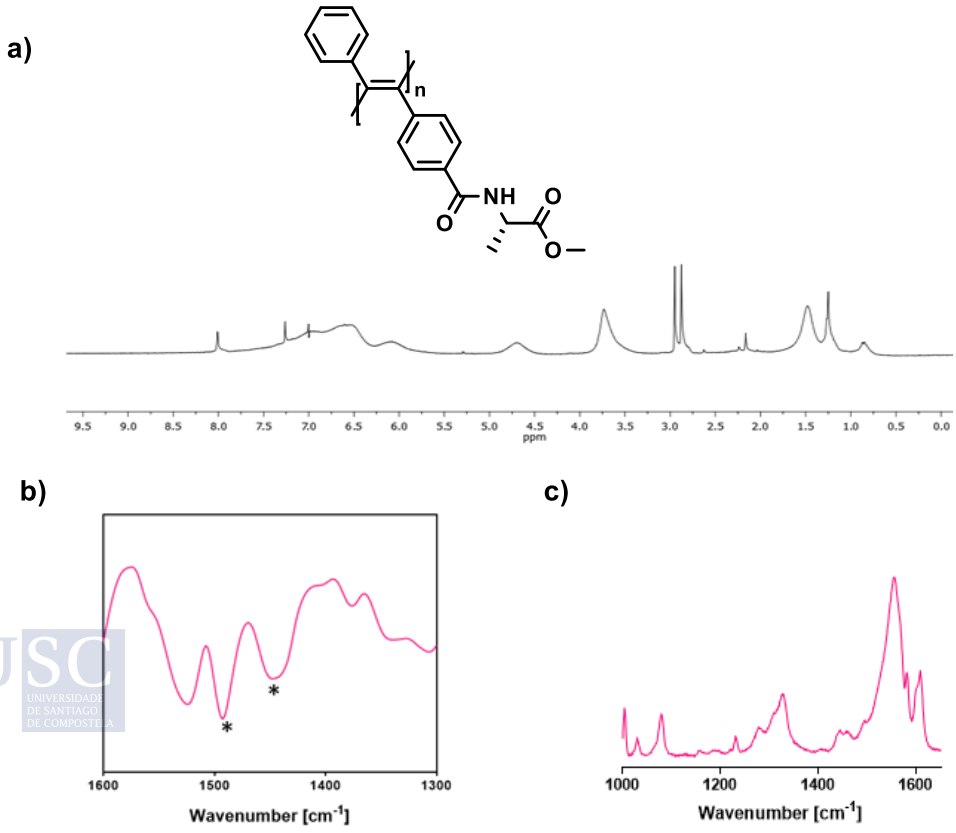

Figure S4. a) ^{1}H, b) IR and c) Raman spectra of Poly-(*L*)-**1**

4. CD studies of Poly-(*L*)-1$_P$ solutions with Li^+

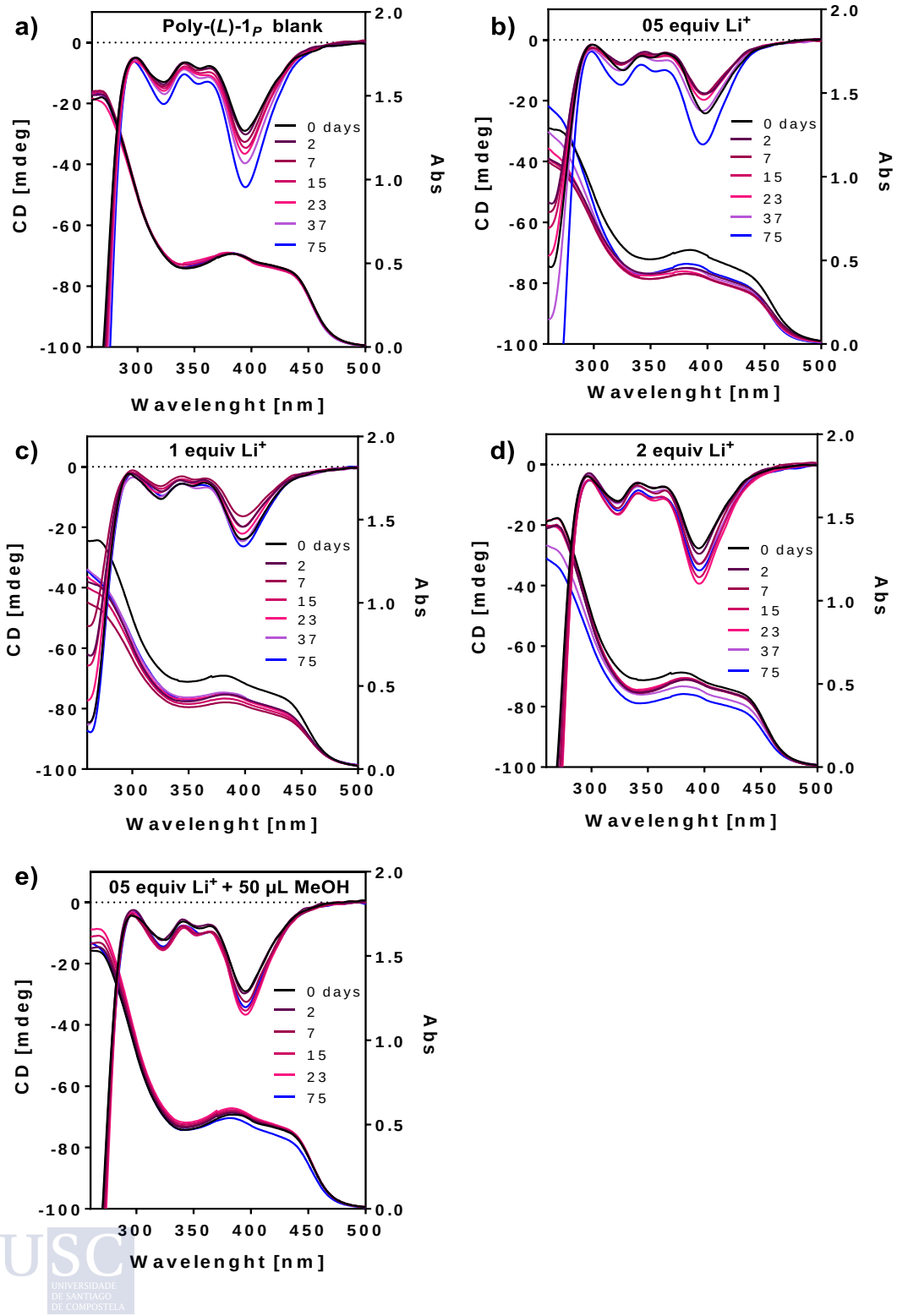

Figure S5: CD and UV spectra of Poly-(*L*)-**1**$_P$ solutions in DCE (0.5 mg/mL) with: a) 200 µL MeOH, b) 0.5 equiv $LiClO_4$, c) 1 equiv $LiClO_4$, d) 2 equiv $LiClO_4$ and e) 0.5 equiv $LiClO_4$ + 50 µL of MeOH.

5. CD studies of Poly-(*L*)-1$_P$ solutions with Ba^{2+}

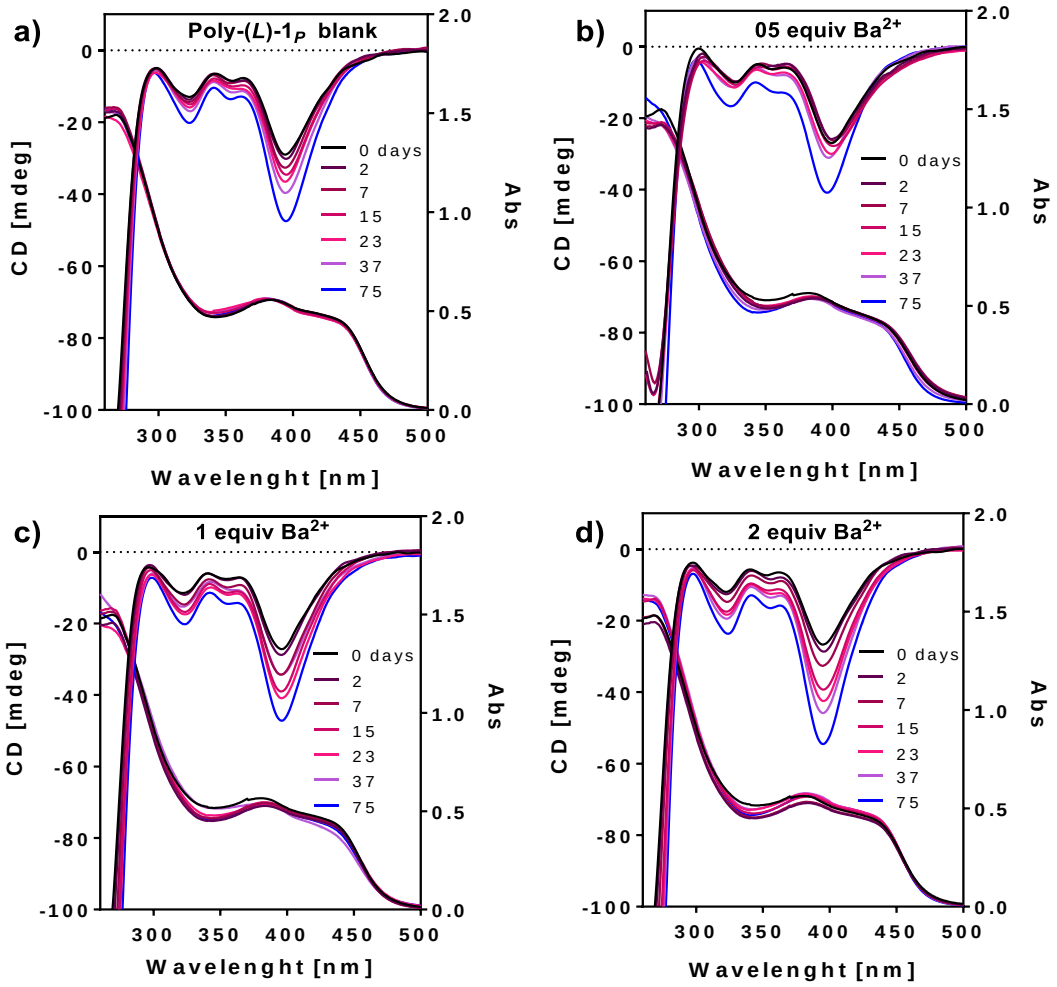

Figure S6: CD and UV spectra of Poly-(*L*)-**1**$_P$ solutions in DCE (0.5 mg/mL) with: a) 200 µL MeOH, b) 0.5 equiv $Ba(ClO_4)_2$, c) 1 equiv $Ba(ClO_4)_2$ and d) 2 equiv $Ba(ClO_4)_2$.

6. Normalized I_{CD}/I_{UV} of Poly-(*L*)-1_P solutions with Li^+

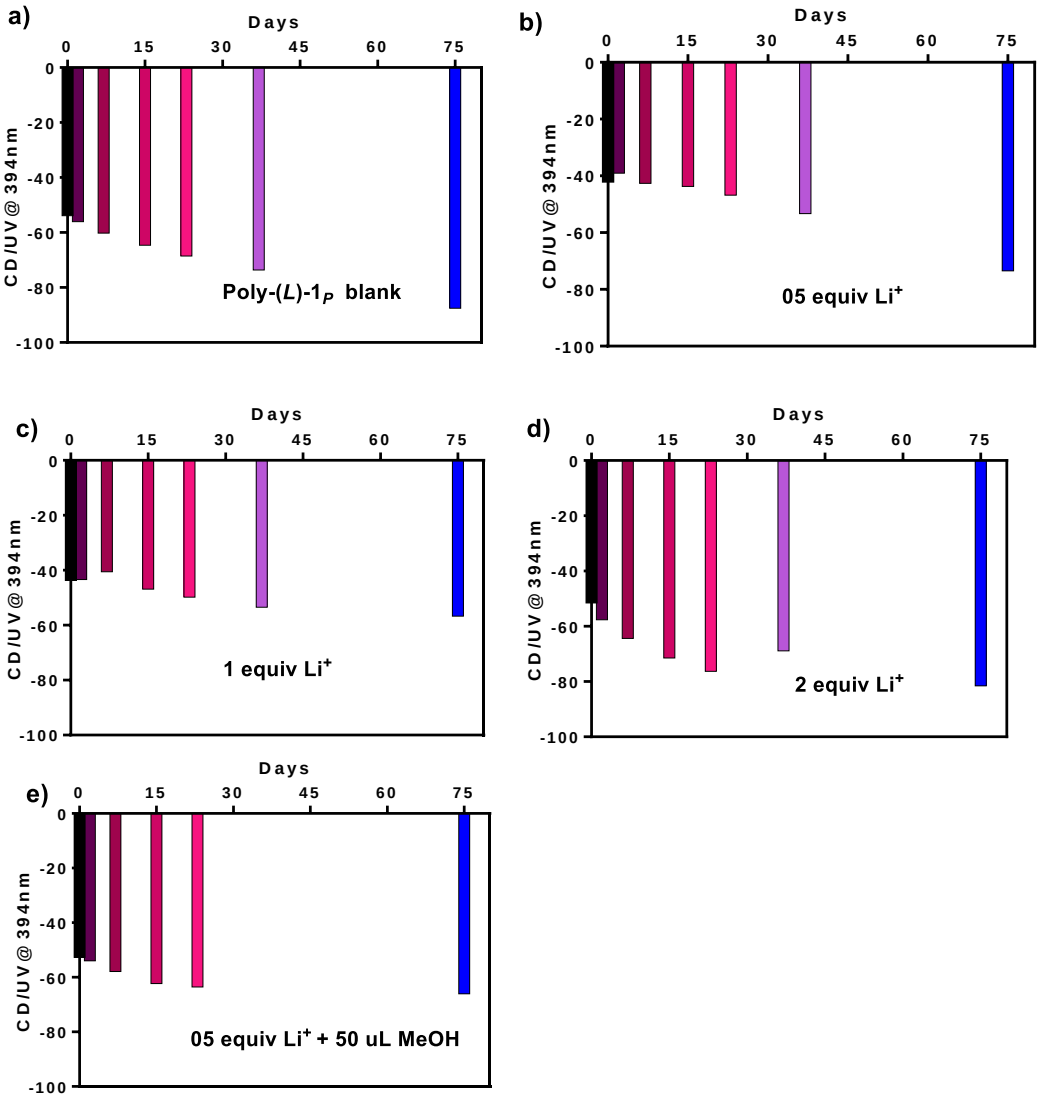

Figure S7: I_{CD}/I_{UV} spectra of Poly-(*L*)-**1**$_P$ solutions in DCE (0.5 mg/mL) with: a) 200 µL MeOH, b) 0.5 equiv $LiClO_4$, c) 1 equiv $LiClO_4$, d) 2 equiv $LiClO_4$ and e) 0.5 equiv $LiClO_4$ + 50 µL of MeOH.

7. Normalized I_{CD}/I_{UV} of Poly-(*L*)-1_P solutions with Ba^{2+}

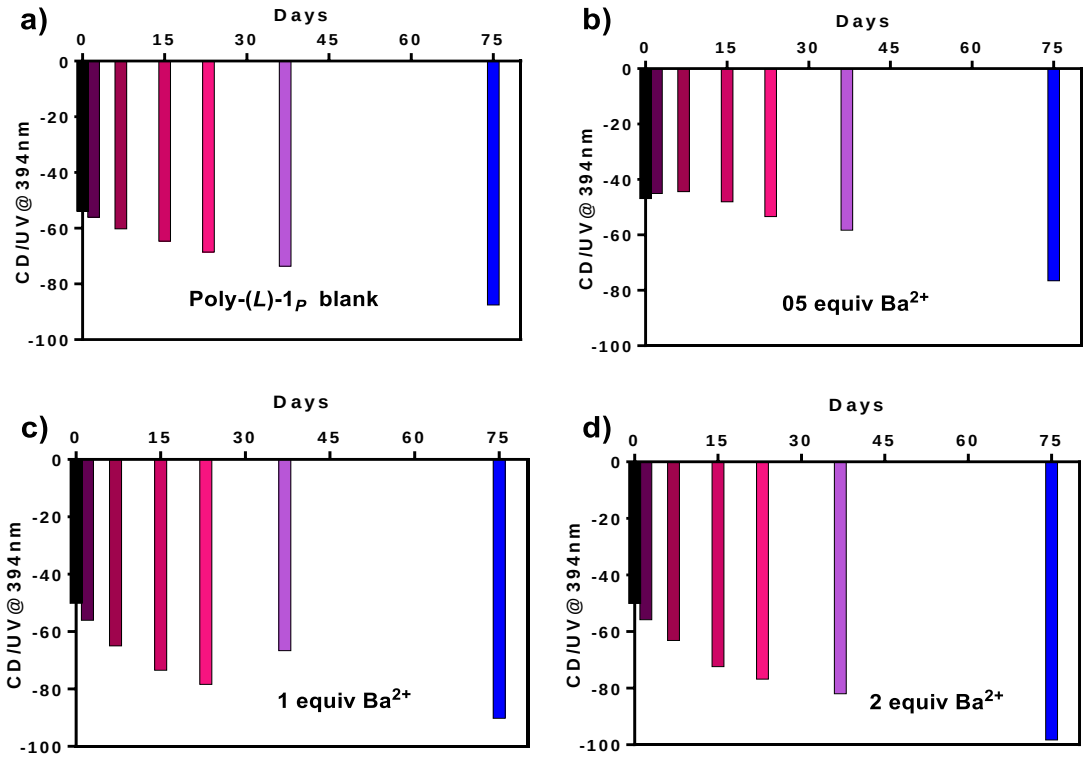

Figure S8: I_{CD}/I_{UV} spectra of Poly-(*L*)-**1**$_P$ solutions in DCE (0.5 mg/mL) with: a) 200 µL MeOH, b) 0.5 equiv $Ba(ClO_4)_2$, c) 1 equiv $Ba(ClO_4)_2$ and d) 2 equiv $Ba(ClO_4)_2$.

8. CD studies of Poly-(*L*)-1$_M$ solutions with Li^+

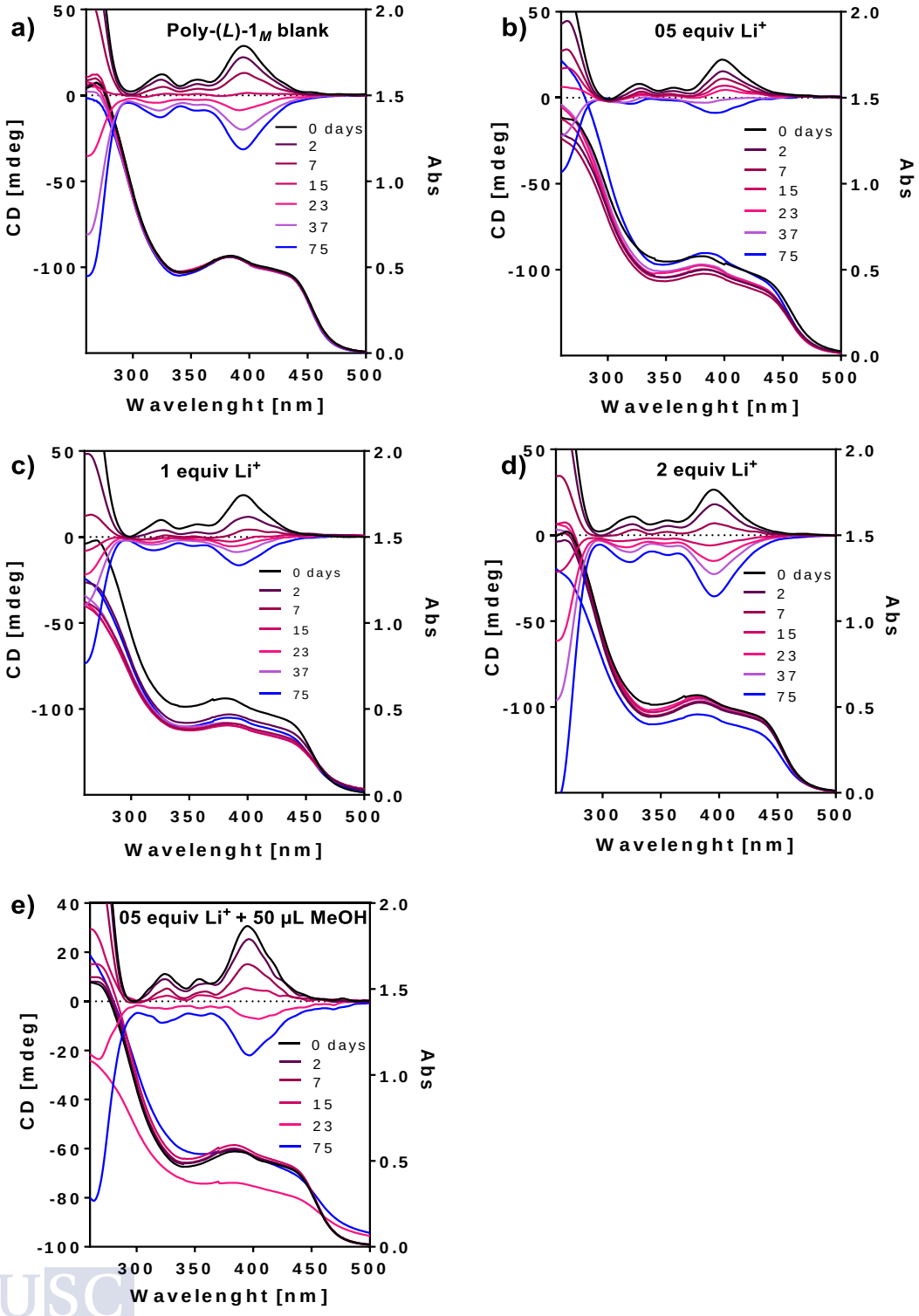

Figure S9: CD and UV spectra of Poly-(*L*)-**1**$_M$ solutions in DCE (0.5 mg/mL) with: a) 200 µL MeOH, b) 0.5 equiv $LiClO_4$, c) 1 equiv $LiClO_4$, d) 2 equiv $LiClO_4$ and e) 0.5 equiv $LiClO_4$ + 50 µL of MeOH.

9. CD studies of Poly-(*L*)-1_M solutions with Ba^{2+}

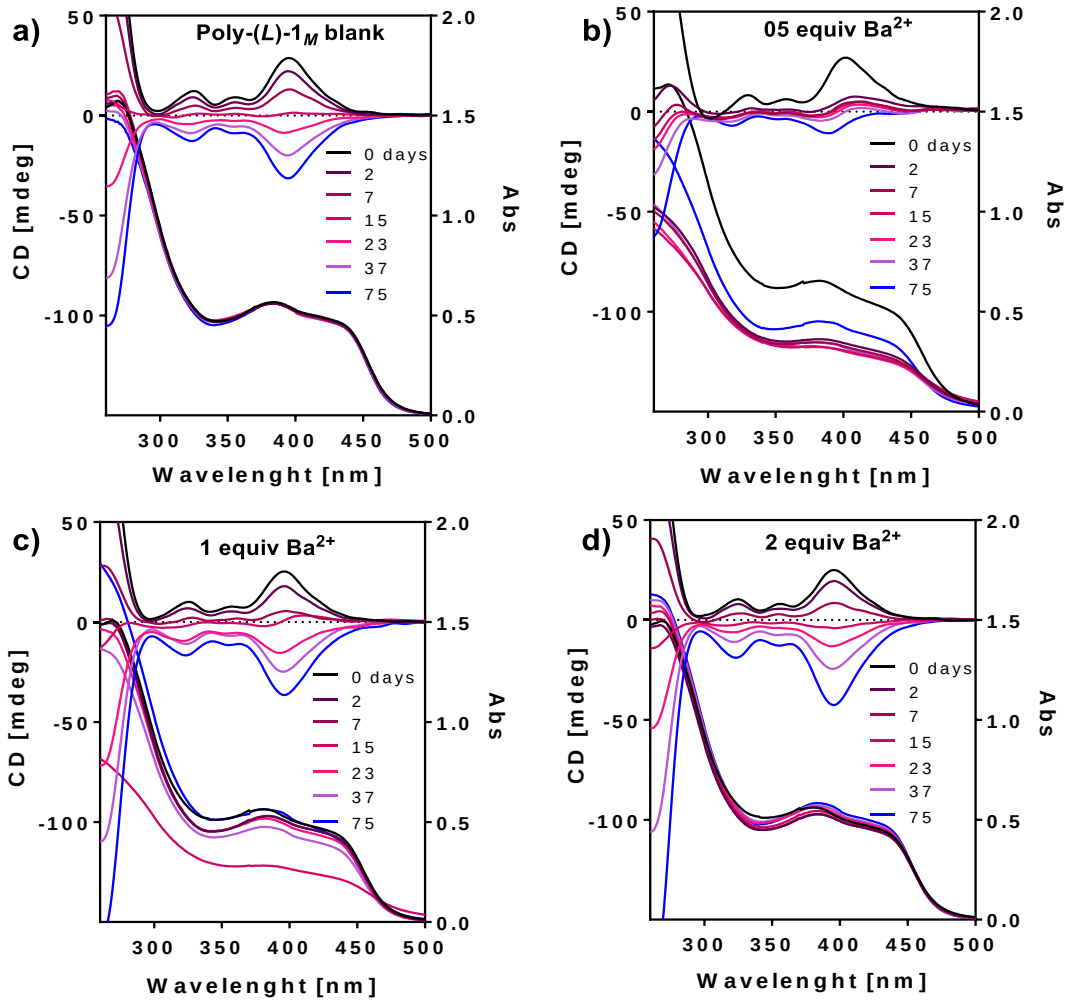

Figure S10: CD and UV spectra of Poly-(*L*)-**1**$_M$ solutions in DCE (0.5 mg/mL) with: a) 200 µL MeOH, b) 0.5 equiv $Ba(ClO_4)_2$, c) 1 equiv $Ba(ClO_4)_2$ and d) 2 equiv $Ba(ClO_4)_2$.

10. Normalized I_{CD}/I_{UV} of Poly-(*L*)-1_M solutions with Li^+

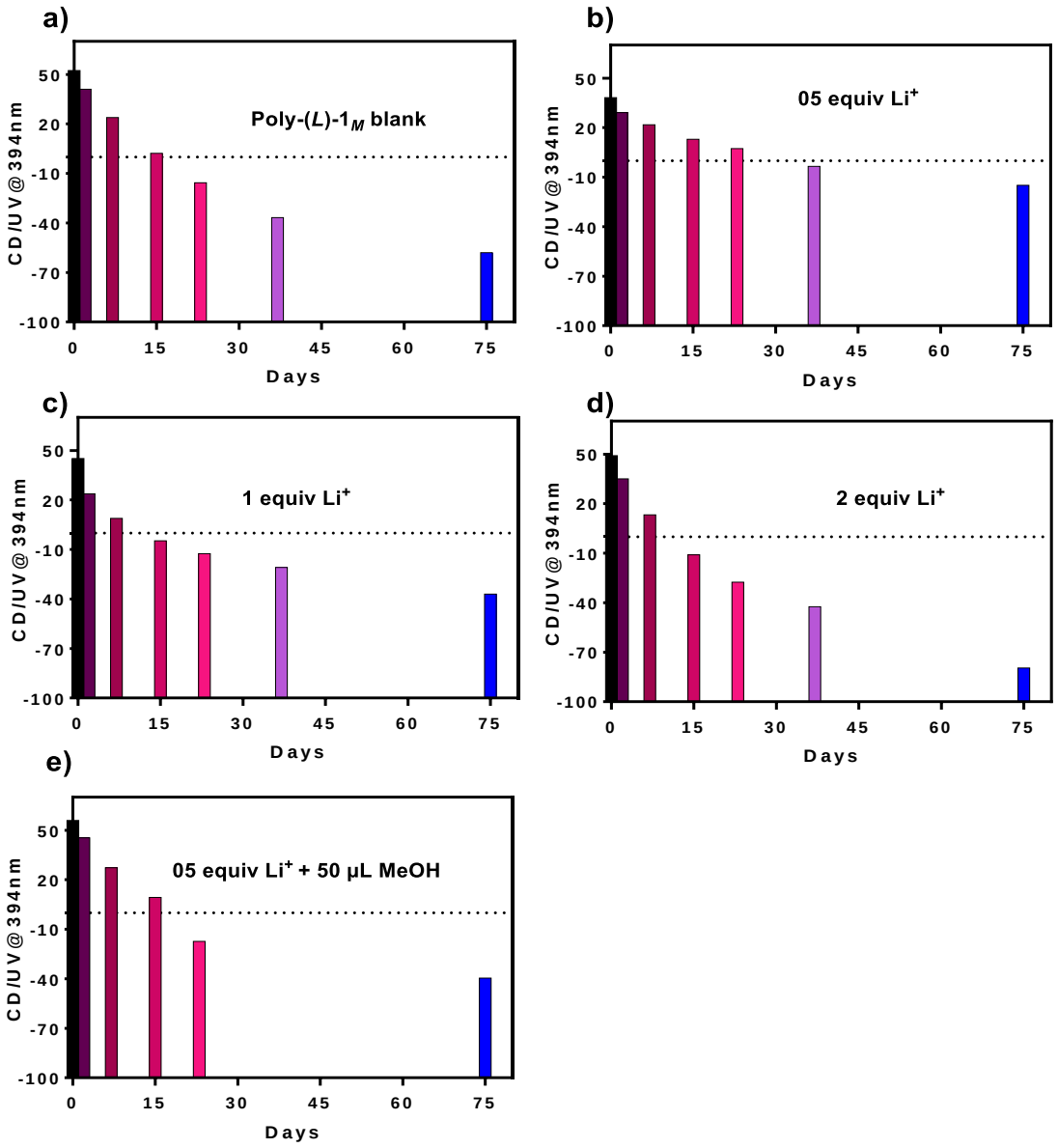

Figure S11: I_{CD}/I_{UV} spectra of Poly-(*L*)-**1**$_M$ solutions in DCE (0.5 mg/mL) with: a) 200 µL MeOH, b) 0.5 equiv $LiClO_4$, c) 1 equiv $LiClO_4$, d) 2 equiv $LiClO_4$ and e) 0.5 equiv $LiClO_4$ + 50 µL of MeOH.

11. Normalized I_{CD}/I_{UV} of Poly-(*L*)-1_M solutions with Ba^{2+}

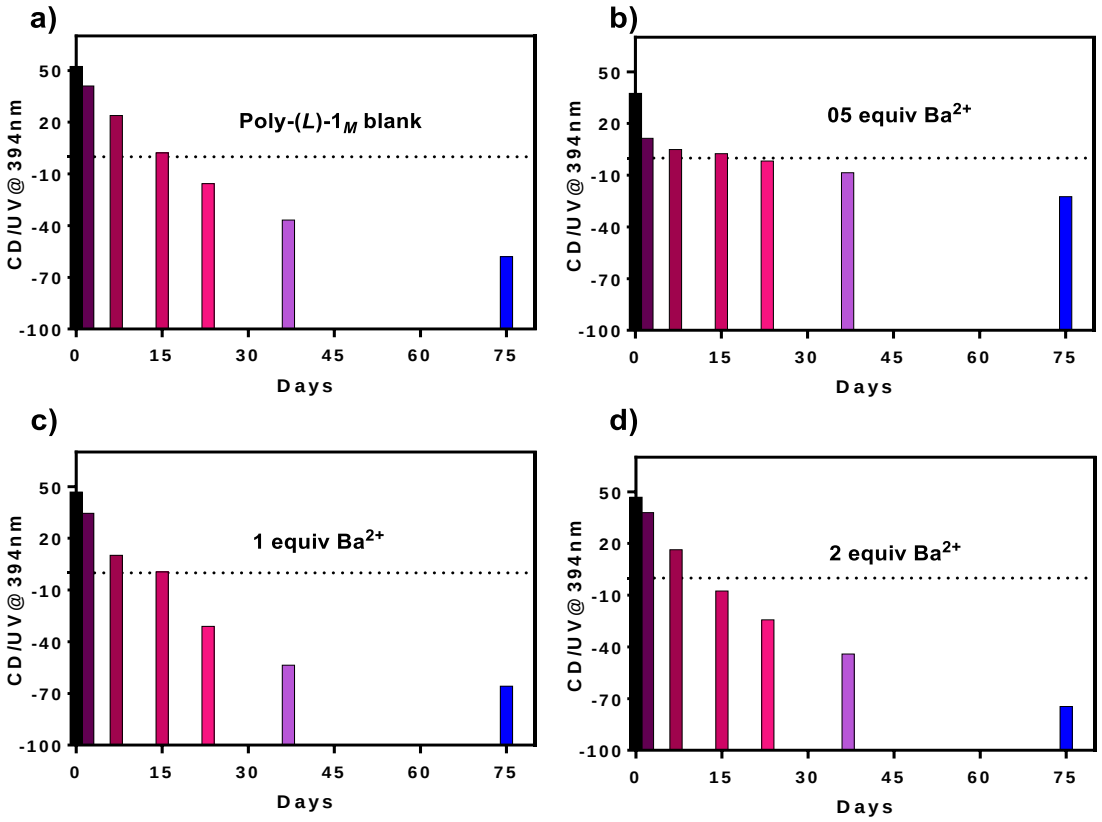

Figure S12: I_{CD}/I_{UV} spectra of Poly-(*L*)-**1**$_M$ solutions in DCE (0.5 mg/mL) with: a) 200 µL MeOH, b) 0.5 equiv $Ba(ClO_4)_2$, c) 1 equiv $Ba(ClO_4)_2$ and d) 2 equiv $Ba(ClO_4)_2$.

12. CD studies of Poly-(*L*)-1$_M$ in THF

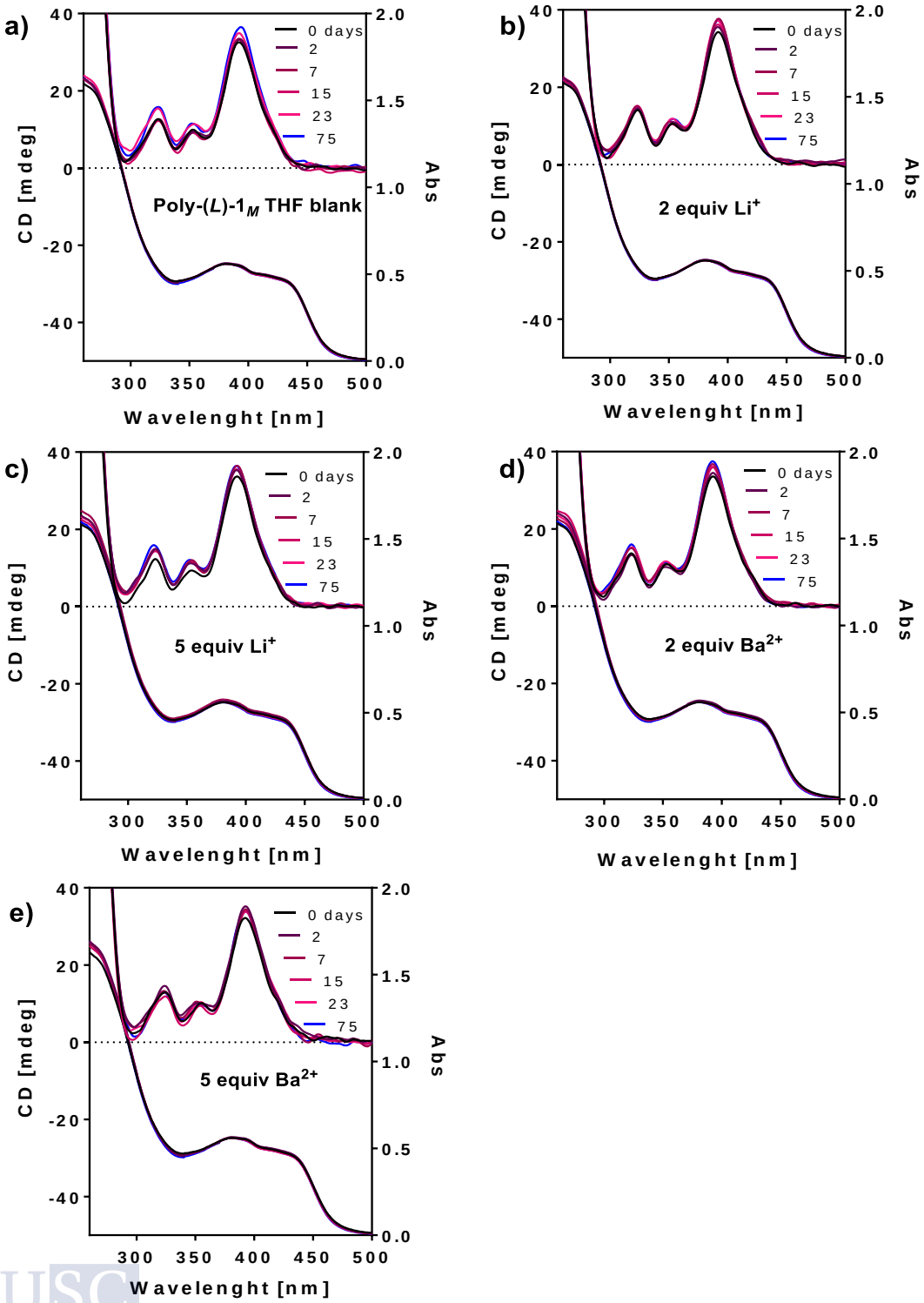

Figure S13: CD and UV spectra of Poly-(*L*)-**1**$_M$ solutions in THF (0.5 mg/mL) with: a) 500 µL MeOH, b) 2 equiv $LiClO_4$, c) 5 equiv $LiClO_4$, d) 2 equiv $Ba(ClO_4)_2$ and e) 5 equiv $Ba(ClO_4)_2$.

13. Normalized I_{CD}/I_{UV} of Poly-(*L*)-1_M in THF

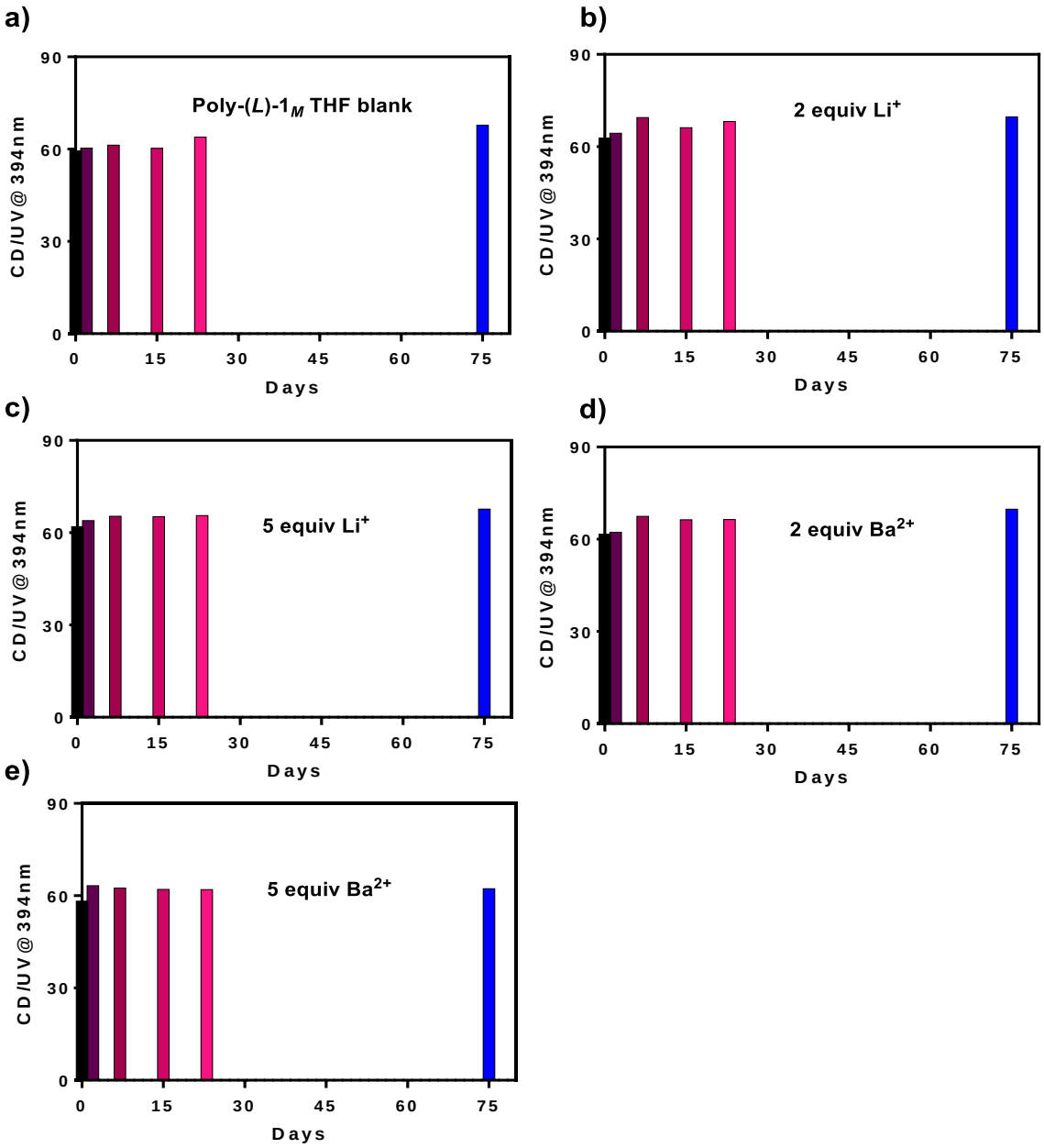

Figure S14: I_{CD}/I_{UV} spectra of Poly-(*L*)-**1**$_M$ solutions in THF (0.5 mg/mL) with: a) 500 µL MeOH, b) 2 equiv $LiClO_4$, c) 5 equiv $LiClO_4$, d) 2 equiv $Ba(ClO_4)_2$ and e) 5 equiv $Ba(ClO_4)_2$.

14. IR studies with metals

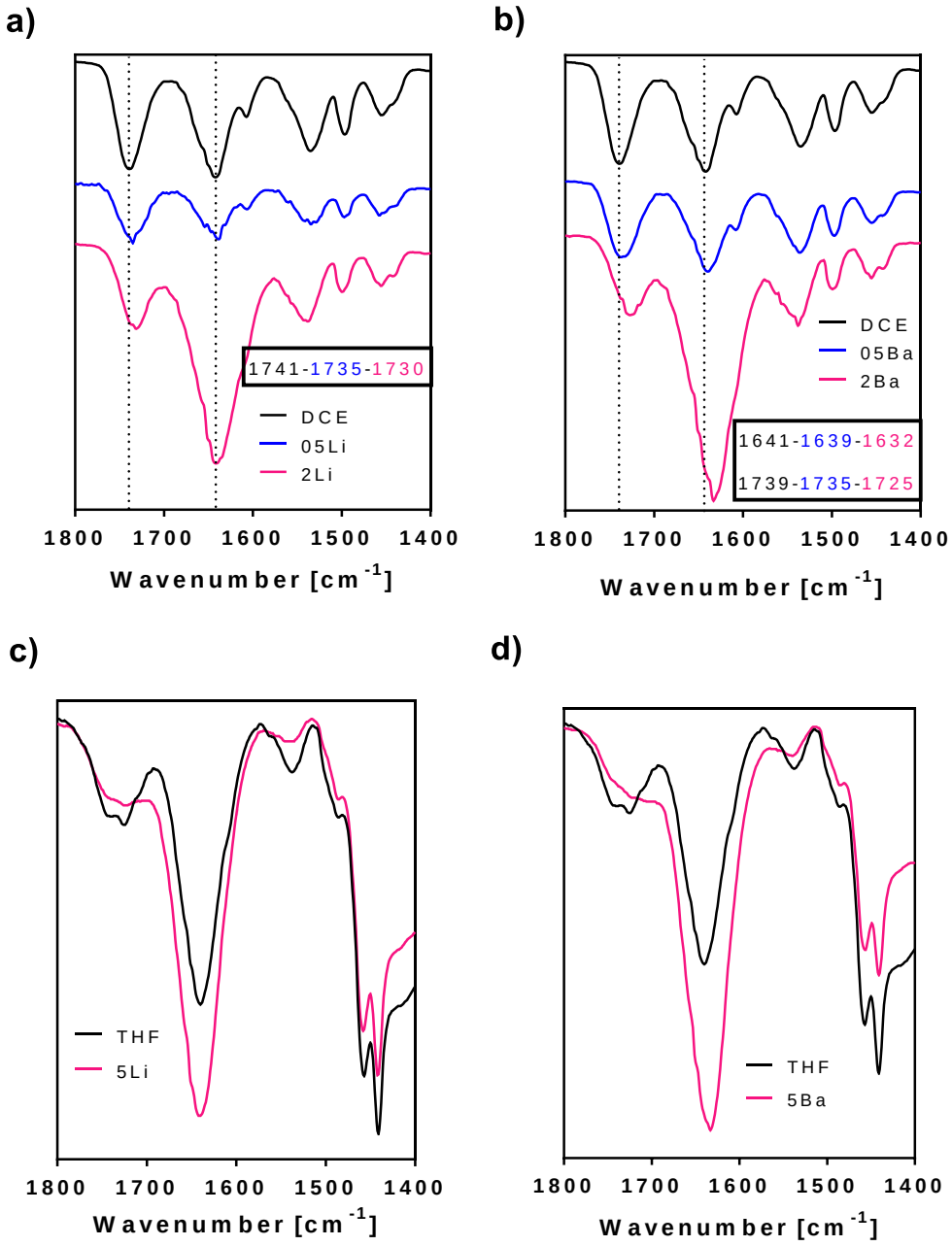

Figure S15: Comparative among several IR studies of Poly-(*L*)-**1** with different amounts of a) $LiClO_4$ and b) $Ba(ClO_4)_2$ in DCE. The same comparative in THF with higher amounts of c) $LiClO_4$ and d) $Ba(ClO_4)_2$.

15. DLS measurements and SEM images of Poly-(*L*)-1 with metals

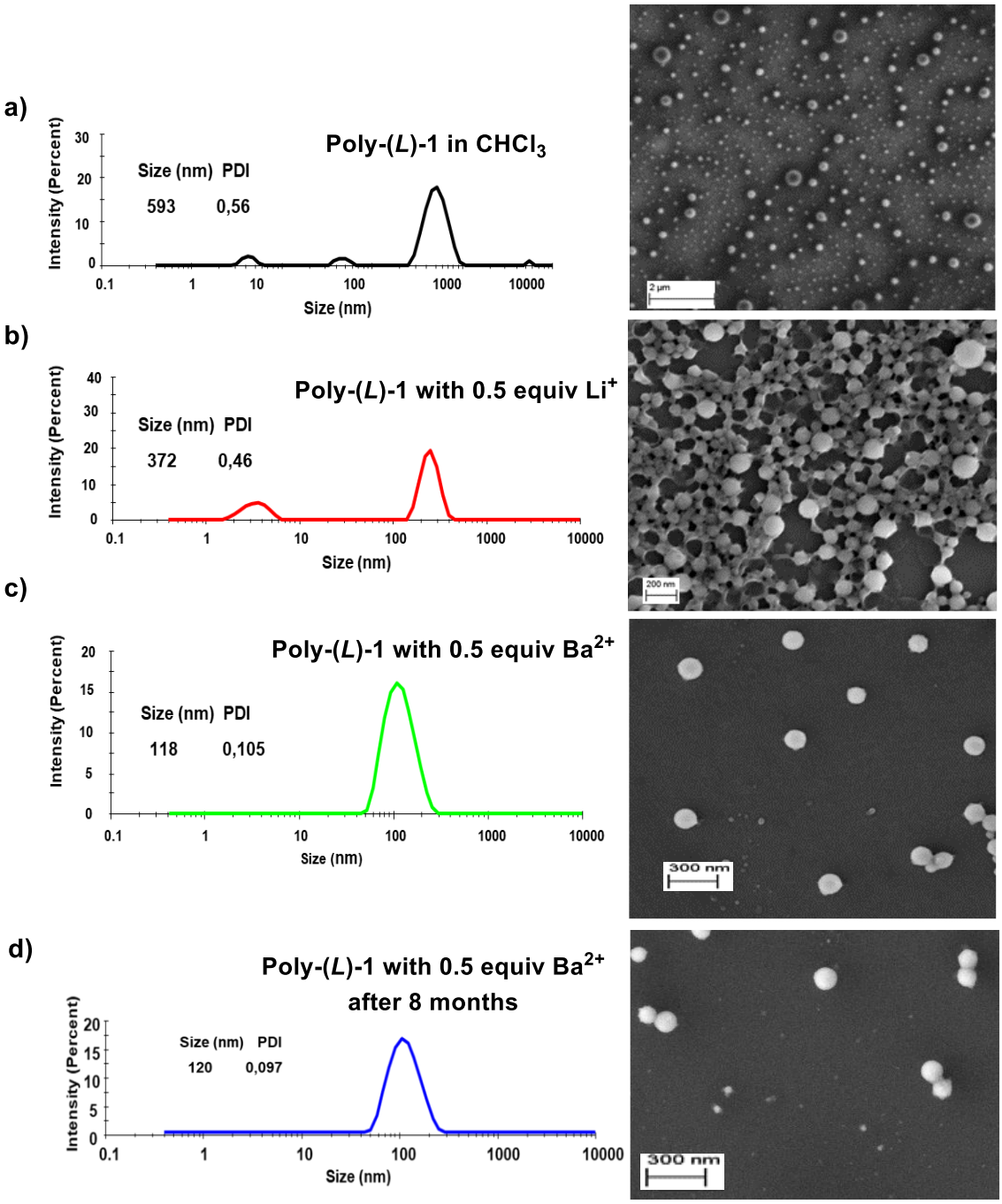

Figure S16: DLS studies and SEM images of Poly-(*L*)-**1** with different metals.

16. Supporting References

S1. Tarrío, J. J.; Rodríguez, R.; Fernández, B.; Quiñoá, E.; Freire, F. Dissymmetric Chiral Poly (diphenylacetylene) s: Secondary Structure Elucidation and Dynamic Luminescence. *Angew. Chem. Int. Ed.*, **2022**, *61*, e202115070.

Experimental Section Chapter VII

1. Materials and Methods

CD measurements were done in a Jasco-720. The amounts of polymer used for CD measurements were 0.5 mg/mL in DCM, 1,2-DCE, $CHCl_3$, THF, Acetone, MeCN, Dioxane, DMF and DMSO.

UV spectra were registered in a Jasco V-630. The amounts of polymer used for UV measurements were 0.5 mg/mL in DCM, 1,2-DCE, $CHCl_3$, THF, Acetone, MeCN, Dioxane, DMF and DMSO.

GPC studies were carried out in a Waters Alliance equipped with Phenomenex GPC columns. The amount of polymer used for GPC measurements was 0.5 mg/mL.

CPL spectra were recorded on a Jasco CPL-300 at a scanning rate of 100nm/min over an average of 5 scans, using a 10 mm quartz cell.

2. Synthesis of monomers

The synthesis of *p*-M-**1** was made following the steps depicted in the SI of Ref. **S1**. An example of the synthesis of *m*-M-**1** is depicted bellow.

Perfluorophenyl 4-iodobenzoate

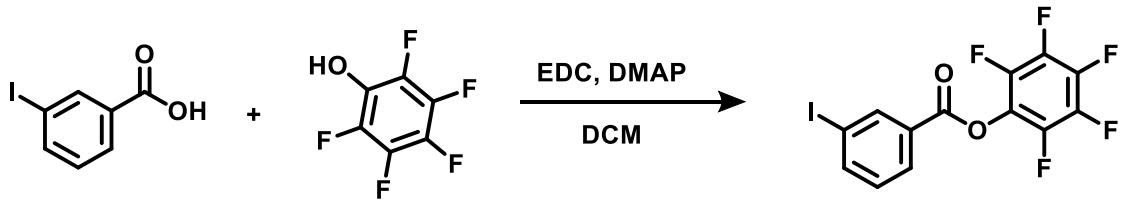

1 **2** **3**

3-iodobenzoic acid (**1**, 1.48 g, 5.97 mmol), EDC (1.19 g, 6.24 mmol), DMAP (0.073 g, 0.6 mmol) and 50 mL dry DCM were added into a 250 mL flask. After activation, pentafluorophenol (**2**, 1.00 g, 5.43 mmol) was added. The mixture was stirred at rt for 12 h and a white precipitate was formed. Then, the solid was filtrated and washed with hexane. After concentration in a rotary evaporator, the crude product was purified by silica gel column chromatography (40-63 mesh) using a mixture of hexane and ethyl acetate (95:5 by volume) as eluent. After evaporation of solvents in a rotary evaporator, a white solid was obtained in 76% yield.

^{1}H NMR (300MHz, $CDCl_3$) δ (ppm): 8.52 (1H, s), 8.16 (1H, d), 8.01 (1H, d), 7.28 (1H, t)

^{19}F NMR (282.3 MHz, $CHCl_3$) δ (ppm): -152.4, -157.7, -162.2

^{13}C NMR (75MHz, $CDCl_3$) δ (ppm): 161.1, 143.4, 141.3, 139.3, 138.0, 136.3, 130.4, 129.7, 128.7, 125.2, 94.0.

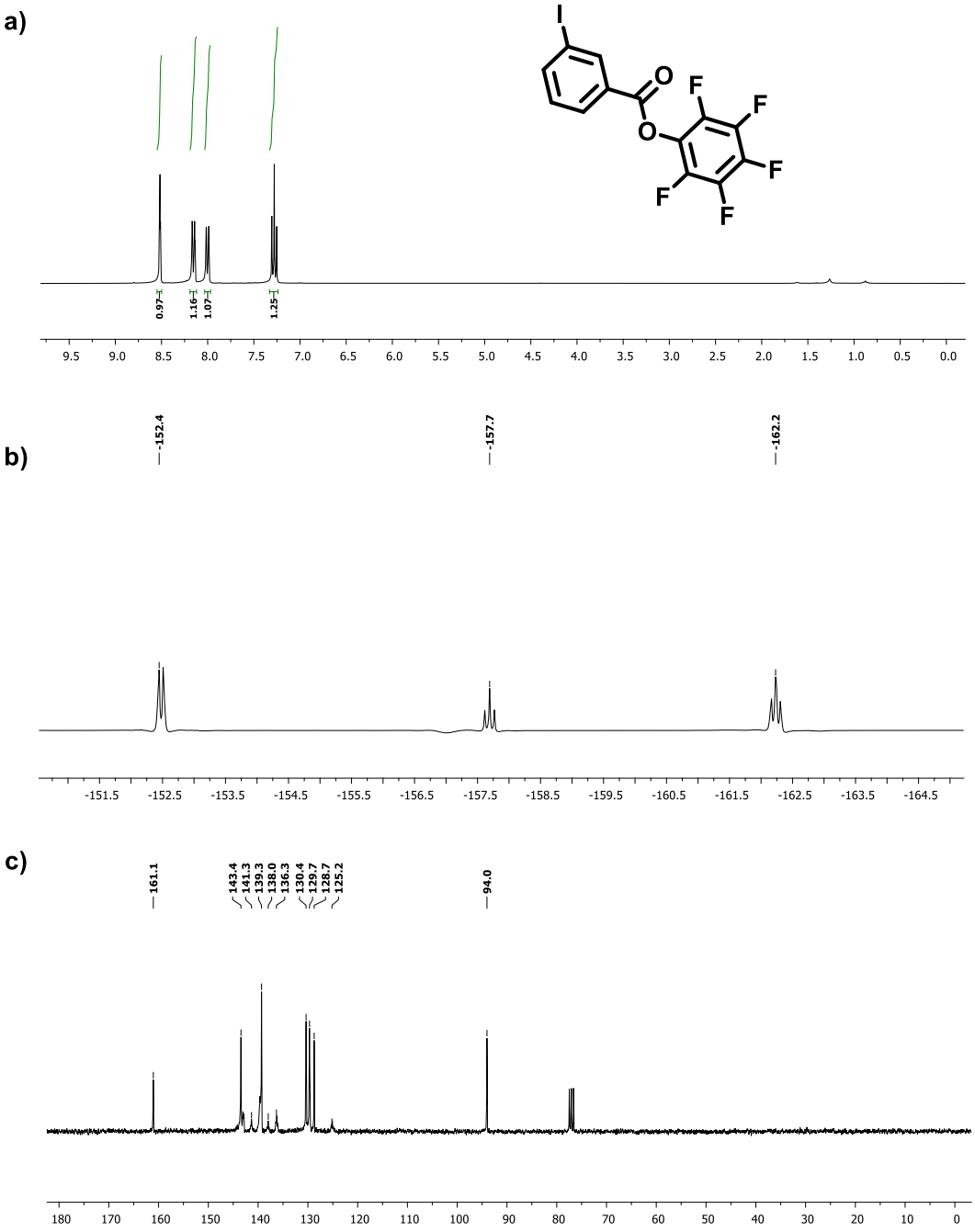

Figure S1. a) 1H, b) 19F and c) 13C NMR spectra of **3** (perfluorophenyl 3-iodobenzoate).

Perfluorophenyl 4-(phenylethynyl)benzoate

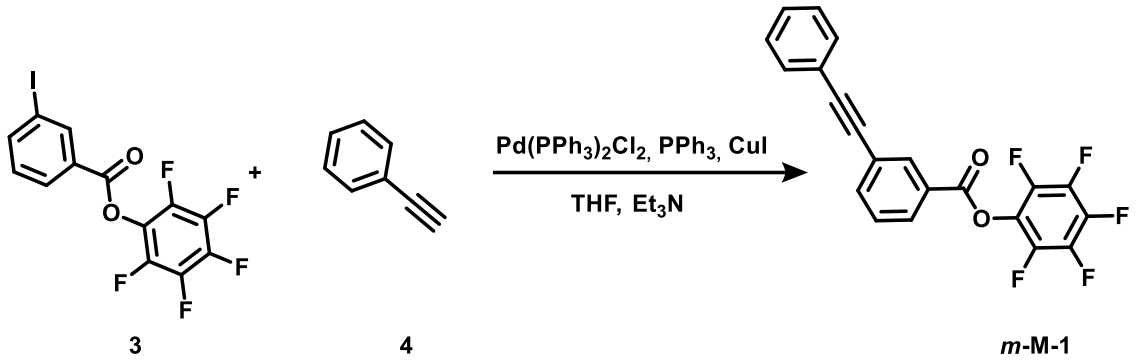

3 **4** ***m*-M-1**

Perfluorophenyl 3-iodobenzoate (**3**, 1.7 g, 4.1 mmol), $PdCl_2(PPh_3)_2$ (143 mg, 0.205 mmol), CuI (78 mg, 0.41 mmol), PPh_3 (107 mg, 0.41 mmol) were added to 20 mL of THF and 2.7 mL of Et_3N (20.5 mmol) under nitrogen. After the catalysts was completely dissolved, phenylacetylene (0.67 mL, 6.15 mmol) was injected into the flask and the mixture was stirred at rt for 24 h. The solid was removed by filtration and washed with diethyl ether. The filtrate was then concentrated in a rotary evaporator. The crude product was purified by silica gel column chromatography (40-63 mesh) using a mixture of hexane and ethyl acetate (95:5 by volume) as eluent. *m*-**M-1** was obtained as a white solid in 67% yield.

1H NMR (300MHz, $CDCl_3$, δ, TMS, ppm): 8.39 (1H, s), 8.15 (1H, d), 7.85 (1H, d), 7.60 (2H, m), 7.53 (1H, t), 7.39 (3H, m).

^{19}F NMR (282.3 MHz, $CHCl_3$) δ (ppm): -152.4, -157.8, -162.3

^{13}C NMR 75 MHz, $CDCl_3$, δ, TMS, ppm): 162.0, 137.3, 133.6, 131.7, 130.0, 129.0, 128.8, 128.4, 127.3, 124.5, 122.6, 91.1, 87.6

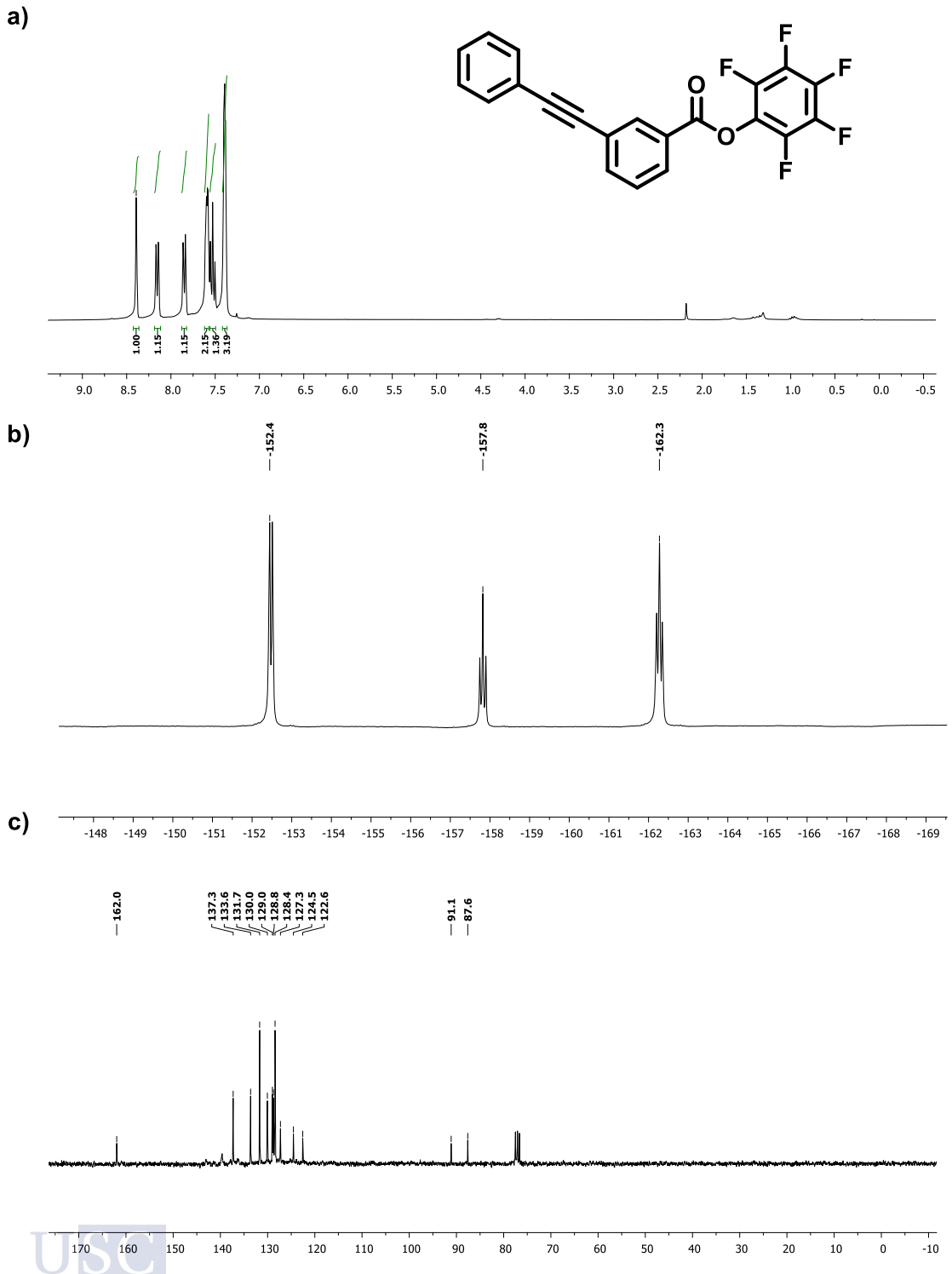

Figure S2. a) ^{1}H, b) ^{19}F and c) ^{13}C NMR spectra of *m*-M-**1**.

3. Synthesis of Polymers

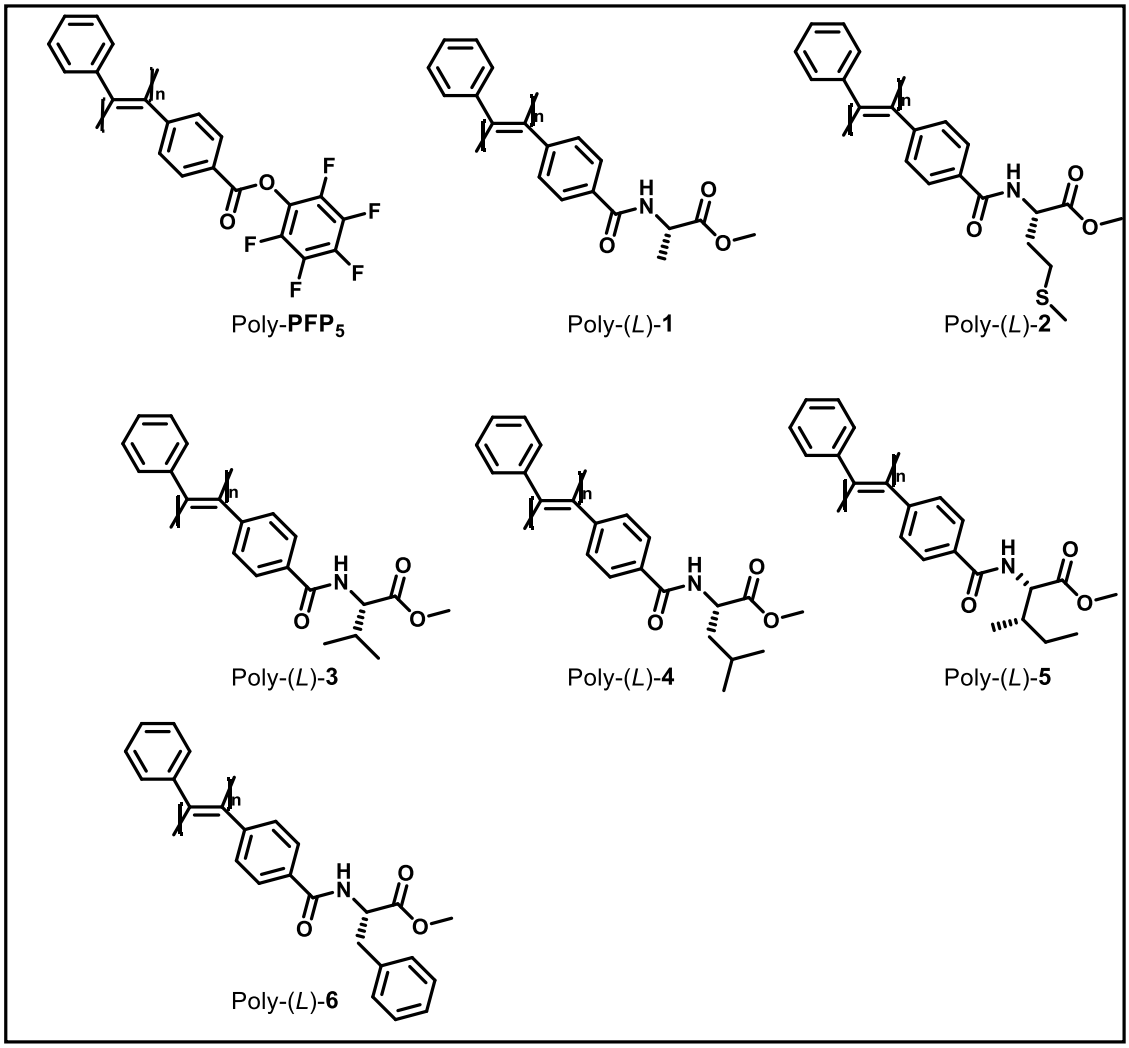

Figure S3: Structure of the *para*-substituted polymers synthesized in this work.

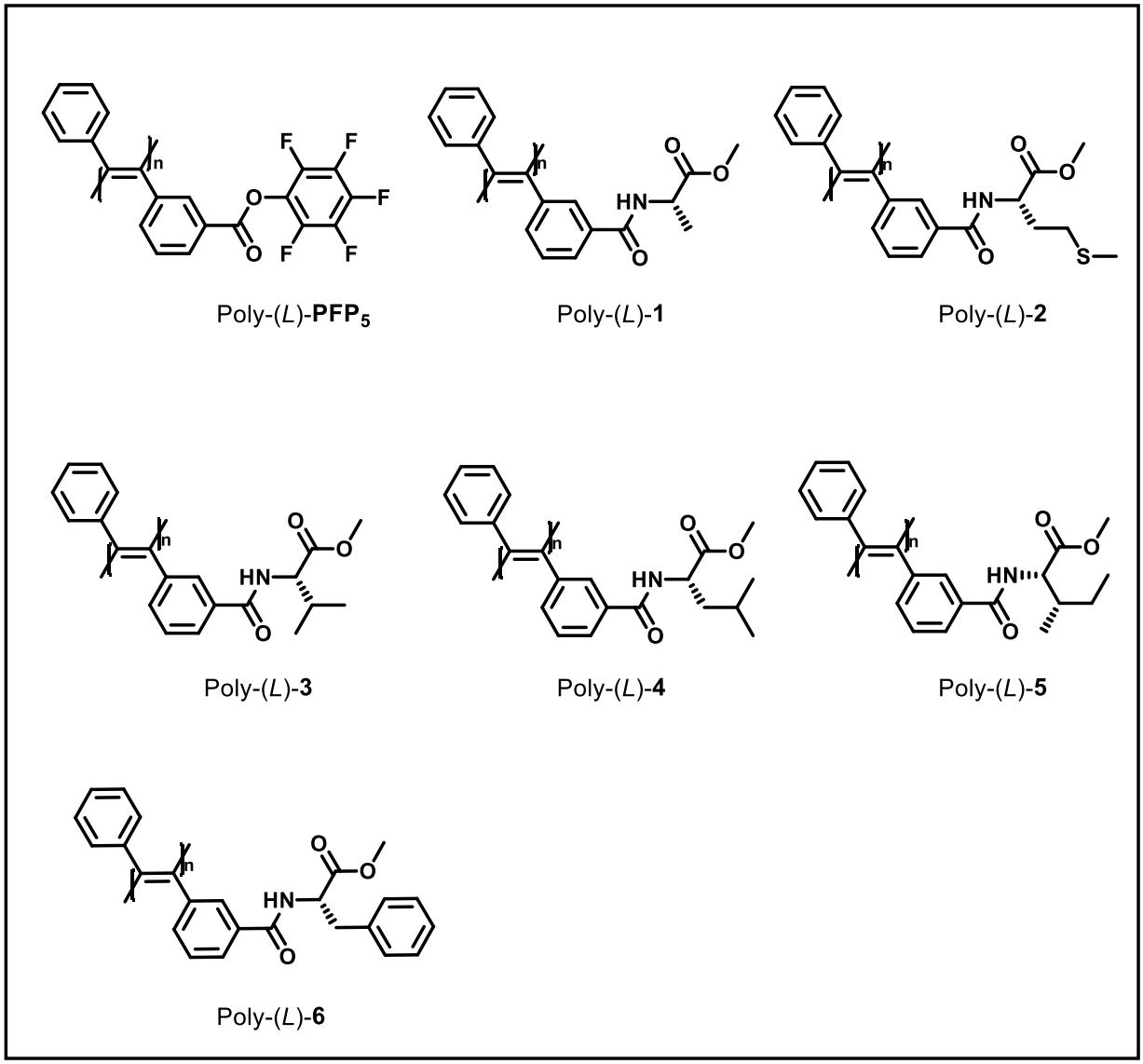

Figure S4: Structure of the *meta*-substituted polymers synthesized in this work.

Trans Polymerization Reaction

The polymerization reaction was carried out under a nitrogen atmosphere using standard Schlenk technique, unless otherwise specified. A typical procedure for the polymerization of *m*-M-**1** is given below as an example following the conditions of Ref. **S1**.

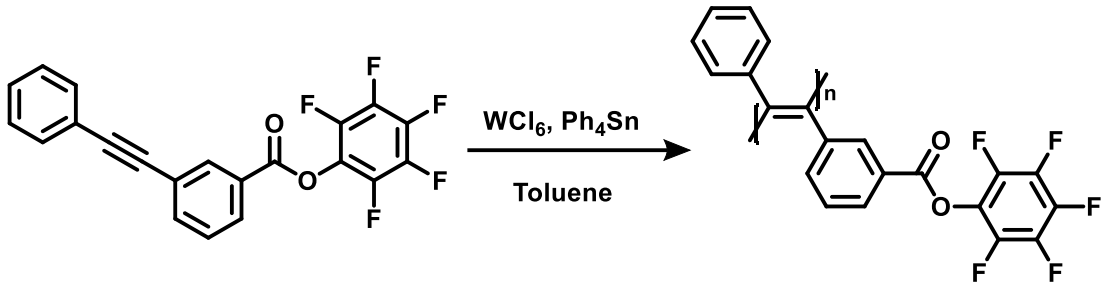

***m*-M-1** ***m*-Poly-PFP$_5$**

20.4 mg of WCl_6 and 44.0 mg of Ph_4Sn were added into a baked 10 mL Schlenk tube with a stopcock in the side arm. The tube was evacuated under vacuum and then flushed with dry nitrogen three times through the side arm. Freshly distilled toluene (1 mL) was injected into the tube to dissolve the mixture of catalysts and then, the catalyst solution was aged at 100 °C for 10 min. The monomer solution was prepared in another tube by dissolving 200 mg of *m*-**M-1** in 1.6 mL of toluene and was transferred to the catalyst solution using a hypodermic syringe. The reaction mixture was stirred at 100 °C for 24 h. The solution was cooled to rt, diluted with CH_2Cl_2 and then precipitated in a large amount of methanol. The precipitate was allowed to stand overnight and then collected by filtration. The polymer was washed with methanol and hexane and dried under vacuum at room temperature to a constant weight. *m*-Poly-**PFP$_5$** was obtained as a brown solid in 71% yield.

^{1}H-NMR (300MHz, $CDCl_3$), δ (TMS, ppm): 7.70-7.30, 7.06-6.05, 6.05-5.55.

^{19}F NMR (282.3MHz, $CDCl_3$), δ (TMS, ppm): -153.4, -157.6, -162.6.

Post-polymerization Coupling

The post-polymerization reaction was carried out using standard peptide coupling conditions. A typical procedure for the coupling of alanine methyl ester is given below as an example following the conditions of Ref. **S1**. Other amino acids are coupled following the same conditions.

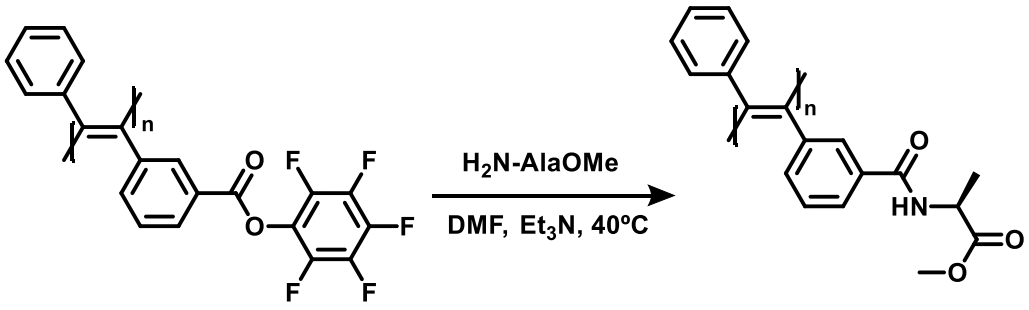

***m*-Poly-1** ***m*-Poly-2**

20 mg (0.052 mmol) of *m*-Poly-**1**, 8.6 mg (0.062 mmol) of *L*-alanine methyl ester hydrochloride and 2 mL dry DMF with a drop of TEA were added into a 10 mL reaction tube with magnetic stirring bar under nitrogen. The reaction solution was stirred for 12 h at 40 °C. Next, the solution mixture was added dropwise to 300 mL methanol through a cotton filter under vigilant stirring. The precipitate was kept still overnight and then filtered. The obtained polymer was washed with water and hexane several times and dried at rt to a constant weight. *m*-Poly-**2** was obtained as a yellow solid in 89 % yield.

^{1}H NMR (300 MHz, $CDCl_3$), δ (TMS, ppm): 7.73, 6.92, 6.48, 5.98, 4.59, 3.74, 1.42.

^{19}F NMR (282.3 MHz, $CDCl_3$), δ (TMS, ppm): no signals.

4. ^{1}H and ^{19}F NMR experiments of the polymers

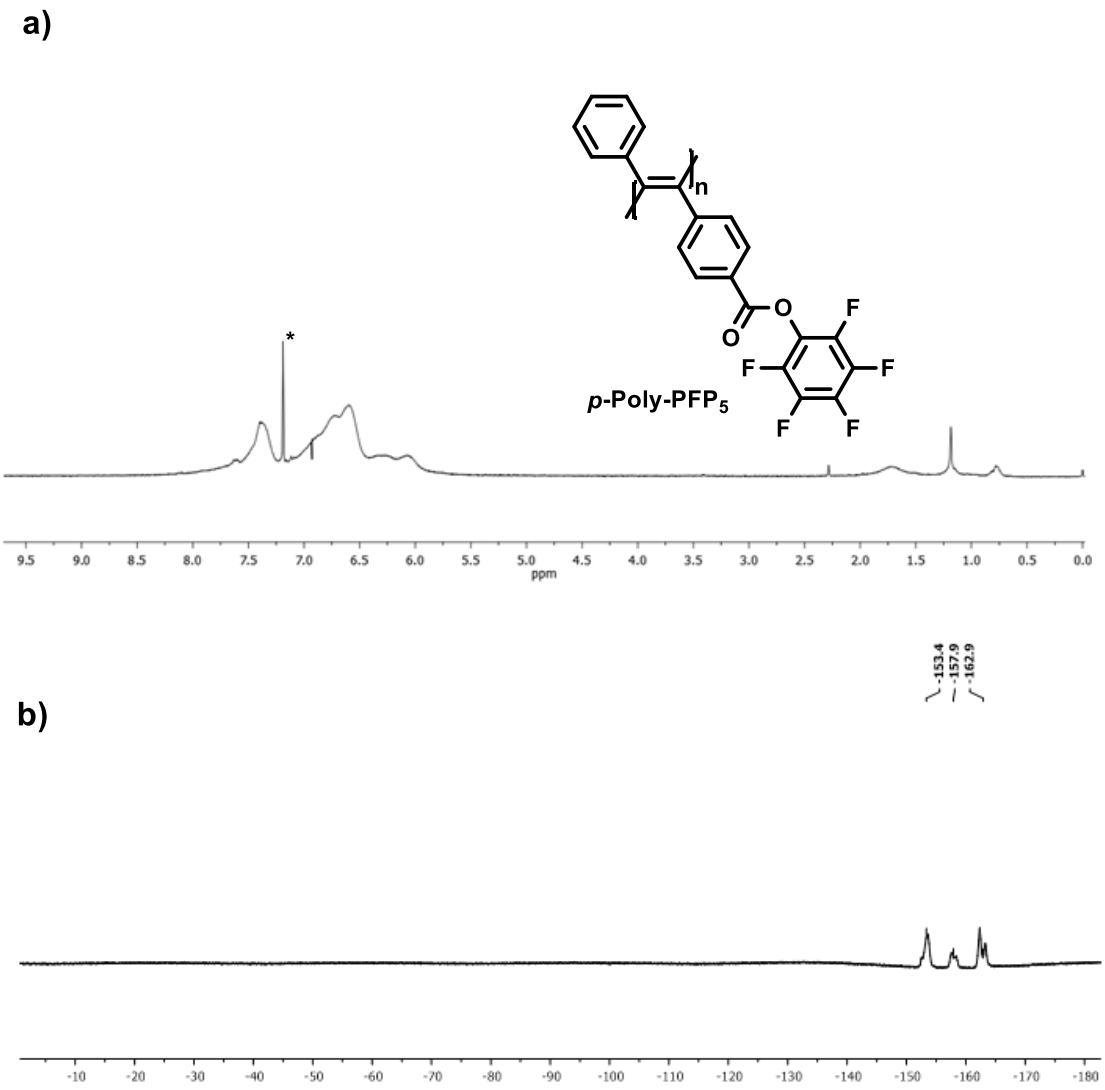

Figure S5. a) ^{1}H-NMR and b) ^{19}F-NMR spectra of *p*-Poly-**PFP$_5$**.

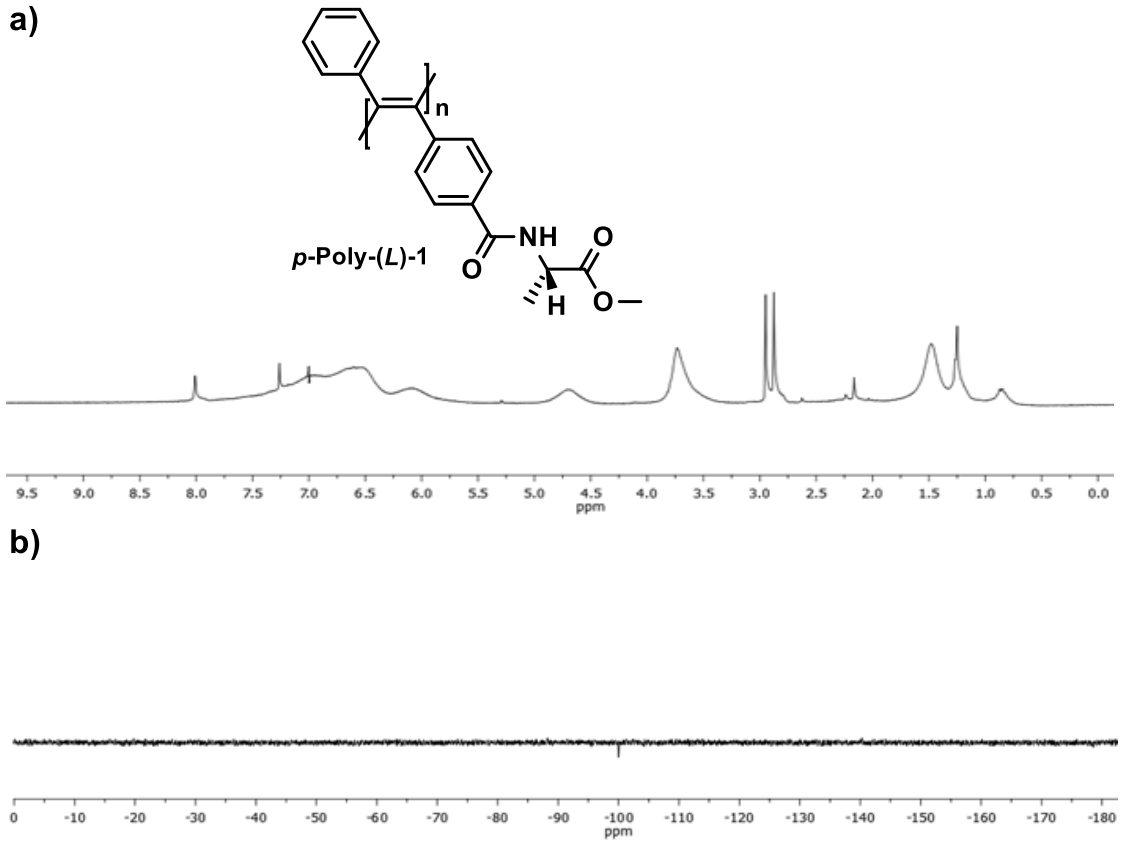

Figure S6. a) ^{1}H-NMR and b) ^{19}F-NMR spectra of *p*-Poly-(*L*)-**1**.

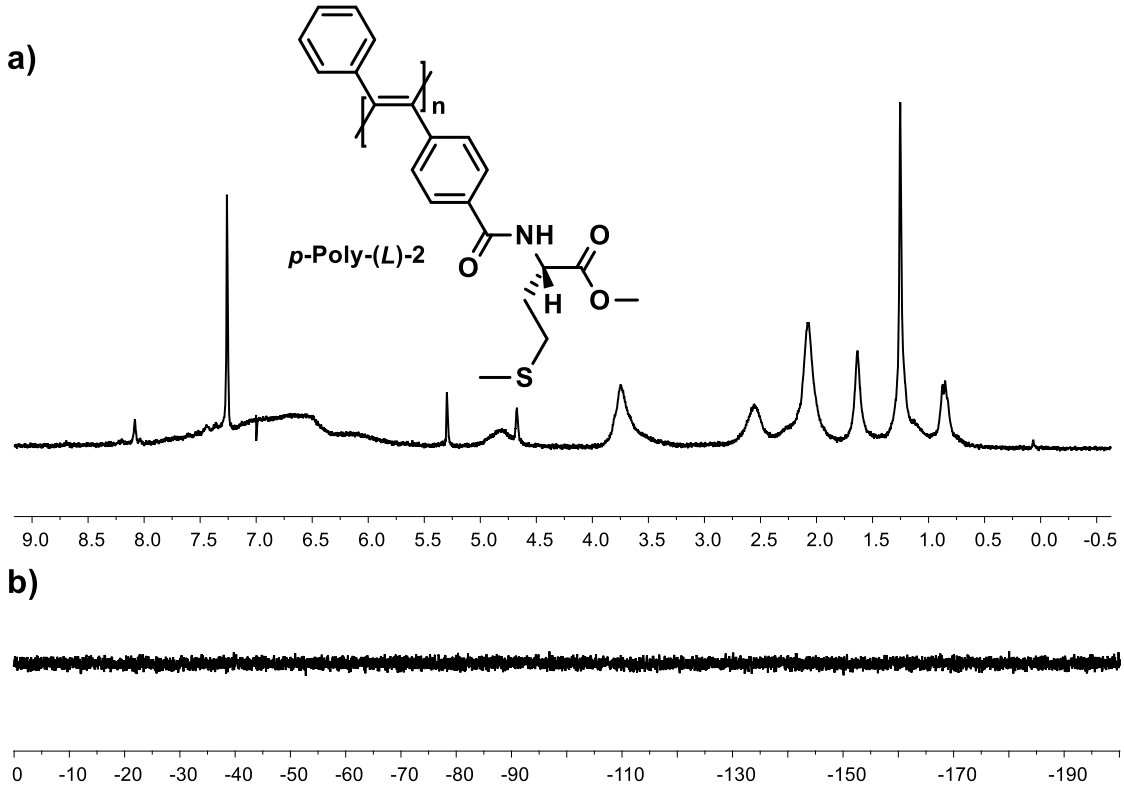

Figure S7. a) ^{1}H-NMR and b) ^{19}F-NMR spectra of *p*-Poly-(*L*)-**2**.

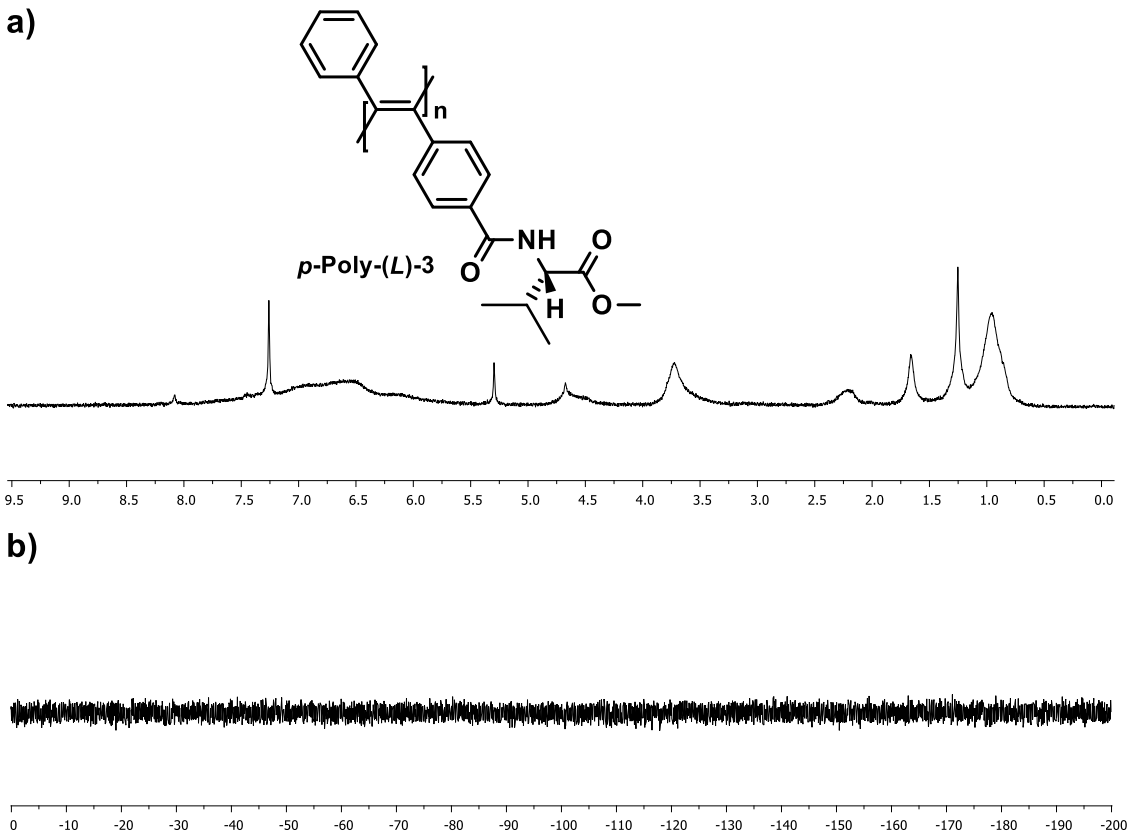

Figure S8. a) ^{1}H-NMR and b) ^{19}F-NMR spectra of *p*-Poly-(*L*)-**3**

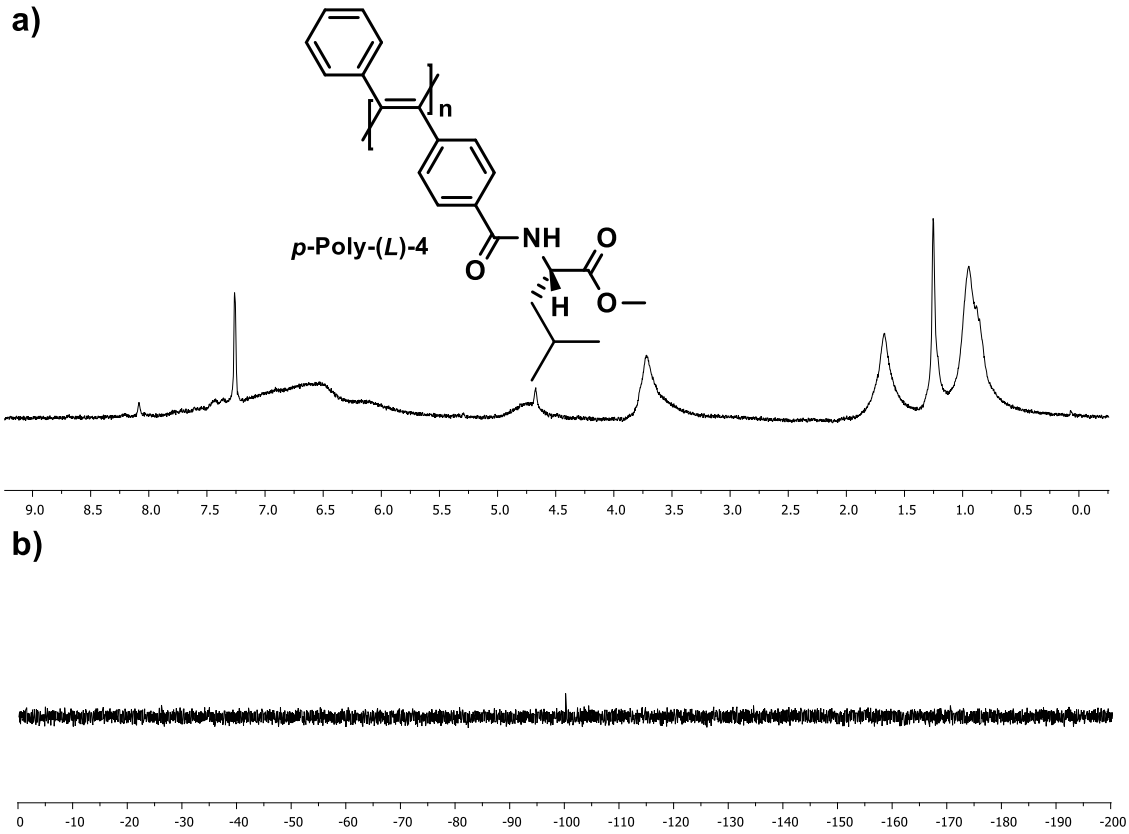

Figure S9. a) ^{1}H-NMR and b) ^{19}F-NMR spectra of *p*-Poly-(*L*)-**4**.

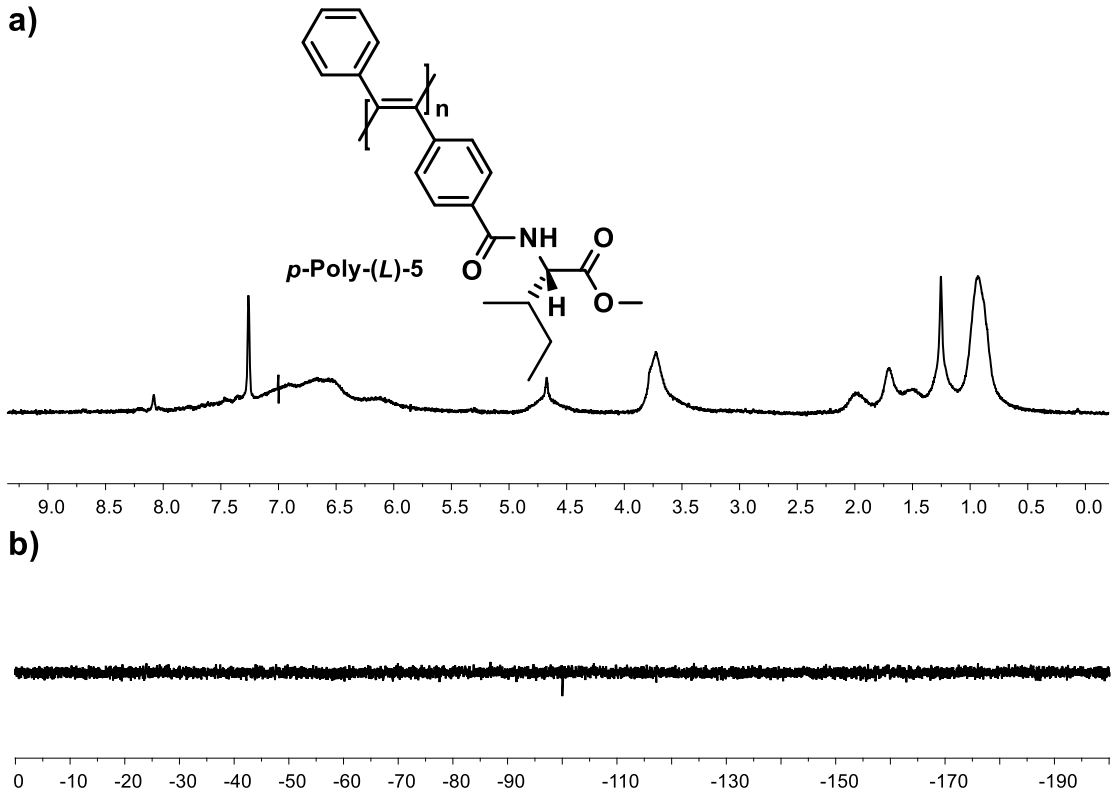

Figure S10. a) ^{1}H-NMR and b) ^{19}F-NMR spectra of *p*-Poly-(*L*)-**5**.

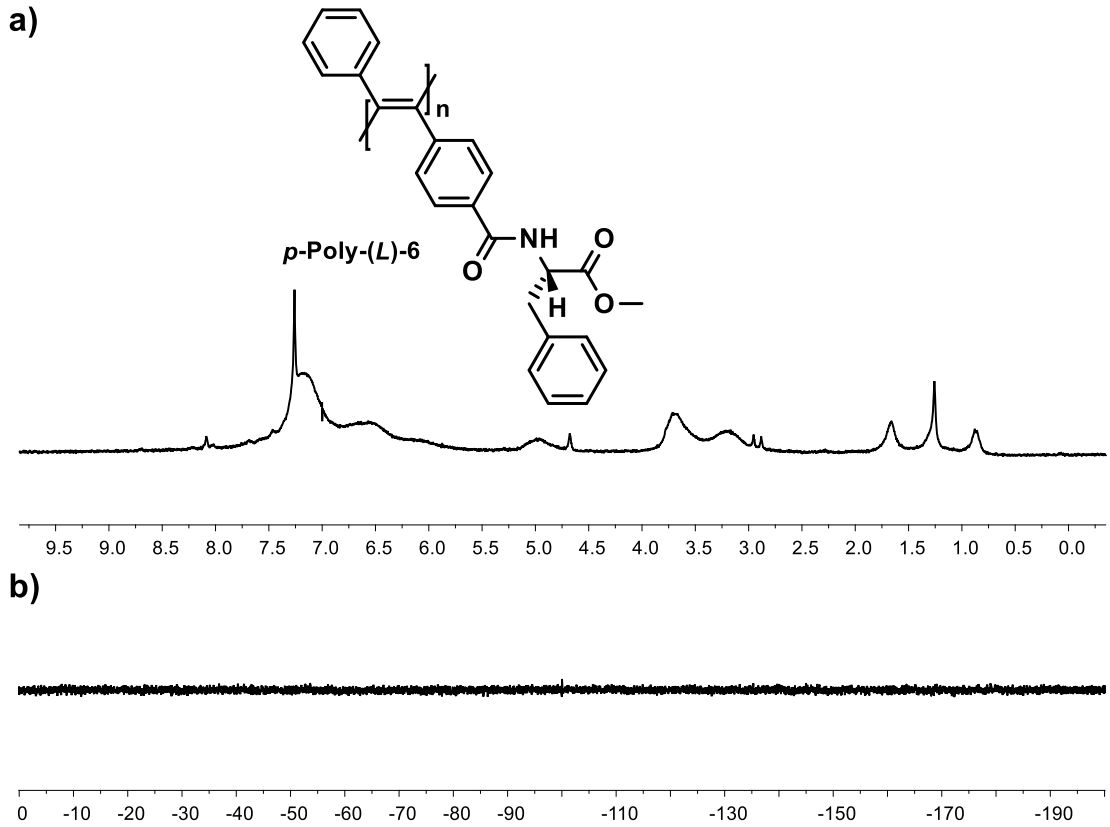

Figure S11. a) ^{1}H-NMR and b) ^{19}F-NMR spectra of *p*-Poly-(*L*)-**6.**

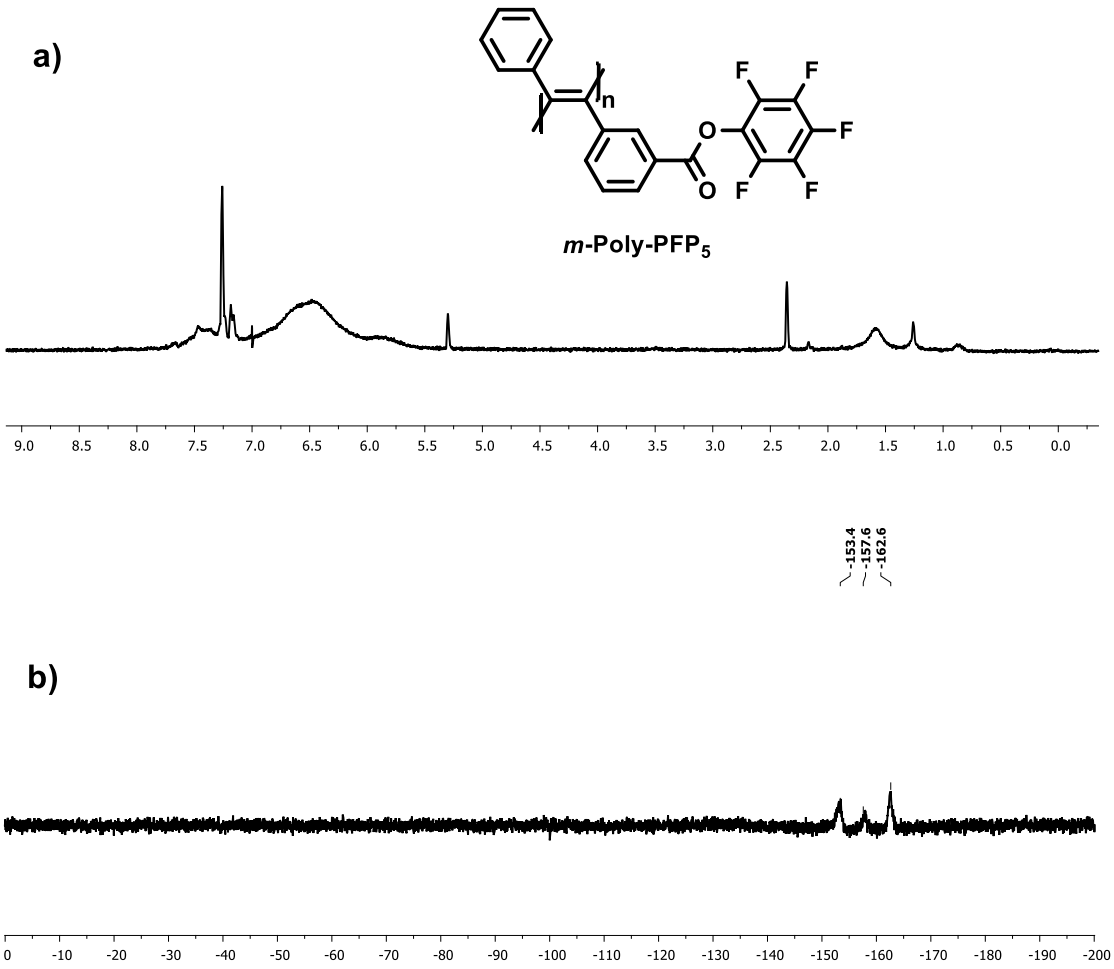

Figure S12. a) ^{1}H-NMR and b) ^{19}F-NMR spectra of *m*-Poly-**PFP$_5$**.

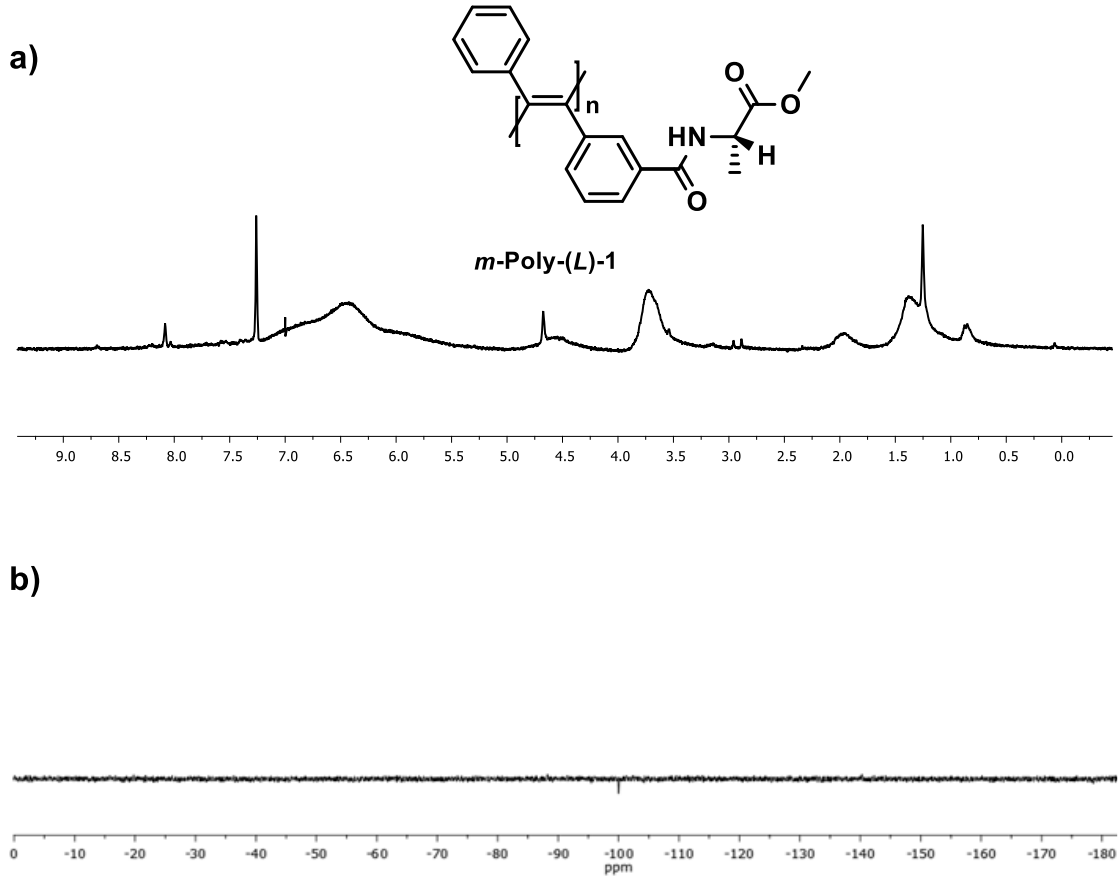

Figure S13. a) ^{1}H-NMR and b) ^{19}F-NMR spectra of *m*-Poly-(*L*)-**1**.

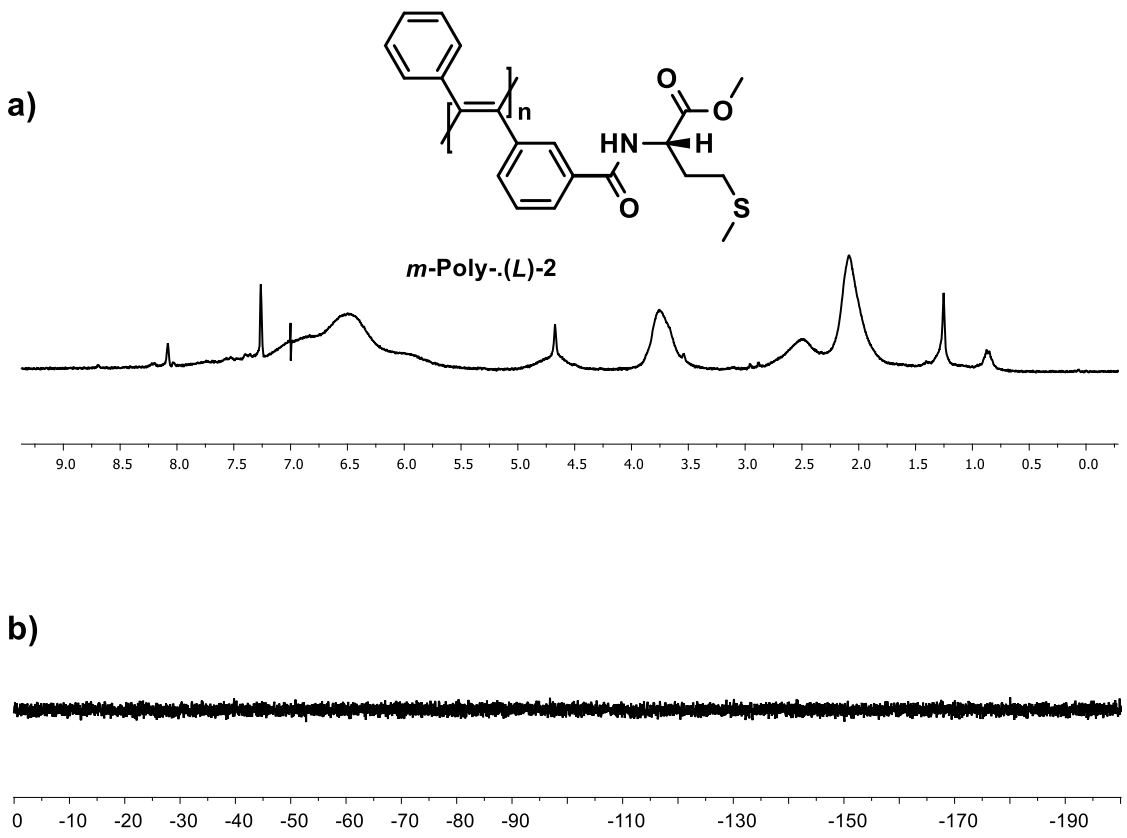

Figure S14. a) ^{1}H-NMR and b) ^{19}F-NMR spectra of *m*-Poly-(*L*)-**2**.

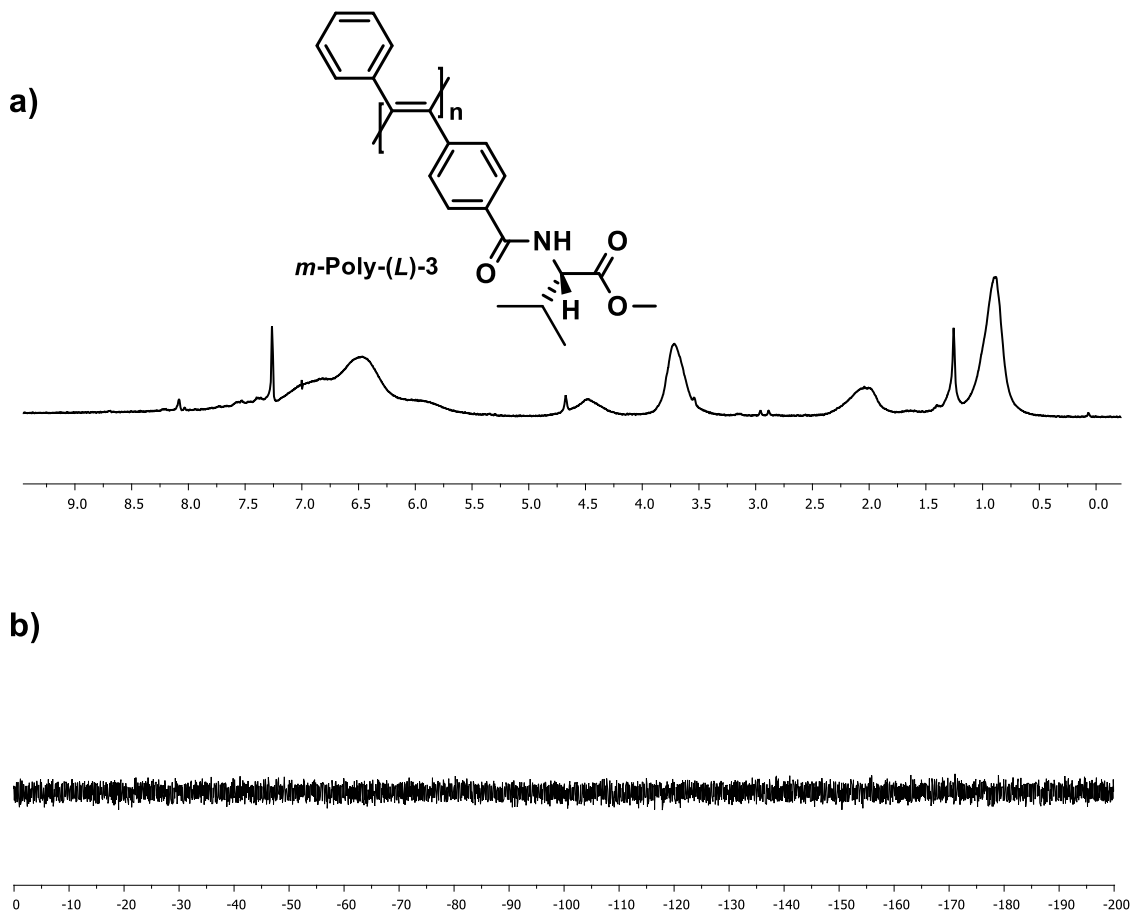

Figure S15. a) ^{1}H-NMR and b) ^{19}F-NMR spectra of *m*-Poly-(*L*)-**3**.

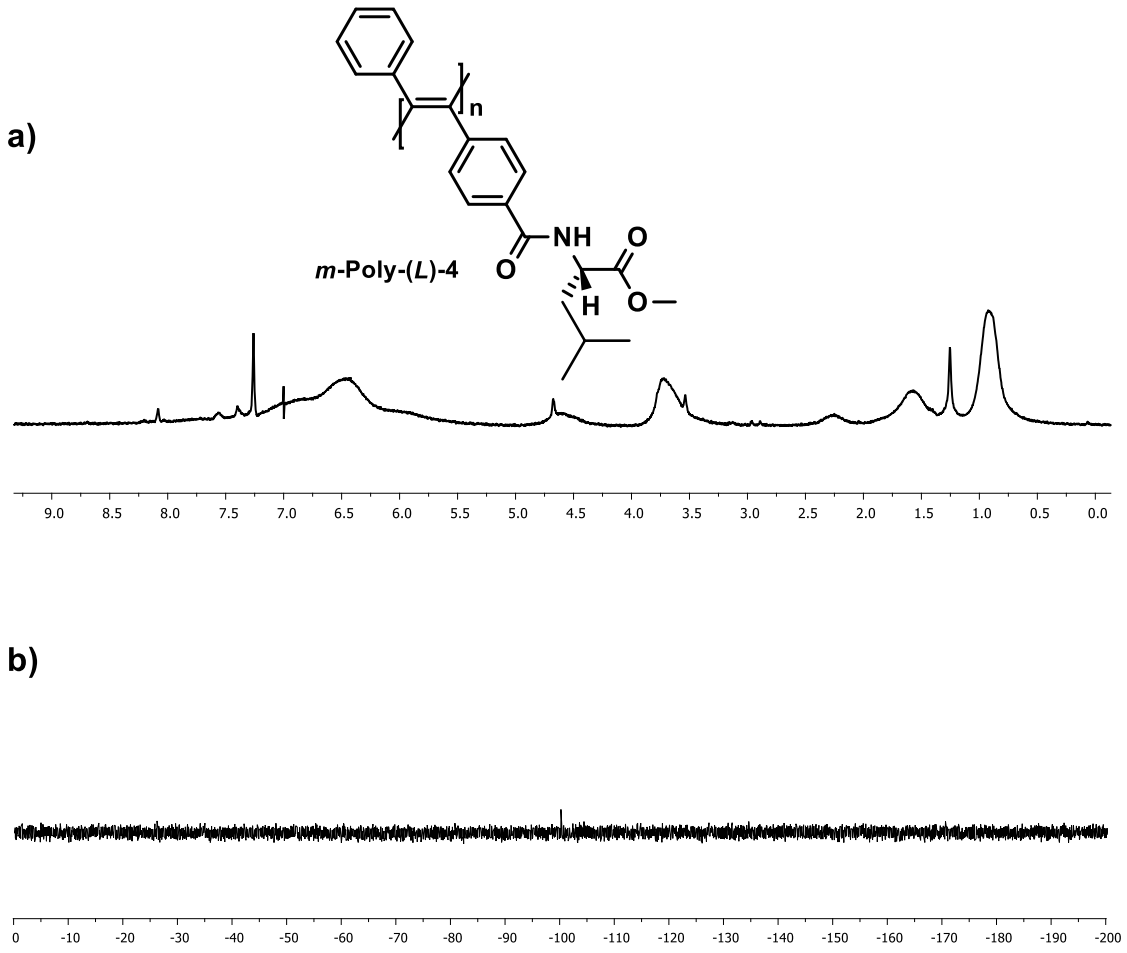

Figure S16. a) ^{1}H-NMR and b) ^{19}F-NMR spectra of *m*-Poly-(*L*)-**4**.

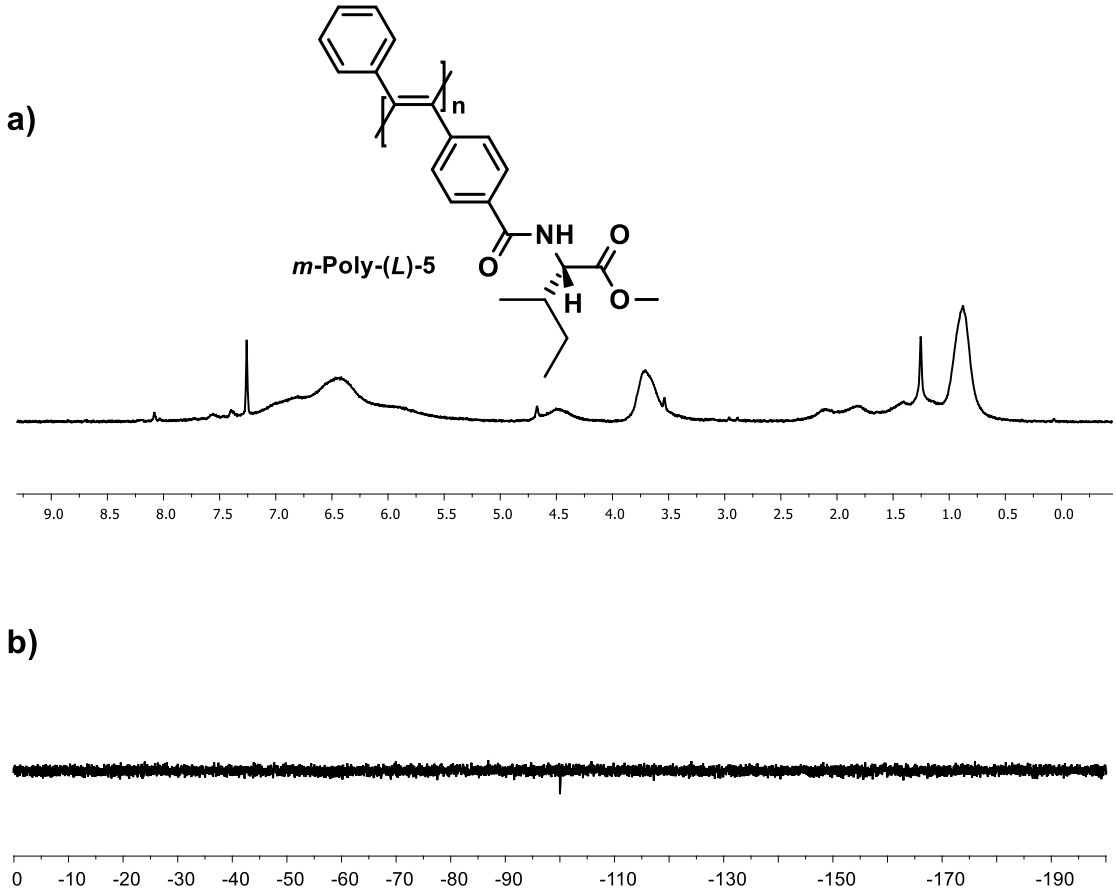

Figure S17. a) ^{1}H-NMR and b) ^{19}F-NMR spectra of *m*-Poly-(*L*)-**5**.

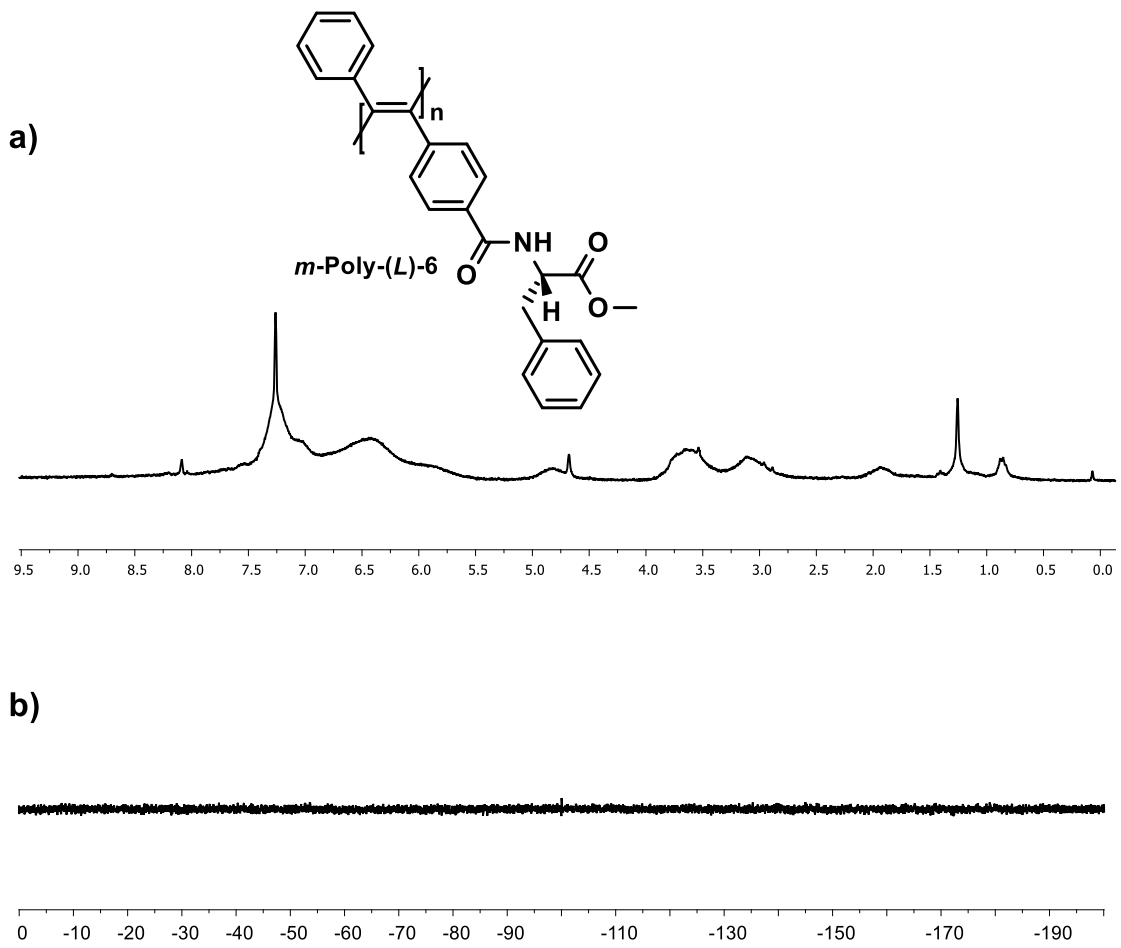

Figure S18. a) ^{1}H-NMR and b) ^{19}F-NMR spectra of *m*-Poly-(*L*)-**6**.

5. CD studies of the *para*-substituted polymers in different solvents

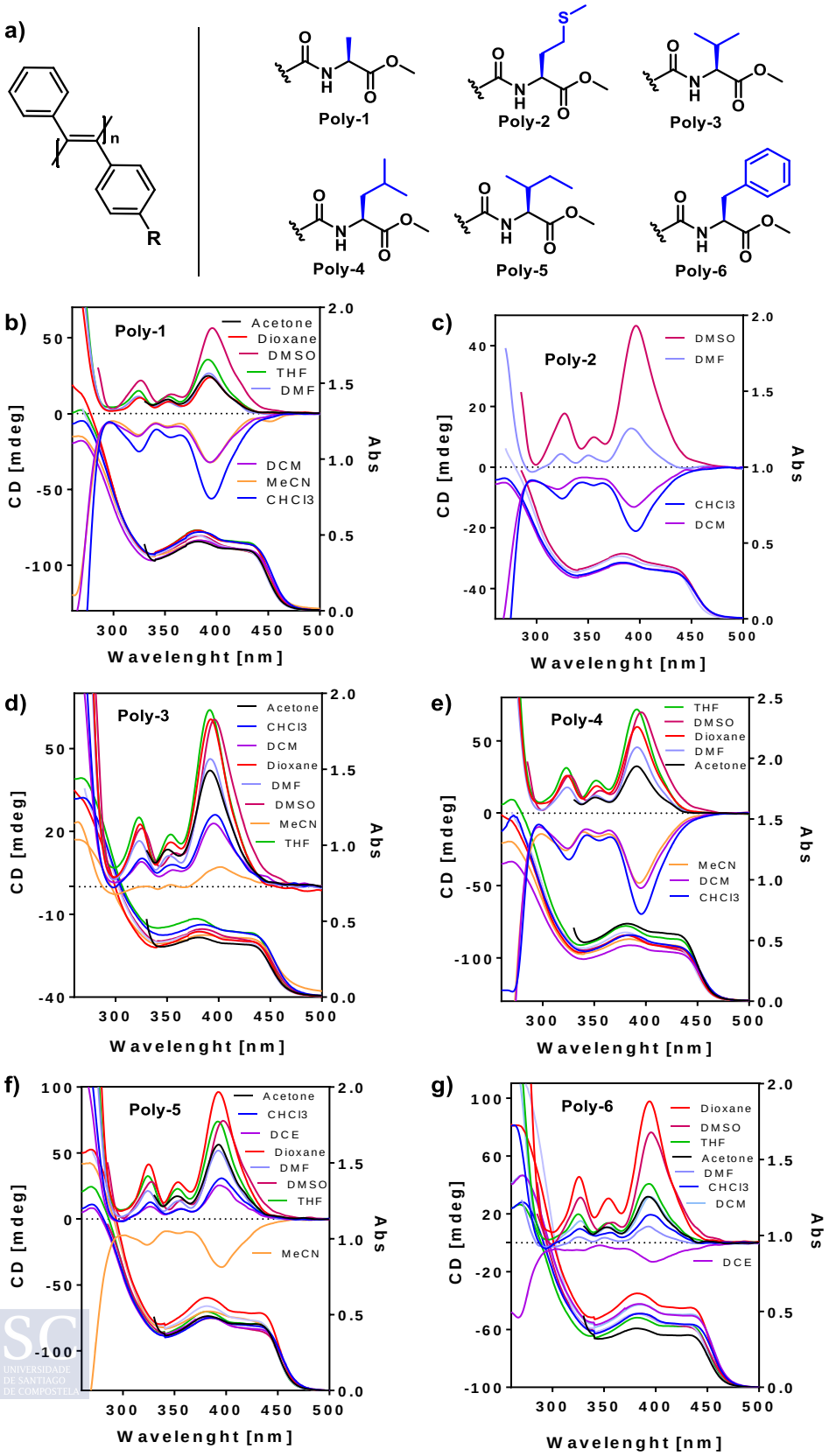

Figure S19: a) Schematic representation of the *para*-substituted polymers synthetized. CD and UV in different solvents (0.5 mg/mL) of b) *p*-poly-(*L*)-**1**, c) *p*-poly-(*L*)-**2**, d) *p*-poly-(*L*)-**3**, e) *p*-poly-(*L*)-**4**, f) *p*-poly-(*L*)-**5** and g) *p*-poly-(*L*)-**6.**

6. CPL studies of *para*-substituted polymers in different solvents

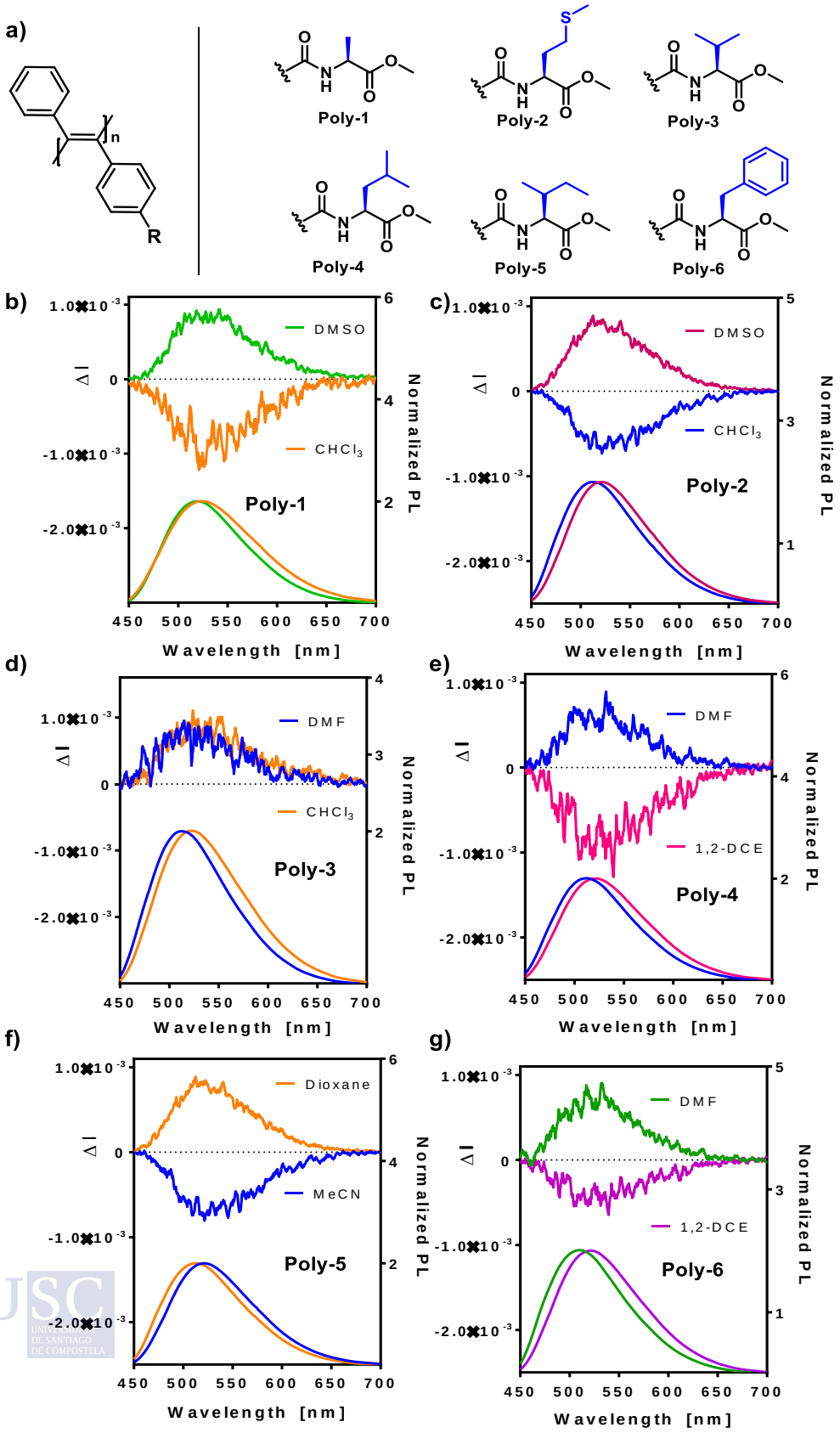

Figure S20: a) Schematic representation of the polymers synthetized. CPL and PL spectra in different solvents (0.3 mg/mL) of b) *p*-poly-(*L*)-**1**, c) *p*-poly-(*L*)-**2**, d) *p*-poly-(*L*)-**3**, e) *p*-poly-(*L*)-**4**, f) *p*-poly-(*L*)-**5** and g) *p*-poly-(*L*)-**6.**

7. CD studies of the *meta*-substituted polymers in different solvents

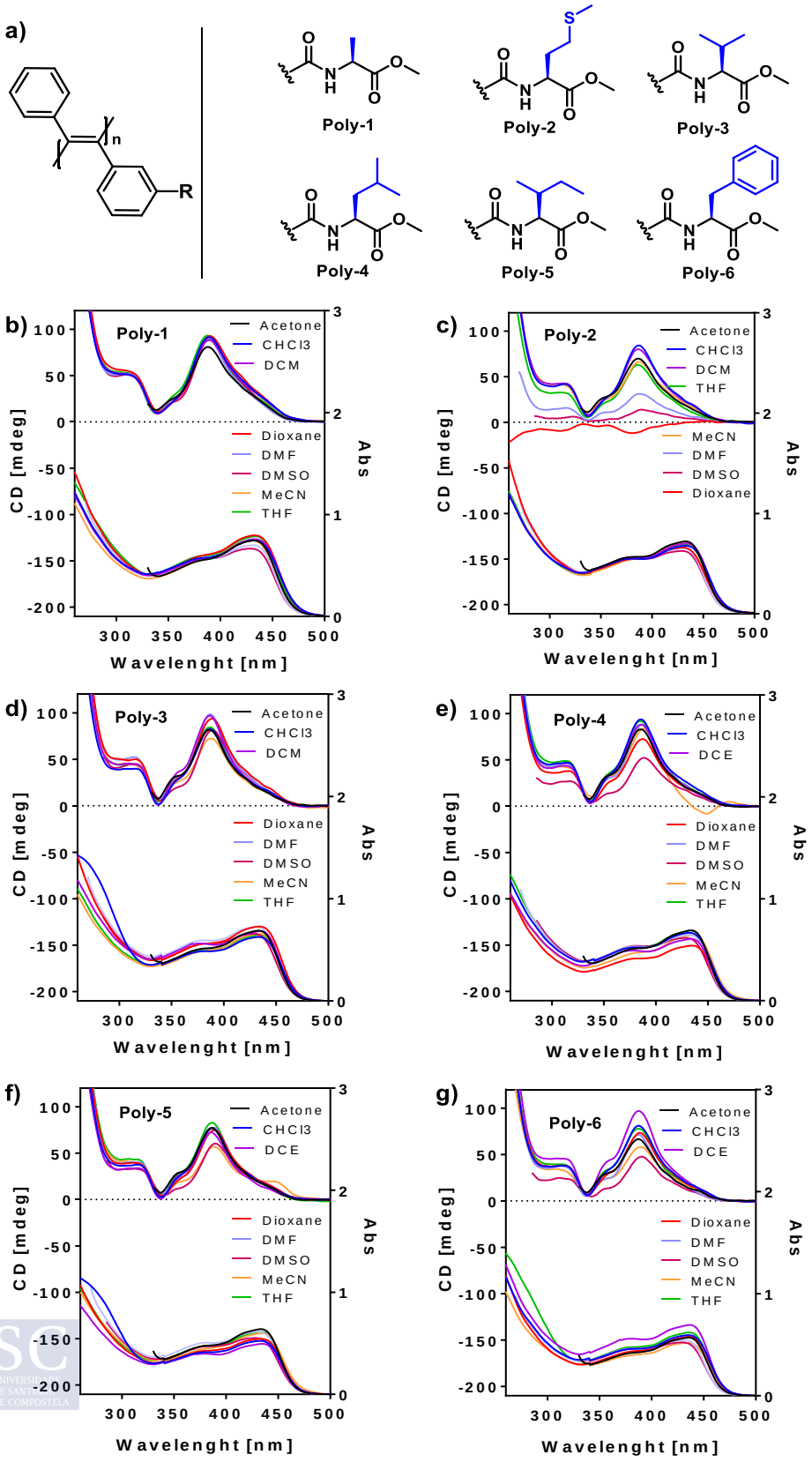

Figure S21: a) Schematic representation of the *meta*-substituted polymers synthetized. CD and UV in different solvents (0.5 mg/mL) of b) *m*-poly-(*L*)-**1**, c) *m*-poly-(*L*)-**2**, d) *m*-poly-(*L*)-**3**, e) *m*-poly-(*L*)-**4**, f) *m*-poly-(*L*)-**5** and g) *m*-poly-(*L*)-**6.**

8. CPL studies of the *meta*-substituted polymers in different solvents

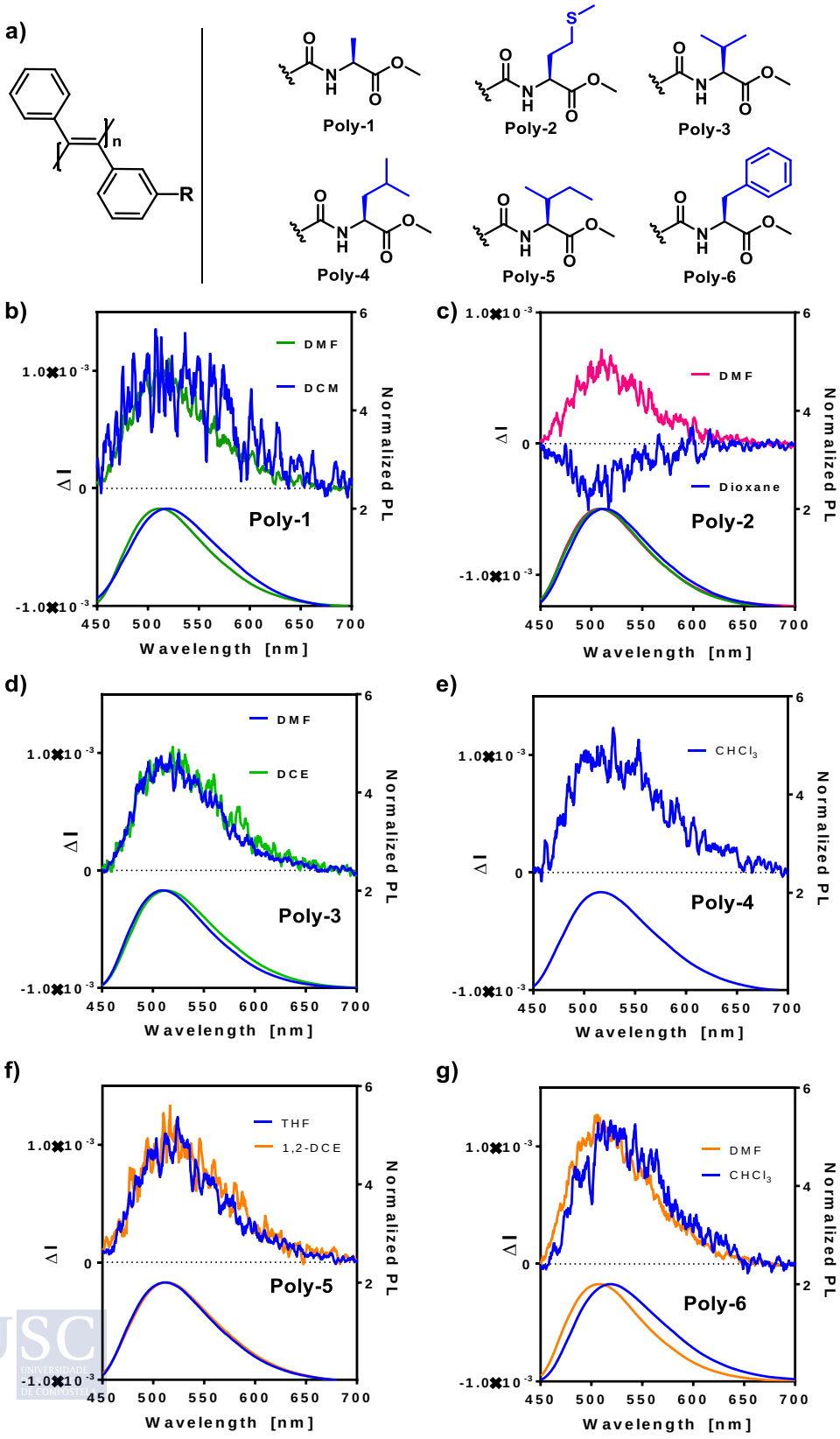

Figure S22: a) Schematic representation of the *meta*-substituted polymers synthetized. CPL and PL spectra in different solvents (0.3 mg/mL) of b) *m*-poly-(*L*)-**1**, c) *m*-poly-(*L*)-**2**, d) *m*-poly-(*L*)-**3**, e) *m*-poly-(*L*)-**4**, f) *m*-poly-(*L*)-**5** and g) *m*-poly-(*L*)-**6.**

9. References

S1. Tarrío, J. J.; Rodríguez, R.; Fernández, B.; Quiñoá, E.; Freire, F. Dissymmetric Chiral Poly (diphenylacetylene) s: Secondary Structure Elucidation and Dynamic Luminescence. *Angew. Chem. Int. Ed.*, **2022**, *61*, e202115070.

This Doctoral Thesis is focused on the development of new chiral materials based on poly(diphenylacetylene)s (PDPA). PDPAs are a family of helical polymers generally described as very stable and static, where the secondary structure — helical sense and/or elongation— cannot be modulated by external stimuli. Therefore, in this work we have explored different approaches to synthesize the first reported dynamic PDPAs, which has allowed us to create new stimuli-responsive materials. In addition, we have also focused on the elucidation of the secondary structure of those polymers to understand their structure-function relationship. These results can help the future rational design of novel smart materials with specific properties.